Mechanisms of TonB-Dependent Protein Import in *Pseudomonas aeruginosa*

By

Jonathan Goult

The Queen's College

A thesis presented for the degree of Doctor of Philosophy at the University of Oxford

Trinity Term 2021

Supervised by

Professor Colin Kleanthous
Professor Christina Redfield

Declaration

I hereby confirm that the work presented in this thesis, submitted for the degree of Doctor of Philosophy, is my own original work. Work that is not my own is referenced appropriately. This thesis has not been previously submitted at this or any other university.

Jonathan Goult

May 2021

Acknowledgements

Over the course of my DPhil, I have been supported by a multitude of people, to whom I am deeply grateful for their support, advice, and friendship, throughout this enjoyable and rewarding (and at times somewhat painful) endeavour. First and foremost, I would like to thank both my supervisors Professor Colin Kleanthous and Professor Christina Redfield. I thank Colin for the opportunity to undertake a DPhil in his lab, in addition to his continued guidance and mentorship over the years. I thank Christina for her support and guidance during my second rotation project, particularly concerning NMR experiments. I am supremely grateful for all the help, advice and support provided by Dr. Nicholas Housden, including the foundations of several aspects of the project, training me on a wide variety of lab techniques, and his utmost patience when I had questions. Many thanks are also due to Dr. Renata Kaminska for her assistance with the production of several plasmids and protein constructs during this project. I would also like to thank Martin Vesely for trialling the expression of some PyoS2 disulphide constructs (including one particularly egregious one) during his Part II project.

Within the Biochemistry department, I would like to mention Dr. Edward Lowe and Dr. David Staunton. I thank Ed for sharing his crystallographic expertise and for his help with solving the $PyoSN_{NTD}$ structure. I thank David for his help and support with several biophysical techniques, and for performing DSC and ESI-MS on several of my protein samples. Outside the University of Oxford, I would like to thank my collaborators – parts of this project would not have been possible without their input. I thank Professor Daniel Walker and Dr. Khedidja Mosbahi at the University of Glasgow for screening PyoSN against a Pseudomonas clinical isolate library. I thank Dr. Emanuele Paci, Daniel Van and Yasmin Taylor for performing molecular dynamics simulations during investigations into the structural constraints of PyoS2 import, in addition to their contributions to a paper written on the topic. I would also like to thank Professor Isabelle Schalk for provision of the several reagents, including *Pseudomonas* strains, plasmids and anti-FpvAI antibodies.

I would also like to thank members of the Kleanthous group, both past and present, for their friendship, scientific conversations, and for being wonderful colleagues to interact with on a daily basis. For this I thank current members: Nick, Renata, Jo, Melissa, Nathalie, Sandip, Gideon, Ruth, Patrick, Iva, Cara and Vivian, in addition to previous members Patrice, Katarina, Paul, Connor, Soumik, Hannah and Marie-Louise.

Finally, I would like to thank my family, who were instrumental in making all this possible. I thank both my parents, Kevin and Beverley, for their love and support, in addition to their encouragement from an early age. I also thank my brother Christopher, who has provided both friendship and healthy competition in the race for thesis submission. I would also like to thank my fiancée Lettie, who has supported me through the highs and lows of my DPhil, celebrated my achievements, patiently read through countless thesis edits and applications, and has always been there with love and support for me.

Abstract

The rise of multidrug resistance in several bacterial families is an emerging therapeutic crisis, with the potential to revert society to a pre-antibiotic era. Of particular concern is the opportunistic pathogen, *Pseudomonas aeruginosa*, a major causative agent of hospital-associated infections. As such, the development of novel therapeutics to target multidrug resistant *P. aeruginosa* is critical. Protein antibiotics synthesised by *P. aeruginosa*, known as pyocins, have recently become the focus of concerted efforts to develop new treatments to combat bacterial infections. Pyocins are fundamental for interbacterial competition, but the mechanisms by which they translocate across the Gram-negative cell envelope are poorly understood. The work presented in this thesis explores the mechanism by which two nuclease-type pyocins, pyocin S2 (PyoS2) and pyocin SN (PyoSN) exploit target proteins within the *P. aeruginosa* cell membrane to stimulate uptake. The components of the cellular envelope parasitised by PyoSN during import were identified, including a novel OM transporter, CntO. CntO is a 22-stranded β-barrel and virulence factor in *P. aeruginosa* that transports the metallophore pseudopaline across the OM. PyoSN eliminated a broad range of *Pseudomonas* clinical isolates, demonstrating its potent therapeutic potential. The PyoSN transporter binding domain was subsequently isolated ($PyoSN_{NTD}$) and the crystal structure solved. $PyoSN_{NTD}$ possessed a kinked three-helical bundle motif, which is conserved with the $PyoS2_{NTD}$ structure. Finally, the global mechanisms of TonB-dependent pyocin import were investigated in atomistic detail using PyoS2 and its transporter FpvAI. The structural constraints imparted on protein import across the OM were identified, confirming partial unfolding of the $PyoS2_{NTD}$ is a requirement for translocation through FpvAI. Interestingly, structural flexibility of transport was much greater than expected, with a PyoS2 disulphide construct retaining translocation activity *in vivo*. Hence, this study demonstrates a conserved mechanism of import for TonB-dependent protein antibiotics through exploitation of energised nutrient transporters in the OM.

Table of Contents

List of Figures

List of Tables

Abbreviations List

ABC	ATP-binding cassette
ADP	Adenosine diphosphate
AF488	Alexa Fluor 488
AFM	Atomic force microscopy
AMS	Airway mucus secretion
APS	Ammonium persulphate
ATP	Adenosine triphosphate
ATPase	Adenosine triphosphatase
αKG	α-ketoglutarate
BAM	β-barrel assembly machinery
β-OG	n-Octyl-β-D-glucopyranoside
CD	Circular dichroism
CDI	Contact dependent inhibition
CF	Cystic fibrosis
CFTR	CF transmembrane conductance regulator
CFU	Colony forming units
CLB	Colicin-like bacteriocin
CntO	Pseudopaline receptor
ColE2	Colicin E2
ColE3	Colicin E3
ColE9	Colicin E9
ColIa	Colicin Ia
ColM	Colicin M
CPA	Common polysaccharide antigen
CRISPR	Clustered regularly interspaced short palindromic repeats
Cryo-EM	Cryo-electron microscopy
Diamide	1,1'-Azobis(N,N-dimethylformamide)
DMSO	Dimethylsulfoxide
DMT	Drug/metabolite transporter
DNA	Deoxyribonucleic acid
DNase	Deoxyribonuclease
DSC	Differential scanning calorimetry
DT	Diphtheria toxin
DTT	DL-Dithiothreitol
E. coli	*Escherichia coli*
ECF	Extra-cytoplasmic function
ECL	Enhanced chemiluminescence
EDTA	Ethylenediaminetetraacetic acid
EF2	Elongation factor 2
ER	Endoplasmic reticulum
ERAD	ER-associated degradation
ESI-MS	Electrospray ionisation mass spectrometry
ESRF	European Synchrotron Radiation Facility
ETA	Exotoxin A
Fe^{2+}	Ferrous iron
Fe^{3+}	Ferric iron
Fe^{3+}-PVD	Ferripyoverdine
FptA	Ferripyochelin receptor

FpvAI	Type I Ferripyoverdine receptor
Fur	Ferric utilisation regulator
GTP	Guanosine triphosphate
HB-EGF	Heparin-binding epidermal growth factor
IM	Inner membrane
ImS2	Immunity protein S2
ImSN	Immunity protein SN
IPTG	Isopropyl β-D-1-thiogalactopyranoside
ITC	Isothermal titration calorimetry
IUTD	Intrinsically unstructured translocation domain
K_a	Binding equilibrium association constant
K_d	Binding equilibrium dissociation constant
LB	Lysogeny broth
LC-MS/MS	Liquid chromatography coupled to tandem mass spectrometry
LF	Lethal factor
LIS	Lithium diiodosalicyclic acid
LPS	Lipopolysaccharide
MD	Molecular dynamics
MIC	Minimum inhibitory concentration
MOPSO	3-Morpholino-2-hydroxypropanesulphonic acid
mPEG	Methoxy-Polyethylene glycol
MPP	Mitochondrial processing peptide
MW	Molecular weight
MWCO	Molecular weight cut-off
NADH	Nicotinamide adenine dinucleotide
NAG	N-acetylglucosamine
NAM	N-acetylmuramic acid
NCS	Non-crystallographic symmetry
NEB	New England Biolabs
NTD	N-terminal domain
OBS	OmpF-binding site
OF	Oedema factor
OM	Outer membrane
OMP	Outer membrane protein
OSA	O-specific antigen
P. aeruginosa	*Pseudomonas aeruginosa*
PA	Protective antigen
PAM	Pre-sequence translocase-associated motor
PCR	Polymerase chain reaction
PDB	Protein Data Bank
PEG	Polyethylene glycol
PG	Peptidoglycan
pI	Isoelectric point
PMF	Proton-motive force
PMSF	Phenylmethylsulphonyl fluoride
POTRA	Polypeptide transport-associated
PRR	Proline rich region
PVD	Pyoverdine
PVDF	Polyvinylidene fluoride
PyoG	Pyocin G

PyoS2	Pyocin S2
PyoS2E2	Pyocin S2-colicin E2 chimera
PyoS3	Pyocin S3
PyoS5	Pyocin S5
PyoSN	Pyocin SN
RMSD	Root-mean-square deviation
rRNA	Ribosomal ribonucleic acid
RNase	Ribonuclease
SAD	Single-wavelength anomalous dispersion
SAM	S-adenosyl methionine
SAXS	Small-angle X-ray scattering
SDS	Sodium dodecyl sulphate
SDS-Page	Sodium dodecyl sulphate polyacrylamide gel electrophoresis
SEC	Size exclusion chromatography
SOC	Super optimal broth with catabolite repression
SRP	Signal recognition particle
$t_{1/2}$	Half-life
T1SS	Type I Secretion System
T2SS	Type II Secretion System
T3SS	Type III Secretion System
T4SS	Type IV Secretion System
T5SS	Type V Secretion System
T6SS	Type VI Secretion System
T9SS	Type IX Secretion System
Tat	Twin arginine translocase
TBDT	TonB-dependent transporter
TBE	Tris-borate-EDTA
TBS	Tris-buffered saline
TBST	Tris-buffered saline with Tween-20
TEMED	Tetramethylethylenediamine
TEV	Tobacco etch virus
TGN	trans-Golgi network
TIC	Translocon at the inner membrane of the chloroplast
TIM	Translocase of the inner membrane
T_m	Melting temperature
TOC	Translocon at the outer membrane of the chloroplast
TOM	Translocase of the outer membrane
tRNA	Transfer ribonucleic acid
UV	Ultraviolet
xNT	Extended N-terminal motif
WHO	World Health Organisation
Zur	Zinc utilisation regulator

Chapter 1 – Introduction

1. General Introduction.

Bacteria are primordial, single-cell microorganisms that are found ubiquitously in almost every conceivable environmental niche on the planet. In addition to their environmental omnipresence, they also comprise a fundamental component of the cellular composition of higher eukaryotes, termed the microbiome. This mutualistic relationship contributes to our overall fitness and as such, most bacterial species pose no significant threat (or are actively beneficial) to human health. However, a subset of bacterial species have evolved antagonistic relationships with their human hosts, known as pathogenesis. For millennia, bacterial pathogenesis has precipitated in serious human infections such as leprosy (*Mycobacterium leprae*), the bubonic plague (*Yersinia pestis*) and cholera (*Vibrio cholerae*). The advent of antibiotics, a class of antimicrobial compounds that eliminate bacterial infections, was thought to signal the swansong for pathogeneses caused by bacteria. Yet evolutionary selective pressures have driven development of resistance to these antimicrobial compounds, threatening to render antibiotics obsolete and foreshadowing a return to the pre-antibiotic era. As a result, the continued development of novel antimicrobial therapeutics is an imperative for modern medicine in combating the ever-escalating threat of multidrug resistance in pathogenic bacteria (WHO, 2014).

1.1. Multidrug resistant *Pseudomonas aeruginosa.*

A list of priority pathogens has been compiled by the World Health Organisation (WHO) in response to the rise in bacterial antibiotic resistance, cataloguing bacterial families that pose the greatest threat to human health (WHO, 2017). Those categorised as most critical include various members of the *Enterobacteriaceae* family (such as *Escherichia coli*), *Acinetobacter baumannii* and *Pseudomonas aeruginosa*. Due to its ubiquity in the environment, extreme metabolic versatility and tolerance to many detergents and disinfectants, *P. aeruginosa* has proven particularly adept at persisting in hospital settings, causing serious infections in patients that require support from conventional medical equipment such as catheters and ventilators (Olejnickova *et al.*, 2014; Ramírez-Estrada *et al.*, 2016).

P. aeruginosa is an opportunistic pathogen and major causative agent of disease in both animals and plants (Moradali *et al.*, 2017). In humans, it is typically associated with infections of burn and surgical wound sites, bacterial sepsis, and pneumonia (including

ventilator-associated pneumonia), primarily affecting immunocompromised patients. These infections are often fatal, with increased susceptibility for sufferers of the genetic condition cystic fibrosis (CF). Patients with CF overproduce mucus, due to a defect in the CF transmembrane conductance regulator (CFTR) chloride channel, which subsequently accumulates in the lungs. Inability to clear this excess mucus fosters an ideal environment for *P. aeruginosa* colonisation, with chronic pneumonia related to *P. aeruginosa* infection in CF patients resulting in a higher rate of mortality than the condition itself (Murray *et al.*, 2007). It is thought that all CF patients (approximately 70,000 – 100,000 people worldwide) will suffer from a *P. aeruginosa* lung infection during their lifetime, of which approximately 80% will become chronic (Folkesson *et al.*, 2012).

P. aeruginosa displays intrinsic resistance to many antibiotic compounds through the low permeability of its outer membrane (OM), in addition to the high-level expression of multidrug efflux pumps MexAB-OprM, MexCD-OprJ and MexEF-OprN (Lambert, 2002; Aeschlimann, 2003). Moreover, *P. aeruginosa* also undergoes phenotypic changes during the establishment of chronic infections, transitioning from single free-swimming bacteria to durable biofilm colonies, further protecting itself from external antimicrobial compounds (Whiteley *et al.*, 2001; Harmer *et al.*, 2013). There is increasing concern in the rise of acquired resistances to antibiotics used to treat *P. aeruginosa* infections, particularly carbapenem resistance, which is often the last line of defence against multidrug resistant bacterial infections. In Europe, it was found that antimicrobial resistance in pathogenic *P. aeruginosa* was high, with 13.7% of isolates displaying resistance to at least three antimicrobial groups, and 5.5% were resistant to all antibiotic groups (ECDC, 2015). As a result, the development of novel therapeutics to target multidrug resistant *P. aeruginosa* infections is of paramount importance.

1.2. The Gram-negative Bacterial Cell Envelope.

Bacteria have evolved a complex, multi-layered envelope to isolate and protect themselves from their unpredictable, nutrient-limited, and often hostile environment. Bacteria can be classified into two major groups based on the structure of their cellular envelope. The cellular envelope of Gram-positive bacteria, including *Staphylococcus aureus* and *Bacillus subtilis*, is comprised of a cytoplasmic membrane surrounded by a thick peptidoglycan (PG) cell wall containing teichoic and lipoteichoic acids. In contrast, Gram-negative bacteria, such as *E. coli* and *P. aeruginosa*, have a cellular envelope comprised of two membranes;

termed the inner and outer membranes. These membranes delimit an intervening compartment, which contains a thin layer of PG, known as the periplasm (Figure 1-1) (Silhavy *et al.*, 2010).

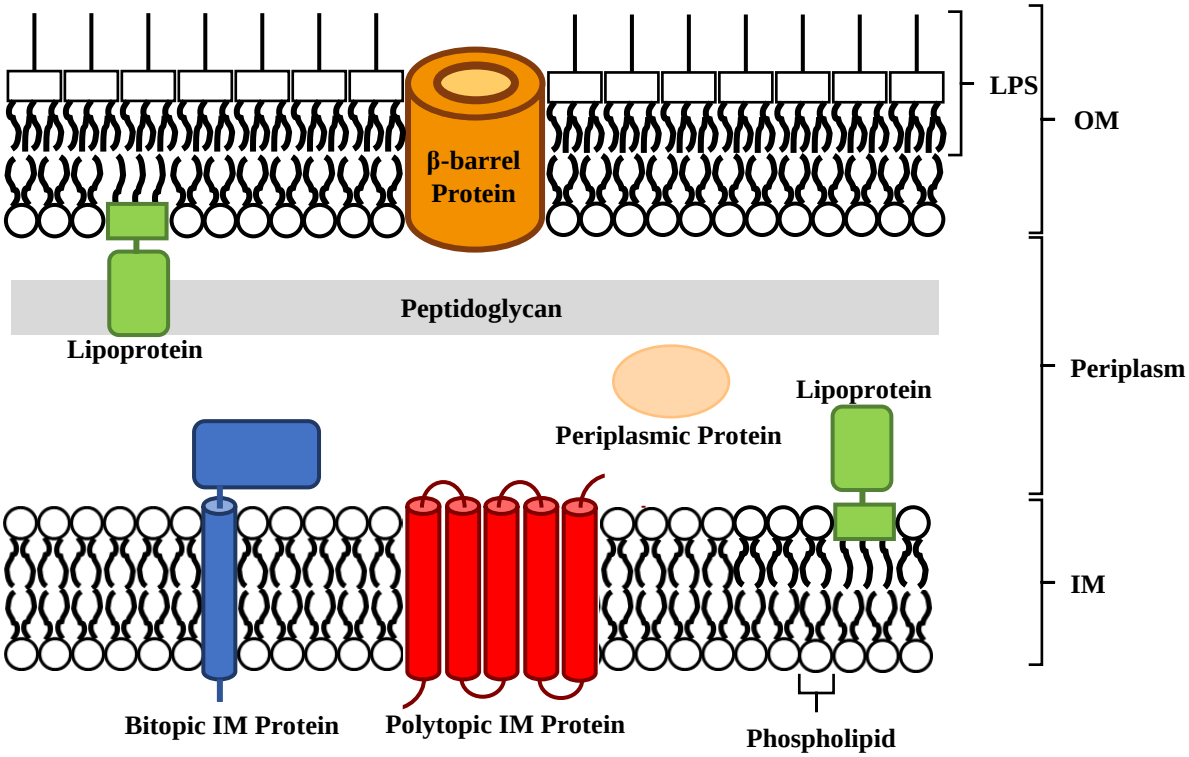

Figure 1-1. The Gram-negative cell envelope.
The *P. aeruginosa* cell envelope is ~38 nm in diameter. The overall thickness of the peptidoglycan layer is similar across Gram-negative bacterial species, including *E. coli* and *P. aeruginosa*, at ~3 nm (Turner *et al.*, 2013). OM = Outer Membrane, IM = Inner Membrane, LPS = lipopolysaccharide. Adapted from Silhavy *et al.*, 2010.

1.2.1. The Outer Membrane.

The outer membrane (OM), a distinguishing feature of Gram-negative bacteria, is asymmetric in nature. Whilst typical biological membranes consist of two symmetric layers of phospholipids, arranged so that hydrophobic acyl chains are protected by hydrophilic phosphate head groups, the outer membrane is instead comprised of distinct inner and outer leaflets. The inner leaflet contains phospholipids, primarily phosphatidylethanolamine, phosphatidylglycerol and cardiolipin (Raetz, 1978), whereas the outer leaflet contains glycolipids, principally lipopolysaccharide (LPS).

LPS is composed of an acylated glucosamine disaccharide, known as lipid A, linked to a "core" oligosaccharide. This oligosaccharide core can also link to an additional extended polysaccharide chain, known as the O-antigen. O-antigen is highly immunogenic, inducing

the secretion of cytokines for stimulation of an inflammatory response during Gram-negative bacterial pathogenesis (Raetz & Whitfield, 2002). This response is infamous for its role in endotoxic shock associated with septicaemia, of which *P. aeruginosa* is a major causative agent (Dudley, 1990). Most *P. aeruginosa* synthesise two distinct forms of O-antigen; the D-rhamnose homopolymer common-polysaccharide antigen (CPA) and the heteropolymer O-specific antigen (OSA), composed of three to five distinct sugars organised in repeated units (Lam *et al.*, 2011).

The OM forms the interface between Gram-negative bacteria and their extracellular environment, and as such, its primary function is to regulate the uptake of nutrients whilst simultaneously excluding toxins (Nikaido, 2003). This is achieved through a repertoire of proteins within the OM, which can be further subdivided into two classes: lipoproteins and β-barrels. Lipoproteins are typically anchored to the inner leaflet of the OM by an acyl chain attached to an N-terminal cysteine residue (Sankaran & Wu, 1994). β-barrels are integral membrane proteins that span the OM and are composed of antiparallel β-strands arranged around a central pore, forming a barrel topology. These barrels are typically comprised of 8 to 24 β-strands but can be as large as 36. Commonly referred to as outer membrane proteins (OMPs), these proteins mediate a diverse range of processes, functioning as porins, transporters and enzymes. The simplest of these OMPs are the porins, comprised of single or trimeric β-barrels. General porins, such as OmpA, OmpC and OmpF in *E. coli*, facilitate passive diffusion of small molecules, including sugars and amino acids, through their lumen across the OM (Nikaido, 2003). In contrast, the *P. aeruginosa* OM is significantly less permeable than that of *E.coli* due to absence of general porins; with expression of substrate-specific porins that can adopt open or closed conformations offering additional protection against antimicrobial penetration of the OM (Nestorovich *et al.*, 2006; Chevalier *et al.*, 2017). Another OMP family are the TonB-dependent transporters (TBDTs), which are required to actively transport larger molecules, in the form of siderophores, metal-chelates and carbohydrates, across the OM (Schauer *et al.*, 2008). These transporters can be distinguished from porins by their larger size (typically 22 β-strands) and presence of an additional N-terminal plug domain that occludes the β-barrel lumen (Noinaj *et al.*, 2010). Some bacterial species, such as *P. aeruginosa*, possess an impressive repertoire of TBDTs that are expressed to scavenge scarce nutrients from their extracellular environment, described in **Table 1-1**. Additionally, some integral β-barrels form large multidrug efflux pumps to extrude antimicrobial compounds from the cell (Delmar *et al.*, 2014). OMPs are

folded and correctly inserted into the OM by the β-barrel assembly machinery, discussed in more detail in section 1.3.2 (Voulhoux & Tommassen, 2004; Wu *et al.*, 2005).

Table 1-1. TonB-dependent Transporters of *P. aeruginosa* strain PAO1.

TBDT Name	Gene Locus	Function	Reference
FiuA	PA0470	Ferrichrome Receptor	(Hannauer *et al.*, 2010)
PirA	PA0931	Ferric Enterobactin Receptor	(Ghysels *et al.*, 2005)
BtuB	PA1271	Putative Cobalamin Transporter	(Hancock & Brinkman, 2002)
HxuC	PA1302	Hemin Transporter	(Otero-Asman *et al.*, 2019)
FemA	PA1910	Ferric Mycobactin Receptor	(Llamas *et al.*, 2008)
SppR	PA2057	Xenosiderophore Receptor	(Pletzer *et al.*, 2016)
FpvAI	PA2398	Ferripyoverdine Receptor	(Poole *et al.*, 1993)
FoxA	PA2466	Ferrioxamine Receptor	(Llamas *et al.*, 2006)
PfeA	PA2688	Ferric Enterobactin Receptor	(Moynié *et al.*, 2019)
HasR	PA3408	Heme Transporter	(Smith & Wilks, 2015)
FptA	PA4221	Fe^{3+}-Pyochelin Receptor	(Ankenbauer & Quan, 1994)
OprC	PA3790	Putative Copper Transporter	(Quintana *et al.*, 2017)
FecA	PA3901	Fe^{3+}-dicitrate Transporter	(Marshall *et al.*, 2009)
FvbA	PA4156	Vibriobactin Transporter	(Elias *et al.*, 2011)
FpvB	PA4168	Ferripyoverdine Receptor B	(Ghysels *et al.*, 2004)
ChtA	PA4675	Aerobactin Receptor	(Cuív *et al.*, 2006)
PhuR	PA4710	Heme/Hemoglobin Receptor	(Smith & Wilks, 2015)
CntO	PA4837	Pseudopaline Receptor	(Lhospice *et al.*, 2017)
	PA0151	Probable TonB-dependent Transporter	
	PA0192		
	PA0434		
	PA0781		
	PA1322		
	PA1365		
	PA1613		
	PA1922		
	PA2070		
	PA2089		
	PA2289		
	PA2335		
	PA2590		
	PA2911		
	PA3268		
	PA4514		
	PA4897		

1.2.2. The Periplasm.

Situated between the OM and IM is an aqueous cellular compartment known as the periplasm. It contains a large assortment of soluble proteins and trans-envelope spanning complexes. These include the multidrug efflux pumps, type III, IV and VI secretion systems and the bacterial flagellum (Delmar *et al.*, 2014; Green & Mecsas, 2016; Armitage & Berry, 2020).

1.2.3. The Peptidoglycan (PG) layer.

The PG layer is a heteropolymer formed by repeating linkages of alternating N-acetylglucosamine-N-acetylmuramic acid (NAM-NAG) disaccharide subunits, which are heavily crosslinked by pentapeptide linkages to form a dense lattice (Vollmer *et al.*, 2008). The PG layer is intimately associated with the OM through covalent interactions with Braun's lipoprotein (Lpp), in addition to non-covalent interactions with other OMPs (V. Braun, 1975; Park *et al.*, 2012). The structure of the PG layer often dictates the bacterial cell shape, in addition to imparting strength and rigidity, but also flexibility and reversible expansion under pressure. The PG layer contains holes that enabling the diffusion of large molecules such as proteins through it (Demchick & Koch, 1996).

1.2.4. The Inner Membrane.

The inner membrane (IM) of Gram-negative bacteria is a symmetric glycerophospholipid bilayer with lipid composition near identical to that of the inner leaflet of the OM (Raetz, 1978; Raetz & Dowhan, 1990). It is the site of many important cellular processes such as PG synthesis during cell growth and division, lipid biogenesis and energy generation via the electron transport chain. Due to the absence of specialised intracellular organelles for metabolic compartmentalisation within bacteria, the IM is fundamental for energy generation in this manner, which is subsequently utilised in ATP synthesis to power cellular processes. Proteins of the IM are associated with the membrane through single- or multi-pass transmembrane α-helices, or anchored to the membrane by an N-terminal acylated chain (Dalbey *et al.*, 2011).

1.3. Protein Transport in Gram-negative Bacteria.

Due its complex tripartite organisation, Gram-negative bacteria require dedicated mechanisms for the import and export of substrates across their cellular envelope. This poses a particular challenge for larger substrates, such as proteins. Proteins are required in all compartments of the cellular envelope, necessitating secretion from the cytosol to reach their active site. As such, Gram-negative bacteria have evolved several distinct secretion systems to translocate proteins between the cellular envelope compartments, the external environment, and even across neighbouring bacterial or host eukaryotic cell membranes.

Whilst the mechanisms of protein secretion are well studied, the import of proteins by Gram-negative bacteria remains poorly resolved.

1.3.1. Secretion across the Inner Membrane – Sec and Tat transport.

All bacterial proteins destined for the cellular envelope are first synthesised on ribosomes in the cytoplasm, and subsequently exported to their correct subcellular compartment. The majority of proteins bound for the OM and the periplasm are synthesised with an N-terminal signal peptide that targets them for secretion across the IM. This signal peptide is recognised by the Sec machinery; comprising the heterotrimeric IM SecYEG complex and the cytosolic motor ATPase SecA (Driessen & Nouwen, 2008). The SecYEG complex is unable to transport folded substrates, therefore pre-proteins are bound by the cytoplasmic chaperone SecB, stabilising the substrate in an unfolded translocation-competent state (Bechtluft *et al.*, 2010). SecB delivers the unfolded substrate to SecA, which binds the chaperone and pre-protein complex. This complex can then engage with SecYEG, allowing intercalation of the signal peptide into the SecYEG channel. The energy for pre-protein translocation through the SecYEG channel into the periplasm is provided by the proton-motive force and SecA-dependent ATP hydrolysis. In addition to post-translational transport, the Sec machinery can secrete nascent proteins co-translationally with assistance from the signal recognition particle (SRP). During protein translation, SRP binds to the nascent signal peptide as it emerges from the ribosome. SRP then associates with FtsY, which delivers the entire ribosome-protein complex onto SecYEG. The nascent polypeptide is translated directly into the SecYEG channel. Once the pre-protein has successfully transported into the periplasm, the signal peptide is cleaved to generate the mature protein.

Bacteria are also capable of translocating proteins in a folded state utilising the Twin-arginine (Tat) system. An N-terminal sequence containing a pair of adjacent arginine residues is recognised by IM proteins TatB and TatC, facilitating the recruitment and oligomerisation of another IM protein, TatA, to form a secretory channel through which the folded substrate translocates (Berks, 2015). Secretion in a folded state is a requirement for some proteins due to the presence of post-translational modifications, such as redox cofactors, that must be synthesised and added to nascent proteins in the cytoplasm prior to export.

1.3.2. Into the Outer Membrane – the β-barrel Assembly Machinery (BAM).

Integral β-barrel pre-proteins destined for the OM require further processing following Sec-mediated translocation to the periplasm. These OMP precursors must undergo successful folding and insertion into the OM in order to perform their cellular functions. This process is mediated by the ~200 kDa BAM complex. The BAM complex is composed of five proteins; an essential core component BamA, which is an OMP itself, and four accessory lipoproteins, BamB, BamC, BamD and BamE, each anchored to the inner leaflet of the OM via an N-terminal acyl chain modification (Wu *et al.*, 2005; Sklar, Wu, Gronenberg, *et al.*, 2007). BamA is a member of the Omp85 superfamily, with a C-terminal 16-stranded integral OM β-barrel domain and five polypeptide transport associated (POTRA) domains at its N-terminus located in the periplasm (Noinaj *et al.*, 2013). Although only BamA and BamD are essential for cell viability in *E. coli*, all components are required for efficient OMP insertion *in vivo* (Malinverni *et al.*, 2006). Upon entering the periplasm, nascent OMPs are bound by chaperones, including SurA, Skp and DegP, protecting them from proteolytic degradation and maintaining substrates in an insertion competent state (Sklar, Wu, Kahne, *et al.*, 2007). Chaperone pathways direct the nascent OMPs to the OM, where they associate with the BAM complex. The mechanism by which the BAM complex is thought to insert and fold OMPs in the OM has been inferred through recent advances in X-ray crystallography, cryo-electron microscopy (cryo-EM) and crosslinking studies. BamA has been demonstrated to exist in an ensemble of conformations, including a 'lateral open' state, in which a portion of the β-barrel has rotated out, separating the β1C and β16C strands, and opening the barrel laterally to the OM (Figure 1-2) (Bakelar *et al.*, 2016; Gu *et al.*, 2016; Iadanza *et al.*, 2016).

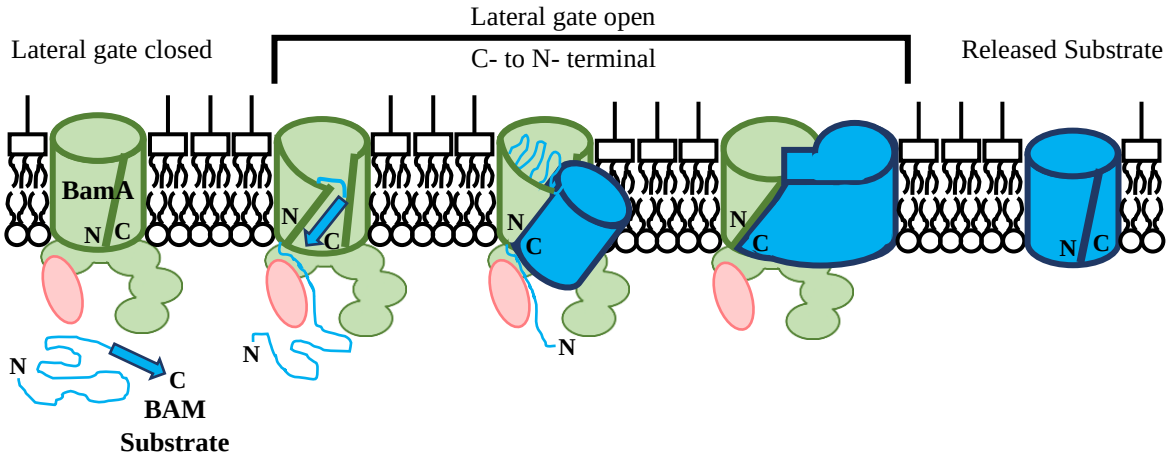

Figure 1-2. Model for β-barrel assembly in the OM by the BAM complex.
Representation of the stages of β-barrel folding and insertion into the OM as described above. BamA (*green*) and BamD (*pink*) alone are shown for simplicity. Adapted from Tomasek *et al.*, 2020.

This facilitates the formation of an antiparallel hydrogen bonded interface between the N-terminal edge of the BamA β-barrel and the C-terminal β-strand of the substrate (Lee *et al.*, 2019; Doyle & Bernstein, 2019; Tomasek *et al.*, 2020). Addition of subsequent β-strands of the nascent OMP generates an asymmetric hybrid β-barrel between the two proteins. Substrate release likely relies on the sequential disruption of hydrogen bonds at the BamA-substrate interface through closure of the mature OMP β-barrel, displacing the hydrogen bond interactions with BamA in a stepwise manner (Tomasek *et al.*, 2020), resulting in the release of the mature OMP from the BAM complex.

1.3.3. Protein secretion systems.

In addition to secretion of proteins to the compartments of the cellular envelope, Gram-negative bacteria have evolved a variety of mechanisms for protein secretion beyond the confines of the cell. This is achieved by dedicated protein secretion systems utilised to shuttle protein cargo across the bacterial cell envelope into the external environment, or in some cases across additional membranes into the cytoplasm of a host eukaryotic or prokaryotic cell. There are seven secretion systems present in Gram-negative bacteria, named type I to type VI, and the recently characterised type IX, which are each utilised for transportation of different subsets of protein substrates (Figure 1-3).

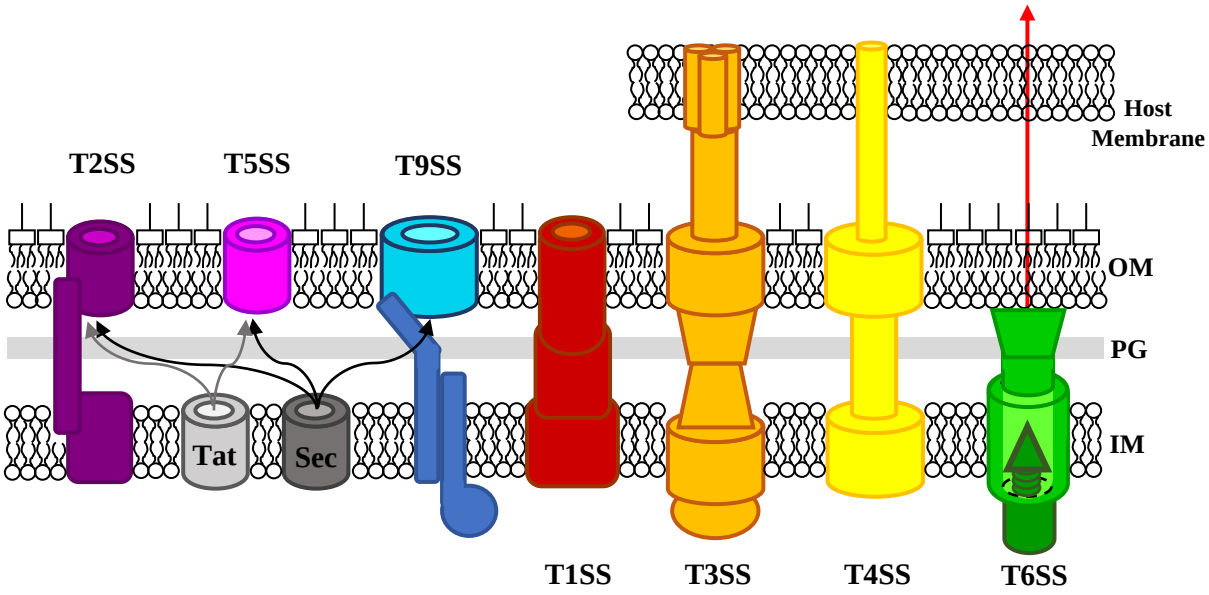

Figure 1-3. Secretion systems of Gram-negative bacteria.
Schematic of the secretion systems present in Gram-negative bacteria. T1SS, T2SS, T5SS and T9SS are utilised to export substrates into the extracellular environment, whereas T3SS, T4SS and T6SS are able to additionally export substrates across host membranes during pathogenesis. Adapted from Green & Mecsas, 2016.

The type I secretion system (T1SS) is composed of three essential structural components: an ABC transporter in the IM, a membrane fusion protein that spans the periplasm and an OMP pore (Thomas *et al.*, 2014). Interestingly, a number of T1SSs utilise the multi-purpose antibiotic efflux protein TolC as their OMP pore (Balakrishnan *et al.*, 2001). Substrates secreted by the T1SS have a diverse range of functions including heme-binding proteins, adhesins and enzymes (Delepelaire, 2004). Type II secretion systems (T2SS) transport folded proteins from the periplasm into the extracellular environment, and thus consist of an OMP pore only. Secreted proteins have a range of biological functions, but are generally enzymatic in nature (Korotkov *et al.*, 2012). The type III secretion system (T3SS) or "injectisome" is a huge trans-envelope spanning complex that is required for secretion of a wide variety of effector proteins across both the IM and OM. In addition, most T3SSs are adapted for direct delivery of substrates across target eukaryotic cell membranes during pathogenesis, transporting effector proteins across three membranes in a single step. The T3SS comprises three main structural components: a basal body spanning the entire cellular envelope, a hollow extracellular needle through which unfolded effectors traverse, and a translocon complex at the needle tip that is essential for effector translocation across target membranes (Radics *et al.*, 2014; Abrusci *et al.*, 2014). The function of T3SS effector proteins vary widely, but those of pathogenic bacteria are often involved in subversion of normal cellular functions, enabling pathogens to establish an infectious niche within a host cell or tissue (Buttner, 2012). The type IV secretion system (T4SS) is an incredibly versatile transport system utilised for exchange of monomeric proteins, multi-subunit protein toxins, DNA and nucleoprotein complexes between bacterial cells, in addition to delivery of effector proteins into target eukaryotic cells during pathogenesis (Cascales & Christie, 2003). The type V secretion system (T5SS) has an atypical secretion mechanism, whereby substrates autocatalyze their translocation across the OM after Sec-mediated secretion to the periplasm. T5SS substrates possess a β-barrel domain that inserts into the OM, forming a channel for secretion of the remaining protein (autotransporter secretion) or an additional specific protein substrate (two-partner and chaperone-usher secretion) across the OM (Leyton *et al.*, 2012). T5SS substrate effectors are predominately associated with virulence, such as proteases, adhesins and host-immune evasion molecules (Pohlner *et al.*, 1987; Brotcke Zumsteg *et al.*, 2014). The type VI secretion system (T6SS) is a widely distributed trans-envelope protein secretion system, capable of contact-dependent delivery of effector proteins between Gram-negative bacteria (Bingle *et al.*, 2008). Comprised of a membrane-spanning complex and central baseplate connected to long needle and sheath (Nguyen *et al.*,

2018), the T6SS has both structural and mechanistic homology to the T4 contractile phage tail (Leiman *et al.*, 2009; Pell *et al.*, 2009). Contraction of the sheath propels the needle out of the cell, delivering effector proteins into target bacteria and some eukaryotes. As a primary mechanism of inter-bacterial competition, T6SS effectors have a diverse range of cytotoxic functions, including nucleases, lipases, peptidoglycan hydrolases and actin crosslinkers (Pukatzki *et al.*, 2007; Alteri & Mobley, 2016). The recently characterised type IX secretion system (T9SS) is a unique secretion system found only in some species of the *Fibrobacteres-Chlorobi-Bacteriodetes* phylum, responsible for secretion of various effector proteins across the OM, such as proteases, adhesins and cellulases. After translocation into the periplasm through the Sec machinery, substrates are targeted to the OM by a C-terminal domain signal, whereby they are secreted into the external environment through the Sov translocon; a process which is thought to be driven by the PorL-PorM stator complex (Gorasia *et al.*, 2020; Hennell James *et al.*, 2021).

1.3.4. Mitochondrial/Plastid protein import.

Whilst bacteria have a plethora of mechanisms for the secretion of proteins across their cellular envelope, no dedicated protein import systems have yet been identified, despite the fundamental importance of protein import for inter-bacterial competition (Kirkup & Riley, 2004; Granato *et al.*, 2019). However, the requirement for dedicated protein import systems has arisen in both mitochondria and plastids; descendants of Gram-negative bacteria. Both mitochondria and plastids are eukaryotic organelles, yet their prokaryotic origins can be traced back to that of free-living α-proteobacteria and cyanobacteria respectively (Yang *et al.*, 1985; Giovannoni *et al.*, 1988). Endosymbiotic theory suggests that ancestors of these bacteria formed an intimate host-symbiont relationship with an archaeon or primitive eukaryote, which in principle resulted in the symbiont residing inside the host (Martin & Müller, 1998; Martin *et al.*, 2015). Horizontal gene transfer between the symbiont and the host, particularly those encoding for metabolic enzymes and substrate transporters, facilitated genetic integration of host and endosymbiont, whilst allowing endosymbionts to maintain a distinct biochemical identity (Martin *et al.*, 2015). This has resulted in transfer of the majority of genes that encode the mitochondrial and plastid proteome to the nuclear genome, with these organelles only maintaining a small genome for expression of components of the respiratory and photosynthetic electron transport chains (Glöckner *et al.*, 2000; Burger *et al.*, 2013). As such, both organelles must possess robust protein import

systems to transport the majority of their proteome from the eukaryotic cytoplasm across their envelope (Wiedemann & Pfanner, 2017).

Pre-proteins destined for the mitochondria are synthesised with an N-terminal presequence, which forms an amphipathic α-helix containing both positively charged and hydrophobic faces (Roise *et al.*, 1986). This presequence is recognised by the translocase of the outer membrane (TOM) complex. The TOM complex is composed of Tom40, a 19-stranded β-barrel that forms the main import channel, and three receptor binding proteins, Tom20, Tom22 and Tom70 (Hill *et al.*, 1998; Shiota *et al.*, 2015). Additional small regulatory subunits Tom5, Tom6 and Tom7 are also associated with the complex (Araiso *et al.*, 2019). Initial recognition of substrates occurs through hydrophobic interactions between the amphipathic α-helix of the presequence with Tom20 (Abe *et al.*, 2000). Tom20 transfers the substrate to the central receptor Tom22, which binds the positively charged surface of the presequence helix. Substrates are then imported across the mitochondrial OM through Tom40. The interior of the Tom40 β-barrel contains both hydrophobic and hydrophilic surfaces, facilitating the import of a diverse range of precursor proteins, including both matrix (hydrophilic) and membrane (hydrophobic) proteins. Preproteins translocated through the TOM complex are further directed through one of several major protein import pathways, depending on their terminal compartment destination within the mitochondria. Mitochondrial β-barrel proteins are trafficked and inserted into the OM by the sorting and assembly machinery complex, constituting Sam50, a member of the Omp85 superfamily, and cytosolic proteins Sam35 and Sam37 (Paschen *et al.*, 2003; Klein *et al.*, 2012). Mitochondrial metabolite carrier proteins are inserted into the IM by the action of the TIM22 complex. Preproteins bound for the mitochondrial matrix and inner membrane are directed to the translocase of the inner membrane (TIM23) complex. Substrate presequences emerging from the Tom40 pore are recognised by the TIM23 complex through Tim50, which activates the IM channel forming Tim23 (Truscott *et al.*, 2001; Lytovchenko *et al.*, 2013). Additionally, Tim17 and Tim21 function as regulatory subunits of the TIM23 complex. Import through the TIM23 complex is primarily driven by membrane potential, with an electrophoretic effect exerted on the positively charged N-terminus of the preprotein as it is drawn towards the negatively charged matrix (Martin *et al.*, 1991). However, complete translocation into the matrix requires a secondary energy source, driven by the ATP-dependant presequence translocase-associated motor (PAM) complex (Chacinska *et al.*, 2009). Mature matrix and inner membrane proteins are generated through cleavage of

the presequence by the mitochondrial processing peptidase (MPP) or the inner-membrane peptidase (Hawlitschek *et al.*, 1988; Mossmann *et al.*, 2012).

The mechanism by which pre-proteins destined for chloroplasts are imported from the cytosol into plastids is remarkably similar to that utilised during mitochondrial protein import. Pre-proteins are synthesised with an analogous N-terminal transit-peptide, targeting them for recognition by the translocon at the outer membrane of the chloroplast (TOC) complex (Bruce, 2001). The TOC complex is composed of Toc75, a 16-stranded β-barrel member of the Omp85 superfamily, and the integral GTP-binding receptors, Toc34 and Toc159, which form the core components required for protein import *in vitro* (Schleiff *et al.*, 2003; Richardson *et al.*, 2014). Additional components Toc64 and Toc12 are also associated with the core components. Toc34 and Toc159 recognise the transit-peptide of the pre-protein, which is subsequently translocated across the plastid outer envelope through Toc75. Translocation into the stroma is facilitated by the translocon at the inner membrane of the chloroplast (TIC) complex, composed of a multitude of protein subunits and associated chaperones (Nakai, 2015). Plastid protein import is energised exclusively through hydrolysis of ATP in the stroma (Theg *et al.*, 1989), unlike the analogous mitochondrial process, which also utilises the membrane potential to drive import. Once in the stroma, the transit-peptide is cleaved by stromal processing peptidase (Shi & Theg, 2013).

1.4. Energy Transduction Systems of Gram-negative Bacteria.

1.4.1. The proton-motive force (PMF).

The proton-motive force (PMF) is the primary method of energy production in Gram-negative bacteria. It is established through differences in chemical and electrical potential across the IM, generally through the accumulation of protons in the periplasm. This generates a proton gradient, which can be utilised to drive energy production and other energetic processes via proton translocation through specialised IM protein transporters into the cytoplasm. The PMF is maintained by the electron transport chain; a series of IM protein complexes containing transition metal redox cofactors that transfers electrons from an initial donor, primarily nicotinamide adenine dinucleotide (NADH), to a terminal electron acceptor. As electrons are shuttled through the electron transport chain, protons accumulate in the periplasm, generating a difference in both proton concentration and electrical potential across the IM (Anraku, 1988).

1.4.2. The Tol and Ton systems.

The primary method of ATP synthesis in Gram-negative bacteria is through the F_0F_1 ATP synthase. This rotary motor catalyses ATP formation in the cytoplasm by harnessing the PMF, coupling the energetically unfavourable ATP synthesis to translocation of protons down their concentration gradient into the cytoplasm. ATP can be subsequently utilised to drive active translocation processes, such as ABC transporter-dependent uptake of nutrients and Sec-mediated protein translocation across the IM. However, active uptake of substrates across the OM presents a significant challenge for Gram-negative bacteria due to absence of ATP or an electrochemical gradient in the periplasm. Therefore, Gram-negative bacteria have evolved trans-envelope complexes to transduce energy from the PMF to the OM. This process is primarily performed by the Tol-Pal and the Ton systems (Figure 1-4).

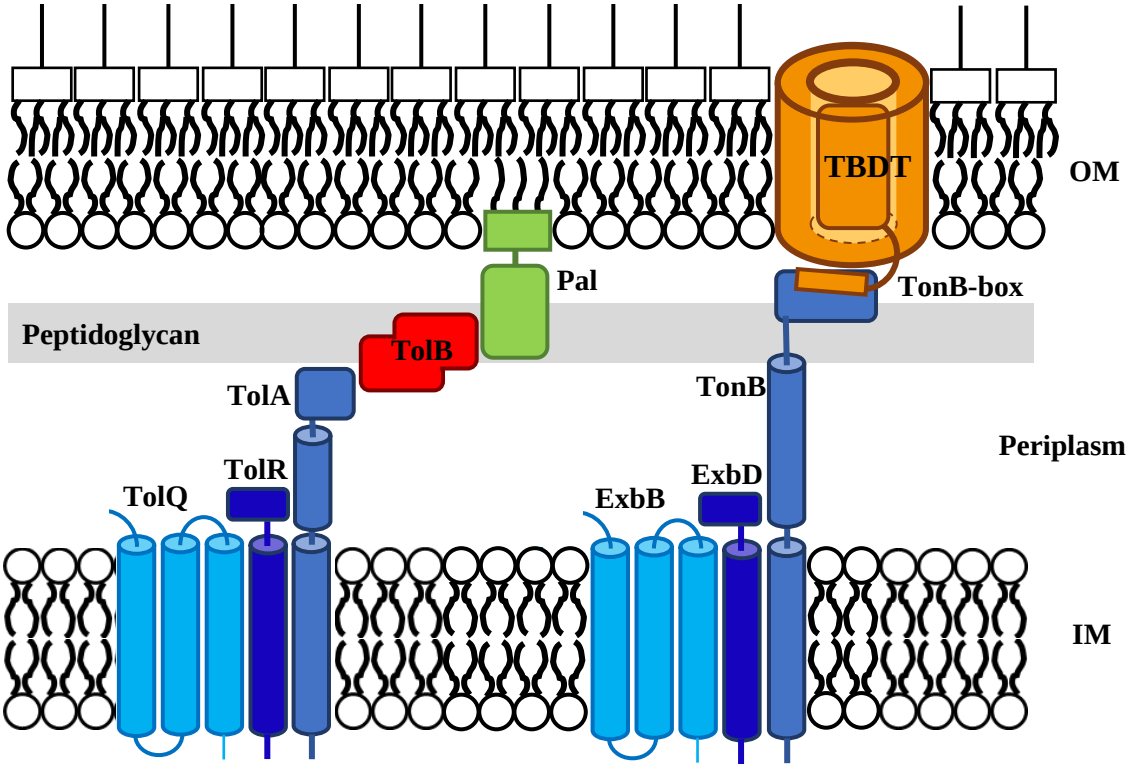

Figure 1-4. Schematic of the Tol and Ton Complexes.
The core Tol complex is composed of TolA, TolQ and TolR. The Tol complex couples the IM and OM through interactions between periplasmic TolB and both TolA and the OM lipoprotein Pal. The Ton complex consists of trans-periplasmic TonB bound to the TonB-box of a TBDT, ExbB and ExbD.

Tol-Pal and Ton are both multiprotein complexes comprised of three analogous IM proteins; TolA/TolQ/TolR for Tol and TonB/ExbB/ExbD for Ton. In addition to these, Tol-Pal also

contains a periplasmic protein, TolB and an OM lipoprotein, Pal. Both complexes contain a membrane protein with an extended periplasmic domain: TolA for Tol-Pal and TonB for Ton, which can interact with proteins at the OM (Levengood *et al.*, 1991; Roof *et al.*, 1991). TolB binds both TolA and Pal (Walburger *et al.*, 2002; Bonsor *et al.*, 2007), coupling signal transduction between the IM and OM. The Tol-Pal system has been demonstrated to be important for maintenance of OM membrane integrity (Cascales *et al.*, 2002), cell division (Szczepaniak *et al.*, 2020) and has been suggested to mediate lipid homeostasis in the OM (Shrivastava *et al.*, 2017). The Ton system is required for nutrient uptake through TBDTs across the OM (Noinaj *et al.*, 2010). Both TolQ/ExbB and TolR/ExbD share sequence homology with proteins of the bacterial stator complex, MotA and MotB, respectively (Cascales *et al.*, 2001). The MotAB stator complex utilises the PMF to drive rotary motion of the bacterial flagellum (Manson *et al.*, 1977). Both the Tol-Pal and Ton systems are hijacked by certain bacteriophages and bacteriocins in order to cross the OM (Cascales *et al.*, 2007).

The TonB and ExbD components of the Ton complex have a similar topology, composed of a short N-terminal domain, followed by a single pass transmembrane α-helix, a flexible linker region, and a C-terminal periplasmic domain. The precise structure that the C-terminal domain of TonB adopts is disputed, with both monomeric and dimeric forms reported (Chang *et al.*, 2001; Sean Peacock *et al.*, 2005). A common three-stranded antiparallel β-sheet structure with $\beta_1\beta_2\alpha_1\beta_3$ topology is shared by both structures; however, additional short α-helix and β-strand motifs are found at the N- and C-termini respectively in the NMR monomer structure (Figure 1-5).

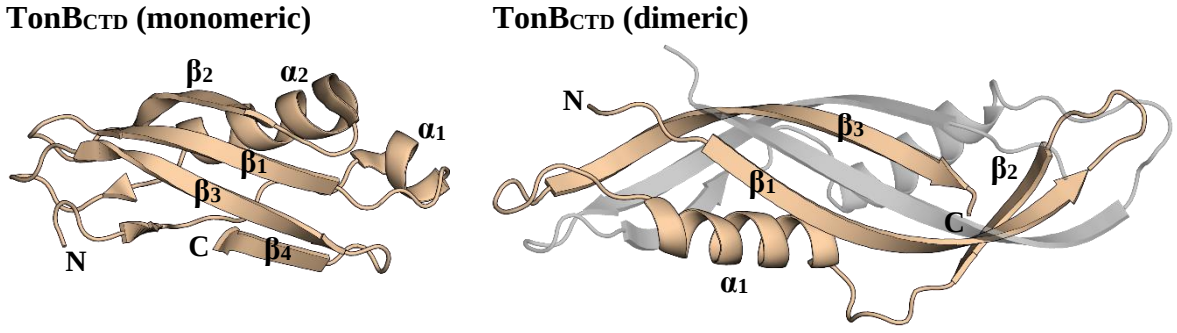

Figure 1-5 Structures of the C-terminal domain of TonB.
Structures of monomeric $TonB_{CTD}$ (residues 103 – 239) (PDB ID = 1XX3 (Sean Peacock *et al.*, 2005)) solved by NMR (*left*) and dimeric $TonB_{CTD}$ (residues 155 – 239) (PDB ID = 1IHR (Chang *et al.*, 2001)) solved by X-ray crystallography (*right*) illustrate two contrasting structures. Structural studies demonstrate that the C-terminal domain of TonB binds TBDTs as a monomer via displacement of the β_4 strand, suggesting this is the likely conformation adopted by the domain *in vivo*.

This additional β-strand (β_4) interacts with β_3 to form a four-stranded antiparallel β-sheet with $\alpha_1\beta_1\beta_2\alpha_2\beta_3\beta_4$ topology, whereas it mediates dimerization in the crystal structures of the TonB C-terminal domain. The C-terminal domain of TonB binds to TBDTs as a monomer, and as such is the likely conformation adopted *in vivo*, through a short, conserved motif within their N-terminus, called the TonB-box. Structures of TonB bound to TBDTs FhuA, BtuB and FoxA demonstrate β-augmentation through the formation of a parallel β-strand interaction between the TonB-box and β_3 of TonB (Figure 1-6) (Pawelek *et al.*, 2006; Shultis *et al.*, 2006; Josts *et al.*, 2019), displacing the β_4 strand, which becomes disordered.

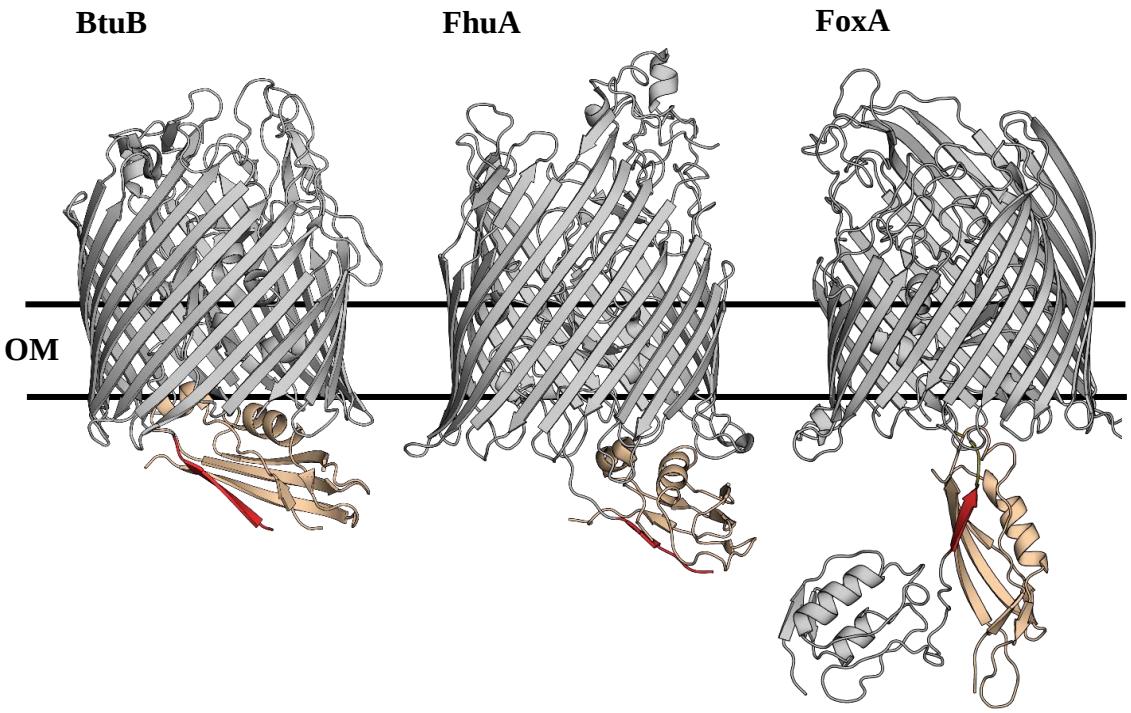

Figure 1-6 Structures of TBDTs in complex with TonB/TonB1.
Crystal structures of BtuB (PDB ID = 2GSK (Shultis *et al.*, 2006)) and FhuA (PDB = 2GRX (Pawelek *et al.*, 2006)) from *E. coli* in complex with the C-terminal domain of TonB (*beige*). The TonB-box (red) complements the TonB β-sandwich fold, contributing a fourth β-strand. The crystal structure of FoxA (PDB ID = 6I97 (Josts *et al.*, 2019)) from *P. aeruginosa* in complex with the C-terminal domain of TonB1 displays a radically different binding orientation to the previous two structures. The TonB1-box (*red*) also contributes a fourth β-strand to TonB1, however residues upstream of the TonB1-box (residues 135-141) form additional interactions with the TonB1 C-terminal domain.

In the *P. aeruginosa* genome, three genes homologous to *tonB* from *E. coli* have been identified, termed *tonB1* (PA5531), *tonB2* (PA0197) and *tonB3* (PA0406). TonB1 is required for siderophore- and heme-mediated iron uptake, with loss of this gene restricting growth in iron-limited media (Takase *et al.*, 2000). TonB2 can partially complement loss of

TonB1, though deletion of TonB2 alone has no adverse effect on iron/heme uptake (Zhao & Poole, 2000). TonB3 is involved in *P. aeruginosa* motility and is required for polar localisation of the flagellum, in addition to formation and localisation of pili. Loss of TonB3 results in swimming and twitching motility defects (Huang *et al.*, 2004; Cowles *et al.*, 2013). Of the three TonB homologous present in *P. aeruginosa*, TonB1 is the most similar to that of TonB found in *E. coli* (Oeemig *et al.*, 2018).

ExbB constitutes the bulk of the IM spanning portion of the Ton complex, comprising seven α-helices of varying lengths, and passing through the IM three times (Hervé Celia *et al.*, 2016). The exact stoichiometry of ExbB within the Ton complex is disputed, with structures of both pentameric and hexameric forms of the ExbB-ExbD subcomplex solved (Hervé Celia *et al.*, 2016; Maki-Yonekura *et al.*, 2018). In both forms, a large central pore is formed by the ExbB monomers. Additional density is observed within the pore, which is thought to correspond to the TM domain of ExbD (Hervé Celia *et al.*, 2016). ExbD is thought to form a dimer within the Ton complex, though the exact number of ExbD subunits within the pore, in addition to how they are accommodated within the overall ExbB architecture, remains contentious (Maki-Yonekura *et al.*, 2018; Herve Celia *et al.*, 2019). However, recent cryo-EM structures of the ExbB-ExbD subcomplex revealed an asymmetric 5:2 stoichiometry, with the TM domains of both ExbD monomers accommodated within the central pore formed by the ExbB pentamer (Figure 1-7) (Herve Celia *et al.*, 2019; Deme *et al.*, 2020).

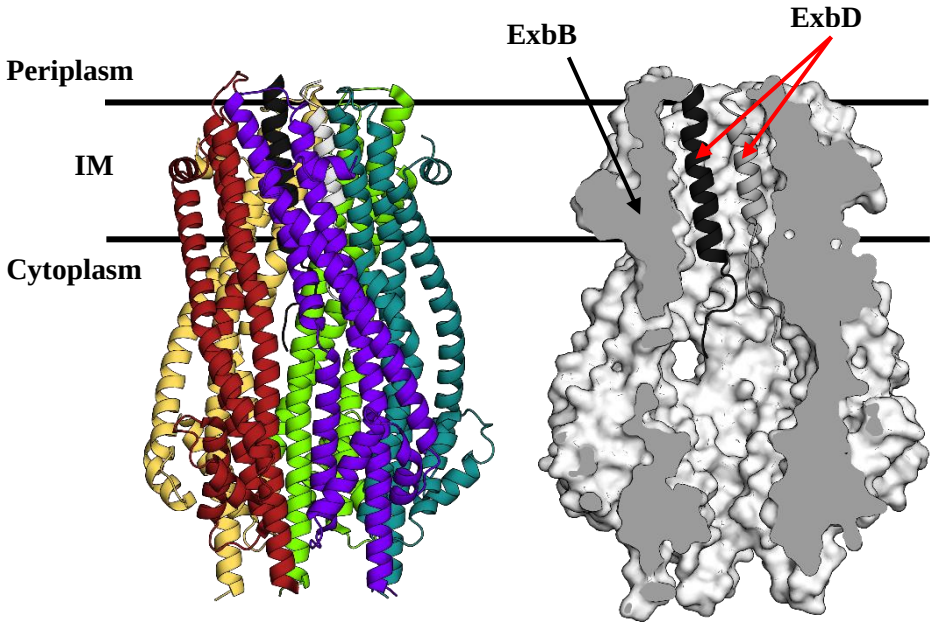

Figure 1-7 Structure of the ExbB-ExbD subcomplex.
Cryo-EM structure of the ExbB-ExbD subcomplex (PDB ID = 6TYI (Herve Celia *et al.*, 2019)) The ExbB-ExbD subcomplex is found to be asymmetric, with a stoichiometry of five ExbB subunits (*red*, *yellow*, *green*, *teal* and *purple*) forming a central pore in which two ExbD subunits (*black* and *dark grey*) are accommodated.

This structural organisation is conserved across other ion-driven force transducing complexes, such as the MotAB stator complex and GldL-GldM gliding motility complex, suggesting a conserved architecture for the generation of mechanical torque through ion flow within bacterial systems (Deme *et al.*, 2020). TonB is thought to reside outside the channel formed by ExbB-ExbD; interacting with ExbB through its transmembrane domain (Larsen *et al.*, 1994; Larsen & Postle, 2001).

The precise mechanism by which the Ton complex transduces conformational changes in TBDTs is currently unknown. It is accepted that through utilising the PMF, TonB exerts "force" via pulling or rotary movement to the TonB-box of an active TBDT (Klebba, 2016; Hickman *et al.*, 2017). This induces conformational change within the TBDT, which is coupled to the subsequent transport of the substrate.

1.5. Transition Metal Acquisition.

Metal ions are essential for a diverse range of biological processes and are a fundamental requirement for all living organisms. Of particular importance are transition metal ions, which can assume multiple discrete oxidation states due to their partially filled *d*-orbitals. As such, they are often employed for the catalysis of enzymatic reactions in the form of essential metal cofactors. Additionally, transition metal ions are integral for macromolecular structure assembly and ligand binding through the formation of elaborate coordination complexes. These essential nutrients are present at low concentrations in the extracellular environment, therefore Gram-negative bacteria have developed a diverse range of mechanisms for active uptake of these metal ions across their cellular envelope. This has resulted in an evolutionary arms race between Gram-negative pathogens and their host organism for control of these essential nutrients (Weinberg, 2009; Kehl-Fie & Skaar, 2010). Expression of proteins required for transition metal uptake are often upregulated during bacterial pathogenesis, functioning as virulence factors (Konings *et al.*, 2013). The metallome of *P. aeruginosa* demonstrates active accumulation of transition metals ions in the cytoplasm that is several orders of magnitude greater than that of the extracellular environment (Cunrath *et al.*, 2016). The two most prevalent transition metals accumulated by *P. aeruginosa* are iron and zinc.

1.5.1. Iron acquisition and metabolism in *P. aeruginosa*.

Iron is the most abundant transition metal ion found in *P. aeruginosa* (Cunrath *et al.*, 2016). It is required for several important biological processes including cellular respiration,

nucleotide synthesis, and DNA replication, transcription and repair (Verkhovtseva *et al.*, 2001). This is due to its characteristic redox activity, with several available oxidation states utilised in biological processes, primarily ferric (Fe^{3+}) and ferrous (Fe^{2+}) iron. Despite its essential role, iron paradoxically has poor bioavailability in the environment due to the low solubility of Fe^{3+} under aerobic conditions. Therefore, all organisms have developed strategies to manage this physiological obstacle. In humans, ferric iron is solubilised and sequestered by the iron binding proteins transferrin and lactoferrin (Skaar, 2010). This immobilisation of free iron poses a significant challenge for pathogenic bacteria, which also require iron for their own cellular processes. As a result, *P. aeruginosa* has developed an impressive array of iron scavenging and uptake mechanisms (Figure 1-8), which are appropriately upregulated during chronic infections (Konings *et al.*, 2013).

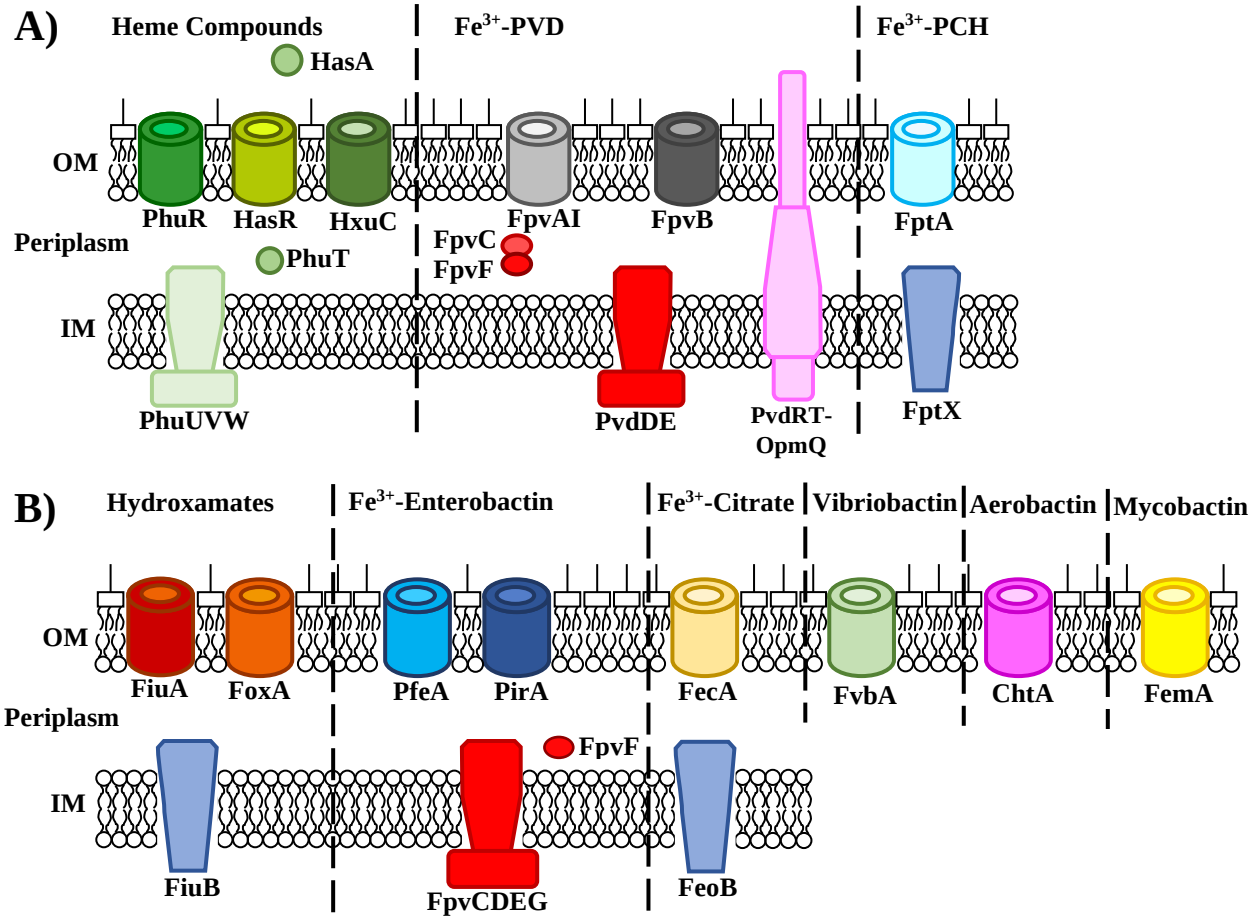

Figure 1-8. Schematic of iron import systems of *P. aeruginosa*.
Proteins of the OM and IM utilised to transport iron across the cell envelope of *P. aeruginosa* strain PAO1. A) Systems involved in the import of endosiderophores and heme-compounds. B) Systems involved in the import of xenosiderophores synthesised by other bacterial species. Adapted from Schalk & Cunrath, 2016.

P. aeruginosa utilises small cyclic peptides called siderophores that bind to iron with high affinity, outcompeting host proteins. The primary siderophore utilised by *P. aeruginosa* strain PAO1 is the fluorescent siderophore type I pyoverdine (PVD). Uptake of this PVD requires the OM protein, type I ferripyoverdine receptor, FpvAI. FpvAI is the best characterised PVD uptake transporter, though others do exist, such as FpvAII, FpvAIII and FpvB (de Chial *et al.*, 2003; Ghysels *et al.*, 2004). FpvAII and FpvAIII are required for uptake of type II and type III PVDs respectively, whereas FpvB is an alternate type I PVD transporter. Additionally, *P. aeruginosa* expresses other TBDTs for iron acquisition, primarily for uptake of xenosiderophores produced by other bacterial species and heme (Figure 1-8).

1.5.2. FpvAI.

FpvAI is a 90 kDa 22-stranded β-barrel TBDT that spans the OM of *P. aeruginosa* PAO1 (Poole *et al.*, 1993). Its biological function is the active uptake of iron in the form of a chelate with the siderophore PVD, a 1.3 kDa mixed hydroxamate-catecholate siderophore with a conserved dihydroxyquinoline chromophore linked to a cyclised peptide of variable length (Visca *et al.*, 2007). The PVD catecholate and hydroxamate groups bind Fe^{3+} with high affinity, with K_a of 10^{32} M^{-1} (Albrecht-Gary *et al.*, 1994). The Fe^{3+}-PVD complex is able to bind to FpvAI with a K_d of 0.5 – 1.5 nM, with subsequent import across the OM utilising energy provided by the TonB1 complex (Schalk *et al.*, 2001; Clément *et al.*, 2004; Hoegy *et al.*, 2005). The structures of FpvAI in complex with Fe^{3+}-PVD and apo-FpvAI, in addition to FpvAI in complex with non-cognate PVDs, have been solved previously (Figure 1-9) (Cobessi *et al.*, 2005; Brillet *et al.*, 2007; Greenwald *et al.*, 2009). FpvAI binds Fe^{3+}-PVD in a siderophore binding pocket located at the top of the β-barrel on the extracellular side of the OM. This binding site is buried within the extracellular loops of FpvAI, with the ligand forming contacts to the plug domain.

It has been proposed that upon binding Fe^{3+}-PVD, conformational changes within the plug domain activate the receptor through exposure of the TonB1-box (Greenwald *et al.*, 2009). This facilitates interactions with the TonB1 complex, energising translocation through coupling to the cellular PMF (Adams *et al.*, 2006; Brillet *et al.*, 2007). The precise mechanism by which FpvAI translocates Fe^{3+}-PVD across the OM has not been fully elucidated. Upon reaching the periplasm, the PVD bound Fe^{3+} is reduced to Fe^{2+}, dissociating it from the siderophore (Greenwald *et al.*, 2007). Fe^{2+} is subsequently bound by

proteins within the periplasm for transport across the IM by the FpvCDEF transporter (Brillet *et al.*, 2012; Bonneau *et al.*, 2020). Unmodified PVD is recycled by the PvdRT-OmpQ system for further iron acquisition from the extracellular environment (Imperi *et al.*, 2009).

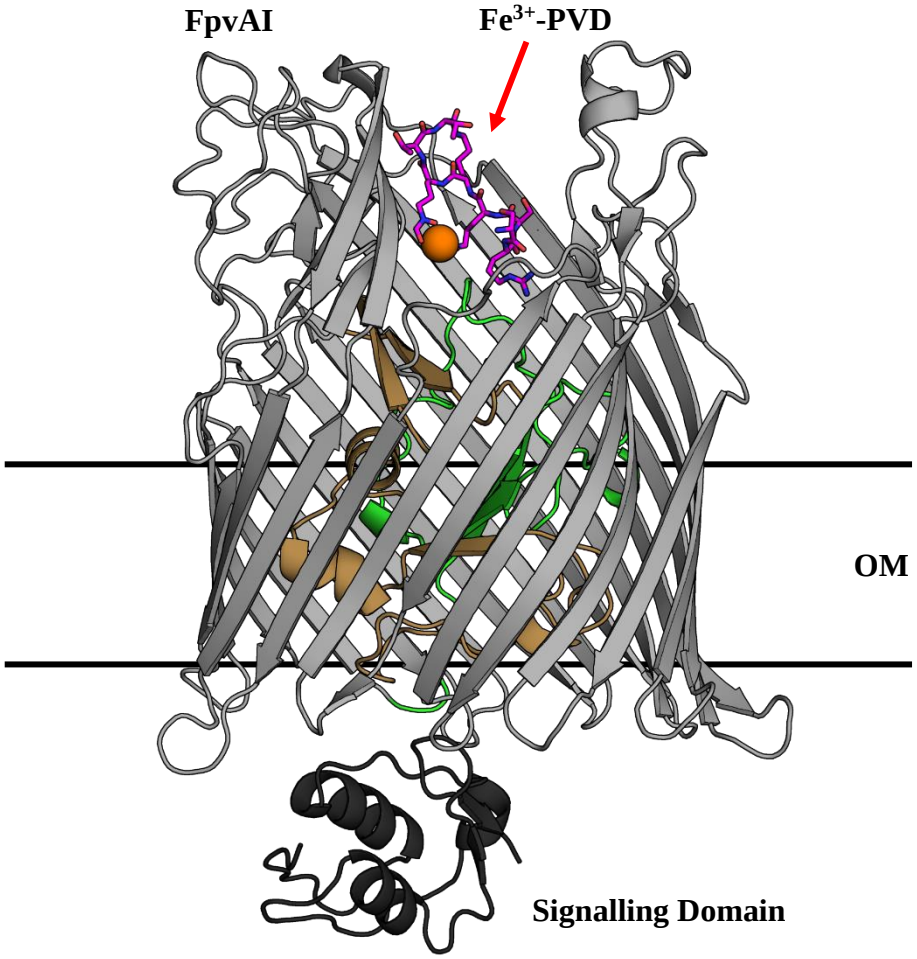

Figure 1-9. Crystal structure of FpvAI in complex with Fe^{3+}-PVD.
Crystal structure of FpvAI (*grey*) bound to Fe^{3+}-PVD (*magenta*). The FpvAI plug domain occludes the β-barrel domain and is predicted to contain two mechanically distinct subdomains; termed force labile (*brown*) and force non-labile (*green*) which are highlighted. A linker region between the signalling (*black*) and plug domains, containing the TonB-box, is absent from this structure (PDB ID = 2W16 (Greenwald *et al.*, 2009)).

In addition to its role in iron uptake, FpvAI is also involved in the regulation of expression of the *fpvA* gene, as well as genes required for PVD synthesis, through an N-terminal extension known as the signalling domain (Shen *et al.*, 2002). In iron-rich environments, FpvAI expression and PVD synthesis are downregulated in a process mediated by a homologue of the *E.coli* ferric utilisation regulator (Fur) (Poole & McKay, 2003; Fillat, 2014). In the absence of Fe^{3+}-PVD, the extracytoplasmic-function (ECF) sigma factors FpvI

and PvdS are bound by the anti-sigma factor FpvR in the IM. Upon activation by Fe^{3+}-PVD, the FpvAI signalling domain contacts FpvR, triggering TonB-dependent proteolysis. This releases FpvI and PvdS to activate transcription of *fpvA* and genes associated with PVD synthesis, respectively (Rédly & Poole, 2005). Fe^{3+}-PVD associated signalling also triggers the upregulation of two genes associated with *P. aeruginosa* virulence, *prpL* encoding an extracellular protease and *exoA* encoding the potent exotoxin A (ETA) (Ochsner *et al.*, 1996; Wilderman *et al.*, 2001).

1.5.3. Zinc acquisition and metabolism in *P. aeruginosa*.

Zinc is the second most abundant transition metal found in *P. aeruginosa*. It is essential for many fundamental bacterial processes, with approximately 6% of prokaryotic proteins predicted to bind Zn (Andreini *et al.*, 2006). Zinc can only adopt a single oxidation state (Zn^{2+}) due to its fully occupied *d*-orbitals and thus is not redox active. However, it still participates in many enzymatic reactions as a soft Lewis acid, or functions as a macromolecular structural cofactor. Like iron, accessibility of free zinc during bacterial pathogenesis is similarly restricted by the host organism through the action of the metal binding proteins calprotectin and psoriasin (Gläser *et al.*, 2005; Corbin *et al.*, 2008). The role of zinc in *P. aeruginosa* pathogenesis is an area of emerging study, with upregulation of virulence factors required for zinc uptake identified during *P. aeruginosa* colonisation in chronic lung infections (Gi *et al.*, 2015; Mastropasqua *et al.*, 2018).

Like many other bacterial species, the primary *P. aeruginosa* Zn^{2+} uptake pathway across the IM is through the ZnuABC transporter (Ellison *et al.*, 2013; Pederick *et al.*, 2015). As a member of the ABC transporter family, ZnuABC is comprised of three proteins; a periplasmic protein that binds Zn^{2+} (ZnuA), an IM permease (ZnuB) and an ATPase (ZnuC) organised in the IM with a complex stoichiometry of $ZnuAB_2C_2$ (Patzer & Hantke, 1998). ZnuA contains two Zn^{2+} binding sites; a high affinity site with a K_d of 22.6 ± 6.4 nM, and a second lower affinity site (~µM range), which likely facilitates relay of Zn^{2+} ions to the adjacent high affinity site (Pederick *et al.*, 2015). *znuB* and *znuC* form a polycistronic operon with an additional upstream gene that encodes for a homologue of the Fur repressor, the zinc utilisation regulator (*zur*). Zur has been demonstrated to function as a zinc-responsive transcriptional repressor; binding to both *znuA* and the *zur-znuBC* operon to repress transcription in zinc-rich conditions (Ellison *et al.*, 2013). Transcriptional analysis of *P. aeruginosa znuA* mutants show up-regulation of the transcription of PA2435, a P-type

ATPase which is predicted to mediate Zn^{2+} uptake (Lewinson *et al.*, 2009), in addition to two putative ABC transporters: PA2912–2914 and PA4063–4066. These ABC transporters contain Zur-binding sites within their promoter regions, strongly suggesting that these gene clusters are also involved in zinc acquisition (Pederick *et al.*, 2015). Therefore, it is likely that *P. aeruginosa* possesses multiple degenerate pathways for zinc import, underlining its metabolic importance.

In contrast, significantly less is known concerning zinc uptake across the OM of *P. aeruginosa*. Transcriptomic analyses have demonstrated that in conditions of Zn^{2+} limitation, the transcription of four genes encoding putative TBDTs are up-regulated (PA0781, PA1922, PA2911 and PA4837) (Pederick *et al.*, 2015). PA0781 shares 27% sequence identity with a TBDT required for zinc uptake from *Neisseria meningitides*, ZnuD (Calmettes *et al.*, 2015). ZnuD is organised and expressed with the ZnuABC transporter gene cluster in *N. meningitides*, suggesting PA0781 may also encode for a ZnuD homologue required for zinc uptake across the OM. Similarly, PA2911 is organised with the PA2912–2914 ABC transporter gene cluster, implying a TBDT (PA2911) and an ABC transporter for zinc uptake across the OM and IM respectively.

The best studied of these specific TBDTs is PA4837 that encodes for CntO; a TBDT required for uptake of the broad spectrum metallophore pseudopaline (Gi *et al.*, 2015; Mastropasqua *et al.*, 2017; Lhospice *et al.*, 2017). Pseudopaline is a nicotianamine-like metallophore and member of the same opine-type metallophore family as staphylopine and yersinopine, synthesised by *S. aureus* and *Y. pestis* respectively (Ghssein *et al.*, 2016; Laffont *et al.*, 2019). It has broad specificity for divalent transition metal ions, however its primary role in zinc uptake is inferred from negative regulation of the *cnt* operon expression by Zur in zinc-rich conditions (Pederick *et al.*, 2015; Lhospice *et al.*, 2017).

The *cnt* operon of *P. aeruginosa* contains four polycistronic genes with partial sequence homology to the *cnt* operon from *S. aureus* (Figure 1-10). This is restricted to the second and third genes that comprise the operon, *cntL* and *cntM*, which encode for two cytoplasmic enzymes that are responsible for the two-step synthesis of pseudopaline (Lhospice *et al.*, 2017). Initially, CntL catalyses the formation of the reaction intermediate yNA from substrates S-adenosine methionine (SAM) and L-histidine, which is followed by an NADH reductive condensation of the yNA with a molecule of α-ketoglutarate (αKG), catalysed by CntM, to produce mature pseudopaline (McFarlane & Lamb, 2017; Lhospice *et al.*, 2017).

The *cnt* operon of *P. aeruginosa* encodes an addition pair of genes located upstream and downstream of *cntL* and *cntM* biosynthetic genes; *cntO* and *cntI*. The first gene, *cntO*, encodes for the OM TBDT CntO and is required for import of pseudopaline across the OM (Mastropasqua *et al.*, 2017; Lhospice *et al.*, 2017). The fourth gene *cntI*, encodes the IM protein CntI; a member of the EamA or drug/metabolite transporter (DMT) family, which is required for secretion of pseudopaline into the periplasm after biosynthesis (Lhospice *et al.*, 2017). Pseudopaline has been shown to secreted across the OM through the multidrug efflux pump MexAB-OprM (Gomez *et al.*, 2021).

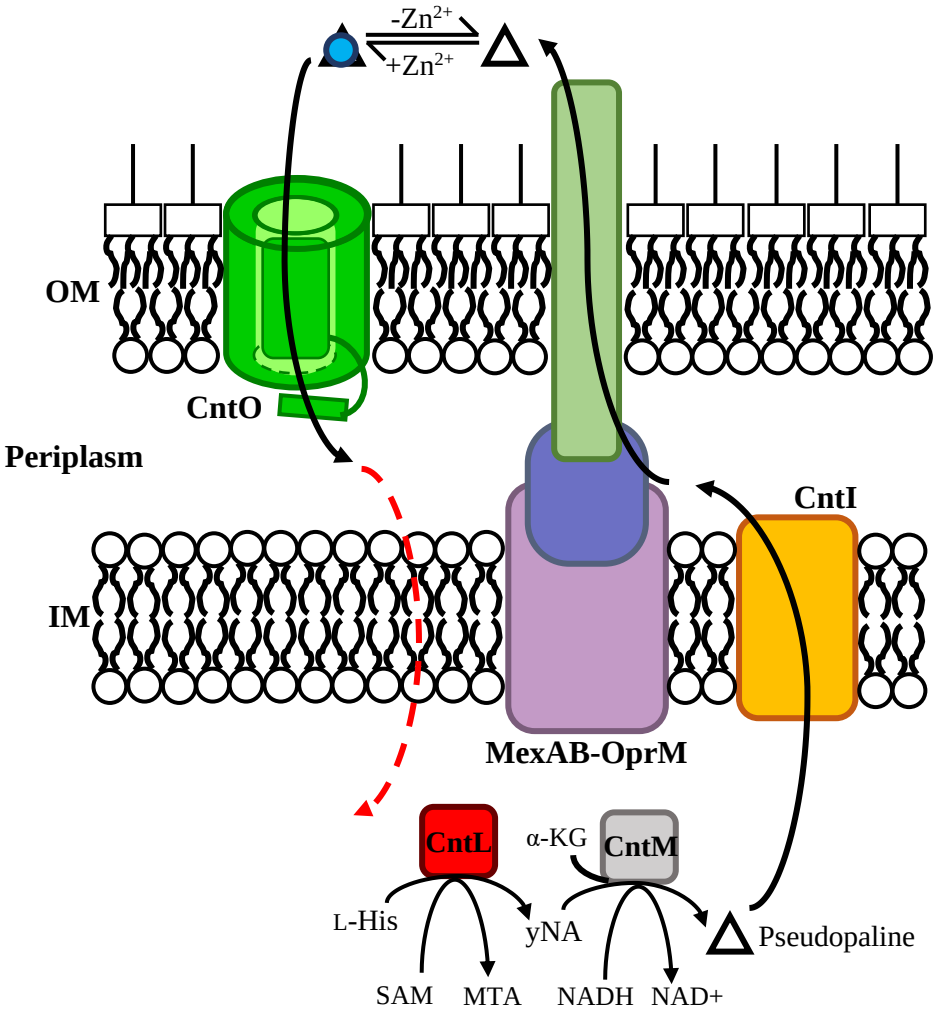

Figure 1-10. Model of pseudopaline synthesis, secretion and import in *P. aeruginosa*. Pseudopaline is synthesised in the cytoplasm by CntL and CntM from L-Histidine (L-His) and α-ketoglutarate (α-KG) using the cofactors SAM and NADH. Pseudopaline (*triangle*) uptake with a divalent metal ion (*blue circle*) across the OM requires CntO. Once in the periplasm, metal ions are released from pseudopaline and imported across the IM by an unknown mechanism. Adapted from Gomez *et al.*, 2021.

Both CntO and CntI have been shown to be essential for *P. aeruginosa* growth in Airway Mucus Secretion (AMS) and for pathogenesis during murine lung infections (Gi *et al.*, 2015; Mastropasqua *et al.*, 2017). Additionally, several transcriptomic analyses show that genes from the *cnt* operon are consistently upregulated during *P. aeruginosa* lung infections (Palmer *et al.*, 2005; Son *et al.*, 2007). Polymorphisms within the *cnt* promotor sequence have been described during establishment of chronic infections, resulting in less stringent repression of the operon by Zur (Hermansen *et al.*, 2018). This suggests that the involvement of the proteins encoded by the *cnt* operon in zinc uptake in zinc-restricted environments is crucial for *P. aeruginosa* survival during lung infections of cystic fibrosis patients.

1.6. Interbacterial Competition Systems.

Bacterial cells are often regarded as autonomous entities that exist in isolation from one another, yet they typically reside in dense, multispecies communities and exhibit a number of cooperative and competitive behaviours. Due to the crowded environment that most bacterial species thrive in, they are often in perpetual competition with one another for the limited space and resources that are required for successful survival and multiplication. This has resulted in an evolutionary arms race in the generation of chemical, mechanical, and biological weapons to eliminate competitors through growth inhibition or cytotoxic activity. Mechanisms of inter-bacterial warfare can be restricted to single cells, such as contact-dependent inhibition or T6SS, or a more general response, through the release of diffusible antimicrobial agents such as microcins and bacteriocins.

1.6.1. Contact-Dependent Inhibition (CDIs).

CDIs are found across many bacterial species. They are a member of the T5SS family, comprising a two-partner secretion system composed of a CdiA toxin and a CdiB transporter. CdiB is a 16-stranded β-barrel OM protein and a membrane of the Omp85 superfamily that facilitates secretion of CdiA from the periplasm onto the bacterial surface (Aoki *et al.*, 2005). CdiA is predicted to form a large elongated β-helical filament that extends several hundred angstroms from the CdiB transporter. This secreted extension is thought to consist of the N-terminal portion of CdiA, which contains a receptor binding domain at its tip that recognises specific OM receptors, such as BamA, on the surface of target cells (Aoki *et al.*, 2008; Ruhe *et al.*, 2018). Receptor binding is thought to trigger a second secretion step, whereby the CdiA C-terminal portion, which was previously localised

in the periplasm, is released and exported to the target cell surface for delivery of a C-terminal toxin domain (Ruhe et al., 2017, 2018). The CdiA toxin domain is cleaved by an unknown mechanism and imported into the cell, independent of its OM receptor, Tol and Ton, and instead through binding to the F-type pilus, which is subsequently internalised (Beck *et al.*, 2014). Growth inhibition or cytotoxicity is elicited by the CdiA effector domain through nuclease, adenosine deaminase, ADP-ribosyl cyclase, metallopeptidase and pore-forming activities (Ruhe *et al.*, 2013).

1.6.2. Bacteriocins.

Bacteriocins are a diverse group of diffusible proteinaceous antimicrobial agents synthesised by bacterial species in order to target and inhibit the growth of competing cells, usually from the same or related species (Cascales *et al.*, 2007). One subset of the bacteriocin family, which have attracted significant interest for therapeutic potential, are the colicin-like bacteriocins (CLBs). CLBs are protein bacteriocins synthesised exclusively by γ-proteobacteria, specifically the *Enterobacteriaceae* and *Pseudomonadaceae* families (Sharp *et al.*, 2017). These large antimicrobial agents are typically produced in response to stress via the SOS pathway, and are subsequently released into the extracellular medium, sometimes via co-expression of a lysis protein (Papadakos *et al.*, 2012). They possess extremely potent bactericidal activity, in addition to their species-specific antagonism, which could potentially enable targeted elimination of pathogenic bacterial species without adverse effects on the host microbiome (Behrens *et al.*, 2017). Indeed, several CLBs have been shown to be active *in vivo* in murine lung infection models (McCaughey, Ritchie, *et al., 2016).*

CLBs have modular structure, consisting of N-terminal and middle domains that parasitize proteins within the bacterial cellular envelope to deliver their cytotoxic C-terminal domain into target cells. Cytotoxicity is elicited through depolarization of the cell by insertion of a pore, or enzymatic cleavage of peptidoglycan precursors or nucleic acids (Volkmar Braun *et al.*, 2002). Nuclease-type CLBs possess C-terminal cytotoxic domains that specifically target DNA, rRNA or tRNA to induce killing.

The majority of nuclease-type CLBs that exhibit DNase activity utilise a HNH-nuclease domain. Members of this protein superfamily are present across all domains of life, and include Type II endonucleases, homing endonucleases, mismatch repair enzymes and the CRISPR/Cas-9 bacterial antiviral defense system (Saravanan *et al.*, 2004; Shen *et al.*, 2004;

Wu *et al.*, 2009; Gasiunas *et al.*, 2012). Despite sharing limited sequence homology, all HNH-nucleases adopt a structurally similar ββα topology, which contains the enzymatic catalytic core (Figure 1-11). The nuclease-type CLB catalytic core comprises a ~30 amino acid motif ($HHX_{14}NX_8HX_3H$) that specifically coordinates a single divalent metal ion, primarily Mg^{2+} or Ni^{2+}, which is required for DNase activity (Pommer *et al.*, 2001; Joshi *et al.*, 2015). The HNH motif binds within the minor groove of DNA, distorting the DNA backbone and positioning a scissile phosphodiester bond in close proximity to the divalent metal cation (Figure 1-11). Nucleophilic attack on the scissile phosphate results in cleavage of the P-O3′ phosphodiester bond, nicking the DNA strand (Hsia *et al.*, 2004). It remains unclear how DNA nicking ultimately translates to cell death, as bacteria possess robust DNA repair mechanisms, induced by the SOS response (Walker *et al.*, 2004). However, it is possible that HNH-DNase mediated nicking overwhelms these repair mechanisms, or generates random lethal double stranded DNA breaks. Though most CLB DNase domains possess HNH motifs, several non-HNH DNase CLBs have recently been identified (Duport *et al.*, 1995; Sharp *et al.*, 2017; Atanaskovic *et al.*, 2020); however their mechanisms of DNA cleavage are currently unknown.

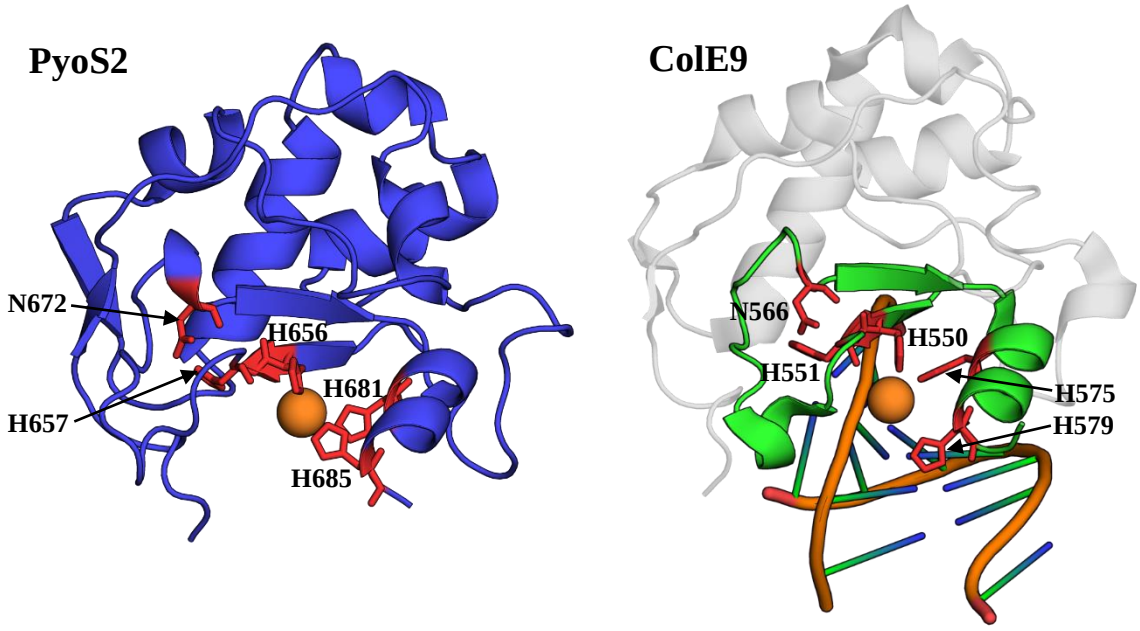

Figure 1-11. Crystal structures of CLB HNH-DNase domains.
Cartoon structures of HNH-DNase domains from pyocin S2 (*blue*) and colicin E9 (*grey*). The colicin E9 DNase is in complex with double stranded DNA, with the ββα HNH-motif highlighted (*green*). Residues that comprise the HNH-motif active sites are also highlighted (*red*), including three histidine residues that coordinate an Mg^{2+} ion (*orange sphere*) in both structures. The RMSD between the two CLB nuclease domains is 1.44 Å. PyoS2 (residues 556 – 686) DNase PDB ID = 4QKO (Joshi *et al.*, 2015). ColE9 (residues 450 – 582) DNase-dsDNA complex PDB ID = 1V14 (Maté & Kleanthous, 2004).

Nuclease-type CLBs that exhibit RNases activity can be classified based on their specific RNA targets. Ribosomal RNases (rRNases), such as colicin E3 (ColE3), cleave the 16S rRNA at the A-site of the ribosome (Bowman *et al.*, 1971), decreasing the stability of codon-recognition complexes during polypeptide elongation and greatly increasing the rate of tRNA rejection (Ng *et al.*, 2010). This reduction in the rate of initiation and elongation causes the build-up of short, truncated peptides, resulting in cell death. Transfer RNases (tRNases) cleave a single phosphodiester bond in specific tRNAs to prevent protein synthesis, resulting in cell death. The colicin E5-like tRNases cleave the anticodon triplet of $tRNA^{Tyr}$, $tRNA^{His}$, $tRNA^{Asn}$ and $tRNA^{Asp}$ (Ogawa *et al.*, 1999), whereas the colicin D-like tRNases cleave the anticodon loop in three of the four $tRNAs^{Arg}$ (Tomita *et al.*, 2000).

To elicit cytotoxic activity, CLBs must deliver their cytotoxic C-terminal domain across the cellular envelope. The best studied CLBs are colicins; toxins synthesized by and specific for, *E. coli*. Colicins exploit a wide variety of cell envelope proteins in order to deliver their cytotoxic domain to its site of action, as described in **Table 1-2** (Kleanthous, 2010).

Table 1-2. Mechanisms of colicin import and cytotoxicity.
Compiled using Cascales *et al.*, 2007 unless noted otherwise. References for subsequent findings shown below.

Colicin	OM Receptor	Translocator	OM Translocation Energisation	Cytotoxic Activity
ColA[1]	BtuB	OmpF	Tol	Pore-Forming
ColB	FepA		Ton	Pore-Forming
ColD	FepA		Ton	tRNase
ColE1	BtuB	TolC	Tol	Pore-Forming
ColE2, E7, E8, E9	BtuB	OmpF	Tol	DNase
ColE3, E4, E6	BtuB	OmpF	Tol	rRNase
ColE5	BtuB	OmpF	Tol	tRNase
ColIa, Ib	Cir	Cir[3]	Ton	Pore-Forming
ColK	Tsx	OmpF, OmpA	Tol	Pore-Forming
ColM	FhuA		Ton	Lipid II-Hydrolysis
ColN	OmpF[4]		Tol	Pore-Forming
ColR	OmpA[5]	N.D.	Tol[4]	Pore-Forming[5]
ColS4	OmpW[6]	OmpF[6]	Tol[5]	Pore-Forming[6]
ColU[2]	OmpA	OmpF	Tol	Pore-Forming
ColY	OmpA[7]	N.D.	Tol[7]	Pore-Forming[7]
ColZ	N.D.	N.D.	N.D.	Lipid II-Hydrolysis[8]
Col5, Col10	Tsx	TolC	Ton	Pore-Forming

N.D. indicates not determined. [1] and [2] were isolated from *Citrobacter freundii* and *Shigella boydii* respectively. [3](Jakes & Finkelstein, 2010), [4](Jansen *et al.*, 2020), [5](Rendueles *et al.*, 2014), [6](Arnold *et al.*, 2009), [7](Bosák *et al.*, 2016), [8](Micenková *et al.*, 2019).

Colicins generally contain two distinct domains involved in uptake across the OM – a receptor binding domain and a translocation domain (Cascales *et al.*, 2007). These are primarily organised with the translocation domain at the N-terminus, followed by the receptor binding domain. Whilst this is considered to be the typical domain organisation for colicins, atypical assemblies including domain duplications (Arnold *et al.*, 2009) and merged receptor/translocation domains do exist (Devanathan & Postle, 2007). Information concerning the structure of these domains is available for several colicins in the form of full-length colicin structures, individual domains and/or colicin-receptor complexes.

The earliest full-length colicin structure solved was colicin Ia (ColIa), published in 1997 (Wiener *et al.*, 1997). ColIa was found to adopt a highly elongated structure composed predominantly of α-helices, including two exceptionally long (~160 Å) helices (Figure 1-12). A TonB-box motif is located at the N-terminus of the structure, which is required for energisation of uptake across the OM (Schramm *et al.*, 1987).

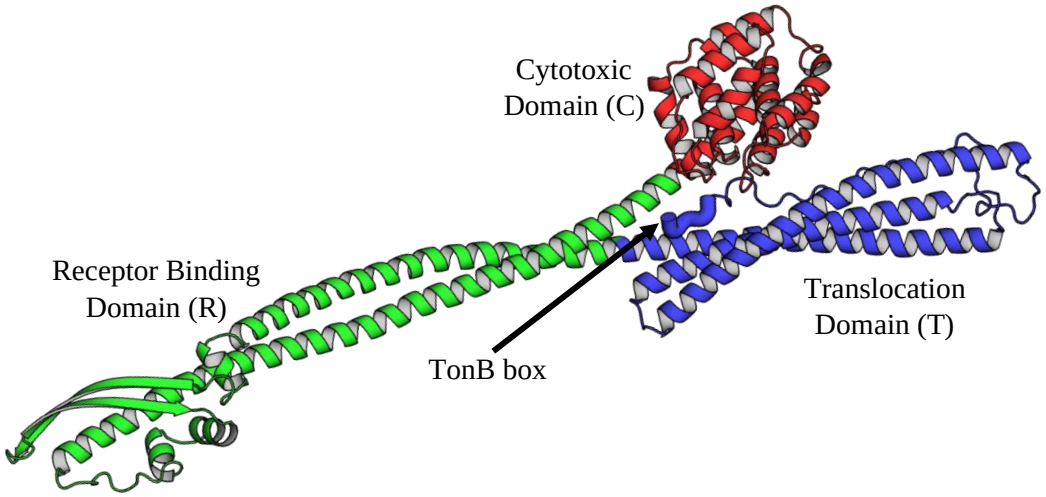

Figure 1-12. Crystal structure of colicin Ia.
Cartoon structure of colicin Ia (PDB ID = 1CII (Wiener *et al.*, 1997)) coloured by its domain architecture; translocation domain (*blue*), receptor binding domain (*green*) and cytotoxic domain (*red*). The TonB-box motif (residues 23 – 27) is found at the N-terminus of the translocation domain.

Additional full-length colicin structures have been published for colicins N, E3, B, M, S4 and E9 (Vetter *et al.*, 1998; Soelaiman *et al.*, 2001; Hilsenbeck *et al.*, 2004; Zeth *et al.*, 2008; Arnold *et al.*, 2009; Klein *et al.*, 2016). Interestingly, despite possessing conserved domain organisation to ColIa, the receptor binding and translocation domains of these colicins have adopted dramatically different three-dimensional structures (Figure 1-13).

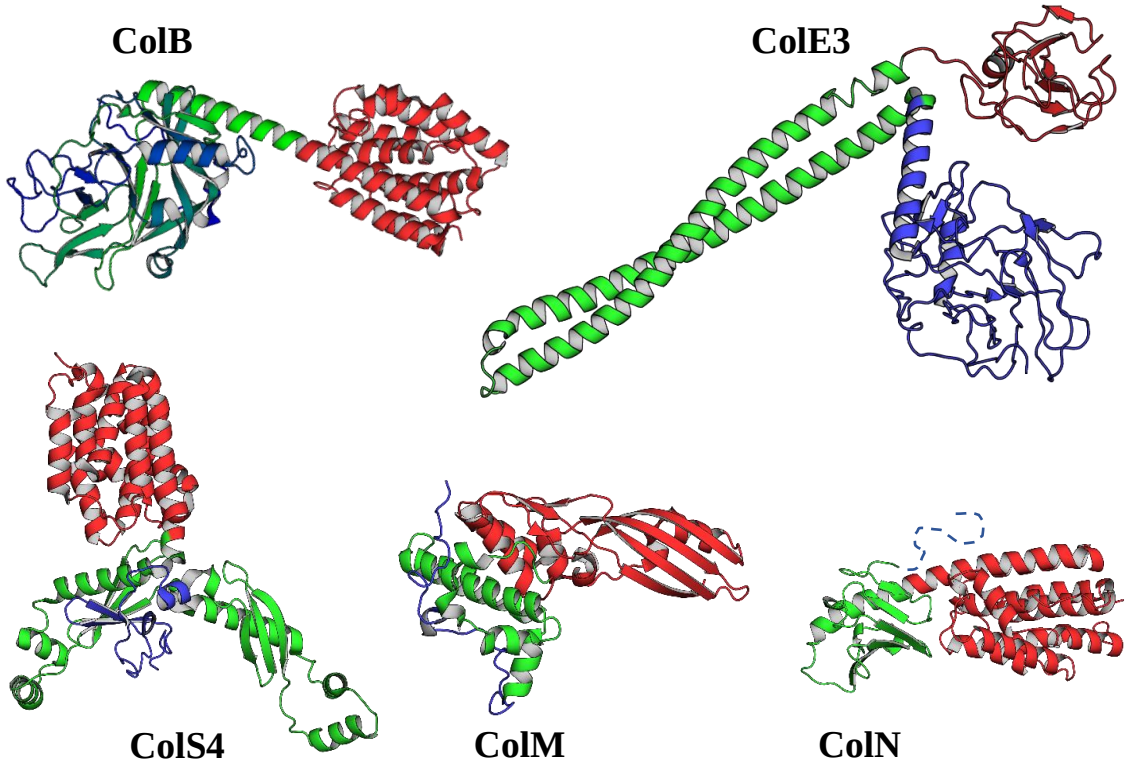

Figure 1-13. Structural diversity amongst colicins.
Cartoon structure of colicins coloured by their domain architecture; translocation domain (*blue*), receptor binding domain (*green*) and cytotoxic domain (*red*). Colicin B contains a dual function receptor binding/translocation domain (*blue/green gradient*). The translocation domain of colicin N (*dotted blue line*) is absent from the crystal structure. Colicin B PDB ID = 1RH1 (Hilsenbeck *et al.*, 2004), colicin E3 PDB ID = 1JCH (Soelaiman *et al.*, 2001), colicin M PDB ID = 2XMX (Zeth *et al.*, 2008), colicin N PDB ID = 1A87 (Vetter *et al.*, 1998), colicin S4 PDB ID = 3FEW (Arnold *et al.*, 2009).

Colicins form high-affinity interactions with primary receptors in the target cell's OM, typically a porin or a TBDT. For example, colicin E9 binds to BtuB with a K_d of 153 nM, which increases to 2.4 nM when calcium ions are present (Housden *et al.*, 2005). Several structures of colicin-receptor/translocation complexes have also been solved. The crystal structure of the ColE3 receptor binding domain, in complex with its primary receptor BtuB, demonstrates that the extended coiled-coil structure of ColE3 inserts into the BtuB β-barrel at an oblique 45° angle (Figure 1-14), primarily interacting with the TBDT's extracellular loops (Kurisu *et al.*, 2003).

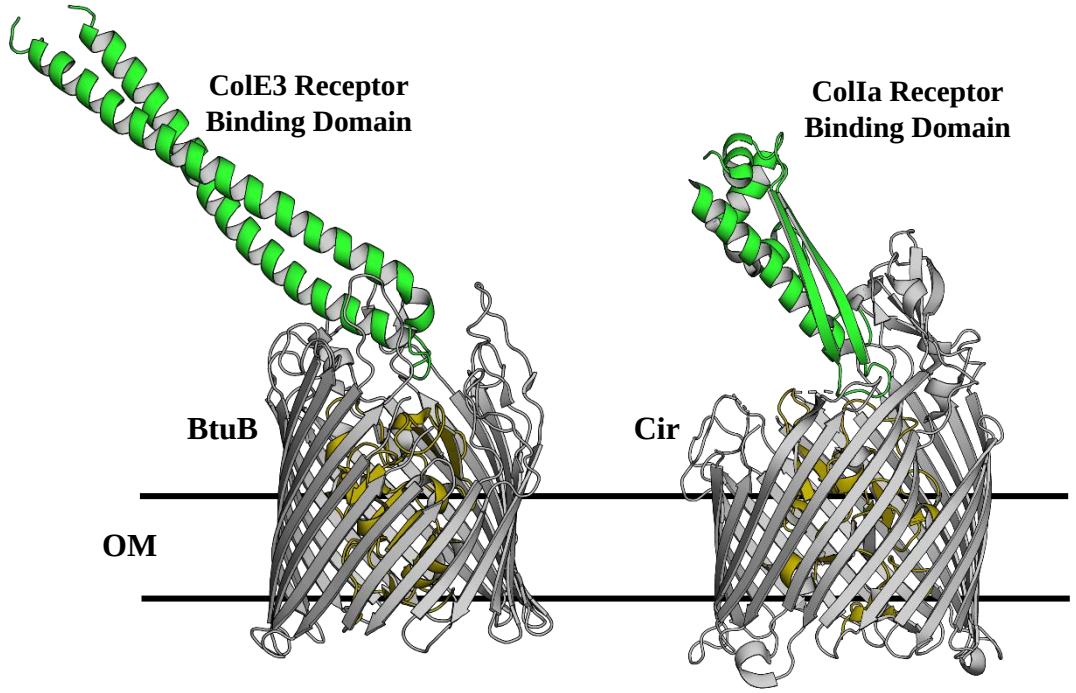

Figure 1-14. Structures of colicin-receptor complexes.
Cartoon representations of the receptor binding domains of ColE3 (residues 316 – 448) and ColIa (residues 282 – 385) (*green*) in complex with their primary OM receptors BtuB and Cir, respectively. Both receptor binding domains interact primarily with extracellular loops from their respective OMP receptors, forming minimal intermolecular interactions with the TBDT plug domain (*olive*). Additionally, both structures display an oblique 45° binding angle, positioning the translocation domain distally to the bound OMP. BtuB:ColE3 PDB ID = 1UJW (Kurisu *et al.*, 2003), Cir:ColIa PDB ID = 2HDI (Buchanan *et al.*, 2007).

This functions to position the ColE3 translocation domain distally from the TBDT, facilitating recruitment of a secondary OMP, OmpF. Structures of the receptor binding domains of colicin E2 (ColE2) and ColIa in complex with their respective OMP receptors, BtuB and Cir, exhibit similar angular binding (Sharma *et al.*, 2007; Buchanan *et al.*, 2007) (Figure 1-14). Both colicins require the recruitment of an additional OMP to successfully translocate across the OM. Like ColE3, ColE2 utilises OmpF, whereas ColIa requires an additional copy of the Cir receptor (Housden *et al.*, 2005; Jakes & Finkelstein, 2010).

After binding their specific receptor, colicins hijack the Tol/Ton complex to energize import across the OM, either through the primary receptor, or via subsequently recruited OM proteins (Figure 1-15) (Housden *et al.*, 2005).

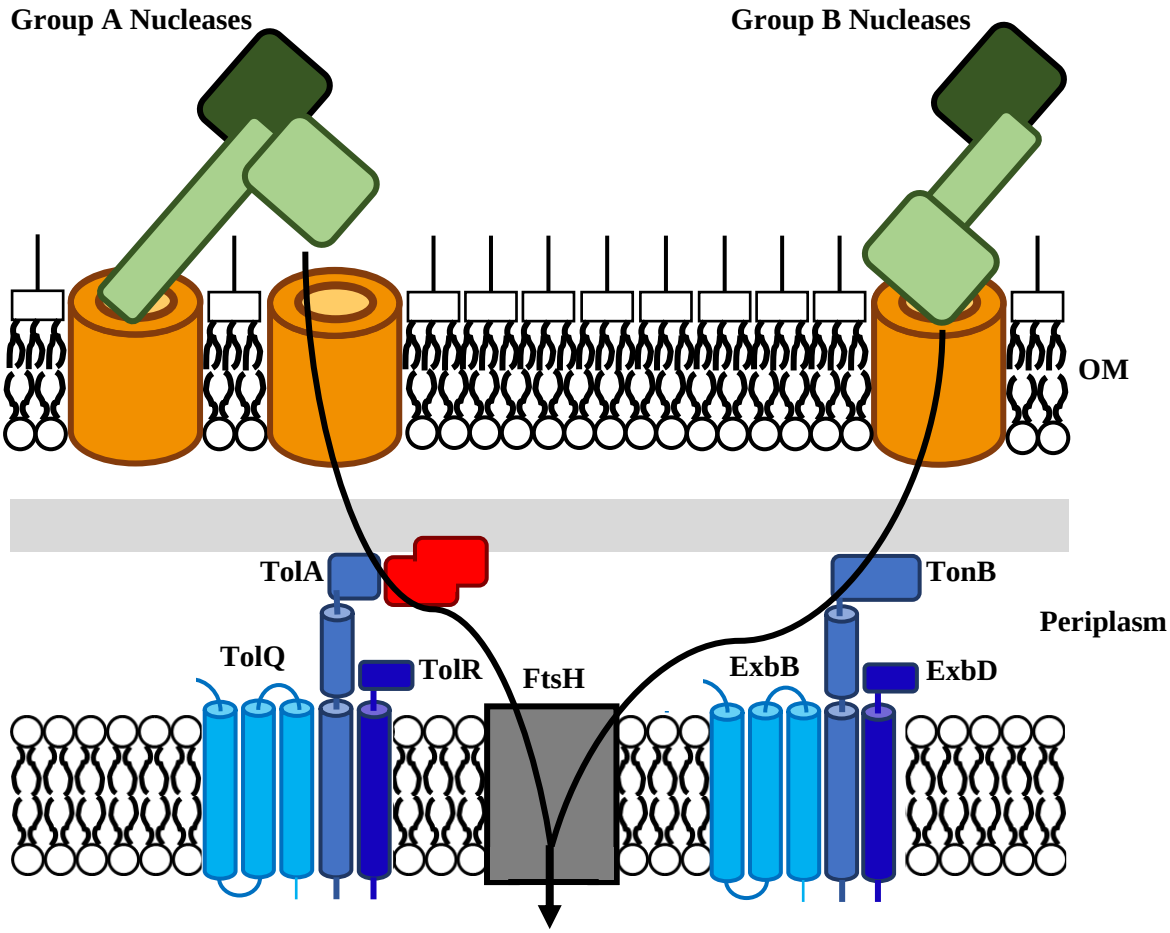

Figure 1-15. Schematic of nuclease-type colicin translocation across the *E. coli* cell envelope. Colicins (and other CLBs) can be subdivided into Group A or Group B in relation to the OM energisation system parasitized; Group A use Tol whereas Group B use Ton. Both Group A and Group B nuclease-type colicins translocate across the OM, with Group B nuclease-type colicins translocating directly through their receptor (e.g.: colicin D) whereas Group A nuclease-type colicins require an additional translocator (e.g.: ColE9). Nuclease-type colicins must additionally translocate across the IM, likely through involvement of FtsH. Adapted from Kleanthous 2010.

Additionally, nuclease-type colicins must also translocate across the IM to reach their site of action. This is thought to occur via the AAA+ ATPase/protease FtsH, which cleaves the cytotoxic domain and mediates translocation into the cytoplasm (Walker et al., 2007; Chauleau et al., 2011). Enzymatic colicins are co-transcribed with a cognate immunity protein to prevent cell suicide. Cognate immunity proteins bind their target colicin C-terminal domain with very high affinity, inhibiting cytotoxic activity (Kleanthous & Walker, 2001).

1.6.3. Pyocins.

Pyocins, bacteriocins specific for strains of *Pseudomonas*, are notably more structurally diverse than their proteinaceous relatives, colicins. All pyocins can be subdivided into three groups based on their structure: S-type pyocins, lectin-like pyocins, and tailocins (Ghequire & De Mot, 2014).

S-type (soluble) pyocins possess a similar modular structure to colicins. They are extended, α-helical, multidomain proteins, consisting of N-terminal and middle domains that parasitize cellular envelope proteins for delivery of their cytotoxic C-terminal domain into target cells as described in **Table 1-3** (Ghequire & De Mot, 2014).

Table 1-3. Mechanisms of pyocin import and cytotoxicity.
Compiled using Ghequire & De Mot, 2014 unless noted otherwise. References for subsequent findings shown below.

Pyocin	OM Receptor/Translocator	CPA Binding Motif	OM Energisation System	Cytotoxic Activity
PyoAP41	N.D.	No[5]	N.D.	DNase
PaeM1	FiuA[7]	N.D.	TonB1[1]	Lipid II-Hydrolysis
PaeM2[1]	FiuA[1]	N.D.	TonB1[1]	Lipid II-Hydrolysis
PaeM4[2]	HxuC/Hur[8]	N.D.	N.D.	Lipid II-Hydrolysis[8]
PyoG[3]	HxuC/Hur[3]	No[3]	TonB1[3]	Putative DNase[3]
PyoS1	N.D.	No[5]	N.D.	DNase
PyoS2	FpvAI	Yes[5]	TonB1[9]	DNase
PyoS3	FpvAII	Putative[5]	N.D.	DNase
PyoS4	FpvAI	N.D.	TonB1[10]	tRNase
PyoS5	FptA	Yes[5]	TonB1[10]	Pore-Forming
PyoS6	N.D.	N.D.	N.D.	rRNase
PyoS8[4]	N.D.	N.D.	N.D.	DNase
PyoSD1[5]	N.D.	No[5]	N.D.	tRNase
PyoSD2[5]	FpvAI[5]	Yes[5]	Putative TonB1[9]	tRNase
PyoSD3[5]	FpvAII[5]	Yes[5]	N.D.	tRNase
PyoSN[6]	N.D.	N.D.	N.D.	Putative DNase[6]

N.D. indicates not determined. [1](Latino *et al.*, 2019), [2](Paškevičius *et al.*, 2017), [3](Atanaskovic *et al.*, 2020), [4](Turano *et al.*, 2017), [5](McCaughey, Josts, *et al.*, 2016), [6](Sharp *et al.*, 2017), [7](Ghequire *et al.*, 2017), [8](Ghequire & Öztürk, 2018), [9](White *et al.*, 2017), [10](Behrens *et al.*, 2020).

The receptor-binding domain tends to be present directly at the N-terminus, unlike colicins, which generally possess central receptor-binding domains (Sano *et al.*, 1993). Their size varies significantly; ranging from 32 kDa for pyocin PaeM1 to 89 kDa for pyocin SN (Latino

et al., 2019; Sharp *et al.*, 2017). S-type pyocins elicit cytotoxicity through intrinsic enzymatic (nuclease or lipid II-hydrolysis) or pore-forming activity (Michel-Briand & Baysse, 2002; Ghequire & De Mot, 2014). Like colicins, S-type pyocins are also co-transcribed with a cognate immunity protein, which forms a very high affinity complex with the cytotoxic domain and inhibits activity (Duport *et al.*, 1995; Joshi *et al.*, 2015). The structures adopted by S-type pyocins, in addition to the mechanisms utilised during translocation across the OM, will be discussed in detail in the prefaces of Chapters 4 and 5, respectively.

Lectin-like pyocins, so named for their tandem monocot mannose-binding lectin motif, exhibit genus-specific cytotoxic activity against *Pseudomonas*. Unusually, they contain no known cytotoxic domain and cognate immunity protein (Ghequire, Öztürk, *et al.*, 2018). The most well characterised member of the lectin-like pyocins is pyocin L1, specific for *P. aeruginosa*. The C-terminal domain of Pyocin L1 binds with high affinity to D-rhamnose moieties that comprise CPA; the major oligosaccharide component of the *P. aeruginosa* OM (McCaughey *et al.*, 2014). Pyocin L1 is then able to interact with the polymorphic external loop L6 of BamA, which is thought to inhibit OMP biogenesis and elicit cytotoxicity through an unidentified mechanism (Ghequire, Swings, *et al.*, 2018).

Tailocins are large pyocins synthesised by *Pseudomonas* that resemble phage tail-like structures (Michel-Briand & Baysse, 2002). Tailocins can be further subdivided into two groups based on their structural architecture. R-type tailocins resemble a double hollow cylinder; composed of a rigid inner core and a contractible outer sheath (Ghequire & De Mot, 2014). Attached to the sheath is a baseplate that forms a docking point for six tail fibres. These fibres are required for anchoring R-type tailocins to target cells in manner analogous to phage recognition, usually though binding of LPS. Strain-specificity is defined by proteins located at the distal portion of the fibres (Ohsumi *et al.*, 1980; Kumazaki & Ishii, 1982). F-type tailocins are similar in structure to R-type tailocins, however they lack the contractile outer sheath. Both elicit cytotoxicity through insertion into the inner membrane of target cells, resulting in depolarisation and cell death (Ghequire & De Mot, 2014).

1.7. Aims of this study.

As prefaced in this introduction, the Gram-negative cellular envelope presents a significant challenge for the transport of molecules from the cytoplasm to the extracellular medium and vice versa. As such, Gram-negative bacteria have evolved several well characterised secretion systems that translocate targeted protein substrates from the cytoplasm across the cellular envelope and into the external environment. However, no dedicated mechanism for the import of proteinaceous substrates has been elucidated. Interestingly, the descendants of Gram-negative bacteria, mitochondria and plastids, have well established protein import systems as a necessity, due to the extraneous synthesis of the majority of their proteome.

Yet proteins are imported across the Gram-negative cell envelope. CLBs are a family of protein toxins that have evolved mechanisms of retrograde translocation through parasitizing proteins within the cellular envelope to deliver their cytotoxic C-terminus into target cells. Understanding this import process could be revolutionary for the development of new antibiotic therapies to relieve the pressures currently exerted on conventional treatments through increasing development of multidrug resistance in pathogenic bacteria. Thus, this study aims to characterise the mechanisms utilised by CLBs during import from macromolecular to atomistic detail through a multidisciplinary approach involving cell biology, biophysics, structural biology, and protein engineering.

A recently identified nuclease-type bacteriocin, pyocin SN (PyoSN), has been demonstrated to kill strains of *P. aeruginosa.* It possesses a unique N-terminal domain, which suggests a novel import pathway across the OM. Characterising the proteins involved in PyoSN import could facilitate identification of new therapeutic targets to combat increasing multidrug resistance in *P. aeruginosa*. Whilst we aim to increase our understanding of new CLBs, investigations into the mechanisms of better characterised CLBs must also continue. A significant proportion of our understanding of pyocin translocation comes from studies of pyocin S2 (PyoS2) and its interactions with the FpvAI receptor. However, there remain unanswered questions concerning the precise mechanism utilised during import across the OM. Delineation of this process in atomistic detail could potentially pave the way for rational drug design, allowing us to better understand the structural constraints of CLB import in *P. aeruginosa*.

Chapter 2 – Materials and Methods

2.1.Strains, Media, and Growth Conditions.

E. coli and *P. aeruginosa* bacterial strains that were utilised throughout this study are described in **Table 2-1** and **Table 2-2**. *P. aeruginosa* clinical isolates provided by the Walker lab are described in **Appendix Table S1**. Bacteria were typically cultured in Miller Lysogeny Broth (LB) medium (10 g/L tryptone, 10 g/L NaCl, 5 g/L yeast extract, pH 7.2) at 37 °C with shaking unless stated otherwise. Single colony isolates for initiation of bacterial cultures were generated after plating bacterial strains or plasmid expressing cells on LB-agar (LB + 1.5% (w/v) agar) plates. Strains were maintained as glycerol stocks (LB + 50% (v/v) glycerol) for long term storage at -80 °C.

Table 2-1. *E. coli* strains used in this study.

Name	Relevant Characteristics	Source
NEB5α	*fhuA2 Δ(argF-lacZ)U169 phoA glnV44 Φ80 Δ(lacZ)M15 gyrA96 recA1 relA1 endA1 thi-1 hsdR17*	New England Biolabs
BL21 (DE3)	*fhuA2 [lon] ompT gal (λ DE3) [dcm]* Δ*hsdS (λ DE3) = λ sBamHIo* Δ*EcoRI-B int::(lacI::PlacUV5::T7 gene1) i21* Δ*nin5*	New England Biolabs
BL21 ΔABCF	*F− ompT hsdS(rB− mB−) dcm+ Tetr gal (λ DE3) endA Hte.. ΔompA ΔlamB ΔompC ΔompF*	Leo Lab Addgene Reference 102270
S17-1λpir	*pro thi hsdR recA; chromosomal RP4 (Tra+ Tcs Kms Aps); Tpr Smr*	American Type Culture Collection

Table 2-2. *P. aeruginosa* strains used in this study.

Name	Relevant Characteristics	Source
PAO1	Clinical isolate, burn wound	Manoil Lab Washington Mutant Library
PAO6609	*met-901,1 amiE200, strA, pvd-9*	Lamont Lab
K1407	PAO6609 *tonB1*$^{-}$	
K1408	PAO6609 *tonB2*$^{-}$	
MS231	PAO6609 *tonB3*$^{-}$	

PAO1 Δrmd	PAO1 *PA5454*$^{-}$ (CPA-deficient)	Khursigara Lab
PW1255	PAO1 *PA0151*$^{-}$	Manoil Lab Washington Mutant Library
PW1334	PAO1 *PA0192*$^{-}$	
PW1793	PAO1 *PA0434*$^{-}$	
PW1861	PAO1 *PA0470*$^{-}$ (*fiuA*)	
PW2418	PAO1 *PA0781*$^{-}$	
PW2689	PAO1 *PA0931*$^{-}$ (*pirA*)	
PW3296	PAO1 *PA1271*$^{-}$ (*btuB*)	
PW3356	PAO1 *PA1302*$^{-}$ (*hxuC/hur*)	
PW3399	PAO1 *PA1322*$^{-}$	
PW3483	PAO1 *PA1365*$^{-}$	
PW3881	PAO1 *PA1613*$^{-}$	
PW4347	PAO1 *PA1910*$^{-}$ (*femA*)	
PW4367	PAO1 *PA1922*$^{-}$	
PW4597	PAO1 *PA2089*$^{-}$	
PW4870	PAO1 *PA2289*$^{-}$	
PW4938	PAO1 *PA2335*$^{-}$	
PW5348	PAO1 *PA2590*$^{-}$	
PW5503	PAO1 *PA2688*$^{-}$ (*pfeA*)	
PW5892	PAO1 *PA2911*$^{-}$	
PW6483	PAO1 *PA3268*$^{-}$	
PW6749	PAO1 *PA3408*$^{-}$ (*hasR*)	
PW7180	PAO1 *PA4221*$^{-}$ (*fptA*)	
PW7415	PAO1 *PA3790*$^{-}$ (*oprC*)	
PW7590	PAO1 *PA3901*$^{-}$ (*fecA*)	
PW8043	PAO1 *PA4156*$^{-}$ (*fvbA*)	
PW8599	PAO1 *PA4514*$^{-}$	
PW8871	PAO1 *PA4675*$^{-}$ (*chtA*)	
PW8934	PAO1 *PA4710*$^{-}$ (*phuR*)	
PW9128	PAO1 *PA4834*$^{-}$ (*cntI*)	
PW9131	PAO1 *PA4835*$^{-}$ (*cntM*)	
PW9132	PAO1 *PA4836*$^{-}$ (*cntL*)	
PW9134	PAO1 *PA4837*$^{-}$ (*cntO*)	
PW9241	PAO1 *PA4897*$^{-}$	
PW9719	PAO1 *PA2057*$^{-}$ (*sppR*)	

PW10299	PAO1 *PA5498*$^{-}$ (*znuA*)	
PW10303	PAO1 *PA5500*$^{-}$ (*znuC*)	
PW10306	PAO1 *PA5501*$^{-}$ (*znuB*)	
PW10435	PAO1 *PA2070*$^{-}$	
PAS033	*pvdF::kana, fpvAI*$_{\Delta 139\text{-}276}$	Schalk Lab

2.2. Plasmids.

Plasmids utilised throughout this study are described in **Table 2-3.**

Table 2-3. Plasmids used in this study.
See **Appendix Table 2** for pET-21a(+), pET-24a(+), pACYCDuet-1, pMMB190, pETM11 and pBAD-Myc-HisB genotypes and vector maps.

Plasmid Name	Description	Source
pPW06	**PyoS2-ImS2**‡ cloned into pET-21a(+) at *NdeI*/*XhoI* sites	Paul White
pREN79	**PyoS2(1-556)-ColE2(449-581)-Im2**‡ chimera cloned into pET-21a(+) at *NdeI*/*XhoI* sites	Renata Kaminska
pJDG07	**PyoS2-ImS2**‡ **(K103C;L186C)** mutant cloned into pET-21a(+) at *NdeI*/*XhoI* sites	This Study
pJDG10	**PyoS2-ImS2**‡ **(P28C;D157C)** mutant cloned into pET-21a(+) at *NdeI*/*XhoI* sites	This Study
pREN120	**PyoS2-ImS2**‡ **(M11C;Y26C)** mutant cloned into pET-21a(+) at *NdeI*/*XhoI* sites	Renata Kaminska
pREN121	**PyoS2-ImS2**‡ **(Y128C;E162C)** mutant cloned into pET-21a(+) at *NdeI*/*XhoI* sites	Renata Kaminska
pPW11	**PyoS2(1-209)**‡ cloned into pET-21a(+) at *NdeI*/*XhoI* sites	Paul White
pJDG23	**PyoS2(1-209)**‡**-Cys** mutant cloned into pET-21a(+) at *NdeI*/*XhoI* sites	This Study
pJDG18	**PyoS2(1-209)**‡ **(M11C;Y26C)** mutant cloned into pET-21a(+) at *NdeI*/*XhoI* sites	This Study
pJDG20	**PyoS2(1-209)**‡ **(K103C;L186C)** mutant cloned into pET-21a(+) at *NdeI*/*XhoI* sites	This Study
pJDG21	**PyoS2(1-209)**‡ **(Y128C;E162C)** mutant cloned into pET-21a(+) at *NdeI*/*XhoI* sites	This Study

pJDG15	**PyoS2(10-689)-ImS2**‡ mutant cloned into pET-21a(+) at *NdeI*/*XhoI* sites	This Study
pJDG48	**PyoSN(1-16)-PyoS2(17-689)-ImS2**‡ mutant cloned into pET-21a(+) at *NdeI*/*XhoI* sites	This Study
pMMB-SD-TB-Plug	**FpvAI(1-276)*** encoding signalling domain, TonB box and plug domain cloned into pMMB190 at *BamHI*/*HindIII* sites	Schalk Lab
pMMB-$Plug_{NL}$	**FpvAI(215-276)*** encoding non-labile plug subdomain cloned into pMMB190 at *BamHI*/*HindIII* sites	This Study
pNGH252	**PyoSN-ImSN**‡ cloned into pET-24a(+) at *NdeI*/*XhoI* sites	Nicholas Housden
pJDG51	**PyoSN(53-832)-ImSN**‡ cloned into pET-24a(+) at *NdeI*/*XhoI* sites	This Study
pNGH260	**ImSN**‡ cloned into pACYCDuet-1 at *NcoI*/*HindIII* sites	Nicholas Housden
pJDG22	**PyoSN(1-699)**‡ cloned into pET-24a(+) at *NdeI*/*XhoI* sites	This Study
pJDG34	**PyoSN(1-205)**‡ cloned into pET-24a(+) at *NdeI*/*XhoI* sites	This Study
pJDG52	**PyoSN(53-205)**‡ cloned into pET-24a(+) at *NdeI*/*XhoI* sites	This Study
pJDG25	**CntO*** cloned into pMMB190 at *BamHI*/*HindIII* sites	This Study
pJDG26	**CntO*** cloned into pBAD-Myc-HisB at *NdeI*/*HindIII* sites	This Study
pJDG27	**CntO*** with OmpF signal sequence cloned into pBAD-Myc-HisB at *NdeI*/*HindIII* sites	This Study
pJDG28	**CntO*** with OmpF signal sequence cloned into pET-24a(+) at *NdeI*/*HindIII* sites	This Study
pPW17	†**TEV-TonB1(109-342)** cloned into pETM11 at *NcoI*/*SacI* sites	Paul White

‡Cloned without a stop codon such that a C-terminal His_6-Tag was provided by the vector.
†Cloned with an N-terminal His_6-Tag provided by the vector.
*Cloned with a signal sequence for OM secretion.

2.3.Molecular Biology.

2.3.1. Extraction of genomic DNA.

P. aeruginosa strain PAO1 was grown overnight at 37 °C in 10 ml LB. Cells were pelleted by centrifugation at 6800 ×g for 7 minutes and genomic DNA was purified using a DNeasy Blood & Tissue Kit (Qiagen) as per the manufacturer's instructions, including the pre-treatment step recommended for Gram-negative bacteria.

2.3.2. Polymerase Chain Reaction (PCR).

PCR was utilised to amplify DNA fragments, in addition to introduction of mutations into plasmids via whole plasmid mutagenesis PCR. All primers used for DNA manipulations were purchased from Sigma-Aldrich and are listed in **Table 2-4**. The standard 50 µl PCR reaction mixture used is described in **Table 2-5**. Dimethylsulfoxide (DMSO) concentration varied between 2 – 4% to reduce any secondary structure propensity of primers. PCR was performed in an Eppendorf Mastercycler Nexus, programmed as described in **Table 2-6** and **Table 2-7** for DNA amplification and whole plasmid mutagenesis, respectively. Methylated template DNA was removed by the addition of 1 µl DpnI to the PCR reaction mix, followed by incubation at 37 °C for a minimum of 1 hour. PCR products were analysed using gel electrophoresis (Section 2.3.8).

Table 2-4. Primers used in this study.

Name	Sequence 5′ → 3′	Use
M11C_F	GATTACGAACCTGGTTCGTGCGTTATTACACATGTGCAGG	Introduction of Cys into *pyoS2* at position M11 to generate pREN120.
M11C_R	CCTGCACATGTGTAATAACCGCAGAACCAGGTTCGTAATC	
Y26C_F	GGGCGTGACATAATCCAGTGTATTCCTGCTCGATCAAGC	Introduction of Cys into *pyoS2* at position Y26 to generate pREN120.
Y26C_R	GCTTGATCGAGCAGGAATACACTGGATTATGTCACGCCC	
P28C_F	GCGTGACATAATCCAGTATATTTGTGCTCGATCAAGCTACG	Introduction of Cys into *pyoS2* at position P28 to generate pJDG10.
P28C_R	CGTAGCTTGATCGAGCACAAATATACTGGATTATGTCACGC	
K103C_F	CAATGACATCCGCGATGAATGCAGTATCGTTGATGCACTC	Introduction of Cys into *pyoS2* at position K103 to generate pJDG07.
K103C_R	GAGTGCATCAACGATACTGCATTCATCGCGGATGTCATTG	
Y128C_F	CGCCCGGCCAATCTTTGTACGGCTTCAGACTTTC	Introduction of Cys into *pyoS2* at position Y128 to generate pREN121.
Y128C_R	GAAAGTCTGAAGCCGTACAAAGATTGGCCGGGCG	

D157C_F	CTATGGAGAGTTCCTGTGTCGCCACATGAGTGAGCTGG	Introduction of Cys into *pyoS2* at position D157 to generate pJDG10.
D157C_R	CCAGCTCACTCATGTGGCGACACAGGAACTCTCCATAG	
E162C_F	GGATCGCCACATGAGTTGTCTGGCCAAAGCGTACAGC	Introduction of Cys into *pyoS2* at position E162 to generate pREN121.
E162C_R	GCTGTACGCTTTGGCCAGACAACTCATGTGGCGATCC	
L186C_F	CTTGAAACAAACGTCTCAAGAGTGTGAGAATAAAGCCCGGTC	Introduction of Cys into *pyoS2* at position L186 to generate pJDG07.
L186C_R	GACCGGGCTTTATTCTCACACTCTTGAGACGTTTGTTTCAAG	
S2del9_F	GTTTAACTTTAAGAAGGAGATATACATATGTCGATGGTTATTACACATGTGCAGG	Removal of residues 1-9 from *pyoS2* to generate pJDG15.
S2del9_R	CCTGCACATGTGTAATAACCATCGACATATGTATATCTCCTTCTTAAAGTTAAAC	
SN(TB)_S2_F	ATATACATATGGCATTGCCCGTAGAAAATTGGAATGATACCACCGTAGTGGGATATCAGGGTGGTGGGCGTGACATAATC	Substitution of *pyoS2* residues 1-16 with *pyoSN* residues 1-16 to generate pJDG48.
SNS2_Fusion_R	GGTGGTGGTGGTGCTCGAGACCGGCCTTAAAGCC	
S2_NTD_F	GGAGGCGGACTACAAGCTCGAGGCAAATGTCGAG	Introduction of XhoI site into *pyoS2* after residue 209. Used to generate plasmids pJDG18, pJDG20 and pJDG21 from pREN120, pJDG07 and pREN121, respectively.
S2_NTD_R	CTCGACATTTGCCTCGAGCTTGTAGTCCGCCTCC	

S2_NLink_Cys_F	GCACCACCACCACCACCACGGCAGCG GCTGTTGAGATCCGGCTGCTAACAAA GC	Introduction of a Cys residue with a GSG linker into *pyoS2*$_{NTD}$ after the His_6 provided by the vector.
S2_NLink_Cys_ R	GCTTTGTTAGCAGCCGGATCTCAACAG CCGCTGCCGTGGTGGTGGTGGTGGTG C	
FpvAI_PlugNL_F	GGCGGGATATGTCCAGGCGCAGATCA ACAACTTCCAGTACGACGGG	Removal of residues 45-213 from *fpvAI*$_{1-276}$ to generate pMMB-$Plug_{NL}$.
FpvAI_PlugNL_ R	CCCGTCGTACTGGAAGTTGTTGATCTG CGCCTGGACATATCCCGCCAGCG	
SN_TR_F	CCATTATACCTGGTCTTTCTCGAGCCG CCGGTTTCTGC	Introduction of XhoI site into *pyoSN* after residue 699. Used to generate plasmid pJDG22.
SN_TR_R	GCAGAAACCGGCGGCTCGAGAAAGAC CAGGTATAATGG	
SN_NTD_F	CCTTCCGGAGCTGGAGAAACTCGAGG CGCCGTTAGTCGCCG	Introduction of XhoI site into *pyoSN* after residue 205. Used to generate plasmid pJDG34.
SN_NTD_R	CGGCGACTAACGGCGCCTCGAGTTTCT CCAGCTCCGGAAGG	
SNdel52_F	GGAACTGTCTCCGATGAGCCATATGTT CGATGCGTTTGAAGATAACGC	Removal of residues 1-52 from *pyoSN* to generate pJDG51 and pJDG52.
SNdel52_R	GCGTTATCTTCAAACGCATCGAACATA TGGCTCATCGGAGACAGTTCC	
CntO_BamHI_F	AGTTCCGGATCCATGAGAGTCAGTGT GTCGCTTGTCCTCG	Used for amplification of *cntO* from PAO1 genomic DNA; CntO_BamHI_F and CntO_NdeI_F were used (in conjunction with CntO_HindIII_R) to generate pJDG25 and pJDG26, respectively.
CntO_NdeI_F	AGTTCCCATATGAGAGTCAGTGTGTCG CTTGTCCTCG	
CntO_HindIII_R	AGGCGTAAGCTTTCAGTAGTTCAGGG TCAGGCTCATGGTCAGG	
OmpF_SS_F	CAGTGATCGTCCCTGCTCTGTTAGTAG CAGGTACTGCAAACGCTGCGGAAACG GAAAGTCCCGCGGAGCTGG	Used for mutagenesis of CntO signal sequence (residues 1-22) to that of *E. coli* OmpF to generate pJDG27.
OmpF_SS_R	GCTACTAACAGAGCAGGGACGATCAC TGCCAGAATATTGCGCTTCACCATATG GAATTCCTCCTGCTAGCCC	

Table 2-5. Standard PCR Reaction Mixture.
Total volume adjusted to 50 µl with dH_2O. Reagents purchased from NEB.

Component	Final Concentration	Volume [µl]
5x Reaction Buffer	1x	10
dNTPs	0.4 mM	2.0
Forward Primer	0.4 µM	2.0
Reverse Primer	0.4 µM	2.0
Template DNA	100 ng	1.0
DMSO	2 – 4%	1.0 – 2.0
Phusion-HF DNA Polymerase	2 units	1.0

Table 2-6. PCR thermal cycler programme for amplification PCR.

Step	Temperature [°C]	Duration
Initial Denaturation	98	3 minutes
Denaturation*	98	10 seconds
Annealing*	50	30 seconds
Extension*	72	2 minutes
Final Extension	72	10 minutes
Hold	4	Indefinitely

*repeat steps for 45 cycles

Table 2-7. PCR thermal cycler programme for mutagenesis PCR.

Step	Temperature [°C]	Duration
Initial Denaturation	98	2 minutes
Denaturation*	98	1 minute
Annealing*	50 – 60	30 seconds
Extension*	72	5 minutes
Final Extension	72	5 minutes
Hold	4	Indefinitely

* repeat steps for 16 cycles

2.3.3. Restriction enzyme digestions.

Restriction enzyme digests were performed in CutSmart Buffer (NEB) in a 10 µl reaction mix, where up to 2 µg of DNA was digested with 0.5 µl of requisite restriction enzymes (NEB) at 37 °C for at least 2 hours. Digested DNA was separated through gel electrophoresis (Section 2.3.5) and extracted by gel extraction using a Monarch DNA Gel Extraction kit as per the manufacturer's instruction.

2.3.4. DNA ligation.

DNA ligation reactions were performed with T4 DNA ligase (NEB). 10 µl ligase reactions containing 1 µl of ligase and 1 µl 10 x T4 DNA ligase buffer (NEB) were performed at room temperature for 15 minutes with vector/insert ratios of 1:3, 10:3 and 100:3.

2.3.5. DNA gel electrophoresis.

1% (w/v) agarose gels were prepared by melting agarose in 0.5x TBE buffer (44.5 mM Tris-HCl pH 8.3, 44.5 mM boric acid, 1 mM ethylenediaminetetraacetic acid (EDTA)) with 1x SybrSafe dye and left to set in a gel electrophoresis tank. 2 µl of 6x DNA loading buffer (30% (v/v) glycerol, 6 mM EDTA, 0.4% (w/v) bromophenol blue) was added to 10 µl sample and loaded onto the gel, with an additional 1 kb DNA ladder (NEB) for comparison. Electrophoresis was conducted at constant voltage of 80 V in 0.5x TBE buffer.

2.3.6. Preparation of chemically competent cells.

Chemically competent NEB5α and BL21(DE3) *E. coli* cells were purchased from NEB. These were utilised for high efficiency transformation, pertaining to adducts generated by PCR, or propagated further to generate additional competent cells for routine plasmid preparation and expression. NEB5α, BL21(DE3), BL21 ΔABCF and S17-1λpir *E. coli* were grown as 5 ml cultures to an optical density (OD_{600nm}) of 0.3 in LB at 37 °C. Cultures were pelleted by centrifugation at 6800 xg for 7 minutes at 4 °C. Cells were resuspended in 10 ml ice cold 10 mM Tris-HCl pH 8.0, 50 mM $CaCl_2$ and incubated on ice for 1 hour. Cells were centrifuged again at 1664 xg for 6 minutes at 4 °C, followed by resuspension in 2 ml ice cold 10 mM Tris-HCl pH 8.0, 100 mM $CaCl_2$, 15% (v/v) glycerol. Competent cells were stored in 100 µl aliquots at -80 °C.

2.3.7. Chemical transformation of *E. coli.*

Competent NEB5α, BL21(DE3), BL21 ΔABCF or S17-1λpir *E. coli* were thawed on ice and incubated with 100 ng plasmid DNA for 30 mins. Cells were heat shocked at 42 °C for 45 seconds, followed by immediate incubation on ice for 2 minutes. Cells were then outgrown in SOC (Super Optimal broth with Catabolite repression) medium (2% (w/v) vegetable peptone, 0.5% (w/v) yeast extract, 10 mM NaCl, 2.5 mM KCl, 10 mM $MgCl_2$, 10 mM $MgSO_4$, 20 mM glucose) for 1 hour at 37 °C before being plated out onto LB-agar plates containing relevant antibiotic/s for selection as described in **Table 2-8**. Plates were incubated at 37 °C for 16 hours.

Table 2-8. Antibiotics used in this study for *E. coli* selection with working concentrations.

Antibiotic	Compatible Plasmid Vectors	Working Concentration
Ampicillin	pET-21a(+), pBAD-Myc-HisB	100 µg/ml
Chloramphenicol	pACYCDuet-1	34 µg/ml
Kanamycin	pET-24a(+), pETM11	30 µg/ml

2.3.8. Transformation of *P. aeruginosa* by conjugation.

Chemically transformed S17-1λpir *E. coli* expressing pMMB190 derived plasmids (Section 2.3.6) and *P. aeruginosa* strains PAS033 and PW9134 were incubated overnight in LB at 37 °C and 43 °C respectively, without antibiotic selection. Each *P. aeruginosa* culture (2 ml) was mixed with S17-1λpir culture expressing the desired plasmid for conjugation (2 ml). Cells were then pelleted by centrifugation at 6800 xg for 7 minutes, followed by resuspension in 100 µl LB. The 100 µl cellular suspensions were spotted in the centre of a pre-warmed LB-agar plates and incubated at 37 °C for 8 hours. The bacterial spot was then harvested and resuspended in LB. Serial dilutions of the cellular suspension were plated onto LB-agar plates containing relevant antibiotics to select for plasmid containing *P. aeruginosa*, described in **Table 2-9**. Plates were incubated at 37 °C for 20 hours.

Table 2-9. Antibiotics used in this study for *P. aeruginosa* selection with working concentrations.

Antibiotic	Working Concentration
Carbenicillin	150 µg/ml
Chloramphenicol	10 µg/ml
Gentamycin	50 µg/ml
Kanamycin	30 µg/ml
Tetracycline	10 µg/ml

2.3.9. Purification and sequencing of plasmid DNA.

Transformed NEB5α cultures were grown in 5 ml LB at 37 °C with appropriate antibiotics overnight, and subsequently harvested by centrifugation at 6800 xg for 7 minutes. Plasmid DNA was isolated from cells using Monarch Plasmid Miniprep and Promega PureYield Plasmid Midiprep kits. Plasmid DNA yields from the kits were typically 50 – 250 ng/µl and 200 – 500 ng/µl respectively, with A_{260nm}/A_{280nm} values between 1.8 and 2.0. Plasmid DNA

was stored at -20 °C. DNA sequencing was performed by Genewiz from plasmid samples at 60 ng/µl.

2.4. Sodium Dodecyl Sulphate Polyacrylamide Gel Electrophoresis (SDS-PAGE).

Tris-buffered acrylamide gels (10 – 15% (w/v) acrylamide (37.5:1 acrylamide/bis-acrylamide), 250 mM Tris-HCl pH 8.8, 0.1% (w/v) SDS, 0.08% (w/v) APS, 0.1% (v/v) TEMED) were left to set in a Hoefer Mighty Small SE250 tank assembled to the manufacturer's instruction. An additional stacking gel, prepared as above but with 5% (w/v) acrylamide and 250 mM Tris-HCl pH 6.8, was layered on top of the acrylamide gels and left to set, prior to sample application. Samples for SDS-PAGE analysis were mixed with 4x loading buffer (200 mM Tris-HCl pH 6.8, 8% (w/v) SDS, 0.4% (w/v) bromophenol blue, 40% (w/v) glycerol, 10% (v/v) β-mercaptoethanol) in a ratio of 3:1 and were boiled for 5 minutes prior to use. Appropriate volumes of sample were loaded onto the acrylamide gel alongside an unstained protein marker comprised of 116, 66.2, 45.0, 35.0, 25.0, 18.4 and 14.4 kDa molecular weight (MW) standards (Pierce). Electrophoresis was typically run at a constant current of 30 mA per gel in Tris-glycine buffer (25 mM Tris, 192 mM glycine, 0.1% SDS). Gels were stained with 50% (v/v) ethanol, 10% (v/v) acetic acid, 0.2% (w/v) Coomassie Brilliant Blue R-250 for 20 minutes, followed by destaining with 10% (v/v) ethanol, 10% (v/v) acetic acid.

2.5. Protein Expression and Purification.

2.5.1. Expression and purification of PyoS2, PyoSN and their derivatives.

PyoS2-ImS2, PyoSN-ImSN and their derivatives were expressed in BL21(DE3) cells grown in LB media. Expression of PyoSN-ImSN, which required co-transformation with pNGH260 carrying a second copy of the ImSN immunity protein gene, was performed at 28 °C, whereas all other constructs were expressed at 37 °C. Expression was induced at an OD_{600nm} of 0.6 by the addition of 1 mM isopropyl-β-D-1-thiogalactopyranoside (IPTG) for 4 hours. Cells were harvested by centrifugation at 5050 xg for 12 minutes, and subsequently resuspended in binding buffer (20 mM Tris-HCl pH 7.5, 500 mM NaCl, 5 mM imidazole) supplemented with 1 mM phenylmethylsulfonyl fluoride (PMSF). Cells were lysed through

sonication on ice using a Misonix S-4000 ultrasonic liquid processor fitted with a 3/8-inch stud probe at 70% maximum amplitude for 3 minutes, with 3 seconds on, 7 seconds off intervals (total processing time of 180 seconds). Cellular debris was removed by centrifugation at 12,500 xg for 30 minutes at 4 °C, and the soluble lysate cleared by filtration through a 0.45 µm syringe filter (Millipore). The cleared lysate was loaded onto a 5 ml HisTrap FF column (GE Healthcare) equilibrated in binding buffer and the tagged protein of interest eluted by a 5 – 250 mM linear imidazole gradient. Fractions adjudged to contain the protein by SDS-PAGE were pooled and 1 mM EDTA added to remove contaminating Ni^{2+}. Protein was dialysed into 25 mM Tris-HCl pH 7.5, 150 mM NaCl overnight at 4 °C. The dialysed protein was subsequently filtered through a 0.45 µm syringe filter and further purified by size exclusion chromatography using HiLoad 26/60 Superdex 75 pg or 26/60 Superdex 200 pg columns (GE Healthcare) (depending on the molecular weight of the purified protein) equilibrated in dialysis buffer.

2.5.2. Expression and purification of TonB1 soluble fragment.

Residues 109 to 342 of TonB1, lacking the transmembrane region, were purified as previously described (White *et al.*, 2017). Briefly, TonB1 was expressed and purified by Ni^{2+}-affinity chromatography as described above for pyocin variants (Section 2.5.1). Fractions containing TonB1were pooled and incubated in 50 mM Tris-HCl pH 7.0, 300 mM NaCl with 0.1 mg/ml His_6-Tobacco etch virus-protease (TEV) at room temperature for 5 hours to cleave the N-terminal His_6-tag. TonB1 was subsequently purified by further Ni^{2+}-affinity chromatography on a HisTrap FF column and size exclusion chromatography on a HiLoad 26/60 Superdex 200 pg column equilibrated in 50 mM Tris-HCl pH 7.5, 300 mM NaCl.

2.5.3. OM fractionation of *E. coli* BL21 ΔABCF expressing CntO.

E. coli BL21 ΔABCF cells (*ompA*$^{-}$, *lamB*$^{-}$, *ompC*$^{-}$, *ompF*$^{-}$) were transformed (Section 2.3.7) with the pJDG28 plasmid containing the *cntO* gene from *P. aeruginosa* strain PAO1 with an N-terminal *ompF* signal sequence from *E. coli*. Cells were grown in Lennox LB media (10 g/L tryptone, 5 g/L NaCl, 5 g/L yeast extract, pH 7.2) at 30 °C to an OD_{600nm} of 1.0, upon which the temperature was dropped to 20 °C and cells continued growth overnight (~16 hours). Cells were harvested and lysed by sonication, as described previously (Section 2.5.1), in 10 mM Tris-HCl pH 8.0, 0.25% (w/v) lithium diiodosalicyclic acid (LIS), 1 mM PMSF. Cellular debris was removed by centrifugation at 10,000 xg for 5 minutes at 4 °C,

followed by isolation of the total membrane fraction through ultracentrifugation at 200,000 xg for 45 minutes at 4 °C. The total membrane pellet was homogenised in 10 mM Tris-HCl pH 8.0, 0.25% (w/v) LIS, 2% (v/v) Triton X-100 to solubilise IM proteins, which were subsequently extracted by ultracentrifugation. The OM pellet was re-homogenised in 10 mM Tris-HCl pH 8.0 to minimise Triton X-100 contamination, followed by ultracentrifugation again. OMPs were extracted by homogenisation of the pellet in 10 mM Tris-HCl pH 8.0, 5 mM EDTA, 2% (w/v) n-octyl-β-D-glucopyranoside (β-OG). Solubilised OMPs were isolated from the insoluble debris by a final ultracentrifugation step.

2.5.4. Purification of the CntO:PyoSN$_{NTD}$ complex.

The OM extract containing CntO (see section 2.5.3) was concentrated down to ~30 ml using VivaSpin 20 centrifugal concentrators (Satorius) with a molecular weight cut-off (MWCO) of 30 kDa. His-tagged PyoSN$_{NTD}$ (purified as described in section 2.5.1) was added at a final concentration of 0.5 mg/ml to the OM extract, which was then loaded onto a 5 ml EDTA-resistance cOmplete^{TM} HisTag purification column (Roche) equilibrated in 20 mM Tris-HCl pH 7.5, 500 mM NaCl, 5 mM imidazole, 1% (w/v) β-OG. Non-specific proteins were washed from the column with 10 column volumes of buffer, and the CntO:PyoSN$_{NTD}$ complex eluted by a 5 – 250 mM linear imidazole gradient. The complex was further purified by size exclusion chromatography on a HiLoad 16/60 Superdex 200 pg column (GE Healthcare) equilibrated in 25 mM Tris-HCl pH 7.5, 150 mM NaCl, 1% (w/v) β-OG. The complex was concentrated down to ~10 mg/ml for crystallisation trials using VivaSpin Turbo 4 centrifugal concentrators (Satorius) with a MWCO of 50 kDa.

2.6. Protein Manipulation and Quantification.

2.6.1. Oxidation, reduction, and alkylation of PyoS2 disulphide mutants.

PyoS2 disulphide mutants were diluted to appropriate concentrations with 25 mM Tris-HCl pH 7.5, 150 mM NaCl. 1,1'-Azobis(N,N-dimethylformamide) (diamide) and DL-Dithiothreitol (DTT) were added when required for disulphide bond oxidation and reduction, respectively. Proteins were incubated with either diamide or DTT, at final concentrations of 1 mM and 5 mM respectively, for 45 minutes in the dark with gentle inversion at room temperature. To prevent the spontaneous reformation of disulphides, DTT reduced disulphide mutants were buffer exchanged into 25 mM Tris-HCl pH 7.5, 150 mM NaCl, 6 M guanidine-HCl using a 5 ml HiTrap Desalting column (GE Healthcare) and incubated for 30 minutes at room temperature to ensure complete protein unfolding. Proteins

were then alkylated with 200 µM iodoacetamide for 1 hour at room temperature, and subsequently desalted back into 25 mM Tris-HCl pH7.5, 150 mM NaCl.

2.6.2. Disulphide bond formation verification via AlexaFluor 488 labelling.

PyoS2 disulphide mutants treated with diamide or DTT and denatured through buffer exchange into 20 mM Tris-HCl pH7.5, 150 mM NaCl, 6 M guanidine-HCl, as described in section 2.6.1, were labelled with Alexa Fluor 488 C5 maleimide (AF488). AF488 (10 mM working stock in DMSO) was added in a fivefold molar excess for 1 hour in the dark with gentle inversion at room temperature. Excess AF488 was removed through buffer exchange into 25 mM Tris-HCl pH 7.5, 150 mM NaCl using a 5 ml HiTrap Desalting column (GE Healthcare). Samples were analysed by SDS-PAGE on a 12% (w/v) acrylamide gel and imaged in the light and fluorescence channels with a GBOX-CHEMI-XRQ.

2.6.3. Protein quantification.

Protein concentration was determined by absorbance at 280 nm using an Eppendorf Biophotometer with a 10 mm pathlength cuvette. The theoretical molecular weights and molar extinction coefficients of the proteins were predicted using ExPASy ProtParam Tool and are listed in **Table 2-10** (oxidised (*left*) and reduced (*right*) forms are denoted where appropriate). Protein masses were confirmed using denaturing electrospray ionisation mass spectrometry (ESI-MS) by Dr. David Staunton (Molecular Biophysics Suite, Department of Biochemistry, University of Oxford) and are listed in **Table 2-10** (oxidised (*left*) and alkylated (*right*) forms are denoted where appropriate).

Table 2-10. Protein molecular weights and molar extinction coefficients used in this study.

Protein	Molar Extinction Coefficient [$M^{-1}cm^{-1}$]		Predicted Molecular Weight [Da]	Observed Molecular Weight by denaturing ESI-MS [Da]	
PyoS2‡-ImS2	77240		84827.2	84828.1	
PyoS2E2‡-Im2	68760		85697.8	85699.3	
PyoS2Δ1-9‡-ImS2	75750		83981.3	83982.8	
$PyoS2_{SN1-15}$‡-ImS2	82740		84873.2	84873.8	
PyoS2(C11-C26)‡-ImS2	75875	75750	84739.1	84739.8	84853.4$^{\overline{\mathbf{T}}}$
PyoS2(C28-C157)‡-ImS2	77365	77240	84821.1	84820.9	84938.9$^{\overline{\mathbf{T}}}$

PyoS2(C103-C186)‡-ImS2	77365	77240	84792.1	84792.7	84906.2₸
PyoS2(C128-C162)‡-ImS2	75875	75750	84741.1	84741.4	84859.4₸
$PyoS2_{NTD}$‡	16390		24116.1	24116.9	
$PyoS2_{NTD}$-Cys‡	16390		24420.4	24422.4	
$PyoS2_{NTD}$(C11-C26)‡	10525	14900	24028.0	24026.2	24142.5₸
$PyoS2_{NTD}$(C103-C186)‡	16515	16390	24081.0	24079.2	24195.9₸
$PyoS2_{NTD}$(C128-C162)‡	15025	14900	24030.0	24028.2	24144.4₸
CntO*	84690		76879.2	Not Tested	
PyoSN‡-ImSN	70250		107325.4	107327.4	
PyoSNΔ1-52‡-ImSN	61770		102117.9	102117.2	
$PyoSN_{NTD}$‡	18910		23625.0	23625.0	
$PyoSN_{NTD}$Δ1-52	10430		18548.7	18548.9	
CntO*-$PyoSN_{NTD}$‡	103600		100504.2	Not Tested	
†TonB1(109-342)	6990		25473.4	25473.0	

‡Initiator Methionine cleaved.
†Includes TEV cleavage scar and GAM linker.
*N-terminal Signal sequence (residues 1-23) cleaved.
₸Contains two carboxyamidomethylcysteine residues.

2.7. Immunoblot Analysis.

P. aeruginosa strains PAO1, PAS033 and pMMB-SD-TB-Plug transformed PAS033 were grown overnight at 30 °C in an iron-deficient succinate medium (6 g/L K_2HPO_4, 3 g/L KH_2PO_4, 1 g/L $(NH_4)_2SO_4$, 0.2 g/L $MgSO_4.7H_2O$, 4 g/L succinic acid). Cells were harvested and lysed as described previously, and total cellular lysates run on a 12% acrylamide gel, followed by semi-dry blotting at 80 mA for 1 hour onto a Sequi-Blot polyvinylidene fluoride (PVDF) membrane (Bio-Rad). The blot was then blocked with 8% Marvel dried skimmed milk in Tris-buffered saline buffer (20 mM Tris-HCl pH 7.5, 500 mM NaCl) with 0.05% (v/v) Tween-20 (TBST) overnight at room temperature. The membrane was washed with TBST (5 times for 1 minute) then probed with primary rabbit α-FpvAI Antiserum, kindly provided by the Schalk lab (Voulhoux *et al.*, 2006) in TBST with 4% Marvel milk (1:250), for 1 hour at room temperature. Membrane was washed again with TBST (5 times for 1 minute) followed by incubation with secondary goat anti-rabbit IgG conjugated to horseradish peroxidase (A6154; Sigma-Aldrich) in TBST with 4% Marvel milk (1:1000) for

1 hour at room temperature. Membrane was washed again with TBST (5 times for 1 minute), followed by protein detection using Amersham enhanced chemiluminescence (ECL) Western Blotting Select Detection Reagent (GE Lifesciences), according to the manufacturer's instruction, in a GBOX-CHEMI-XRQ.

2.8.Pyocin Cytotoxicity and Activity Assays.

2.8.1. Plate-killing assays.

P. aeruginosa strains were grown in 5 ml LB unless stated otherwise, with antibiotics where appropriate, and incubated at 37 °C until an OD_{600nm} of 0.6 was attained. Bacterial lawns were prepared by addition of 200 µl culture to 10 ml of molten soft LB-agar (0.75% (w/v) agar in LB) at 50 °C and poured onto LB-agar plates. Once set and dry, 2 µl of serially diluted pyocin construct ranging from 10 µM to 57 pM were spotted onto the lawn. Plates were incubated overnight at 37 °C and cytotoxicity was determined through observation of clearance zones.

2.8.2. PyoS2 disulphide mutant Colony Forming Unit (CFU) quantification.

P. aeruginosa strain YHP17 was grown in 50 ml LB at 37 °C to an OD_{600nm} of 0.4. Cultures were subsequently split into 3 ml triplicates and 10 nM PyoS2 or PyoS2 variant was added. Cultures were incubated at 37 °C and the OD_{600nm} was monitored, with readings taken at 30 minute timepoints for 180 minutes. After 180 minutes, 1 ml of culture was taken and serially diluted between 10^0 to 10^6 -fold with LB, and 50 µl plated out onto LB-agar plates. Plates were incubated at 37 °C for 16 hours and the resulting colonies counted and utilised to calculate YHP17 colony forming unites per ml (CFU/ml) per culture.

2.8.3. PyoS2 kinetic time-course cytotoxicity assay.

P. aeruginosa strain YHP17 was grown in 50 ml LB at 37 °C to an OD_{600nm} of 0.4 and 10 nM of PyoS2 or PyoS2 variant was added. At time points of 0, 2, 5, 10, 15, 20, 25, 30, 45 and 60 minutes following incubation with pyocin, 900 µl sample of culture was removed and added to 100 µl of trypsin (final concentration of 1 mg/ml) in 20 mM $CaCl_2$, 0.1 M HCl pH 3.0. Samples were incubated with trypsin at 37 °C for 30 minutes. 100 µl of each time point were serially diluted from $10^0 – 10^8$ -fold with LB, and 3 µl spotted out onto LB-agar plates. Plates were incubated at 37 °C for 16 hours. Colonies were counted from each spot and the CFU/ml values were calculated and plotted as a pseudo-first order model for

translocation against time. The translocation rate constant was calculated from the fit gradient allowing calculation of the $t_{1/2}$ ($t_{1/2}$ = ln2/k). Experiments were performed in triplicate to generate standard errors.

2.9. Binding Assays.

2.9.1. Analytical Size Exclusion Chromatography.

Analytical size exclusion chromatography was performed on a Superdex 75 Increase 10/300 GL column (GE Healthcare) at a flow rate of 0.8 ml/min in 20 mM Tris-HCl pH 7.5, 150 mM NaCl. 100 µl protein samples were loaded onto the column using a 100 µl sample loop, which was filled with 150 µl of sample.

2.9.2. Isothermal Titration Calorimetry (ITC).

ITC was performed in a MicroCal iTC200 thermostated at 25 °C in 25 mM Tris-HCl pH 7.5, 150 mM NaCl. The sample cell contained TonB1 at 15 µM and the syringe contained either $PyoSN_{NTD}$ or $PyoSN\Delta1\text{-}52_{NTD}$ at 150 µM. After an initial injection of 0.5 µl, 15 injections of 2.0 µl were performed, spaced by 180 seconds. Binding isotherms were fitted with a single set of binding sites in Microcal LLC Origin software.

2.10. Biophysical Techniques.

2.10.1. Circular Dichroism (CD).

Proteins were dialysed into 10 mM potassium phosphate buffer pH 7.5 and concentration adjusted to 0.1 mg/ml. Far-UV spectra were obtained in triplicate using a Jasco J-815 Spectropolarimeter over a wavelength range of 260 – 190 nm, with a digital integration time of 1 second and a 1 nm bandwidth. Molar ellipticity was calculated by multiplying the baseline subtracted sample spectra by the molecular weight, then dividing by the molar concentration and the pathlength. Protein melting temperatures (T_m) were determined by measuring ellipticity at 222 nm across a temperature gradient of 20 °C to 86 °C.

2.10.2. Differential Scanning Calorimetry (DSC).

Proteins were dialysed into 20 mM Tris-HCl pH 7.5, 150 mM NaCl and analysed using a MicroCal VP-Capillary DSC System (Malvern). DSC was performed by Dr. David Staunton (Molecular Biophysics Suite, Department of Biochemistry, University of Oxford).

2.11. X-ray Crystallography.

2.11.1. Crystallisation.

The CntO:PyoSN$_{NTD}$ complex (11.0 mg/ml) and the isolated PyoSN$_{NTD}$ (15.7 mg/ml) were crystallised by sitting drop vapour diffusion in 96-well MRC 2-drop plates (SWISSCI) at 18 °C. A Mosquito robot (TTP Labtech) was used to mix and dispense a 200 nl drop into the plates with a 1:1 ratio of protein to crystallant. Crystallisation of the CntO:PyoSN$_{NTD}$ complex was trialled in MemGold, MemGold2, MemPlus, PGA and ProPlex commercial screens (Molecular Dimensions). Crystallisation of the isolated PyoSN$_{NTD}$ was trialled in Morpheus, Morpheus II, MIDAS and JCSG+ commercial screens (Molecular Dimensions). Crystals of the CntO:PyoSN$_{NTD}$ complex were observed across multiple conditions (discussed in Chapter 4), whereas PyoSN$_{NTD}$ only crystallised in Morpheus II screen condition E3 containing 10% (w/v) PEG 8000, 20% (v/v) 1,5-pentanediol, 0.1 M MOPSO, Bis-Tris pH 6.5, 0.02 M lanthanides (0.005 M yttrium(III) chloride hexahydrate, 0.005M erbium(III) chloride hexahydrate, 0.005M terbium(III) chloride hexahydrate, 0.005M ytterbium(III) chloride hexahydrate). Crystals were harvested 40 days after appearance and flash cooled in liquid nitrogen prior to data processing.

2.11.2. X-Ray diffraction data collection.

X-ray diffraction data was collected for a single cryo-cooled crystal at the European Synchrotron Radiation Facility (ESRF) on the beamline IO-4 microfocus with a beam size of 31.7 x 20.0 µm using an Eiger2 XE 16M detector (Dectris). X-ray wavelength was fixed at 0.9795 Å. Diffraction data was collected for a total of 360° extending to a resolution of 1.8 Å with a 0.1° oscillation using an exposure time of 0.01 seconds at 20% transmission.

2.11.3. Data processing, refinement, and validation.

Initial X-ray diffraction data processing was indexed and integrated using Dials v3.4.0 and scaled initially with Aimless, before returning to DIALS in CCP4i2 v7.1.009 suite. The

initial structure was solved by Dr. Edward Lowe (Crystallisation Facility, Department of Biochemistry, University of Oxford) by experimental phasing using single-wavelength anomalous dispersion (SAD) utilising Shelxd for initial substructure identification, followed by Phaser for phase calculation and completion of the substructure (McCoy *et al.*, 2007). This revealed an anomalous substructure containing 10 metal ions. These were modelled as Er^{3+}. Parrot was utilised for density modification for management of NCS within the model. Crystallographic refinement was performed using Phenix v1.19 (Adams *et al.*, 2010) and REFMAC v5.8.0267 (Murshudov *et al.*, 2011). Subsequent manual model building and manipulation was carried out in Coot v0.8.9.2 (Emsley *et al.*, 2010). The final structure was validated using MolProbity (Williams *et al.*, 2018).

2.11.4. Structure analysis.

The molecular graphics program PyMOL v2.4.1 (Delano, 2002) was used for protein structure analysis and for generation of figures.

2.12. Fluorescence Microscopy.

2.12.1. Conjugation of maleimide fluorophores to proteins.

A C-terminal cysteine residue with an intermediate flexible GSG linker was introduced following the HisTag of PyoS2$_{NTD}$ by site directed mutagenesis. The protein was expressed as described previously, followed by incubation with 5 mM DTT for 2 hours at room temperature to reduce cysteines, ensuring a monomeric population. The protein was buffer exchanged into 20 mM potassium phosphate pH 7.0, 500 mM NaCl to remove DTT using a 5 ml HiTrap desalting column (GE Healthcare). A fivefold molar excess of AF488 C5 maleimide was added to the protein sample to label free cysteines. The labelling reaction was incubated for 1 hour with gentle inversion in the dark at room temperature. The reaction was subsequently quenched with 10 mM DTT and the protein-fluorophore conjugate separated from excess free dye using a HiTrap desalting column. The protein-fluorophore conjugate was then further purified using a HiLoad 16/60 Superdex 200 pg column (GE Healthcare). The absorbance of PyoS2$_{NTD}$-AF488 was measured at 280 nm and 494 nm using a V-550 UV-Visible Spectrophotometer (Jasco). The labelling efficiency was estimated spectrophotometrically utilising the protein and fluorophore extinction co-

efficients ($PyoS2_{NTD}$ ε_{280nm} = 163900 $cm^{-1}M^{-1}$, Alexa Fluor 488 ε_{max} = 71,000 $M^{-1}cm^{-1}$) and correction factors for absorption at 280 nm by the fluorophore (A_{280nm} = 0.11 x A_{494nm}).

2.12.2. Fluorescent labelling of *P. aeruginosa* cells.

Overnight cultures of *P. aeruginosa* were used to inoculate 5 ml M9-glucose media (6.78 g/L Na_2HPO_4, 3 g/L KH_2PO_4, 0.5 g/L NaCl, 10 mM D-glucose, 1 mg/ml NH_4Cl, 2 mM $MgSO_4$) and incubated at 37 °C. Once an OD_{600nm} of 0.6 was reached, 1 ml of culture was pelleted by centrifugation at 7000 g for 3 minutes. Cells were resuspended in M9-glucose media with 1 µM $PyoS2_{NTD}$-AF488 and incubated for 15 minutes in the dark with gentle inversion at room temperature. Cells were washed to remove excess $PyoS2_{NTD}$-A488 label through pelleting and resuspension in M9-glucose media three times. After a final resuspension into an appropriate volume of M9-glucose (typically 10 – 100 µl dependent on cell pellet size), 10 µl of cellular suspension was loaded onto a 1% (w/v) agarose pad for imaging. 1% (w/v) agarose pads were prepared by loading 190 µl of molten M9-glucose media with 1% (w/v) agarose into a Geneframe matrix (Thermo Scientific) adhered to a clean microscope slide. A clean coverslip was then added on top to flatten the pad surface. Once solidified, the coverslip was removed and bacterial suspensions were loaded onto the pad, followed by the addition of a new coverslip to the adhesive side of the Geneframe matrix to seal.

2.12.3. Image acquisition and processing.

All images were collected on an Oxford Nanoimager S microscope at 100 ms exposure. For every image 200 frames were collected and averaged. Green fluorescence was measured at 35% A474 laser power. Frames were averaged together in the z direction in Fiji (Schindelin *et al.*, 2012) to generate an averaged image, and single cells identified in binarized trans-illumination images. Regions of interest were subsequently transferred to images taken in the fluorescence channel and average fluorescence intensity in regions of interest was extrapolated. A minimum of 50 bacterial cells were quantified for each sample. Students t-tests were performed to determine *p*-values.

Chapter 3 – Identification of the Pyocin SN Translocation Components

3.1. Introduction.

Identification of novel CLBs from Gram-negative bacterial genomes has often proven challenging due to the diversity of the sequences encoding them. Functional domains required for bacteriocin cytotoxic activity and translocation across the cell envelope exhibit extensive sequence variability, with reorganisation between these modular domains producing a plethora of unique and highly distinct bacteriocin sequences. However, recent developments have facilitated the identification of several putative nuclease-type CLBs *in silico* through a bioinformatic pipeline that applies Hidden-Markov models to search for conserved motifs within bacteriocin nuclease domains, and their associated immunity proteins (Sharp *et al.*, 2017). One such gene identified was *pyoSN*; a nuclease-type pyocin with confirmed cytotoxic activity against *P. aeruginosa* (Sharp *et al.*, 2017).

pyoSN encodes an 832 amino acid protein toxin containing a putative C-terminal non-HNH cytotoxic DNase domain. This domain is homologous to the C-terminal domain of Pyocin S3 (PyoS3), which has previously been demonstrated to exhibit DNase activity *in vitro* (Duport *et al.*, 1995). Alignment of PyoSN with PyoS3 (**Appendix Alignment I and II**) shows high sequence identity between the two proteins, localised to the middle and C-terminal domains. However, the sequence identity diverges significantly in the N-terminal regions (Figure 3-1), with PyoSN encoding a novel N-terminal domain that is unique within the S-type pyocin family. S-type pyocins are known to bind their target OM receptors/translocators through their NTDs, which additionally function to energise import across the OM (Sano *et al.*, 1993; White *et al.*, 2017; Behrens *et al.*, 2020). Therefore, it was hypothesised that the unique N-terminal domain of PyoSN likely reflects a novel OM receptor/transporter required for OM translocation, making it an attractive target for the development of new antimicrobial therapeutics to treat *P. aeruginosa* infections.

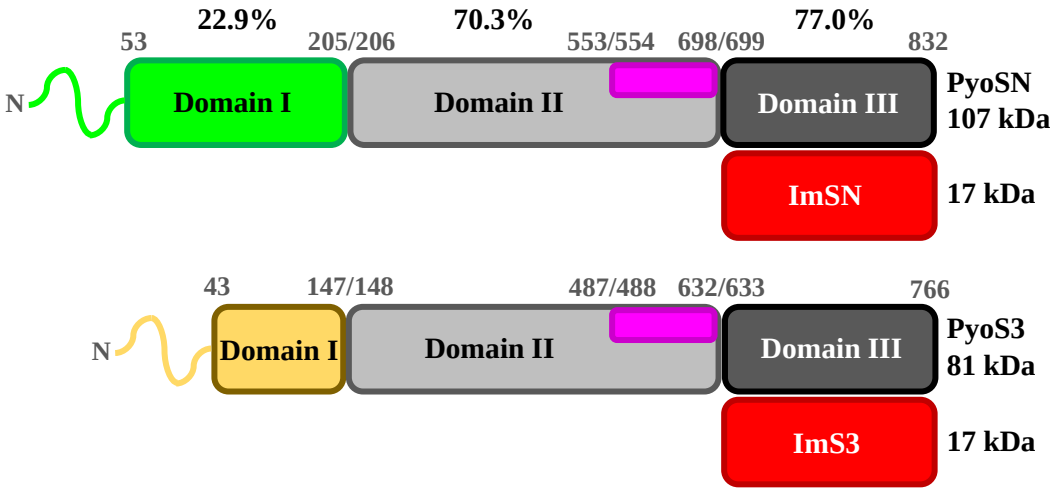

Figure 3-1. Comparison of domain architecture of PyoSN and PyoS3.
Predicted domain architecture and sequence identity (*above*) of PyoSN and PyoS3 aligned using CLUSTAL Omega. Domain boundaries between Domain I and Domain II were identified due to low sequence identity observed (22.9%) at the N-termini of PyoS3 (*beige*) and PyoSN (*green*). Residues 1 – 42 and 1 – 52 of PyoS3 and PyoSN respectively, are predicted to be disordered using PSIPRED (Jones, 1999). Both pyocins contain a Pyocin_S domain (*pink*) (Pfam Domain PF06958) conserved across all nuclease-type bacteriocins, which defines the boundary between Domain II and Domain III. The C-terminal DNase domain (III) is bound by a high affinity immunity protein, ImS3/ImSN. Overall sequence identity between PyoS3 and PyoSN is 62.6%.

In this chapter, I describe the expression and purification of PyoSN and its efficacy as a toxin against a panel of *P. aeruginosa* clinical isolates. I subsequently identified the components of the cellular envelope that are required for PyoSN cytotoxicity *in vivo*, resulting in a proposed model for import. This culminated in the identification of CntO, a novel metallophore receptor, as the primary OM receptor/translocator for PyoSN. Finally, I demonstrate that PyoSN activity is tightly modulated in response to availability of the transition metal ion zinc.

3.2. Results.

3.2.1. Expression and purification of the PyoSN-ImSN Complex.

PyoSN was heterogeneously expressed in *E. coli* BL21(DE3) cells encoded on an IPTG inducible pET24-a(+) plasmid, in complex with its inhibitor ImSN-His_6 to circumvent lethality upon expression. Successful expression also required co-transformation with an additional inducible plasmid carrying the ImSN-His_6 protein alone to further suppress PyoSN-mediated cytotoxicity. The PyoSN-ImSN complex was purified using Ni^{2+}-affinity chromatography, followed by SEC (Figure 3-2).

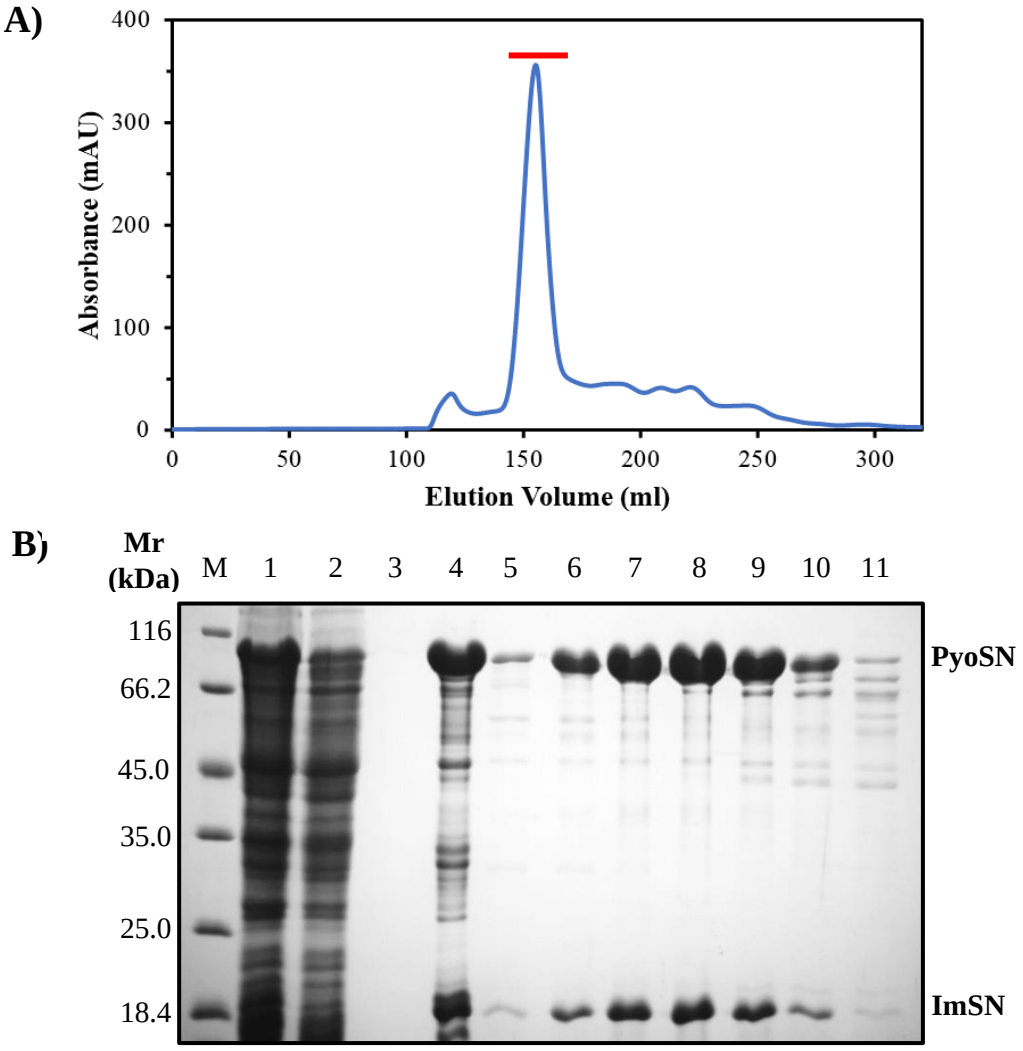

Figure 3-2. Purification of PyoSN-ImSN.
A) Elution profile of the PyoSN-ImSN complex from a Superdex 200 26/60 column with A_{280nm} in blue. Elution fractions for peak corresponding to the complex are highlighted in red. B) 12% polyacrylamide gel of steps of the Ni^{2+}-affinity and size exclusion chromatography purification procedure of PyoSN-ImSN. M, unstained protein marker (Pierce), 1, Cleared cell lysate, 2, HisTrap Flow Through, 3, VivaSpin concentration flow through, 4, SEC Input, 5 – 11, Elution fractions corresponding to UV absorbance peak from A)

The cytotoxic activity of purified PyoSN was assessed using a plate-based toxicity assay. This assay spots purified pyocin onto a lawn of *P. aeruginosa* cells and surveys for areas of clearance indicative of pyocin induced killing. Serial dilutions of the PyoSN-ImSN complex generated zones of clearance in *P. aeruginosa* strain PAO1 lawns down to 1.5 nM (Figure 3-3).

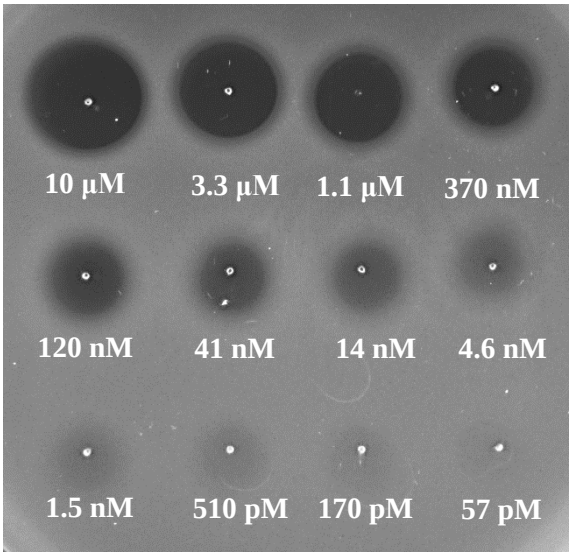

Figure 3-3. Activity of PyoSN against *P. aeruginosa* strain PAO1.
Plate-killing assay demonstrates *P. aeruginosa* strain PAO1 is susceptible to PyoSN activity down to the low nM range. PyoSN serial dilutions were spotted onto *P. aeruginosa* lawns at concentrations ranging from 10 µM (*top left*) to 57 pM (*bottom right*). Zones of clearance result from cell killing.

3.2.2. PyoSN kills a broad range of *P. aeruginosa* clinical isolates.

Despite possessing potent antimicrobial activity against PAO1, the effectiveness of PyoSN against other *P. aeruginosa* strains, particularly ones of clinical relevance, is currently unknown. To investigate the efficacy of PyoSN, killing activity was assessed against a library of 32 *P. aeruginosa* clinical isolates (in collaboration with Dr. Khedidja Mosbahi, University of Glasgow). PyoSN was found to be active against the majority (~85 %) of the clinical isolate strains tested (Figure 3-4). PyoSN displays a broad spectrum of antimicrobial activity against the susceptible strains, with many exhibiting MICs in the nM range. This not only underpins the therapeutic potential of PyoSN to combat pathogenic *P. aeruginosa* strains, but additionally that the import machinery parasitized by PyoSN is well conserved within *P. aeruginosa* genomes.

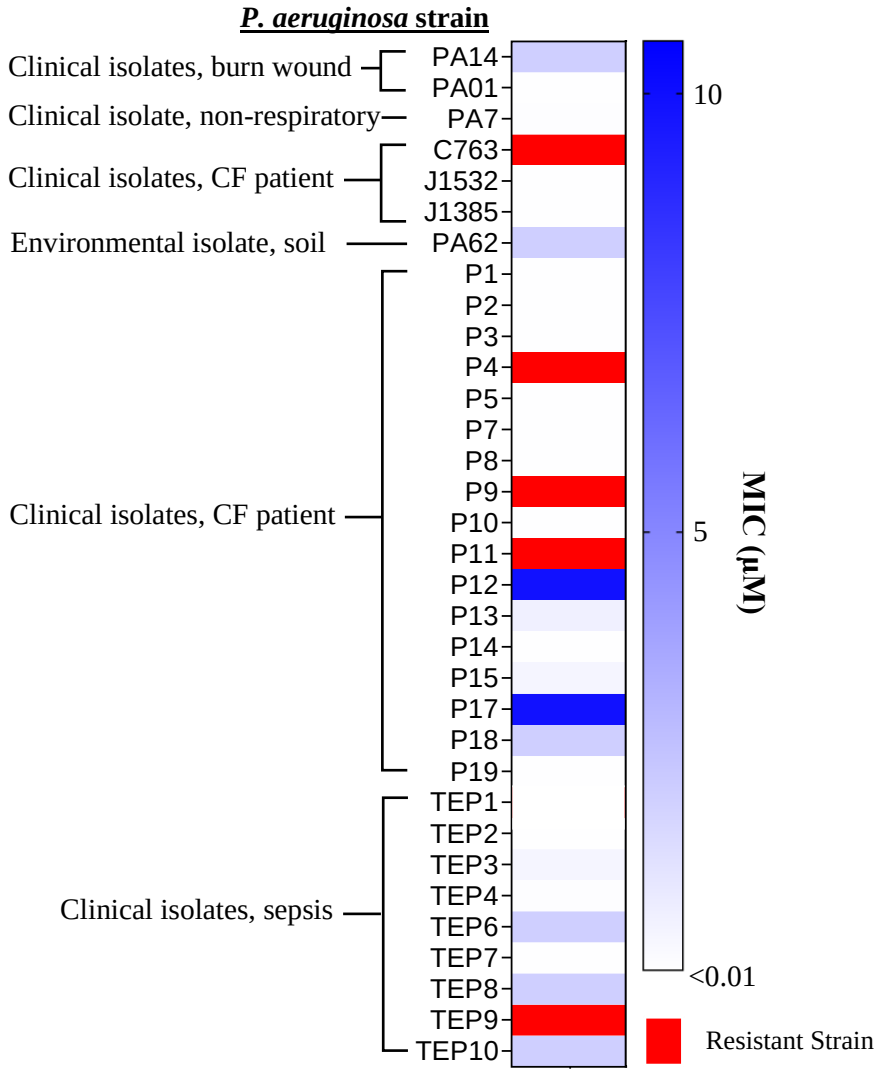

Figure 3-4. Activity of PyoSN against *P. aeruginosa* clinical isolates.
Minimum inhibitory concentrations (MICs) from plate-killing assays for PyoSN-dependent cytotoxicity against *P. aeruginosa* clinical isolate strains. MIC values are represented as increasing intensities of blue for susceptible strains and resistant strains are represented in red. 28 of the 33 of strains screened are sensitive to PyoSN activity. Experiments were performed by Dr. Khedidja Mosbahi, Institute of Immunity, Infection & Inflammation, University of Glasgow.

3.2.3. Identification of components of the cell envelope required for PyoSN cytotoxicity.

Like other S-type pyocins, PyoSN must parasitize proteins within the cell envelope during import. To identify the components utilised by PyoSN during import, PAO1 knockout mutants were assessed for PyoSN susceptibility. In these mutants, genes encoding cell envelope proteins, commonly parasitized during the import of pyocins (and colicins), were knocked out by transposon insertion.

All S-type pyocins to date have been demonstrated to hijack the Ton complex to energise import across the OM (White *et al.*, 2017; Latino *et al.*, 2019; Behrens *et al.*, 2020). Therefore, *P. aeruginosa* knockout strains for the three *tonB* genes present were screened for PyoSN susceptibility. Plate-killing assays show that the *tonB1* knockout (K1040) alone was resistant to PyoSN activity, whereas both *tonB2* (K1407) and *tonB3* (MS231) knockouts remained susceptible (Figure 3-5), demonstrating PyoSN cytotoxicity is TonB1-dependent.

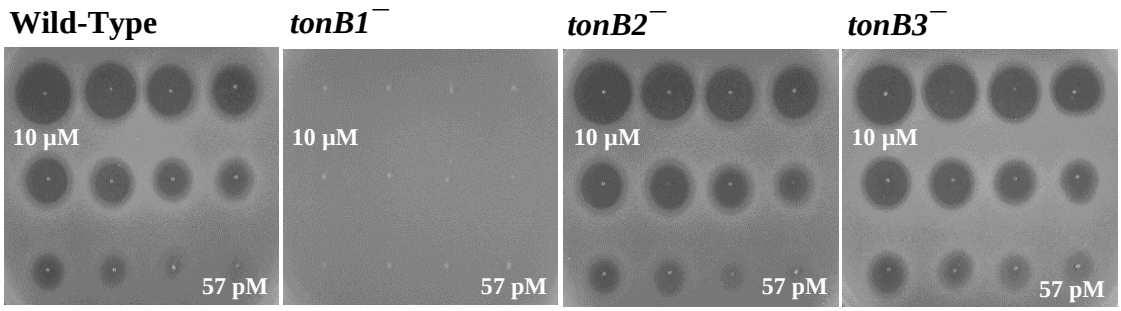

Figure 3-5. PyoSN cytotoxicity is TonB1-dependent.
PyoSN plate-killing assays with *P. aeruginosa tonB* knockout strains PA06609 (parent strain), K1040 (*tonB1*¯), K1407 (*tonB2*¯) and MS231 (*tonB3*¯) grown in LB supplemented with 100 µM $FeCl_3$ to prevent limitation of cell growth. Zones of clearance indicate cell killing. Only the *tonB1* knockout strain was resistant to PyoSN activity.

As PyoSN was found to hijack the Ton complex to induce cell killing, it was reasoned that its OM translocator could also be a member of the TonB-dependent Transporter (TBDT) family – required for the import of other S-type pyocins (White *et al.*, 2017; Behrens *et al.*, 2020; Atanaskovic *et al.*, 2020). To test this hypothesis, a mutant library comprising knockouts of all TBDTs encoded within the PAO1 genome, discussed in **Table 1-1**, was screened for PyoSN susceptibility. This library was assembled through identification of genes containing the 'TonB-dependent receptor plug domain' (Pfam Domain PF07715), which generated 35 prospective TBDTs. Plate-killing assays identified a single PAO1 knockout strain (PW9134) with resistance to PyoSN activity (Figure 3-6). This knockout contained a transposon insertion within the gene locus PA4837, encoding for the putative TBDT *cntO*. Complementation of the knockout strain with a plasmid containing *cntO* (p*cntO*) restored PyoSN killing (Figure 3-7), indicating CntO is the OM translocator for PyoSN.

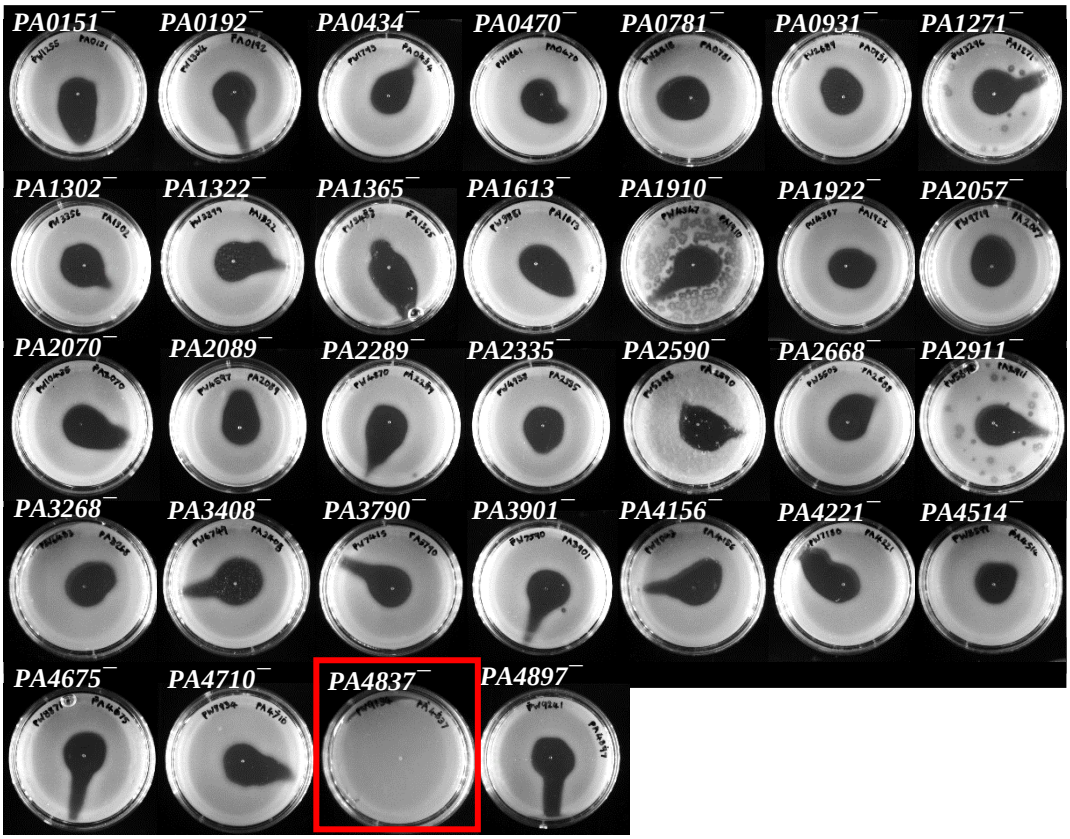

Figure 3-6. Identification of the OM receptor/transporter of PyoSN.
PyoSN plate-killing assays with *P. aeruginosa* TBDT knockout strain library. Knockouts of the genes *fpvAI*, *fpvB* and *foxA* were not screened for PyoSN susceptibility. Zones of clearance result from cell killing. Only the *P. aeruginosa* knockout for the gene PA4837 was found to resistant to PyoSN activity.

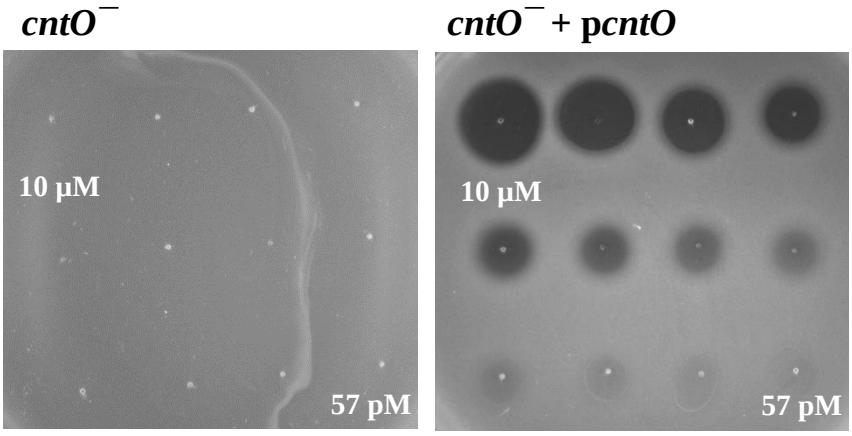

Figure 3-7. PyoSN cytotoxicity is CntO dependent.
Plate-killing assay demonstrates that *P. aeruginosa cntO*⁻ knockout strain (PW9134) is resistant to PyoSN cytotoxicity. Introduction of a plasmid encoding *cntO* restores susceptibility to PW9134 strain, demonstrating PyoSN cytotoxicity is CntO dependent. Zones of clearance result from cell killing.

An additional cell envelope component that could also play a role in PyoSN cytotoxicity is the OM polysaccharide CPA. Several S-type pyocins contain domains that specifically bind CPA *in vitro*, including homologues of PyoS3 (McCaughey, Josts, *et al.*, 2016). Therefore, PyoSN was evaluated for the presence of a putative CPA-binding motif through sequence alignment with the CPA-binding domain (residues 195-315) of PyoS5. No sequence homology to the CPA-binding domain could be identified within the PyoSN sequence (**Appendix Alignment III**), suggesting PyoSN does not bind CPA in the *P. aeruginosa* cell envelope. This was confirmed through killing assays comparing PyoSN activity to that of PyoS5-Ia against a CPA deficient *P. aeruginosa* strain (PAO1*Δrmd*). PyoS5-Ia is an S-type pyocin-colicin fusion (that subverts PyoS5 resistance in the PAO1 parent strain utilising a ColIa cytotoxic domain) containing a well-characterised CPA-binding domain (Behrens *et al.*, 2020) with reduced cytotoxic activity against PAO1*Δrmd*. No significant difference in susceptibility to PyoSN was observed for the CPA-deficient strain *in vivo* (Figure 3-8). Therefore, CntO is likely the sole OM component involved in PyoSN translocation.

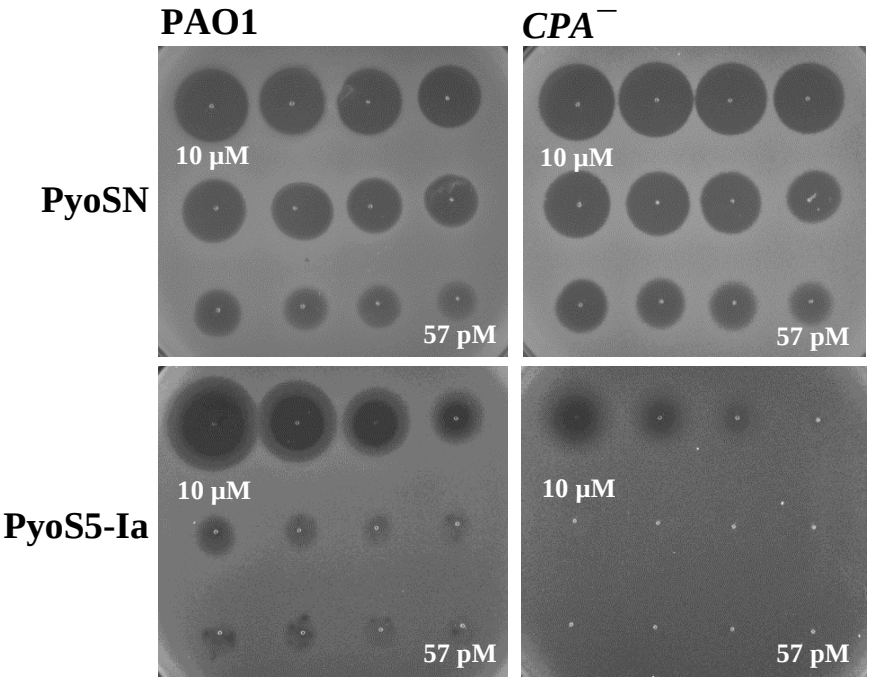

Figure 3-8. PyoSN cytotoxicity is not CPA-dependent.
Plate-killing assay confirm PyoSN cytotoxicity is CPA-independent as no significant decrease in activity is observed against *P. aeruginosa* CPA knockout strain PAO1*Δrmd.* Zones of clearance result from cell killing.

In addition to OM translocation, nuclease CLBs like PyoSN must also deliver their cytotoxic C-terminal domains across the IM to elicit killing. The mechanism by which this process occurs is thought to involve the inner membrane AAA+ ATPase/protease FtsH. The precise role that FtsH plays in the IM translocation step of bacteriocin uptake is currently unknown, however it has recently been shown that it is essential for PyoG activity *in vivo* (Atanaskovic *et al.*, 2020). As PyoSN is also a nuclease-type pyocin, a *P. aeruginosa ftsH* knockout strain (grown in LB with no salt present to subvert sensitivity) was tested for PyoSN sensitivity. Plate-killing assays show the *ftsH* knockout also confers resistance to PyoSN killing (Figure 3-9), supporting its requirement for the import of nuclease-type pyocins in *P. aeruginosa*.

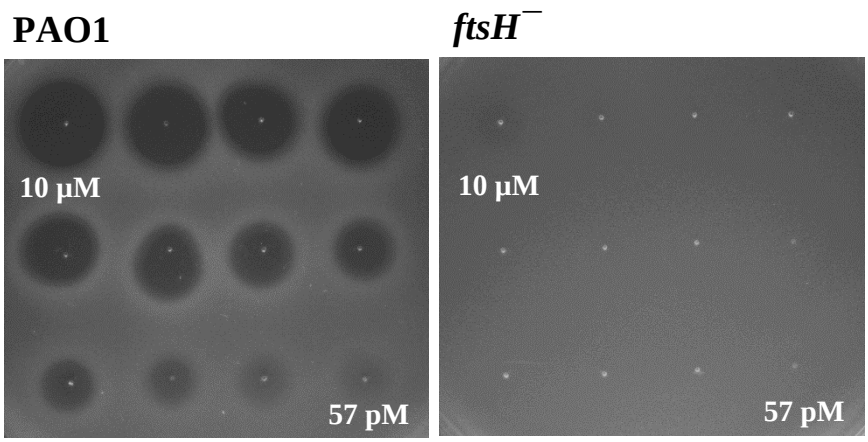

Figure 3-9. PyoSN cytotoxicity is FtsH dependent.
Plate-killing assay demonstrates that *P. aeruginosa ΔftsH* knockout strain is resistant to PyoSN cytotoxicity. Zones of clearance result from cell killing. This loss of activity is likely a result of failure of the PyoSN cytotoxic domain to translocate across the IM.

From the results presented in this subsection, several components of the PyoSN translocation machinery have now been identified. CntO likely functions as the sole OM component, functioning as both a receptor and translocator for PyoSN, with import energised via coupling to the TonB1 complex. Once in the periplasm, PyoSN translocates across the IM in an FtsH-dependent manner.

3.2.4. CntO is the only protein encoded by *cnt* operon involved in PyoSN cytotoxicity.

cntO encodes a putative OMP with predicted TBDT architecture and is organised within the *cnt* operon. This operon comprises four genes that encode proteins required for the synthesis, secretion and uptake of the metallophore pseudopaline (Lhospice *et al.*, 2017). As these

genes are co-transcribed, it was unclear whether the additional three genes within the operon were also involved in PyoSN cytotoxicity. Therefore, PAO1 knockouts of the cognate genes that comprise the *cnt* operon were assessed for PyoSN activity. Both plate- and liquid-killing assays confirmed that only the CntO knockout conferred resistance to PyoSN, whilst knockouts for genes encoding the proteins CntL, CntM and CntI remained susceptible (Figure 3-10).

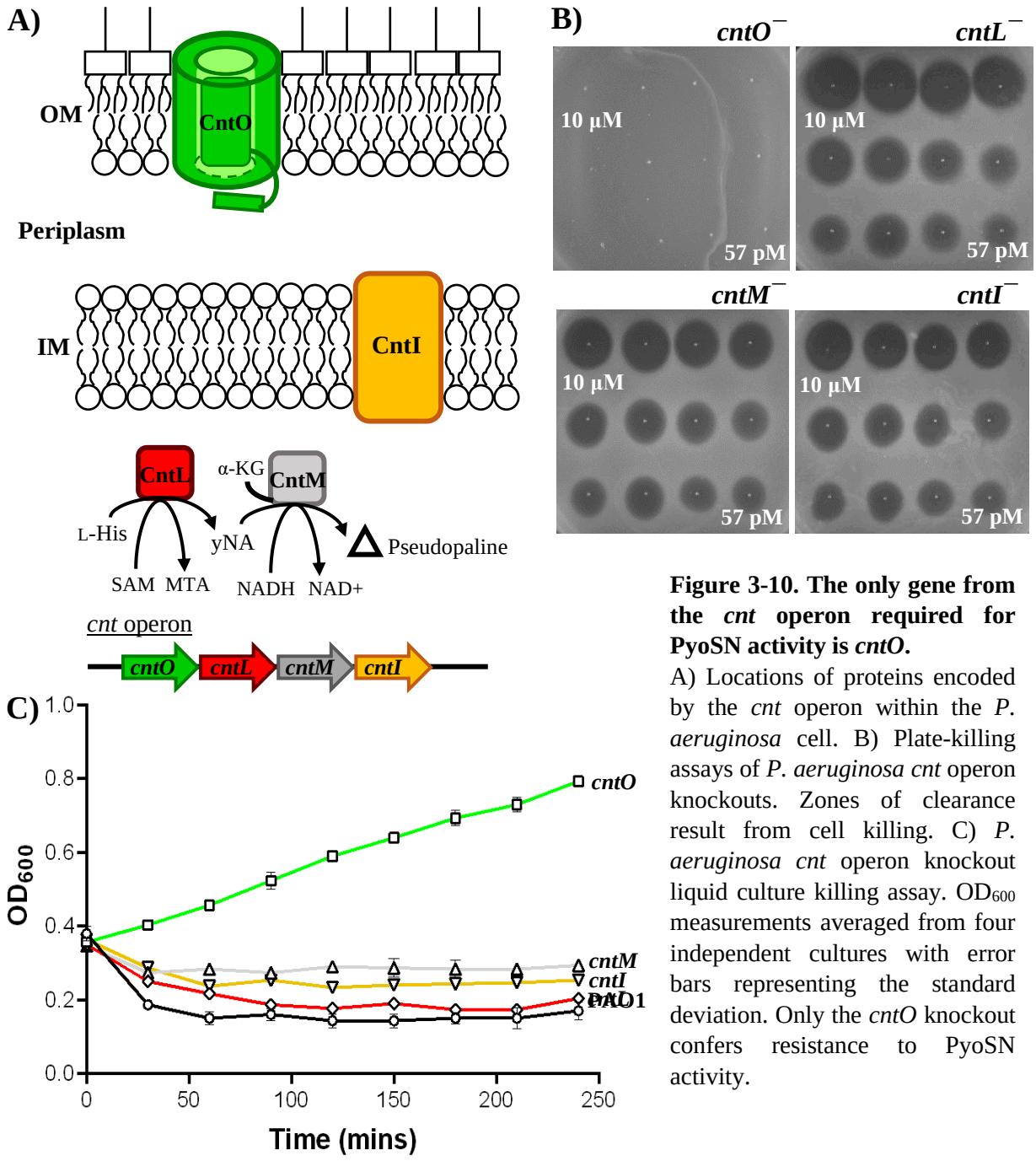

Figure 3-10. The only gene from the *cnt* operon required for PyoSN activity is *cntO*.
A) Locations of proteins encoded by the *cnt* operon within the *P. aeruginosa* cell. B) Plate-killing assays of *P. aeruginosa cnt* operon knockouts. Zones of clearance result from cell killing. C) *P. aeruginosa cnt* operon knockout liquid culture killing assay. OD_{600} measurements averaged from four independent cultures with error bars representing the standard deviation. Only the *cntO* knockout confers resistance to PyoSN activity.

3.2.5. Influence of zinc on PyoSN activity.

Expression of the *cnt* operon has been shown to be regulated in response to intracellular zinc concentrations. The *cnt* operon contains a Zur-binding box at its σ^{70} promotor region that, in Zn-rich conditions, binds the Zur repressor, downregulating operon expression (Lhospice *et al.*, 2017). To assess the influence of zinc on PyoSN activity, PAO1 cells were grown in LB supplemented with 2 mM $ZnSO_4$. Plate-killing assays showed a reduction in PyoSN activity against cells grown in the presence of excess Zn, likely resulting from suppression of CntO expression (Figure 3-11).

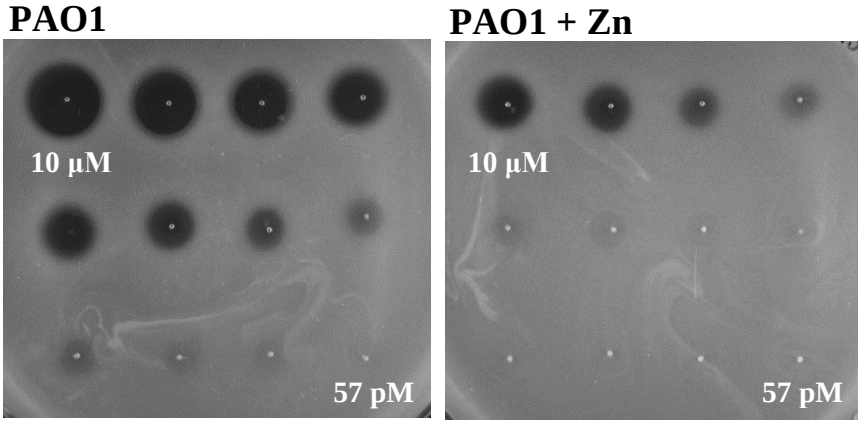

Figure 3-11. Increased zinc concentrations suppress PyoSN cytotoxicity.
Plate-killing assay demonstrates that *P. aeruginosa* PAO1 grown in LB supplemented with 2 mM $ZnSO_4$ have reduced susceptibility to PyoSN cytotoxicity, likely due to downregulation of CntO expression. Zones of clearance result from cell killing.

To further examine the effects of perturbations in zinc homeostasis on PyoSN activity, knockout mutants for components of the Znu transporter (ZnuABC), an IM ABC transporter and primary Zn-uptake pathway of *P. aeruginosa*, were assessed for susceptibility to PyoSN. Plate-killing assays with knockout mutants of the three components that comprise the Znu complex were shown to be increasingly susceptible to PyoSN cytotoxicity when grown in zinc-limited conditions (Figure 3-12). Loss of components of the ZnuABC transporter disrupts the zinc homeostasis of the cell when extracellular zinc is limited, resulting in upregulation of alternative zinc acquisition pathways such as the *cnt* operon (Mastropasqua *et al.*, 2017). Upregulation of CntO expression likely explains the increased susceptibility observed in these cells to PyoSN activity.

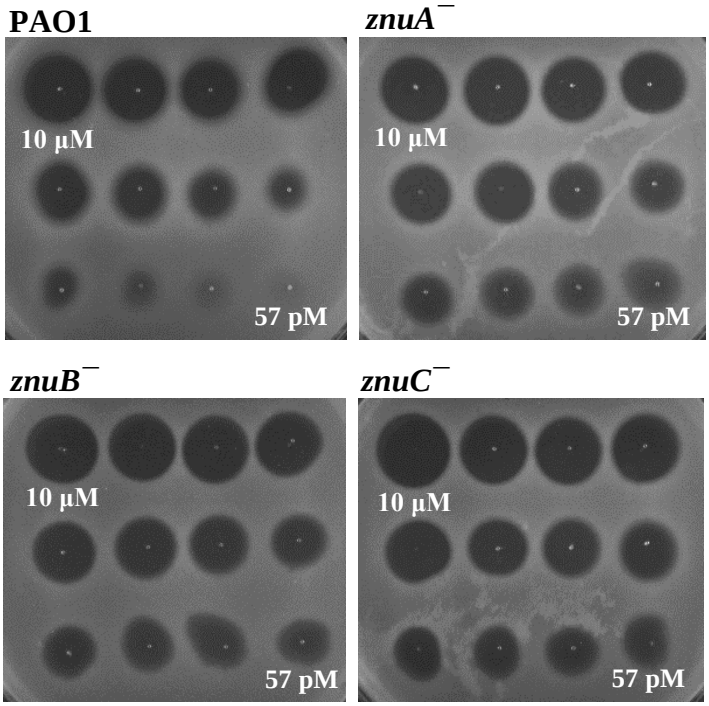

Figure 3-12. Loss of the Znu transporter increases susceptibility to PyoSN.
Plate-killing assay demonstrates that *P. aeruginosa* knockouts PW10299 (*znuA*$^{-}$), PW10306 (*znuB*$^{-}$) and PW1030 (*znuC*$^{-}$) grown in M9-gluocse are significantly more susceptible to PyoSN cytotoxicity that the wild-type PAO1 strain. PAO1 killing efficiency of PyoSN against PAO1 marginally increases under these conditions. Zones of clearance result from cell killing.

3.3. Discussion.

The results presented in this chapter identify several translocon components required for the import of PyoSN, a newly identified pyocin, across the cell envelope. To bypass the OM, PyoSN requires a TBDT, CntO, which likely functions as both the OM receptor and translocator. Import across the OM is energised through coupling to TonB1, part of the IM Ton system. Once in the periplasm, PyoSN translocates across the IM in an FtsH-dependent manner through a presently undescribed mechanism (Figure 3-13).

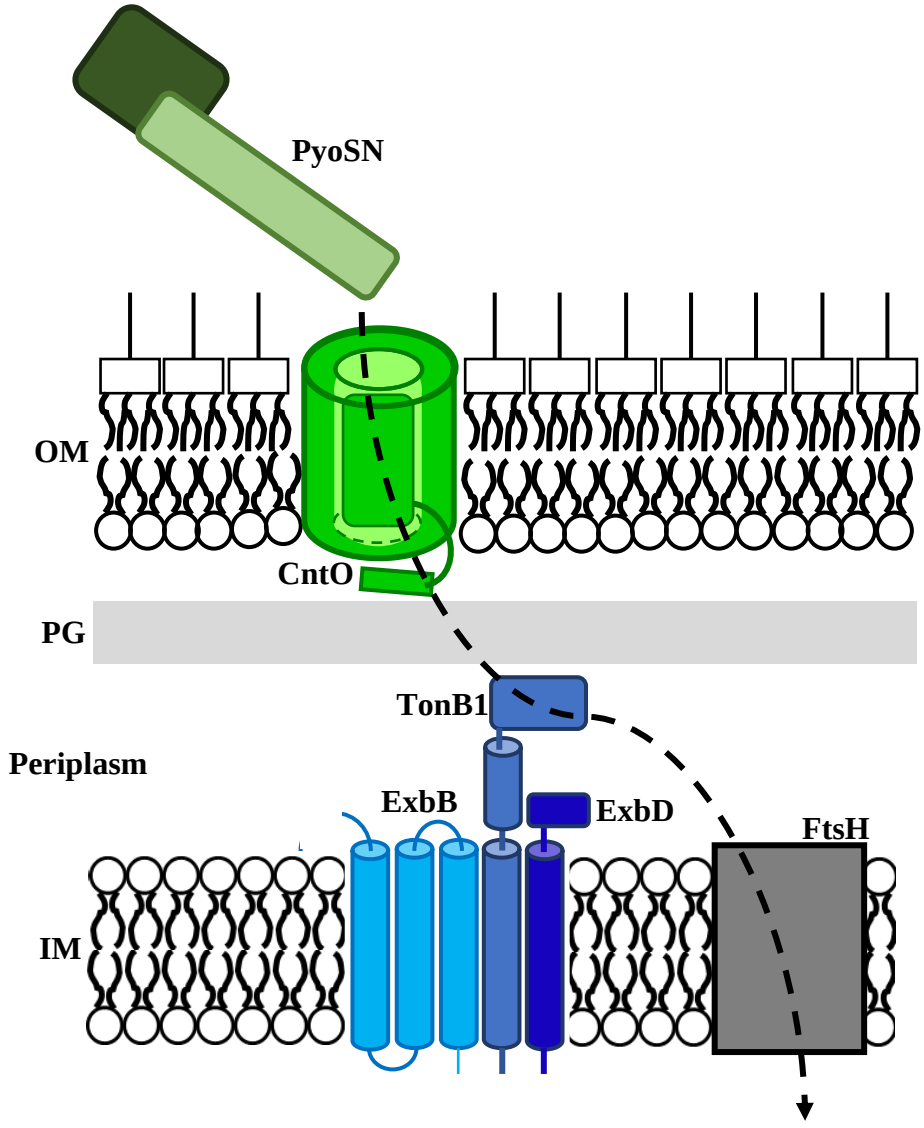

Figure 3-13. Proposed model of PyoSN import across the *P. aeruginosa* cell envelope. PyoSN parasitizes CntO (*light green*) as both the OM receptor and translocator. PyoSN also hijacks the TonB1 complex comprised of TonB1, ExbB and ExbD (*blue*), which links the PMF across IM with pyocin translocation across the OM. Import of the PyoSN cytotoxic domain (*dark green*) across the IM FtsH (*grey*).

Identification of many of these cell envelope components as requisite for PyoSN import is not wholly unsurprising, as they appeared to be well conserved in the import mechanisms of many CLBs (Cascales *et al.*, 2007). For example, the S-type pyocins PyoS2 and PyoS5 both parasitize TBDTs, FpvAI and FptA respectively, for import across the OM. Furthermore, this translocation process is also TonB1-dependent, with TonB1 binding to TonB1 boxes located within both the TBDT and the pyocin N-terminus. These interactions with the Ton system are required to energise import in a PMF-dependent manner (White *et al.*, 2017; Behrens *et al.*, 2020). It is thought that interactions with the TonB1 complex energise the forced remodelling of the TBDT plug domain, generating a pore through which the pyocin diffuses (Hickman *et al.*, 2017; White *et al.*, 2017). This allows exposure of the pyocins TonB box to the periplasm, facilitating energised import through the translocator. The utilisation of a TBDT as an OM receptor/transporter, in addition to hijacking the TonB1 complex for import, suggests that translocation across the OM occurs through a similar mechanism to that demonstrated for PyoS2 (White *et al.*, 2017).

CLBs are dichotomous in the number of OMPs required for translocation; with some requiring a single OMP and others requiring recruitment of additional OMPs. For example, ColE9 initially binds the TBDT BtuB but translocates through the general porin OmpF (Housden *et al.*, 2005). In contrast, all previously described pyocins utilise a sole TBDT during import (White *et al.*, 2017; Behrens *et al.*, 2020), thus it is likely that PyoSN is imported through CntO alone. Whether translocation of PyoSN occurs directly through the specific CntO receptor/translocator, or via the recruitment of an additional CntO transporter, similar to that demonstrated for ColIa import (Jakes & Finkelstein, 2010), is unknown, although the former is more likely to be the case. In addition to binding OMPs, several pyocins have been shown to bind CPA as a cell surface receptor (McCaughey, Josts, *et al.*, 2016). Due to its sequence similarity to PyoS3, which binds CPA *in vitro*, it was initially predicted that PyoSN would also bind to the *P. aeruginosa* cell surface through CPA. However, no homologous CPA binding domain could be identified in PyoSN and furthermore, PyoSN cytotoxicity assays against a CPA-deficient PAO1 mutant strain demonstrated no change in susceptibility. Taken together, it is likely that PyoSN only binds CntO at the extracellular surface.

S-type pyocins have been previously demonstrated to parasitize the TBDT siderophore receptors involved in iron acquisition such as FpvAI, FpvAII, FptA and FiuA (Baysse *et al.*, 1999; Elfarash *et al.*, 2012, 2014; Latino *et al.*, 2019). In addition, the recently characterised

pyocins PaeM4 and PyoG were found to utilise the HxuC/Hur receptor for import, which is required for acquisition of hemin (Ghequire & Öztürk, 2018; Atanaskovic *et al.*, 2020). Instead, CntO functions as the receptor for the broad-spectrum metallophore pseudopaline (Lhospice *et al.*, 2017). Whilst the identity of the primary metal ion chelated by pseudopaline for import is disputed, there is an intimate association between the Cnt machinery and the transition metal ion zinc (Mastropasqua *et al.*, 2017; Lhospice *et al.*, 2017). Expression of the *cnt* operon is negatively regulated by zinc through binding of the Zur repressor under zinc-rich conditions (Lhospice *et al.*, 2017). Indeed, PyoSN cytotoxic activity is severely diminished in *P. aeruginosa* cells supplemented with excess zinc. In addition, loss of the IM ZnuABC transporter, the primary zinc uptake pathway in *P. aeruginosa*, significantly increased susceptibility to PyoSN in zinc-restricted growth conditions. The role of zinc acquisition in *P. aeruginosa* pathogenesis is an emerging topic of study, with several transcriptomic analyses demonstrating upregulation of genes involved in zinc uptake, including CntO, during chronic lung infection, suggesting it is crucial for survival in these zinc-depleted environments (Palmer *et al.*, 2005; Son *et al.*, 2007). In addition, polymorphisms within the *cnt* promotor sequence have been described that result in less stringent repression of the operon by Zur during the establishment of chronic *P. aeruginosa* infections (Hermansen *et al.*, 2018). PyoSN therefore presents a potentially attractive CLB for therapeutic development to target *P. aeruginosa* infections, as demonstrated by the susceptibility of the pathogenic *P. aeruginosa* strain library to PyoSN, with ~85% strain coverage.

In addition to translocation across the OM, PyoSN must also deliver its C-terminal nuclease domain across the IM to elicit cytotoxicity. CLBs are thought to enter the periplasm in an unfolded state (Housden *et al.*, 2013), and as such it is unknown whether refolding in the periplasm is a requirement for IM translocation. Indeed the CLB colicin M (ColM) refolds in the periplasm utilising the chaperone FkpA, in order to elicit cytotoxicity (Hullmann *et al.*, 2008). PyoSN cytotoxicity was demonstrated to be FtsH dependent, suggesting this protein likely plays a role in the IM import step. Nuclease-type CLBs have previously been shown to require FtsH for translocation across the IM (Walker *et al.*, 2007; Atanaskovic *et al.*, 2020), however whether this protein is directly involved in pyocin import remains unclear. Previous studies have demonstrated that FtsH protease and ATPase activities are required for colicin activity (Walker *et al.*, 2007) and that the nuclease domains of colicin D and E3 undergo proteolytic processing during import (Chauleau *et al.*, 2011). Thus, it is

likely that PyoSN similarly requires an FtsH-dependent cleavage step to translocate across IM, but this remains to be demonstrated experimentally.

3.4. Conclusions.

The work presented in this chapter establishes several translocon components required for PyoSN import across the *P. aeruginosa* cellular envelope, from which a model for import was proposed (Figure 3-13). PyoSN was found to utilise the TBDT CntO as its OM receptor/translocator with import across the OM energised by the TonB1 complex. TonB1-dependent force remodelling of the CntO plug domain generates a pore in the TBDT, permitting access to the periplasm. Exposure of a TonB1 box in the periplasm allows PyoSN to contact TonB1 itself, facilitating energised import across the OM. This mechanism is similar to that previously proposed for PyoS2 import across the OM through FpvAI. Once in the periplasm, PyoSN translocates across the IM in an FtsH-dependent manner through a presently undescribed mechanism.

Chapter 4 – Biophysical and Structural Characterisation of the Pyocin SN N-terminal Domain

4.1. Introduction.

The Gram-negative OM poses a formidable barrier for the import of proteins from the extracellular environment. Yet CLBs have evolved to subvert the OM during delivery of their cytotoxic domain across the cellular envelope. CLBs execute this process using modular domains that form specific interactions with the cellular envelope proteins of target cells. CLBs generally contain domains required for binding OMPs at the extracellular surface, in addition to parasitizing energy transducing systems in the periplasm to successfully drive import (Cascales *et al.*, 2007). These domains assume a variety of distinct three-dimensional structures to impart their unique biological function during CLB translocation.

The study of a protein's three-dimensional structure can provide invaluable insights into its biological function. Despite significant improvements in other methods of structural determination such as cryo-EM, X-ray crystallography remains the primary method by which this structural information is obtained. Since the publication of the first protein crystal structure of myoglobin in 1957 (Kendrew & Parrish, 1957), over 170,000 structures have been deposited in the PDB, of which ~90% have been determined by X-ray crystallography (http://www.rcsb.org/pdb/ (Berman *et al.*, 2000)). The basis of macromolecular crystallography is the diffraction of a focused X-ray beam by atoms within an ordered three-dimensional crystal, generating a diffraction pattern. Through rotation of the crystal, a series of diffraction images are collected that represent reflections of X-rays by the atomic planes of the crystal lattice at allowed angles, dictated by the Bragg equation. The angles and intensities of these diffracted X-rays can be converted (using Fourier methods) into a reconstruction of the electron density present within the crystal lattice. Through iterative rounds of density refinement and model building, a three-dimensional atomic model of the macromolecule present in the crystal can be built (Shabalin *et al.*, 2018). This atomic model is often a compromise between the optimal fit for the electron density present, in addition to satisfying the geometric constraints of the polypeptide chain.

Compared to colicins discussed previously (Section 1.6.2.), considerably less structural information is currently available for receptor binding and translocation domains of S-type pyocins. To date, only three S-type pyocin structures encompassing the receptor/translocator binding domains have been delineated: the full-length structures of PaeM and PyoS5, in addition to the N-terminal domain of PyoS2, in complex with the translocator FpvAI. The structure of the FpvAI:PyoS2$_{NTD}$ complex will be discussed in detail in the preface to Chapter 5.

Both PaeM and PyoS5 are found to adopt dramatically different three-dimensional structures, in a manner similar to the structural diversity observed across the colicin family (Figure 4-1).

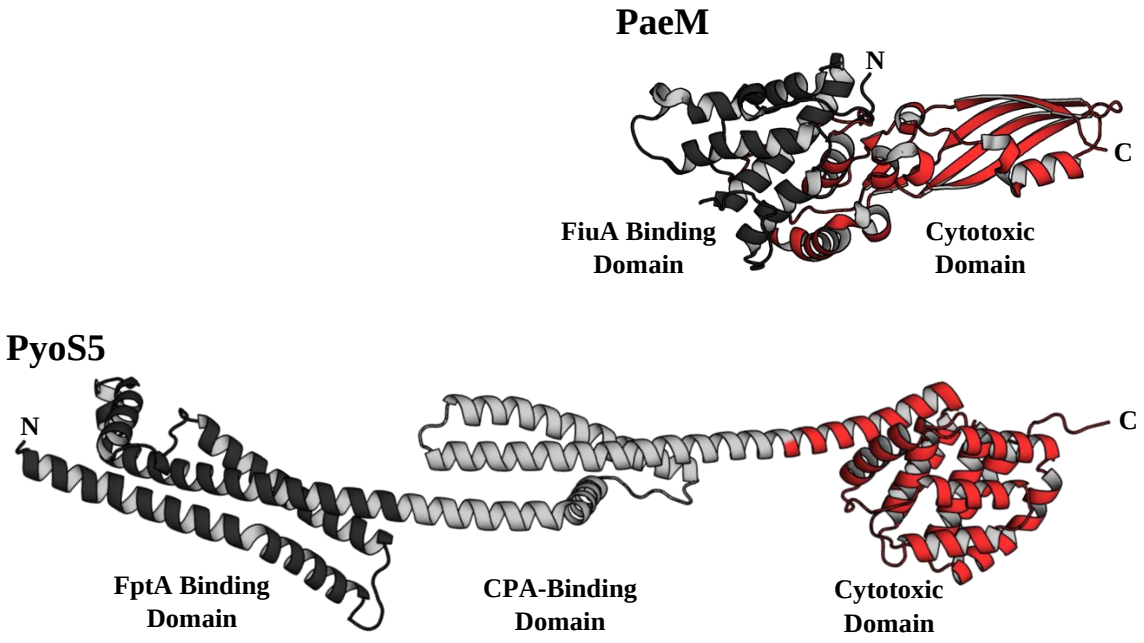

Figure 4-1. Diversity amongst S-type pyocin structures.
Cartoon representations of PaeM (PDB ID = 4G76 (Barreteau *et al.*, 2012)) and PyoS5 (PDB ID = 6THK (Behrens *et al.*, 2020)) coloured by their domain architecture; OM receptor/translocator binding domains (*black*) and cytotoxic domains (*red*). In addition to binding its translocator FptA (via residues 40 – 195), PyoS5 possesses an additional receptor binding domain (residues 196 – 315) utilised to bind CPA (*grey*).

PaeM (also known as PaeM1) is a compact (32 kDa) pyocin with lipid-II hydrolase activity, homologous to ColM from *E. coli* (Barreteau *et al.*, 2012). It adopts a similar three-dimensional architecture to ColM, consisting of an elongated cylindrical structure ~ 90 Å in length, with a receptor/translocator binding domain encompassing residues 1 – 121 respectively (Figure 4-1). The PaeM receptor/translocator binding domain is formed by a four α-helical bundle, displaying 2.3 Å root mean squared deviation (RMSD) from the

analogous domain in ColM. Indeed, both proteins parasitize the ferrichrome receptor expressed by their respective target species during import; FhuA for ColM and FiuA for PaeM (Ghequire, Buchanan, *et al.*, 2018).

The full-length structure of PyoS5 has recently been solved (Figure 4-1), which was found to be highly elongated (194.5 Å in length) and predominantly composed of α-helices (Behrens *et al.*, 2020). PyoS5 has three distinct domains; a cytotoxic C-terminal domain from the E1 pore-forming group, in addition to two domains which adopt a similar tertiary structure. These domains are comprised of a kinked three helical bundle fold and are thought to result from domain duplication. Whilst CLBs containing domain duplications have been identified previously (Arnold *et al.*, 2009), PyoS5 is unique in that both domains possess quite different functions, albeit both functions are involved in OM transport. The PyoS5 N-terminal domain (residues 40 – 195) binds the OM translocator FptA. Preceding this N-terminal domain is an unstructured region containing the TonB1 box (residues 10 – 14) required for coupling to the TonB1 complex that energises import through FptA (Behrens *et al.*, 2020). In contrast, the middle helical domain is required for binding CPA (residues 196 – 315) at the OM, which is thought to localise PyoS5 at the cell surface prior to binding FptA (McCaughey, Josts, *et al.*, 2016; Behrens *et al.*, 2020). Both domains are required for optimal binding to the *P. aeruginosa* OM; however the N-terminal helical bundle alone is sufficient to translocate to the periplasm (Behrens *et al.*, 2020).

In this chapter, I determined the region of PyoSN required for binding to both CntO and TonB1, which are localised to the N-terminal domain of the protein. As a result, the PyoSN N-terminal domain ($PyoSN_{NTD}$) was purified and crystallised. This structure was used to design experiments for biophysical characterisation of regions of the domain that were predicted to be involved in PyoSN translocation. Additionally, an affinity-based purification method was developed for isolation of the CntO:$PyoSN_{NTD}$ complex *in vitro* for future studies.

4.2. Results.

4.2.1. Identification of the PyoSN N-terminal domain.

As discussed in Chapter 3, the PyoSN N-terminal domain likely defines its specificity for the OM receptor/translocator CntO. To delineate the precise N-terminal domain boundary, sequential truncations of PyoSN at its putative domain interfaces were generated, and domain unfolding of the truncations was assessed by DSC. The DSC trace for PyoSN contains three distinct peaks (Figure 4-2), suggesting three independent domain unfolding events and corresponding well with the predicted domain architecture discussed in Chapter 3.

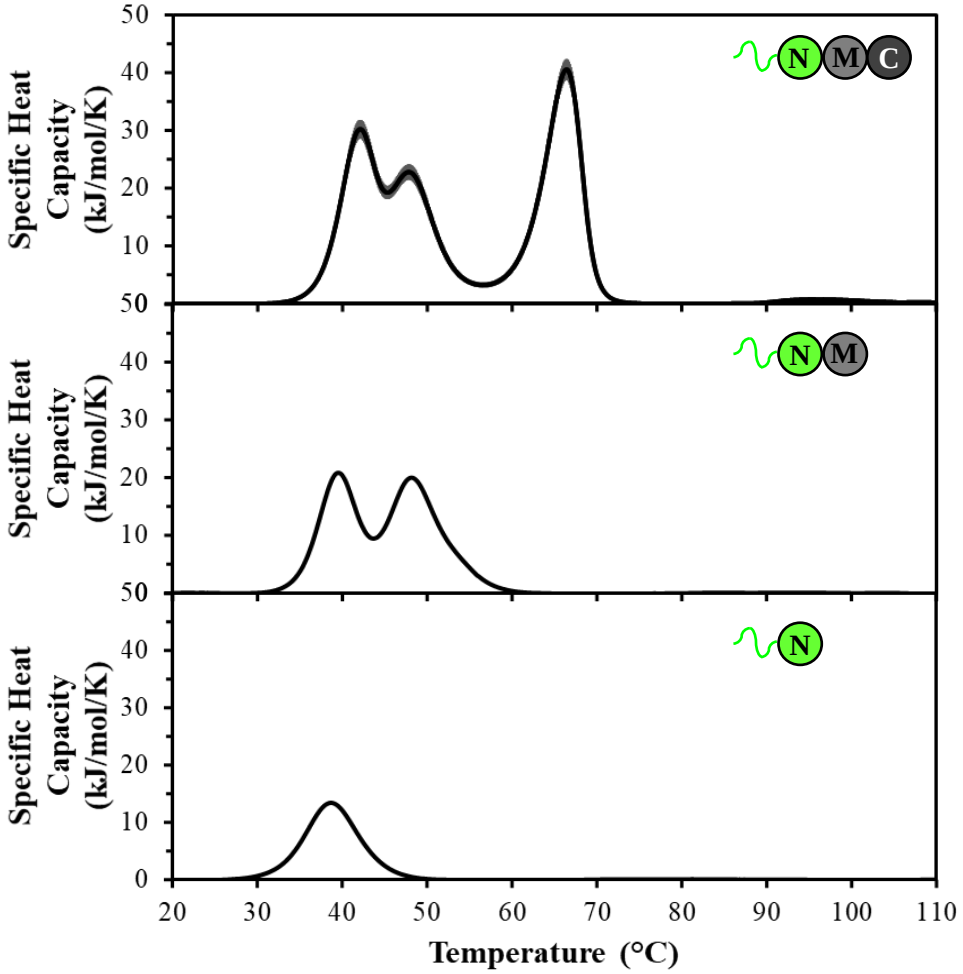

Figure 4-2. PyoSN contains three independently folded domains.
DSC of PyoSN demonstrates three distinct unfolding events, with peaks at 42.1 °C, 49.9 °C and 66.4 °C. Truncation of the cytotoxic domain (residues 700 – 832) results in a loss of the peak at 66.4 °C. Further truncation of the middle domain (residues 206 – 699) left a single peak with a melting temperature of 37.9 °C corresponding to the N-terminal domain alone ($PyoSN_{NTD}$). DSC traces are means of three independent experiments with standard deviation in grey.

Subsequent truncations of the putative C-terminal cytotoxic (predicted from the conserved Pyocin_S Pfam domain) and middle domains (predicted from sequence alignment with PyoS3) resulted in sequential reduction in the number of peaks present in the DSC traces, with a single peak present at 37.9 °C corresponding to the N-terminal domain alone (Figure 4-2).

As a result, the N-terminal domain of PyoSN ($PyoSN_{NTD}$) was mapped to the first 205 residues of the protein. This isolated domain was demonstrated to be folded *in vitro* and possess α-helical secondary structure, by far-UV CD (Figure 4-3).

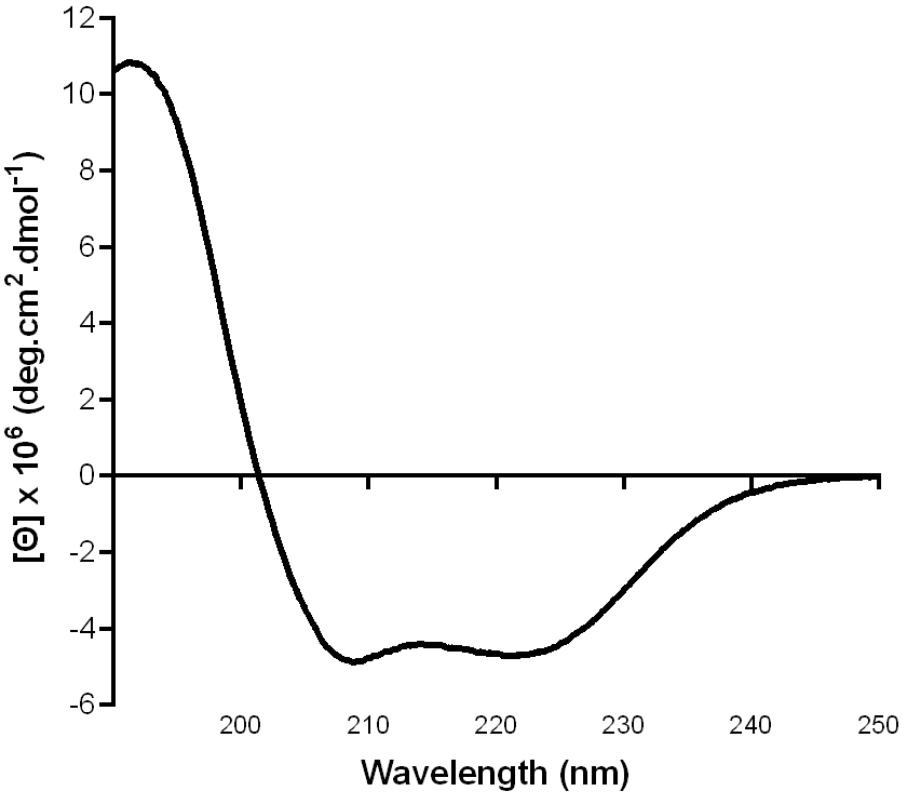

Figure 4-3. $PyoSN_{NTD}$ is folded and α-helical.
Far-UV circular dichroism (CD) spectrum demonstrating a characteristic double minimum at 208 nm and 222 nm indicative of α-helical secondary structure. CD was performed in 10 mM potassium phosphate buffer, pH 7.5.

4.2.2. Co-purification of the CntO:$PyoSN_{NTD}$ complex.

CntO was expressed from an IPTG inducible pET24-a(+) plasmid in *E. coli* BL21ΔABCF cells (*ompA*$^{-}$, *lamB*$^{-}$, *ompC*$^{-}$, *ompF*$^{-}$) to minimise the quantity of contaminating OM porins typical of OMP purification. The *cntO* secretion signal sequence from *P. aeruginosa* (as predicted by SignalP (Nielsen *et al.*, 1997)) was exchanged with that of *ompF* from *E. coli*

to ensure insertion into the native OM. To optimise expression conditions, cells were grown overnight (16 hours) at 20 °C with varying concentrations of IPTG, and the overall OMP composition of the OM was assessed by SDS-PAGE. IPTG induction resulted in substantial deposition of CntO into inclusion bodies. However, a faint additional protein band was detected in detergent extracted OM fractions of cells grown overnight without plasmid induction (Figure 4-4), suggesting some successful insertion of CntO in the native *E. coli* OM.

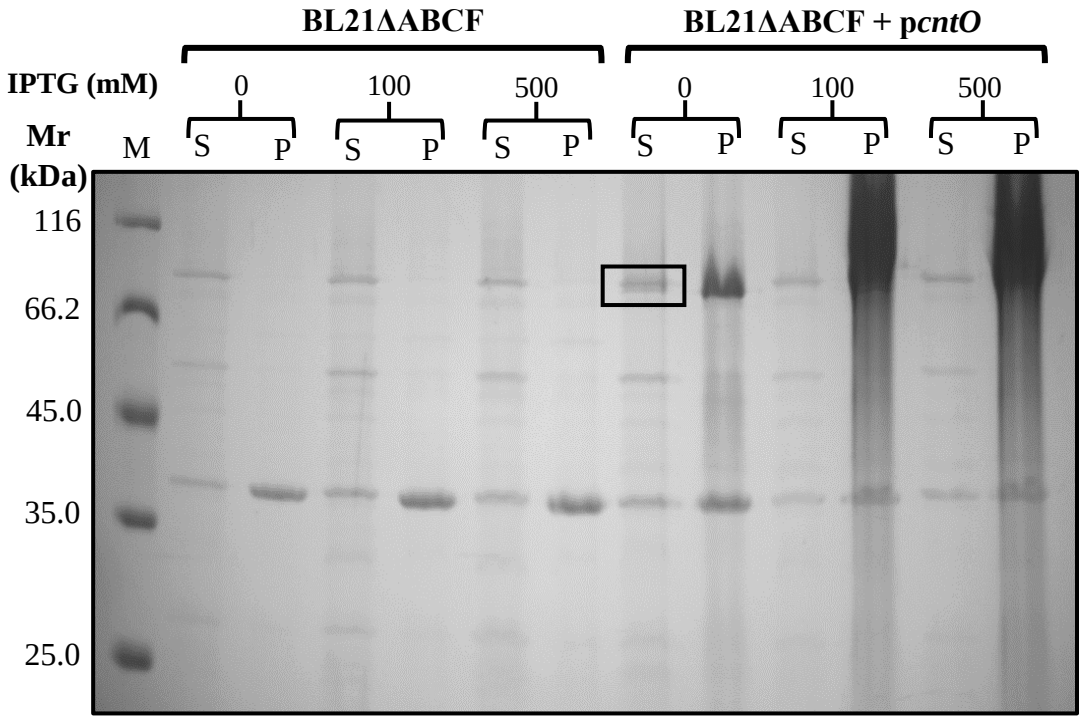

Figure 4-4. Optimisation of CntO expression in *E. coli* BL21ΔABCF.
10% polyacrylamide gel of BL21ΔABCF OM extracts from different expression conditions. M, unstained protein marker (Pierce), S, solubilised OM extract, P, insoluble pellet. Concentrations of IPTG added for induction of expression are denoted above each lane. An additional protein band (*highlighted*) is present in the soluble OM extract with no IPTG induction, suggesting potential CntO expression under these conditions.

His-tagged $PyoSN_{NTD}$ was added to the detergent solubilised OM fraction as "bait", and SDS-PAGE analysis of Ni^{2+}-affinity pulldown assays identified an additional protein band (~80 kDa) that co-eluted with $PyoSN_{NTD}$ (Figure 4-5). The identity of the protein band was confirmed to be CntO by LC-MS/MS (performed by Dr. Melissa Webby, Department of Biochemistry, University of Oxford), demonstrating that the N-terminus of PyoSN and CntO form a complex *in vitro*.

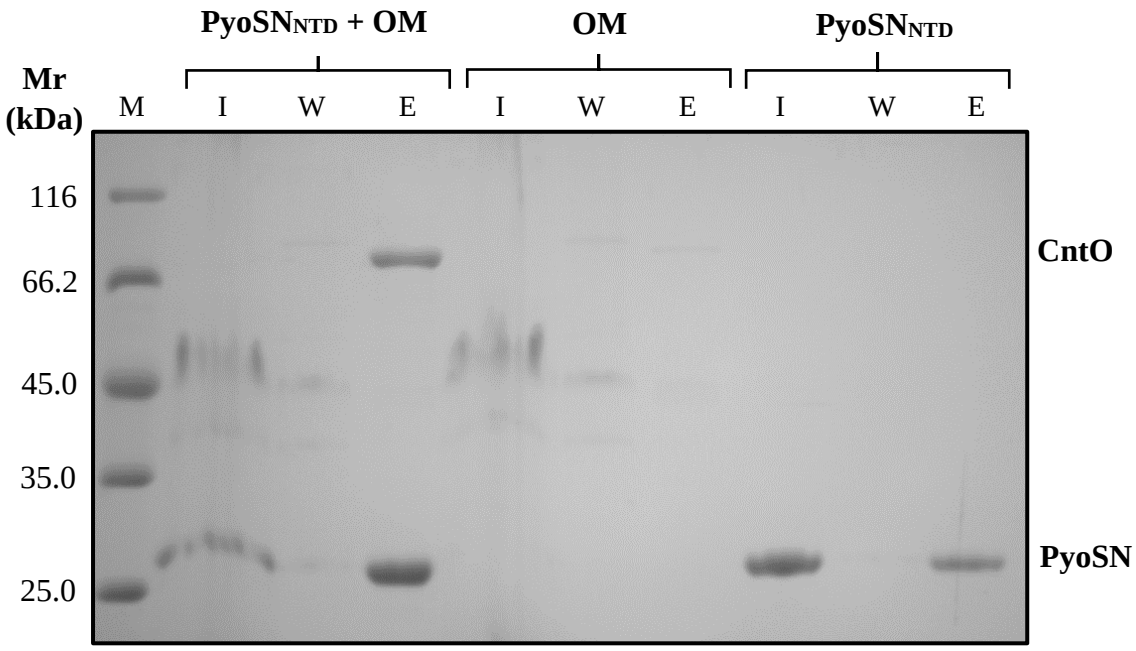

Figure 4-5. PyoSN$_{NTD}$ and CntO form a complex *in vitro*.
12% polyacrylamide gel of Ni^{2+}-affinity pulldowns of PyoSN$_{NTD}$ incubated with BL21ΔABCF OM extract expressing p*cntO*. An additional ~80 kDa protein co-elutes with PyoSN$_{NTD}$ from the OM extract, which was subsequently identified as CntO by LC-MS/MS. M, unstained protein marker (Pierce) I, Ni^{2+}-pulldown input, W, Ni^{2+}-pulldown wash, E, Ni^{2+}-pulldown elution.

This enabled the development of an affinity-based co-purification method to isolate the CntO:PyoSN$_{NTD}$ complex. His-tagged PyoSN$_{NTD}$ was added to detergent and EDTA solubilised *E. coli* OM extract containing CntO as described previously. The resulting complex was co-purified by Ni^{2+}-affinity chromatography using an EDTA-resistant HisTrap column, followed by further purification by SEC to remove excess PyoSN$_{NTD}$ (Figure 4-6).

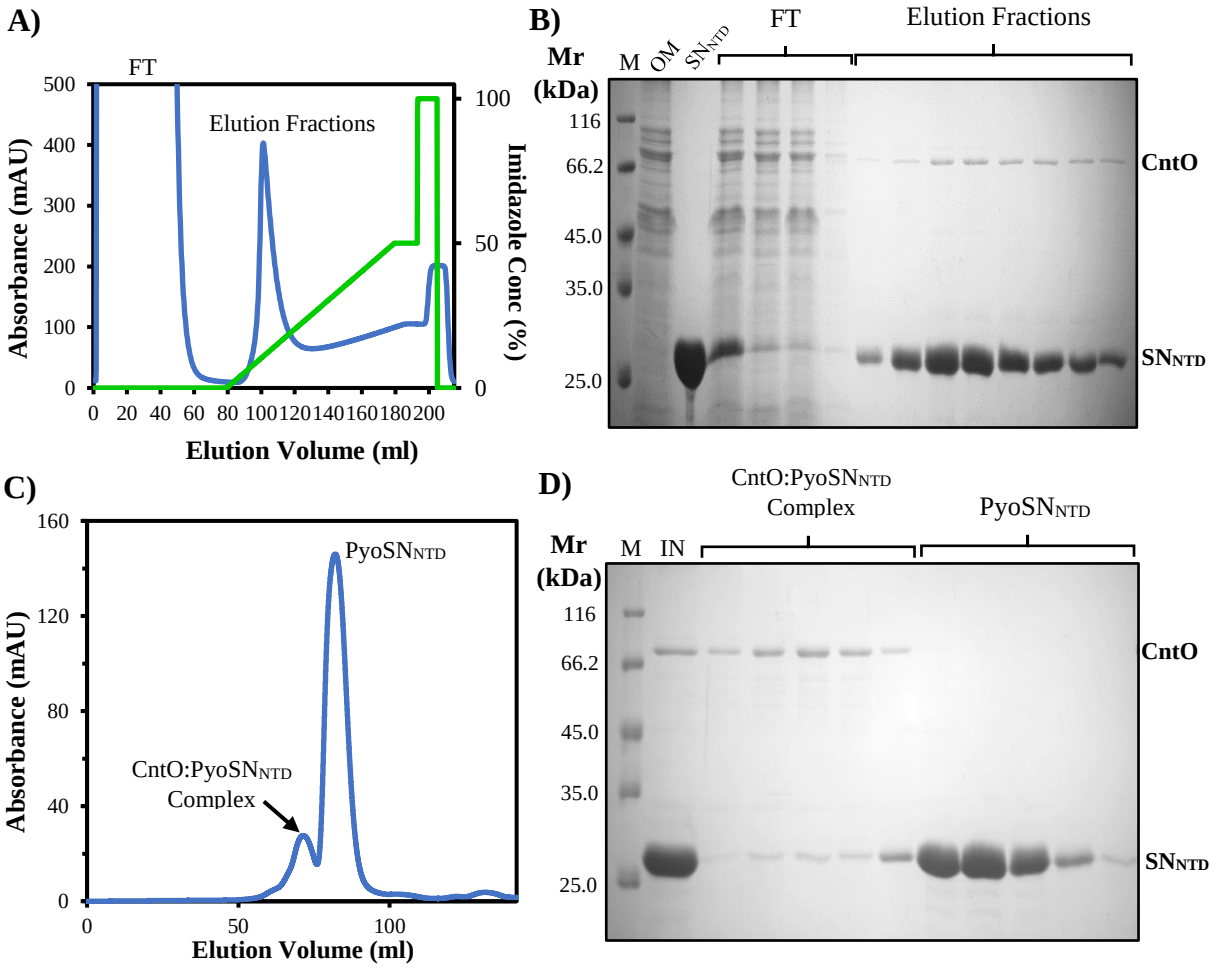

Figure 4-6. Purification of the CntO:PyoSN$_{NTD}$ complex.
A) Ni^{2+}-affinity elution trace of BL21ΔABCF OM extract expressing CntO with addition of PyoSN$_{NTD}$ bait from an EDTA-resistant cOmplete HisTrap column (Roche). Protein was eluted using a linear gradient of 0 – 50% elution buffer *(green)* (5 – 250 mM imidazole), monitored by absorbance at A_{280nm} *(blue)*. B) 12% polyacrylamide gel of Ni^{2+}-affinity co-purification of the CntO:PyoSN$_{NTD}$ complex. PyoSN$_{NTD}$ is massively in excess to ensure saturation of CntO binding. M, unstained protein marker (Pierce), OM, Outer membrane extract, SN$_{NTD}$, PyoSN$_{NTD}$ alone, FT, Ni^{2+}-affinity Flow Through. C) Elution profile of the CntO:PyoSN$_{NTD}$ complex from a Superdex 200 16/600 column with A_{280nm} in blue. D) 12% polyacrylamide gel of size exclusion purification of the CntO:PyoSN$_{NTD}$ complex. The major peak in the trace contained excess PyoSN$_{NTD}$ whereas the minor peak contained the purified complex. M, unstained protein marker (Pierce), IN, SEC input sample.

4.2.3. Crystallisation of PyoSN$_{NTD}$ and the CntO:PyoSN$_{NTD}$ complex.

As PyoSN$_{NTD}$ and CntO were demonstrated to form a complex *in vitro*, I decided to pursue structural characterisation of both the CntO:PyoSN$_{NTD}$ complex, and the PyoSN$_{NTD}$ domain in isolation. Crystallisation trials utilising commercially available screens, specifically

chosen to promote potential crystal formation for each sample, were set up for the CntO:PyoSN$_{NTD}$ complex and the isolated PyoSN$_{NTD}$ domain.

Crystallisation of the CntO:PyoSN$_{NTD}$ complex was trialled in MemGold, MemGold2, MemPlus, PGA and ProPlex. These screens were selected for their previous successes in crystallisation of membrane proteins and complexes; particularly MemGold and MemGold2, which are optimised for α-helical and β-sheet membrane proteins respectively (Newstead *et al.*, 2008; Parker & Newstead, 2012). CntO:PyoSN$_{NTD}$ crystallised in several conditions from the MemGold and MemGold2 screens (Figure 4-7). Crystals were supplemented with cryoprotectant solution (to a final concentration of 1% (w/v) β-OG, 25% (v/v) ethylene glycol), followed by cryo-cooling in liquid nitrogen prior to X-ray diffraction experiments. Whilst CntO:PyoSN$_{NTD}$ complex crystals yielded diffraction patterns, the datasets could not be processed below 10 Å resolution, making them unusable for high-resolution structural determination.

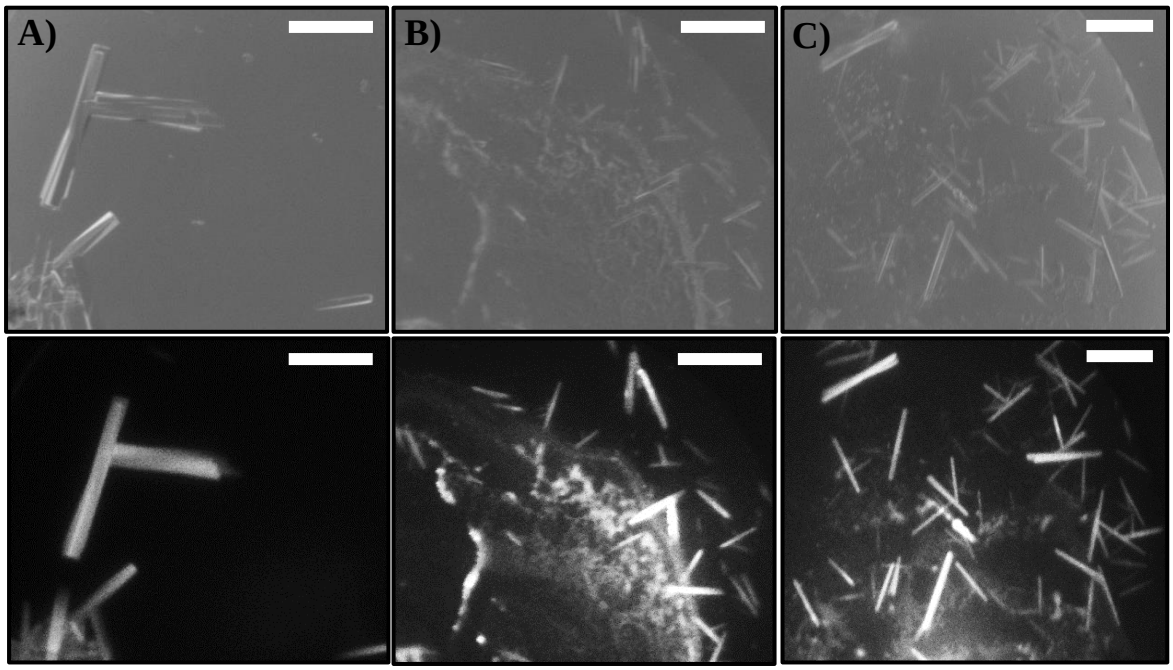

Figure 4-7. CntO:PyoSN$_{NTD}$ crystals from MemGold and MemGold2 screens.
Crystals formed after ~25 days in A) 0.1 M magnesium acetate, 14% (w/v) mPEG 5000, 0.1 M sodium citrate pH 5.8 (MemGold condition A12) B) 0.1 M magnesium chloride, 22% (v/v) PEG 400, 0.1 M Tris pH 7.5 (MemGold condition C2) and C) 0.05 M sodium citrate, 0.12 M potassium chloride, 14% (w/v) PEG 4000, 0.08 M bis-Tris pH 6.2 (MemGold2 condition A12). Scale bars, 0.2 mm. Final protein concentration in the drops was ~5.5 mg/ml. Crystals were imaged via illumination with visible (*top*) and UV (*bottom*) light.

Crystallisation of the isolated $PyoSN_{NTD}$ was trialled in Morpheus, Morpheus II, MIDAS and JCSG+; dynamic screens that cover a wide variety of different conditions. $PyoSN_{NTD}$ was found to crystallise in a single condition from the Morpheus II screen (Figure 4-8). Crucially, this condition contained a cocktail of heavy atoms that could be utilised for experimental phasing (discussed below). As all Morpheus II conditions contain cryoprotectant, crystals could be cryo-cooled directly in liquid nitrogen, prior to diffraction experiments.

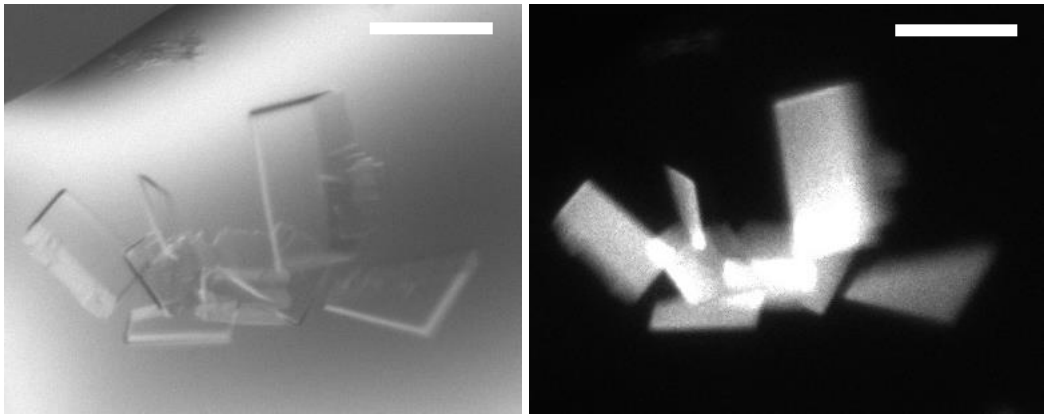

Figure 4-8. $PyoSN_{NTD}$ crystals from the Morpheus II screen.
Crystals formed after 12 days in 1.0 M MOPSO, bis-Tris pH 6.5, 10% (w/v) PEG 8000, 20% (w/v) 1,5-pentanediol, 2 mM lanthanide mix (Morpheus II condition E3). Scale bars, 0.2 mm. Final protein concentration in the drops was ~8.7 mg/ml. Crystals were imaged via illumination with visible (*left*) and UV (*right*) light.

4.2.4. Crystal structure of $PyoSN_{NTD}$ at 2.4 Å.

Diffraction of $PyoSN_{NTD}$ crystals indicated a tetragonal space group P 4_3 with unit cell parameters a = 70.325 Å, b = 70.325 Å, c = 277.931 Å, α = 90°, β = 90°, γ = 90°. The crystal structure of $PyoSN_{NTD}$ was solved to 2.4 Å through experimental phasing by single-wavelength anomalous dispersion (SAD). Four copies of $PyoSN_{NTD}$, related by translational non-crystallographic symmetry (tNCS), were found in the unit cell, in addition to 10 heavy atoms that were prospectively modelled as Er. Discontinuous density was observed encompassing residues 6 – 26 and 39 – 205 of $PyoSN_{NTD}$ (Figure 4-9 and Table 4-1).

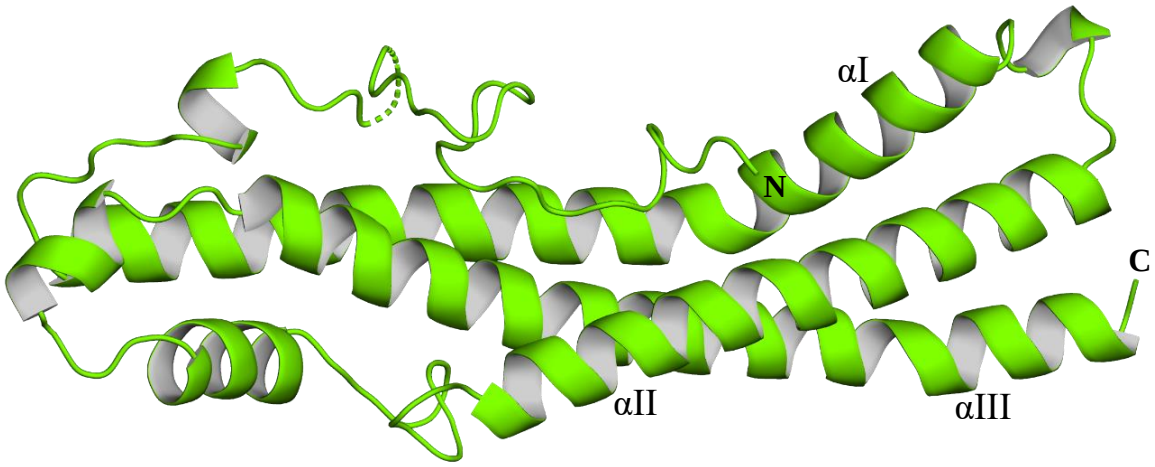

Figure 4-9. The 2.4 Å crystal structure of PyoSN$_{NTD}$.
The structure of the N-terminal domain of PyoSN, comprising residues 1 – 205, at 2.4 Å resolution. N- and C- terminal residues are labelled accordingly. Residues 27 – 38 (in addition to the first five residues of the protein) are not resolved in the structure (*dashed line*) and are presumed disordered.

Table 4-1. X-ray data processing, refinement, and validation statistics.

Data Processing	
X-ray Wavelength (Å)	0.979
Space Group	P 4_3
Cell Dimensions (Å)	a = 70.325 Å, b = 70.325 Å, c = 277.931 Å
Cell angles (°)	α = 90°, β = 90°, γ = 90°
Resolution	70.42 – 2.40 (2.47 – 2.40)
Unique Reflections	52429 (2654)
Completeness (%)	99.97
1/σ	7.5 (0.9)
CC (1/2)	0.997 (0.670)
R_{meas}	0.116 (2.13)
Multiplicity	8.2 (7.8)
Refinement	
R_{work}/R_{free}	0.2405/0.2672
Number of atoms	6221
Number of Er atoms	10
Average B-factor (Å^2)	44.47
Validation	
RMS bonds	0.0178
RMS angles	2.001
Ramachandran favoured (%)	97.62
Ramachandran allowed (%)	2.38
Ramachandran outliers (%)	0.00
MolProbity Clashscore	5.54

PyoSN$_{NTD}$ adopts an α-helical bundle fold composed of three α-helices. The first α-helix (αI) is kinked and α-helices II and III are connected by a helical turn consisting of two shorter helices. Electron density was absent for residues 27 – 38, which are presumed disordered, suggesting conformational flexibility in this region. Residues 6 – 26 and 39 – 52 possessed no significant secondary structure and extend up the proximal face of the α-helical bundle, formed by helices αI and αIII (Figure 4-10). This interface between the extended N-terminal motif (xNT) and the α-helical bundle is particularly pronounced, with a buried surface area of 2960 Å^2.

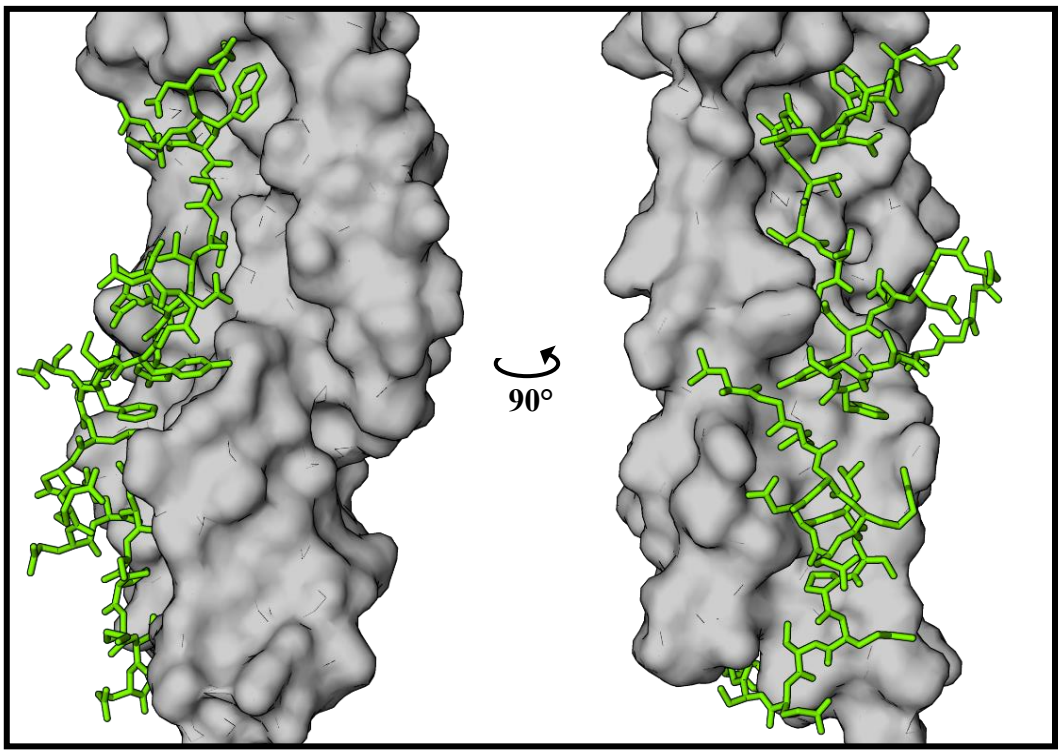

Figure 4-10. The xNT of PyoSN$_{NTD}$ is closely associated with the α-helical bundle.
The PyoSN$_{NTD}$ substructure interface surface is formed by residues that comprise the extended N-terminus (xNT) (*green*) and the main body (*grey*) of the domain. This encompasses residues 6 – 26 and 39 – 52 of the xNT in the structure.

In addition, significant intramolecular interactions are observed between the α-helical bundle and the xNT motif of PyoSN$_{NTD}$. A total of 18 hydrogen bond interactions are formed at the substructure interface, with an extensive hydrogen bonded network formed between residues T11 – G15 and G40 – L46 and the α-helical bundle (Figure 4-11). Residues Gln74 and Asn185 are particularly prolific in their interactions, forming several hydrogen bonds to a short sequence encompassing xNT residues 12 – 15 (TVVG).

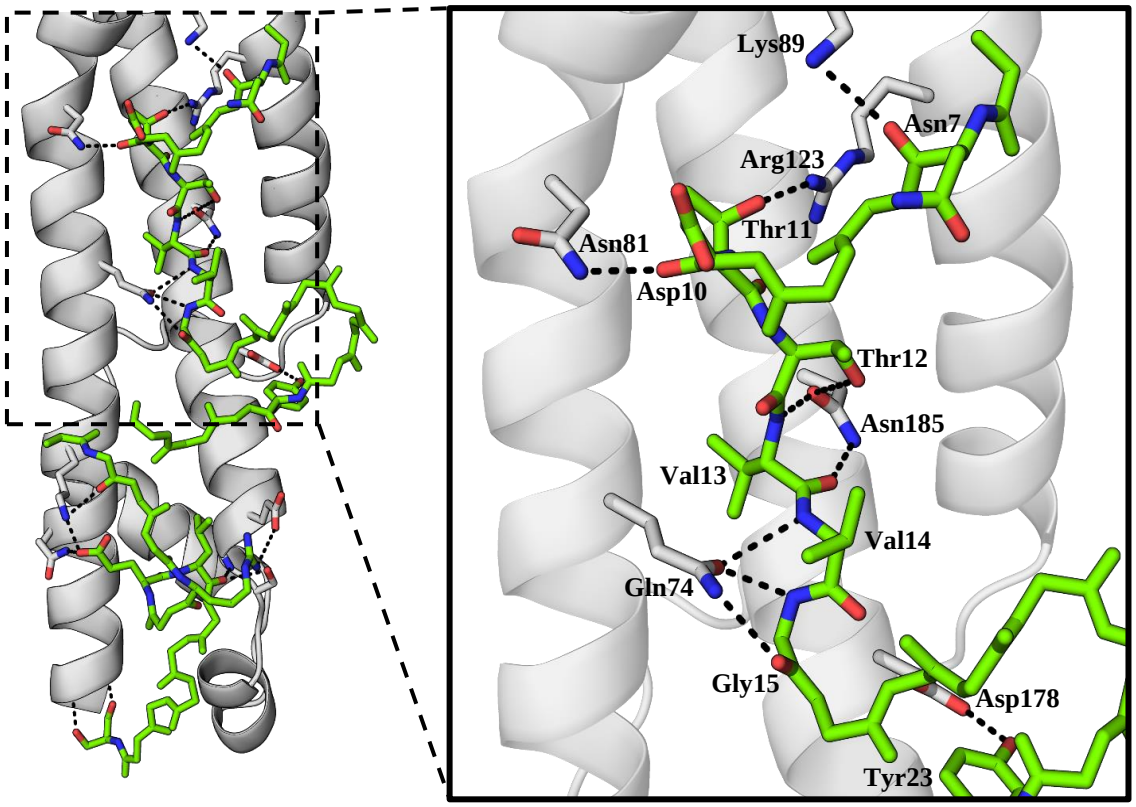

Figure 4-11. Hydrogen bonds at the xNT motif interface within the PyoSN$_{NTD}$ structure. Representation of the interface within PyoSN$_{NTD}$ between its xNT (*green*) and the main α-helical bundle (*grey*). Residues involved in hydrogen bonding are depicted as sticks with the intramolecular bonds highlighted (*black dashes*). Most of the hydrogen bonds at this interface are formed by a short polypeptide motif comprising residues Asn7 to Gly15 of the xNT. Additional hydrogen bond interactions are also observed from residues Gly40 to Ser52.

4.2.5. Conservation of tertiary structure across the S-type pyocin family.

Alignment of PyoSN$_{NTD}$ to the structures of other S-type pyocin N-terminal domains demonstrates a striking conservation of tertiary structure. Of the three known structures of S-type pyocin N-terminal domains, PyoSN$_{NTD}$ is most similar to that of PyoS5, with a RMSD of 2.90 Å over 146 amino acids. Both structures possess an identical α-helical bundle fold, with minor structural deviations in the helical turn connecting αII and αIII, displaying an angular shift of 35° between the two proteins (Figure 4-12). The major structural deviation between the two N-terminal domains occurs within the xNT motif of PyoSN$_{NTD}$, in which an analogous motif remains unresolved in the PyoS5 structure. This structural conservation is surprising given the lack of sequence homology between the two domains, with PyoSN and PyoS5 sharing only 18.8% sequence identity across their N-terminal domains. PyoSN$_{NTD}$ also shares structural homology with that of PyoS2, with an RMSD of

3.13 Å over 163 amino acids. Unsurprisingly, no structural homology is seen between $PyoSN_{NTD}$ and the colicin M-like S-type pyocin, PaeM.

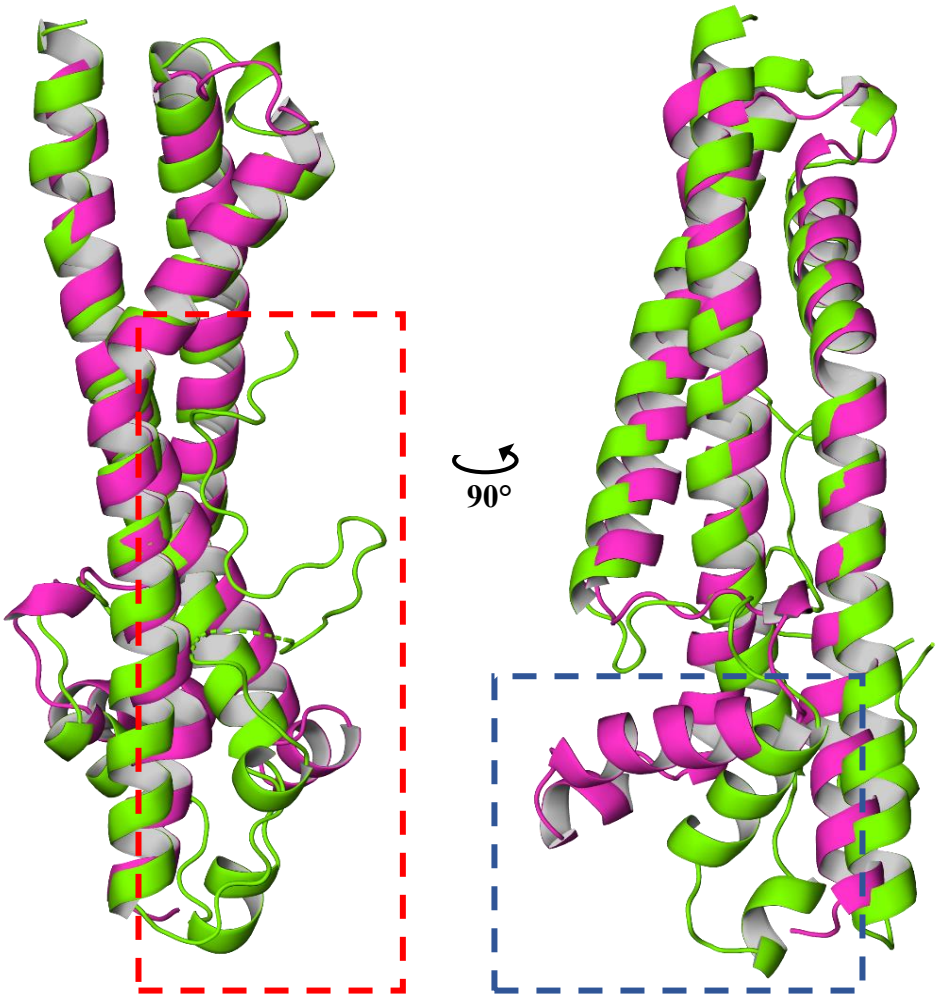

Figure 4-12. Comparison of the $PyoSN_{NTD}$ and $PyoS5_{40\text{-}195}$ structures.
Representation of the alignment of the $PyoSN_{NTD}$ (*green*) with the N-terminal domain (residues 40 – 195) of PyoS5 (*magenta*) from the full-length structure (PDB ID = 6THK (Behrens *et al.*, 2020)). These domains exhibit structural homology, with an RMSD of 2.90 Å. There is significant deviation between the structure at the extreme N-terminus, with $PyoSN_{NTD}$ possessing the xNT motif, which is not present in the PyoS5 structure (*red box*). Additionally, minor structural deviations within the helical turn between αII and αIII are observed between the structures, resulting from a 35° reorientation (*blue box*).

4.2.6. The extended N-terminal motif is required for $PyoSN_{NTD}$ stability.

A significant interface is formed between the $PyoSN_{NTD}$ xNT motif and the α-helical bundle, involving an extensive hydrogen bond network in addition to encompassing a buried surface area of 2960 $Å^2$. The xNT appears to shield a hydrophobic cleft at the apex of the molecule

from the aqueous environment, which may affect the overall stability of $PyoSN_{NTD}$. Therefore, the role of the xNT motif in the thermal stability of $PyoSN_{NTD}$ was investigated using both CD and DSC. Truncation of the xNT ($PyoSN_{NTD}\Delta 1\text{-}52$) resulted in a significant reduction in the α-helical secondary structure present in the domain (Figure 4-13).

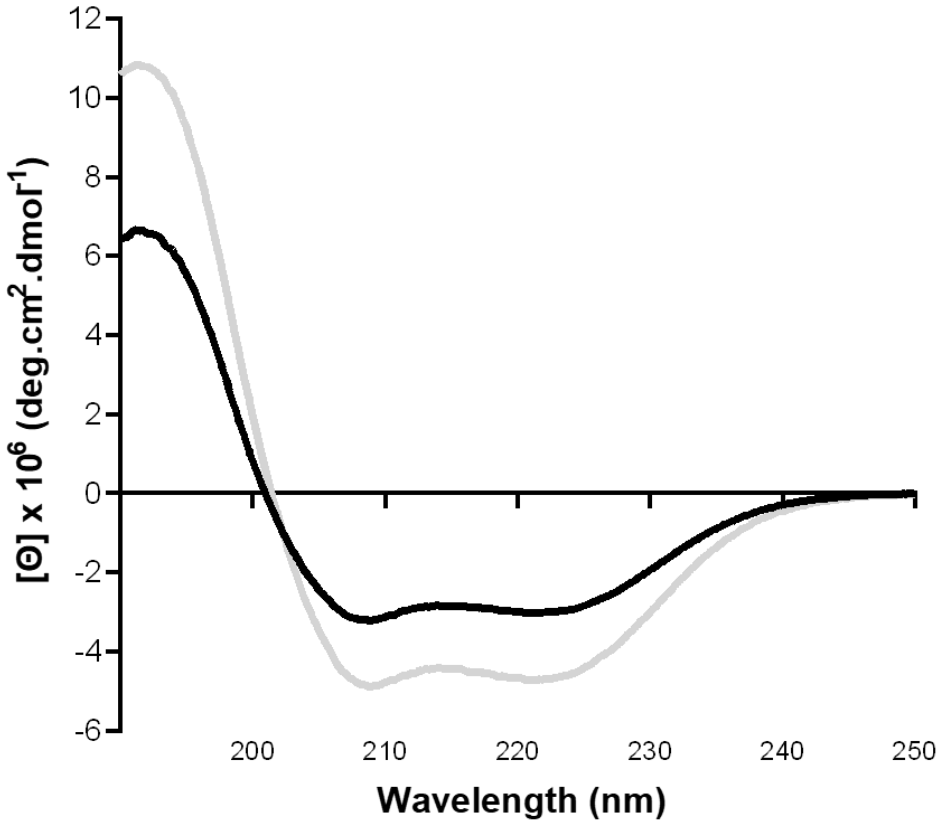

Figure 4-13. Truncation of the xNT motif results in loss of $PyoSN_{NTD}$ secondary structure. Far-UV CD spectrum demonstrates loss of α-helical secondary structure upon truncation of the xNT motif ($PyoSN_{NTD}\Delta 1\text{-}52$) (*black*) compared to the full-length domain (*grey*). CD was performed in 10 mM potassium phosphate buffer, pH 7.5.

This was demonstrated to result from destabilisation of the $PyoSN_{NTD}$ structure, with a significant decrease observed in the thermodynamic transition for domain unfolding in DSC traces (Figure 4-14). The symmetric peak that corresponds to $PyoSN_{NTD}$ unfolding broadens, indicating loss of co-operative unfolding. This peak also shifts from 37.9 °C to 21.9 °C, precipitating in >50% of the $PyoSN_{NTD}$ xNT truncation adopting an unfolded structure at room temperature. Therefore, the xNT motif is essential for $PyoSN_{NTD}$ domain stability.

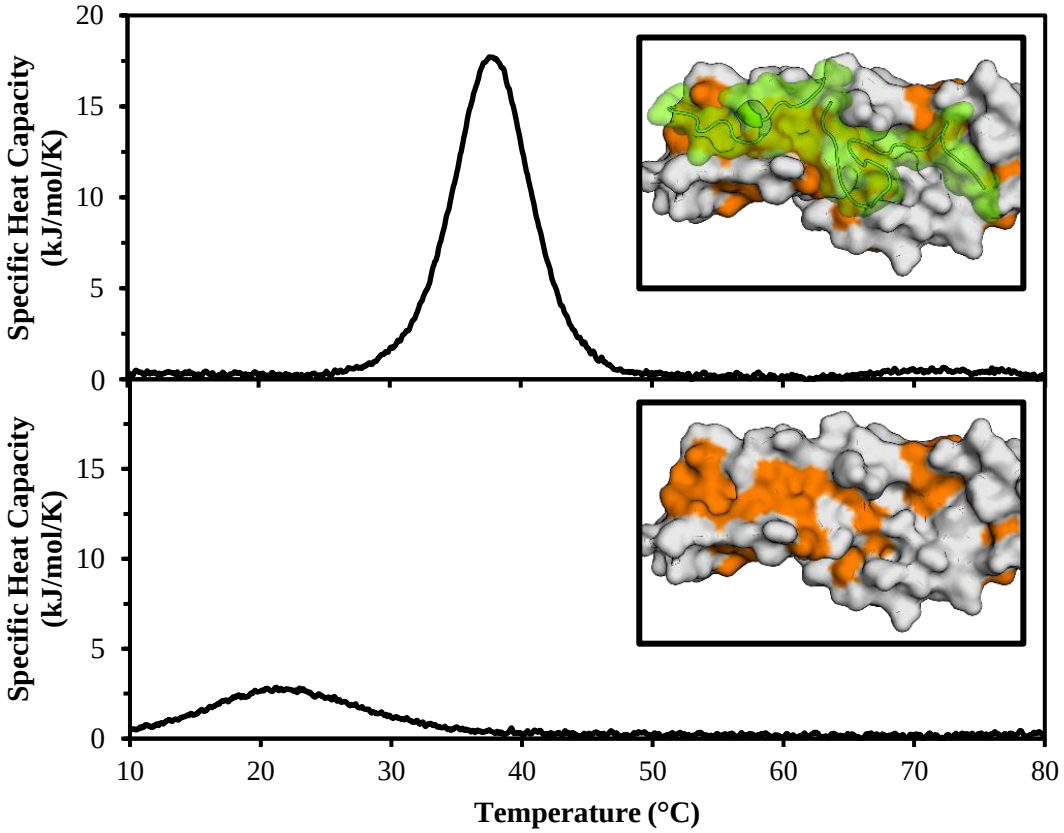

Figure 4-14. The xNT motif stabilises the PyoSN N-terminal α-helical bundle.
DSC traces demonstrate a shift of the unfolding peak that corresponds to the PyoSN N-terminal domain from at 39.7 °C to 21.9 °C upon truncations of the first 52 residues. This likely results from exposure of a hydrophobic cleft (*inset, orange*) in the PyoSN truncation which is normally shielded from the aqueous solution by the xNT (*inset, green*).

4.2.7. PyoSN$_{NTD}$ binds TonB1 *in vitro*.

PyoSN has previously been demonstrated to hijack the TonB1 complex in order to induce cytotoxicity (Section 3.2.3). Due to its structural similarity to PyoS2, it was reasoned that a putative TonB1 box could also be present within the xNT motif of PyoSN$_{NTD}$. Thus, to further explore this hypothesis, potential interactions between the two proteins were investigated by analytical SEC and ITC.

Individually, TonB1 and PyoSN$_{NTD}$ were found to elute at 9.09 ml and 11.40 ml, respectively, from a Superdex 75 Increase 10/300 GL column. However, both proteins co-eluted as a complex at 8.65 ml when loaded onto the column together (Figure 4-15). Truncation of the first 52 residues of PyoSN abrogated complex formation *in vitro*, with TonB1 and PyoSN$_{NTD}$Δ1-52 eluting separately, at 9.09 and 11.66 ml respectively, when applied to the column together (Figure 4-15).

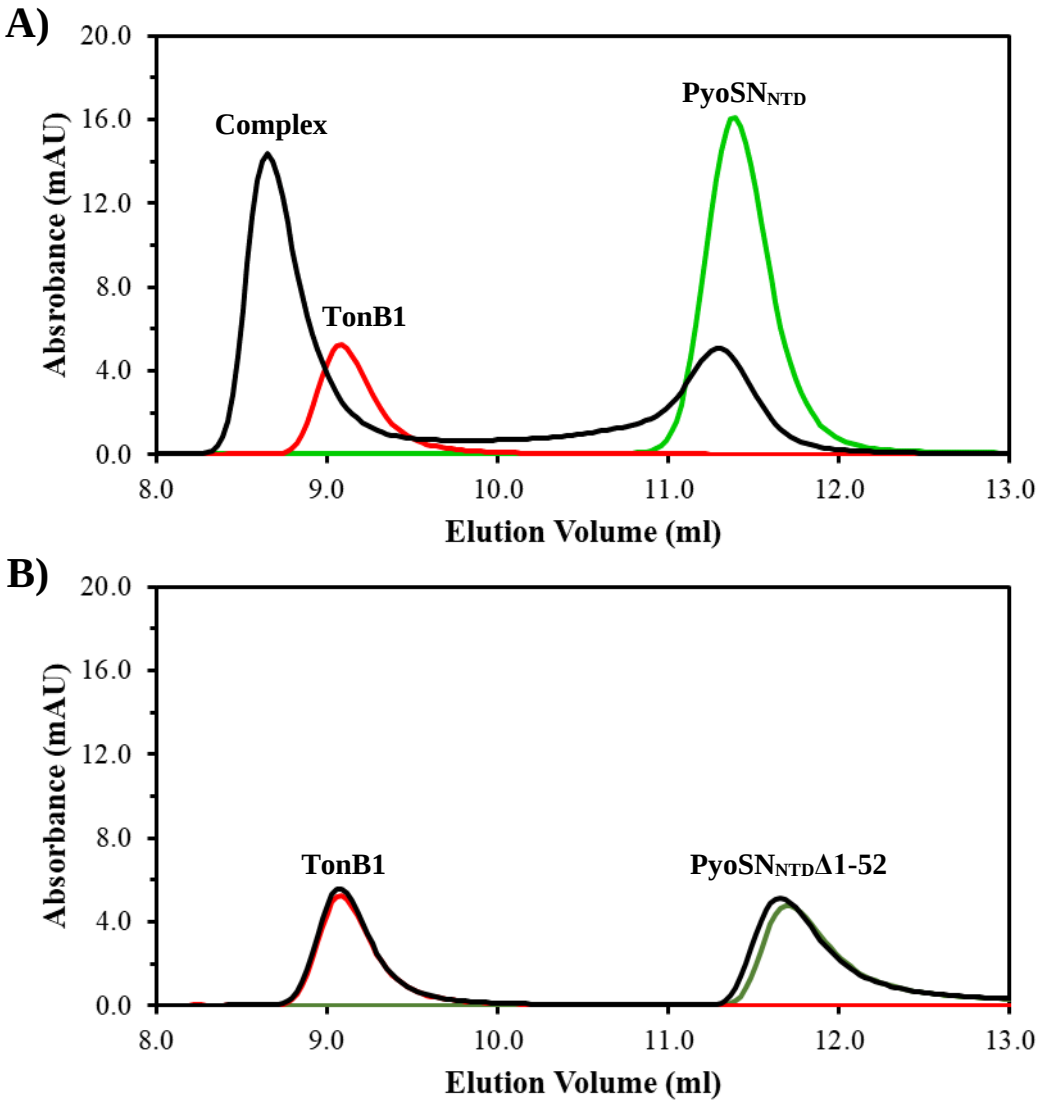

Figure 4-15. The xNT motif of PyoSN binds TonB1 *in vitro*.
A) Analytical SEC of PyoSN$_{NTD}$ (*green*), TonB1 (residues 109 – 342) (*red*) and both (*black*) at 5 µM on a S75 Increase 10/300 GL column in 25 mM Tris-HCl pH 7.5, 150 mM NaCl demonstrates the proteins co-elute as a complex. B) Analytical SEC of PyoSN$_{NTD}$Δ1-52 (*dark green*), TonB1 (residues 109 – 342) (*red*) and both (*black*) at 5 µM on a S75 Increase 10/300 GL column in 25 mM Tris-HCl pH 7.5, 150 mM NaCl demonstrates that proteins elute separately. Therefore, TonB1 binding activity is localised in the first 52 residues of PyoSN.

The binding interaction between TonB1 and PyoSN was further assessed by ITC. Titration of PyoSN$_{NTD}$ into TonB1 generated saturatable exothermic binding, with a K_d of 61 nM (Figure 4-16). Truncation of the first 52 residues significantly perturbs the observable K_d, which increases ~1000-fold to 27 µM. In addition, binding of PyoSN$_{NTD}$Δ1-52 to TonB1 was no longer saturated over the course of the titration. This indicates a significant reduction

in the truncation's ability to bind TonB1 *in vitro*, suggesting the primary binding site for TonB1 is located in the xNT motif of $PyoSN_{NTD}$.

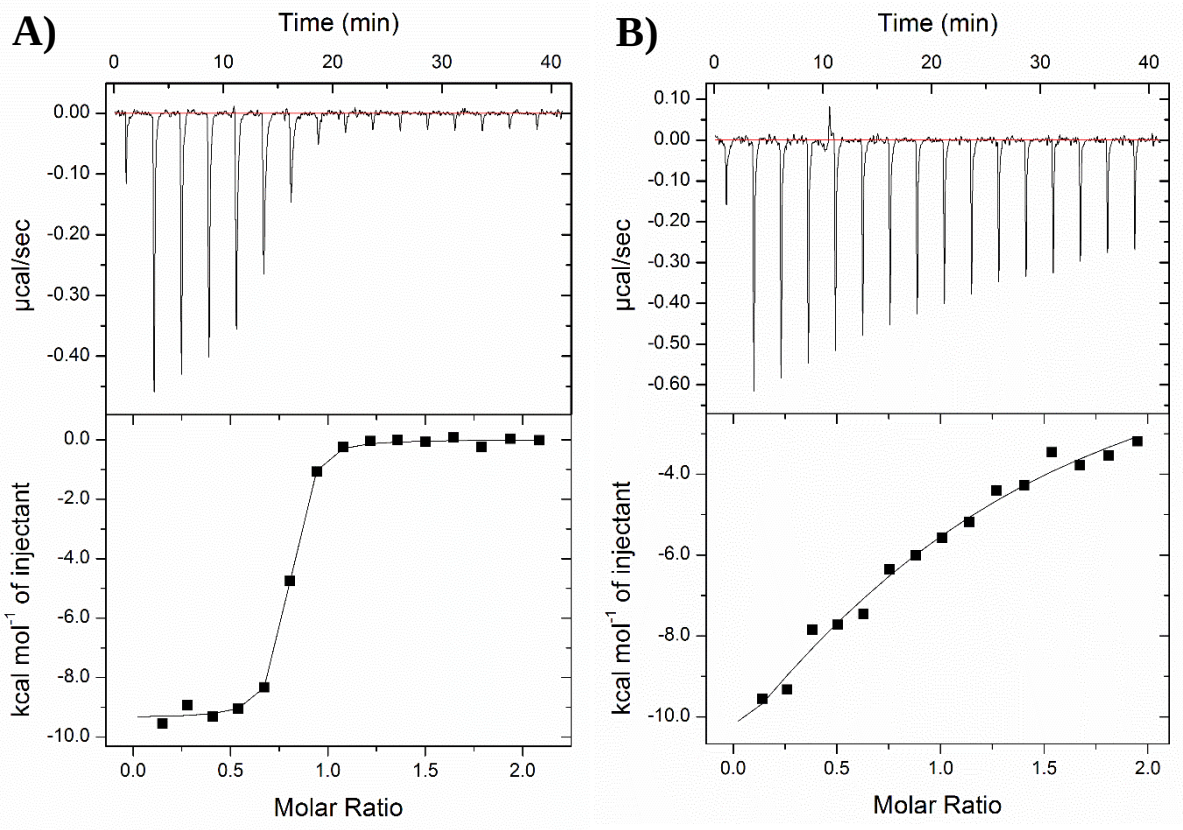

Figure 4-16. Loss of the PyoSN xNT significantly impairs TonB1 binding.
A) Binding of $PyoSN_{NTD}$ to TonB1 (residues 109 – 342) observed by ITC. The following binding parameters were obtained after data fitting to a single site binding model: $\Delta H = -9.4 \pm 0.8$ kcal/mol, $\Delta S = 1.64$ cal/mol/K, $N = 0.75 \pm 0.00$ sites, $K_d = 6.09 \pm 0.35 \times 10^{-8}$ M. B) Binding of $PyoSN_{NTD}\Delta 1$-52 to TonB1 (residues 109 – 342) observed by ITC. The following binding parameters were obtained after data fitting to a single site binding model: $\Delta H = -24.3 \pm 9.5$ kcal/mol, $\Delta S = -60.5$ cal/mol/K, $N = 0.99 \pm 0.26$ sites, $K_d = 2.74 \pm 6.90 \times 10^{-5}$ M. Therefore, loss of the xNT motif reduces TonB1 binding by 1000-fold.

The importance of the first 52 residues was confirmed *in vivo* through plate killing cytotoxicity assays, with loss of PyoSN cytotoxicity observed for the xNT truncation mutant (Figure 4-17). It is therefore likely the xNT motif contains a TonB1 box that is essential for PyoSN activity *in vivo*, in addition to also binding TonB1 *in vitro*.

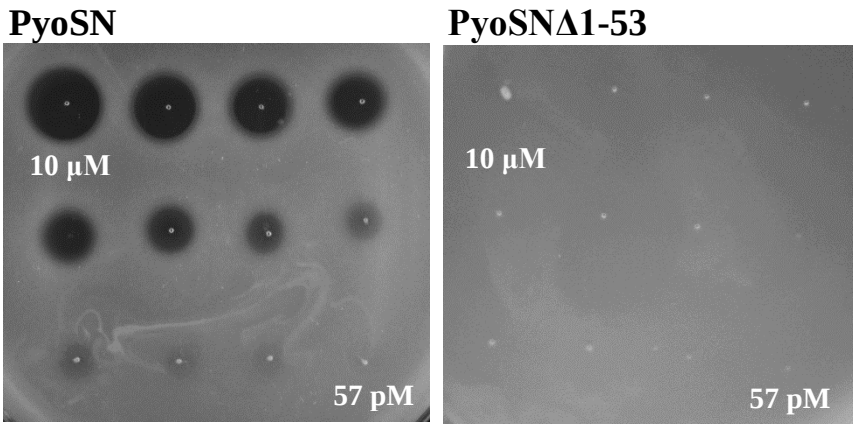

Figure 4-17. Loss of the xNT motif abrogates PyoSN cytotoxicity.
Plate killing assays show abrogation of cytotoxic activity upon loss of the xNT motif in PyoSN. Zones of clearance result from cell killing.

4.3. Discussion.

The biophysical and structural data presented in this chapter demonstrates that PyoSN is comprised of three folded domains. The domain responsible for binding to the OM translocator CntO was successfully delineated and shown to encompass the N-terminal 205 residues, which are sufficient for CntO binding *in vitro*. These experiments confirm that the N-terminal domain of PyoSN is required for translocator binding, as demonstrated previously for the S-type pyocins PyoS2 and PyoS5 (White *et al.*, 2017; Behrens *et al.*, 2020). As such, this facilitated development of an affinity-based purification method for CntO, utilising $PyoSN_{NTD}$ as "bait" to extract the target OMP from fractionated *E. coli* OM. Purification of the CntO:$PyoSN_{NTD}$ complex enabled preliminary crystallisation trials in an attempt to elucidate the complex structure. Despite forming crystals across a number of conditions, they failed to diffract to a high enough resolution for meaningful structural analysis.

However, the structure of $PyoSN_{NTD}$ in isolation was solved, revealing a three α-helical bundle fold with an extended N-terminal motif (xNT). The propensity for α-helical structures within CLBs is perhaps unsurprising due to their requirement to translocate in an unfolded state (Penfold *et al.*, 2004). Despite possessing well-ordered hydrophobic cores, α-helical domains are typically less mechanically stable than β-sheets (Brockwell *et al.*, 2003), which is beneficial for CLBs that require energised unfolding via the Tol/Ton complex for import (Hann *et al.*, 2007; Farrance *et al.*, 2013; Hickman *et al.*, 2017). Indeed, the structures of many colicins and S-type pyocins that have been solved previously are predominantly α-helical (Wiener *et al.*, 1997; Soelaiman *et al.*, 2001; Klein *et al.*, 2016; Behrens *et al.*, 2020).

The N-terminal domain of PyoSN displays significant structural homology to the N-terminal structures of both PyoS2 and PyoS5. Of these two structures, $PyoSN_{NTD}$ was found to be most similar to that of PyoS5 (residues 40 – 194) (Behrens *et al.*, 2020), demonstrating an RMSD of 2.90 Å (Figure 4-18). Within the core α-helical bundle, minor structural deviations between the two domains occur within the helical turn between αII and αIII, with a 35° reorientation of the turn. Interestingly, it is within this region that significant structural deviations are also present within the PyoS2 structure. Alignment of the PyoS2 N-terminal domain (residues 11 – 205) with $PyoSN_{NTD}$ shows more disparate structural identity between the two domains, with an RMSD of 3.13 Å (Figure 4-18). A significant reorientation of this helical turn has occurred in the PyoS2 N-terminal structure, which was solved in complex

with its translocator FpvAI (White *et al.*, 2017). Taken together, this helical turn likely exhibits marked conformation flexibility in solution (as seen from the B-factors of the $PyoSN_{NTD}$ structure (*not shown*)). Potential rearrangement of this helical turn could be a hallmark of translocator binding for these domains. However, to conclusively validate this assessment, further pyocin-translocator structures would have to be solved.

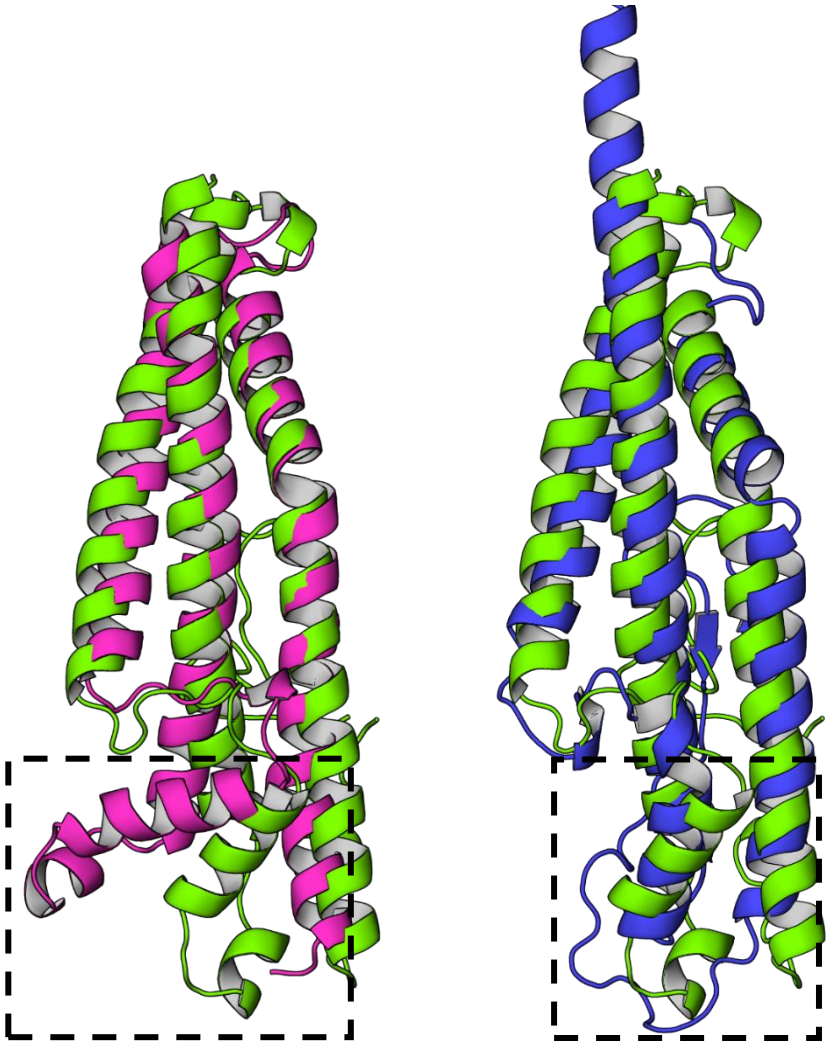

Figure 4-18. Structural comparison of the three S-type pyocin N-terminal domains. Structural alignments of the $PyoSN_{NTD}$ (*green*) (this study) with residues 40 – 195 of PyoS5 (*magenta*) (PDB ID = 6THK (Behrens *et al.*, 2020) and the N-terminal domain of PyoS2 from the FpvAI:$PyoS2_{NTD}$ complex (*blue*) (PDB ID = 5ODW (White *et al.*, 2017)) illustrating the differences in the helical turn between αII and αIII helices of the helical bundle (*dashed square*).

Assuming import of substrates by TBDTs occurs through an analogous mechanism, the structure of $PyoSN_{NTD}$ (and that of other S-type pyocin N-terminal domains) has implications for import across the OM. Upon activation of the TBDT through substrate

binding, force remodelling of the TBDT plug domain occurs through contact with the TonB1 complex, generating a pore through the translocator, through which substrates can enter the periplasm. Uptake of pseudopaline through the CntO lumen can be rationalised due to its small size, whereas PyoSN is significantly larger. Indeed, the PyoSN$_{NTD}$ structure alone is ~74 Å in length, approximately seven times greater than that of pseudopaline in its widest dimension (Figure 4-19). Therefore, it is likely that PyoSN$_{NTD}$ translocates through the CntO lumen in an unfolded conformation, as demonstrated for PyoS2 (discussed in Chapter 5).

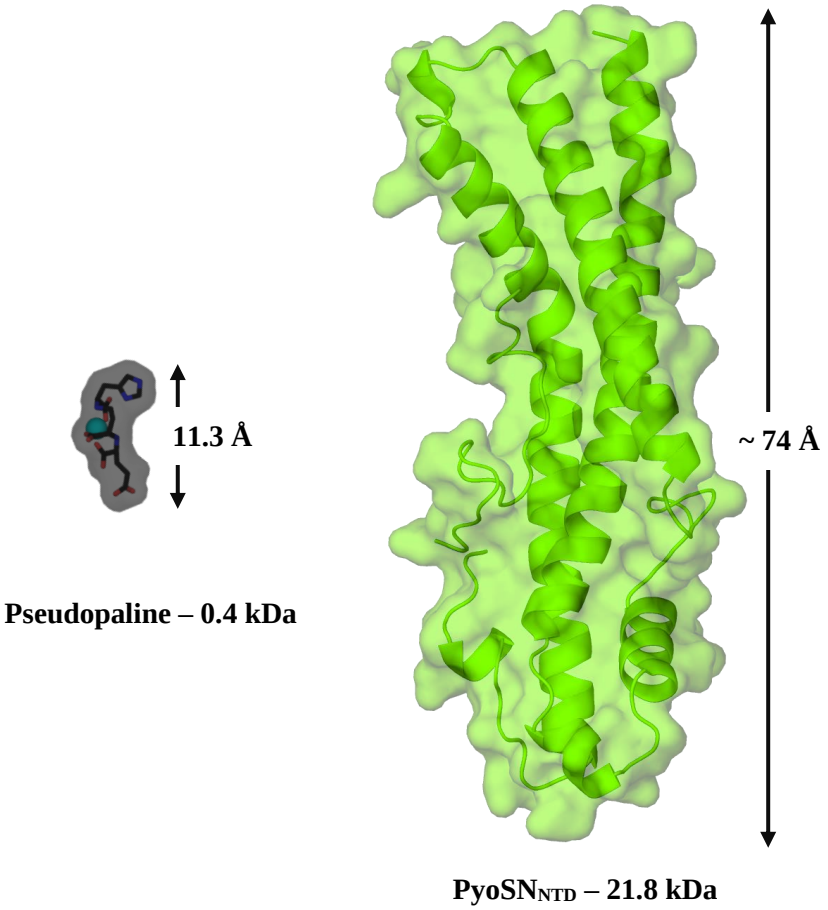

Figure 4-19. Structural comparison of pseudopaline and PyoSN$_{NTD}$.
Surface representations of pseudopaline (*black*) and PyoSN$_{NTD}$ (*green*) illustrate the significant size difference between the two molecules, despite both utilising the same transporter, CntO, for uptake across the OM. Pseudopaline structure was adapted from co-ordination complexes modelled in Zhao *et al.*, 2020.

Both PyoS2 and PyoSN possess a structured, extended N-terminal motif (xNT) that associates laterally with the main α-helical bundle. This N-terminal architecture appears to be unique to the S-type pyocins within the CLB family, with colicin translocation domains instead possessing an N-terminal disordered extension that is utilised to contact the Tol/Ton

systems during import (Cascales *et al.*, 2007). The precise architecture of this xNT varies considerably between PyoS2 and PyoSN – PyoS2 xNT adopts a short β-hairpin motif while the PyoSN xNT possesses no significant secondary structure. The PyoSN xNT additionally forms numerous hydrogen bond interactions with the α-helical bundle, particularly around residues 10 – 15, (DTTVVG) which function to anchor the xNT motif to the domain. As a result, the interface between the xNT motif of PyoSN appears to be much more intimate than that of PyoS2. The calculated buried surface area between the PyoSN xNT and the α-helical bundle is 2960 $Å^2$, whereas the analogous region of PyoS2 has a buried surface area of 1939 $Å^2$. This extensive interaction interface, containing several buried hydrophobic residues shielded by the PyoSN xNT in the crystal structure, could explain the loss of thermodynamic stability observed upon its removal. Thermal denaturation of the $PyoSN_{NTD}$ monitored by DSC showed that the domain unfolded with a T_m of 37.9 °C. This is significantly lower than that which has been reported for other CLBs, with the translocator binding domain of PyoS2 unfolding at a T_m of 50 °C (White *et al.*, 2017) and the receptor binding domain of colicin E1 equally unfolding at a T_m of 52 °C (Griko *et al.*, 2000). The pronounced thermal instability of the $PyoSN_{NTD}$ is further compounded through removal of the xNT motif, which results in a reduction of the domain melting temperature by 18 °C. Removal of the analogous β-hairpin motif of PyoS2 reduces the T_m by 6 °C, suggesting that N-terminal domain of PyoSN is more susceptible to denaturation upon removal of its xNT. This could play a significant role in the import mechanism of PyoSN, whereby xNT removal may expediate helical unfolding of the PyoSN N-terminal domain. Indeed, the formation of a high affinity interaction (K_d = 61 nM) between the xNT and TonB1 supports the denaturation of the domain during import in response to TonB-mediated force.

4.4. Conclusions.

The work presented in this chapter identified that the PyoSN translocator binding domain was located at the N-terminus, forming a complex with CntO *in vitro*. Crystallisation of the $PyoSN_{NTD}$ in isolation revealed a three α-helical fold that is conserved with both PyoS2 and PyoS5. The $PyoSN_{NTD}$ contains an extended N-terminal motif that contains the TonB1 box, required for energisation of import. Removal of the xNT profoundly affects the thermostability of the domain, which could potentially play a role in import across the OM.

Chapter 5 – Structural Constraints of Pyocin S2 Import Through FpvAI

5.1. Introduction.

To reach their specific intracellular targets, CLBs must first pass through the Gram-negative OM. Gram-negative bacteria possess extensive systems for protein secretion to the extracellular environment (Green & Mecsas, 2016), yet no analogous systems have been identified for the import of protein substrates into cells. Instead, CLBs have adapted to parasitize OMPs present in the target cell's OM, through which they translocate.

The precise mechanisms by which CLBs are imported across the OM remains an area of active research. The majority of Group A CLBs are thought to exploit porins to translocate across the OM (Housden *et al.*, 2010), although multidrug efflux pumps can also be utilised (Zakharov *et al.*, 2004). Upon localisation to the cell surface through receptor binding to BtuB, the enzymatic (E) colicins E2 – E9 recruit the general porin OmpF (or OmpC), through which an intrinsically unstructured N-terminal domain (IUTD) sequence is delivered (Housden *et al.*, 2010). The IUTD passes through a single OmpF β-barrel lumen, whereby an OmpF-binding sequence (OBS2) forms a stable association with the β-barrel interior (Housden *et al.*, 2018). An additional OBS sequence, OBS1, located at the N-terminus of the IUTD, is then able to bind within the lumen of a second subunit of the OmpF trimer, in the reverse orientation to OBS2. This allows presentation of a TolB binding epitope in the periplasm at a fixed orientation, presumably initiating contact with TolB in a manner that allows active recruitment of the Tol complex for energised import (Housden *et al.*, 2013, 2018). Therefore, the OmpF pore is most likely exploited as the translocator through which the entire colicin passes.

In contrast, Group B CLBs typically utilise a TBDT for import across the OM. With the exception of ColIa, which requires recruitment of an additional copy of Cir (Jakes & Finkelstein, 2010), Group B CLBs are thought to translocate directly through the primary OMP receptor, bound during localisation on the target cell surface (Devanathan & Postle, 2007). How this occurs remains unclear, however significant insights into the mechanisms of this process have been gained from the structure of the N-terminal domain of PyoS2 ($PyoS2_{NTD}$), in complex with its translocator FpvAI (Figure 5-1). $PyoS2_{NTD}$ forms a high-

affinity interaction with FpvAI, binding with a K_d of ~240 pM and outcompeting binding of the native ligand Fe^{3+}-PVD (White *et al.*, 2017).

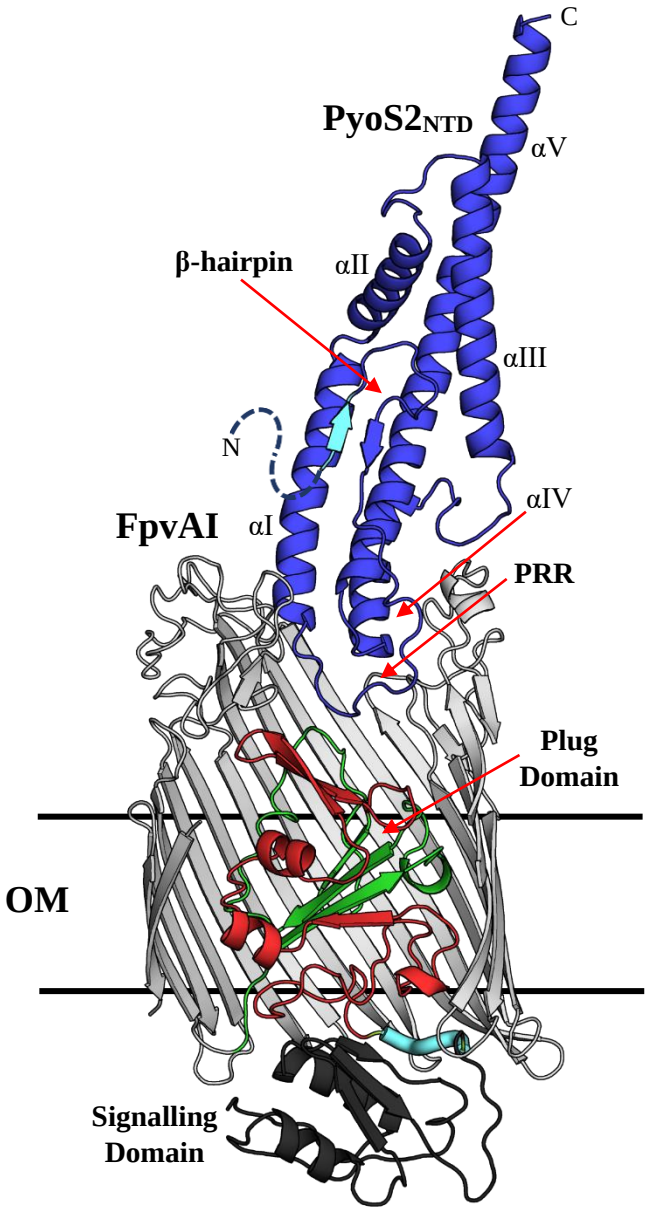

Figure 5-1. Structure of the FpvAI:PyoS2$_{NTD}$ complex.
Cartoon representation of the PyoS2$_{NTD}$ (*blue*) in complex with its translocator FpvAI (*grey*). Several strands that comprise the FpvAI β-barrel have been removed to highlight the plug domain, which is coloured according to its predicted mechanical properties: labile (*red*) and non-labile (*green*) subdomains. TonB1-boxes (highlighted in *cyan*) are present in both proteins; within the β-hairpin motif of PyoS2 and following the signalling domain of FpvAI (*black*). PyoS2$_{NTD}$ helices α1 to αV are denoted in the structure. Residues 2 – 10 of PyoS2$_{NTD}$ are not present in the crystal structure and are presumed disordered (*dashed line*). PDB ID = 5ODW (White *et al.*, 2017)

The structure of the FpvAI:PyoS2$_{NTD}$ complex reveals that, unlike comparable structures of ColE3 and ColIa receptor complexes (Buchanan *et al.*, 2007), PyoS2$_{NTD}$ binds in an

orientation that positions the domain directly above the translocator (White *et al.*, 2017). A short proline rich region (PRR) motif, comprising residues 35 – 45 (TPPFVPPGPSP) forms interactions with the FpvAI PVD binding cleft, mimicking binding of Fe^{3+}-PVD to FpvAI. This suggests PyoS2 translocation occurs through the same mechanism as PVD uptake.

The PyoS2 N-terminal domain is primarily α-helical, with significant structural homology to the N-terminal domains of both PyoS5 and PyoSN, introduced in Chapter 4. However, $PyoS2_{NTD}$ contains an additional short β-hairpin that associates laterally with the α-helical bundle. This β-hairpin contains the TonB1-box, required for energisation of PyoS2 import across the OM through parasitizing the TonB1 complex (White *et al.*, 2017). Preceding the TonB1-box is a short N-terminal sequence that is absent from the crystal structure, and as such, is presumed to be disordered *in vivo*. The FpvAI translocator possesses typical TBDT architecture, with a β-barrel domain occluded by a globular plug (Noinaj *et al.*, 2010). TBDTs also contain TonB-boxes, which are thought to stimulate force remodelling of the plug domain upon contact with the TonB complex. This process generates a pore through FpvAI which PyoS2 translocates, which is supported by *in vitro* crosslinking data (White *et al.*, 2017).

The structural constraints of PyoS2 import through the FpvAI translocator are poorly understood. The FpvAI:$PyoS2_{NTD}$ structure depicts a 'closed state', in which the FpvAI β-barrel is completely occluded by the plug domain (Figure 5-1). As such, it is currently unknown what role, if any, the FpvAI plug domain plays in translocation of PyoS2. This is further confounded by the presence of two mechanically independent subdomains within the plug domain, as demonstrated for the TBDT BtuB. AFM studies on the mechanism of substrate uptake by BtuB have shown that the plug domain is comprised of a labile subdomain that unravels upon TonB1-dependent torque application, and a non-labile subdomain that remains associated with the β-barrel domain (Hickman *et al.*, 2017). Indeed, molecular dynamics (MD) simulations of FpvAI unplugging also demonstrates partial removal of the plug domain in response to the application of force (Dr. Emanuele Paci, University of Leeds, *personal communication*). Structural alignment of the BtuB and FpvAI plug domains reveal that displacement of the FpvAI labile plug subdomain (residues 126 – 215) generates a pore ~13 Å in diameter (Figure 5-2). Whilst this pore diameter is sufficient for Fe^{3+}-PVD uptake, the dimensions do not support $PyoS2_{NTD}$ translocation in a folded state. Thus, PyoS2 is assumed to translocate through FpvAI in an extended conformation; however, no direct evidence is currently available to support PyoS2 unfolding during

translocation across the OM. Furthermore, the TonB1-box motif of PyoS2, required to stimulate import, is located distally from the FpvAI translocator (White *et al.*, 2017). Dissociation of the TonB1-box from the α-helical bundle and into the periplasm is a prerequisite for PyoS2 import (White *et al.*, 2017), though how this process occurs is currently unresolved.

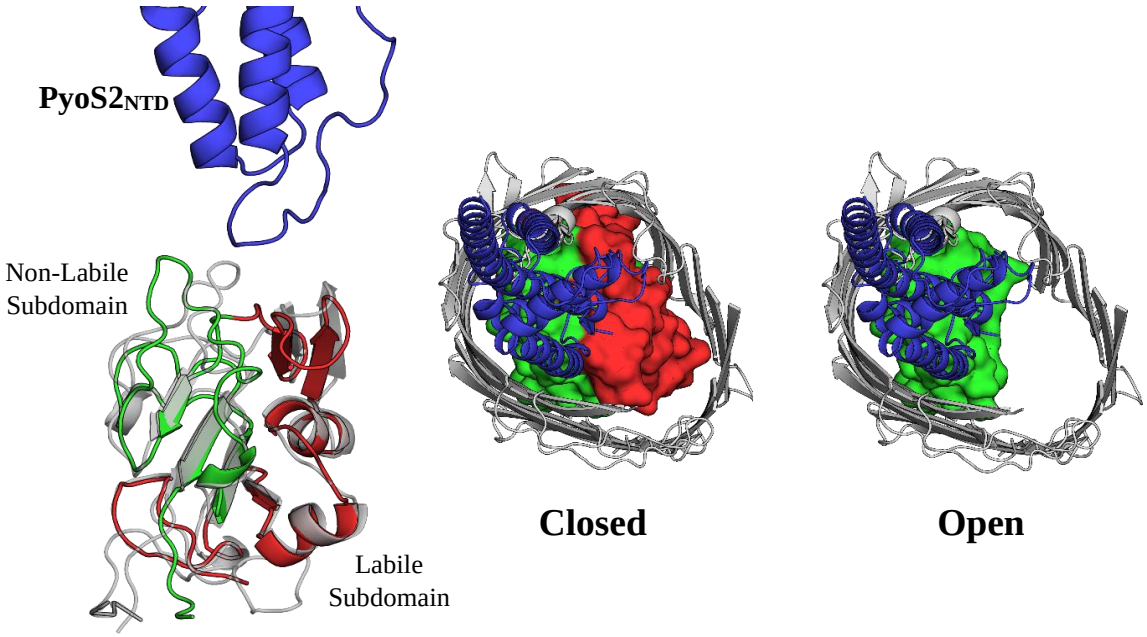

Figure 5-2. Removal of the labile plug subdomain of FpvAI generates a pore.
Structural alignment (RMSD = 1.5 Å) of the FpvAI (*grey*) and BtuB plug domains (PDB ID = 1NQH (Chimento *et al.*, 2003)). The labile (*red*) and non-labile (*green*) plug subdomains of BtuB are highlighted. Extracellular views of the FpvAI:PyoS2$_{NTD}$ complex (PDB ID = 5ODW (White *et al.*, 2017)) in 'closed' and 'open' conformations, resulting from removal of the labile subdomain, reveals a ~13 Å pore through the transporter.

In this chapter, I address the structural constraints of PyoS2 import across the OM through its translocator FpvAI that have been inferred from the crystal structure. Firstly, the role of the FpvAI plug domain in PyoS2 import is investigated. I then characterise the initial stages of PyoS2 translocation, in which the TonB1 sequence is delivered to the periplasm to contact the TonB1 complex. Finally, I delineate the mechanism by which PyoS2 translocates through the FpvAI transporter, utilising disulphide mutants within the PyoS2 N-terminal domain to stall import. As such, an updated model for PyoS2 translocation through the FpvAI transporter was developed, encompassing the structural constraints delineated during this study. This mechanism of import could be conserved across the S-type pyocin family, in addition to bearing some hallmarks to the import systems utilised by mitochondria for protein import.

5.2. Results.

5.2.1. The FpvAI plug domain is required for PyoS2 import

The FpvAI:PyoS2$_{NTD}$ crystal structure depicts FpvAI in a closed state, with the β-barrel completely occluded by the plug domain (Figure 5-1). To explore the role of the FpvAI plug in PyoS2 translocation, a *P. aeruginosa* strain expressing the FpvAI β-barrel domain only (PAS033) was screened for susceptibility to PyoS2. A chimeric PyoS2E2 construct, used to subvert resistance of the *P. aeruginosa* PAO1 parent strain, was found to be inactive against PAS033, despite the presence of the unoccluded FpvAI lumen (Figure 5-3). Therefore, PyoS2 is unable to translocate through the open lumen of the FpvAI β-barrel domain alone.

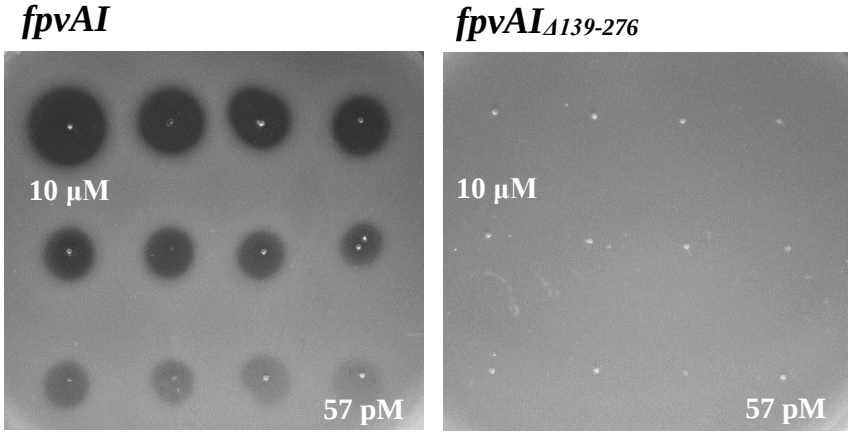

Figure 5-3. Loss of the FpvAI plug abrogates PyoS2E2 cytotoxicity.
Plate-killing assays showing *P. aeruginosa* strain PAS033 (*fpvAI*$_{Δ139-276}$) is resistant to PyoS2E2 activity, in comparison to parent strain PAO1 (*fpvAI*). Zones of clearance result from cell killing.

It has previously been demonstrated that expression of a soluble FpvAI plug domain (*fpvAI*$_{1-276}$) is able to complement a plugless FpvAI β-barrel and partially restore PVD uptake (Nader *et al.*, 2011). However, as a portion of the FpvAI plug is predicted to remain associated with the β-barrel, it is unclear as to the precise role the FpvAI plug undertakes during import. PAS033 was transformed with plasmids encoding for the intact FpvAI plug domain (residues 1 – 276), or the non-labile subdomain alone (residues 216 – 276). Expression of the soluble FpvAI plug domain was found to restore susceptibility to PyoS2E2 *in vivo*, indicating pyocin translocation can also be re-established *in-trans* (Figure 5-4). However, cells expressing the non-labile plug subdomain alone remained resistant to PyoS2E2 activity (Figure 5-4), suggesting that an intact FpvAI plug domain is a requirement for PyoS2 cytotoxicity.

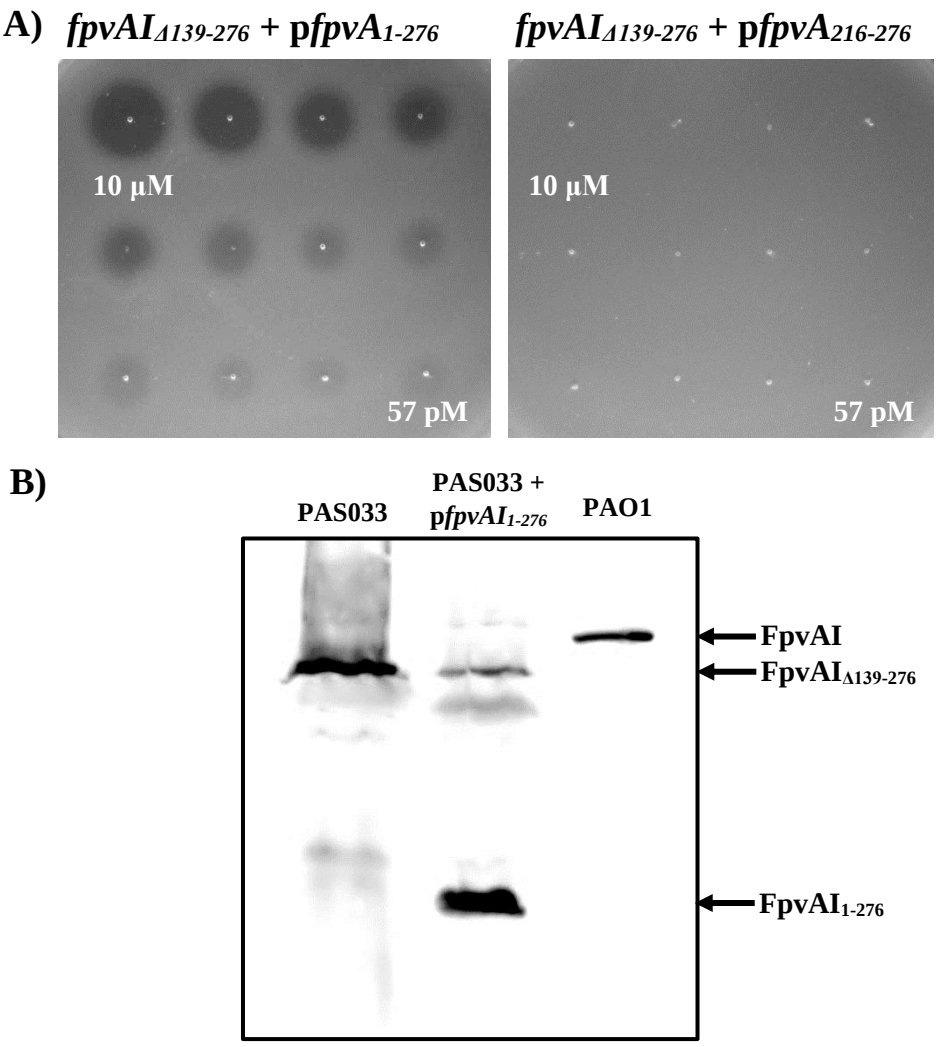

Figure 5-4. An intact FpvAI plug domain is required for PyoS2E2 cytotoxicity. A) Plate-killing assays show expression of an intact plug (p*fpvAI*$_{1-276}$) in *P. aeruginosa* strain PAS033 restores PyoS2E2 cytotoxic susceptibility, whereas PAS033 expressing the non-labile plug subdomain alone (p*fpvAI*$_{216-276}$) remain resistant to PyoS2E2. Zones of clearance result from cell killing. B) Western Blot of total membrane extracts of *P. aeruginosa* strains PAO1 (*fpvAI*), PAS033 (*fpvAI*$_{\Delta 139-276}$) and PAS033 + p*fpvAI*$_{1-276}$. Total membrane extracts, prepared from cells grown for 16 h in succinate medium at 30 °C, were subjected to SDS-PAGE on a 12% polyacrylamide gel followed by transfer onto a PVDF membrane. FpvAI expression was detected with primary rabbit anti-FpvAI antiserum. Expression of the non-labile plug subdomain alone could not be detected by this method.

The role of the FpvAI plug during PyoS2 import was further investigated through fluorescence microscopy using a fluorescently labelled PyoS2$_{NTD}$ (PyoS2$_{NTD}$-AF488) construct to probe interactions with the mutant FpvAI transporter *in vivo*. PyoS2$_{NTD}$-AF488 was unable to specifically label PAS033 in comparison to the PAO1 wild type strain (Figure 5-5). Therefore, PAS033 resistance to PyoS2E2 activity was demonstrated to stem from abrogation of binding between the plugless FpvAI transporter and the PyoS2$_{NTD}$.

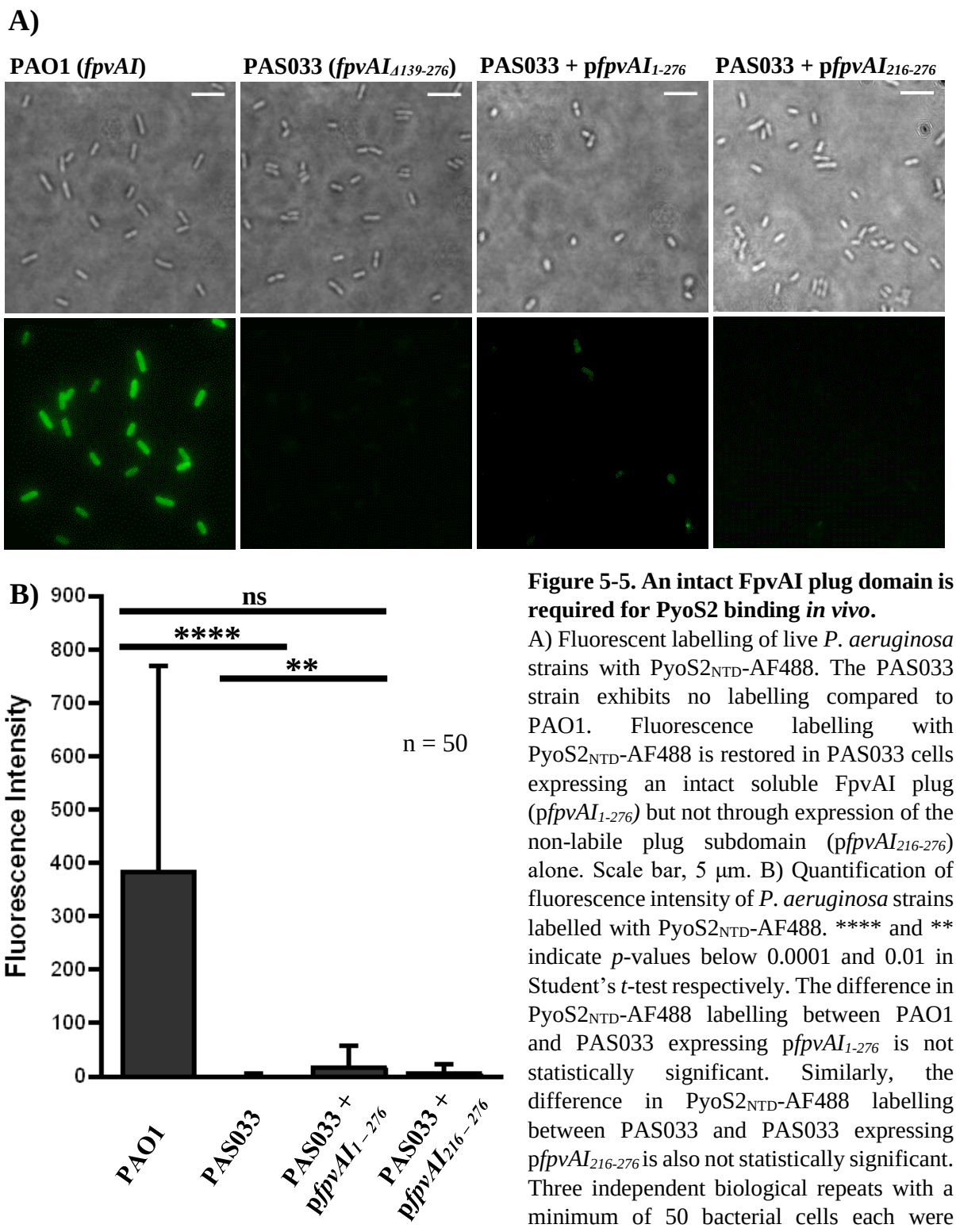

Figure 5-5. An intact FpvAI plug domain is required for PyoS2 binding *in vivo*.
A) Fluorescent labelling of live *P. aeruginosa* strains with $PyoS2_{NTD}$-AF488. The PAS033 strain exhibits no labelling compared to PAO1. Fluorescence labelling with $PyoS2_{NTD}$-AF488 is restored in PAS033 cells expressing an intact soluble FpvAI plug (p*fpvAI*$_{1-276}$) but not through expression of the non-labile plug subdomain (p*fpvAI*$_{216-276}$) alone. Scale bar, 5 μm. B) Quantification of fluorescence intensity of *P. aeruginosa* strains labelled with $PyoS2_{NTD}$-AF488. **** and ** indicate *p*-values below 0.0001 and 0.01 in Student's *t*-test respectively. The difference in $PyoS2_{NTD}$-AF488 labelling between PAO1 and PAS033 expressing p*fpvAI*$_{1-276}$ is not statistically significant. Similarly, the difference in $PyoS2_{NTD}$-AF488 labelling between PAS033 and PAS033 expressing p*fpvAI*$_{216-276}$ is also not statistically significant. Three independent biological repeats with a minimum of 50 bacterial cells each were quantified per sample.

Quantification of fluorescent labelling of PAS033 cells expressing the soluble FpvAI plug domain demonstrated restoration of $PyoS2_{NTD}$ binding at a reduced level compared to PAO1 cells expressing the full length FpvAI transporter (Figure 5-5). This reduction in binding is

analogous to that of reduced rates of PVD uptake observed for the reconstituted transporter (Nader *et al.*, 2011). PyoS2 binding was not restored when PAS033 was complemented with the non-labile subdomain alone (Figure 5-5). Therefore, the presence of an intact FpvAI plug domain is critical for $PyoS2_{NTD}$ binding and is required for import of PyoS2 *in vivo*.

5.2.2. The TonB1-boxes of S-type pyocins are interchangeable.

As mentioned previously, all S-type pyocins to date have also been found to hijack the TonB1 complex to energise import (White *et al.*, 2017; Latino *et al.*, 2019; Behrens *et al.*, 2020; Atanaskovic *et al.*, 2020). This implies an analogous TonB1 binding epitope across the S-type pyocin family, and potentially a conserved mechanism for its delivery into the periplasm. Therefore, the xNTs of S-type pyocins that have been confirmed experimentally to parasitize the TonB1 complex were identified using three-dimensional structural information where possible, or PSIPRED (through identification of residues preceding the first predicted N-terminal α-helix). Alignment of these sequences with those of PyoS2 and PyoS5, which contain well characterised TonB1-boxes (White *et al.*, 2017; Behrens *et al.*, 2020), facilitated identification of homologous pentapeptide motifs possessing considerable amino acid conservation within the S-type pyocin xNTs, designated putative TonB1-boxes (Figure 5-6). These pentapeptide sequences are primarily comprised of hydrophobic and β-branched amino acids, such as threonine, valine, isoleucine, and methionine. In addition, all sequences possess an acidic/hydrophobic amino acid pair preceding their putative TonB1-boxes, though the precise distance from the pentapeptide sequence varies. To confirm the identification of TonB1-box motifs, the N-terminal residues of PyoSN predicted to contain its putative TonB1-box (residues 1 – 16) were substituted for those at the PyoS2 extreme N-terminus, and the resulting construct was assayed for cytotoxicity. The PyoSNS2 chimera ($PyoS2_{SN1-16}$) remained active against *P. aeruginosa* strain YHP17, confirming the presence of a TonB1-box within the first 16 residues of PyoSN (Figure 5-6). This confirms that TonB1-boxes from S-type pyocins are interchangeable and as such, could utilise a conserved mechanism for epitope delivery prior to translocation.

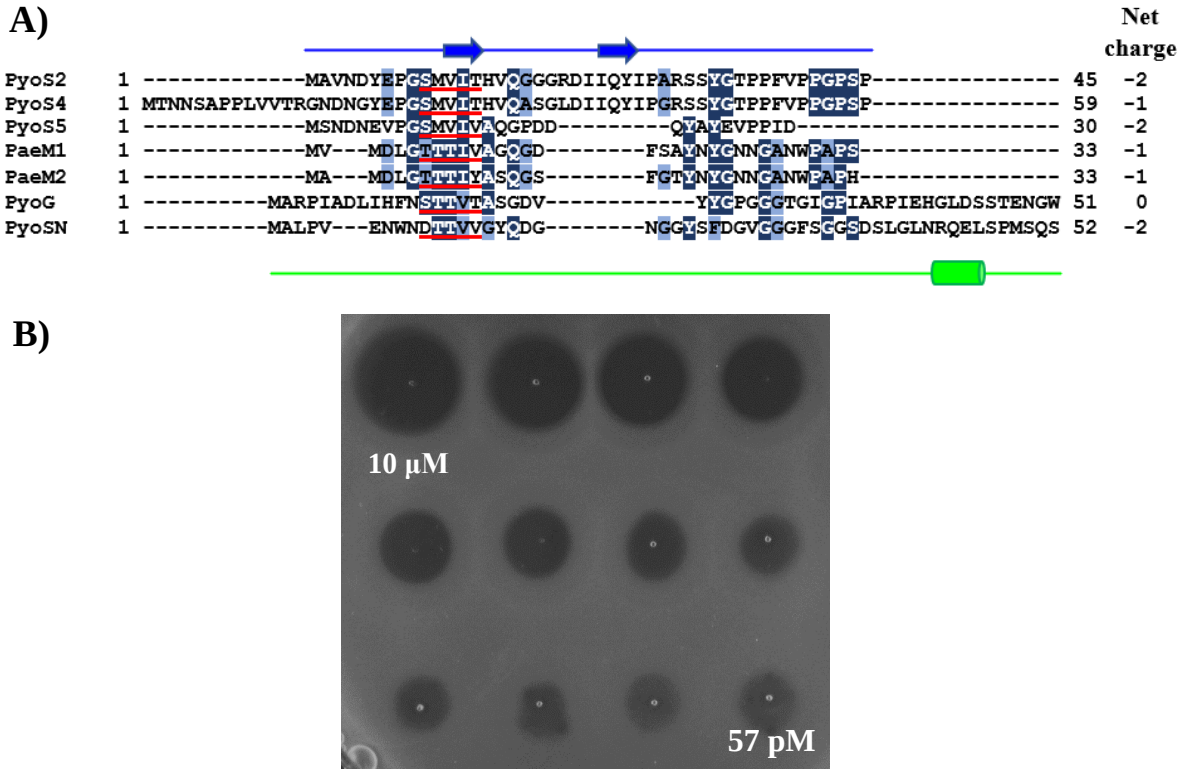

Figure 5-6. The TonB1-boxes of S-type pyocins are interchangeable.
A) Sequence alignment of unstructured residues of confirmed TonB1-dependent S-type pyocins with the net charge of their predicted unstructured N-termini at pH 7.0. Secondary structural elements adopted within the xNTs of PyoS2 (*blue*) and PyoSN (*green*) are displayed above and below the alignment, respectively. Alignment was performed with Clustal Omega and annotated using Boxshade. B) Plate-killing assay demonstrates substitution of the unstructured N-terminus and TonB1-box region of PyoS2 (residues 1 – 16) with that of PyoSN ($PyoS2_{SN1-16}$) does not affect its cytotoxic activity against *P. aeruginosa* strain YPH17, indicating that these residues are interchangeable, provided the presence of a functional TonB1-box. Zones of clearance result from cell killing.

5.2.3. The unstructured PyoS2 N-terminus is required for optimal import.

The PyoS2 TonB1-box is sequestered in a β-hairpin motif within the N-terminal domain in the FpvAI:$PyoS2_{NTD}$ crystal structure (Figure 5-1). To contact TonB1, this motif must dissociate from its current position and enter the periplasm, likely through the FpvAI transporter. It was reasoned that the residues preceding the TonB1-box could be involved in its delivery to the periplasm, as demonstrated previously for the analogous delivery of Tol binding motifs of Group A CLBs (Housden *et al.*, 2013). These residues are unstructured in the FpvAI:$PyoS2_{NTD}$ crystal structure and as such, have no mechanistic role in translocation ascribed to them. To evaluate whether the unstructured N-terminus plays a role in PyoS2 translocation *in vivo*, residues preceding the TonB1-box of PyoS2 were truncated (PyoS2Δ1-

9) and the resulting construct tested for cytotoxic activity. PyoS2Δ1-9 displayed no significant reduction in cytotoxicity against *P. aeruginosa* YHP17 (Figure 5-7).

However, kinetic time-course cytotoxicity experiments showed that deletion of these residues resulted in an increase in colony forming units (CFU) for PyoS2Δ1-9 compared to PyoS2 (Figure 5-7). Calculation of the half-lives ($t_{1/2}$) of pyocin translocation revealed PyoS2Δ1-9 has a $t_{1/2}$ of 3.5 ± 0.4 minutes; approximately three times greater than the $t_{1/2}$ of PyoS2 (1.2 ± 0.2 minutes). Therefore, loss of the N-terminal residues preceding the TonB1-box imparts a kinetic penalty on the PyoS2 translocation rate, slowing import across the OM and increasing the $t_{1/2}$ for pyocin-induced cytotoxicity.

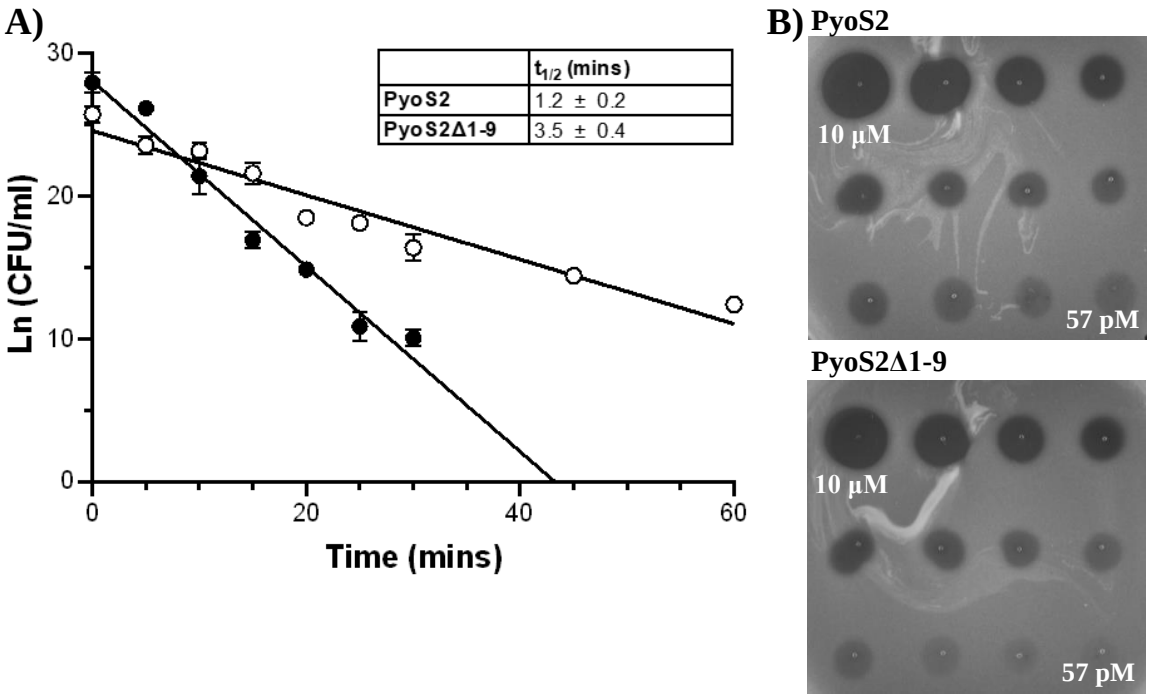

Figure 5-7. The unstructured N-terminus of PyoS2 is required for optimal rate of translocation.
A) PyoS2 kinetic time-course cytotoxicity assay demonstrates that truncation of unstructured residues upstream of the TonB1-box decreases the rate of translocation for PyoS2Δ1-9 (○) compared to PyoS2 (●). Colony counts from four independent YHP17 cultures (with error bars representing standard deviation) were fitted to a pseudo-first order reaction model and translocation half-lives ($t_{1/2}$) were calculated from the linear plot. B) Plate-killing assays demonstrate PyoS2Δ1-9 displays no significant reduction in cytotoxicity against *P. aeruginosa* strain YHP17, compared to PyoS2. Zones of clearance result from cell killing.

5.2.4. Expression and characterisation of PyoS2 disulphide mutants.

To investigate whether unfolding of PyoS2 is a prerequisite for translocation, cysteine mutations were introduced into the PyoS2 N-terminal domain at various positions as predicted by Disulfide by Design (https://doi.org/10.1186/1471-2105-14-346) (Craig & Dombkowski, 2013) from the FpvAI:PyoS2$_{NTD}$ structure (Figure 5-8)

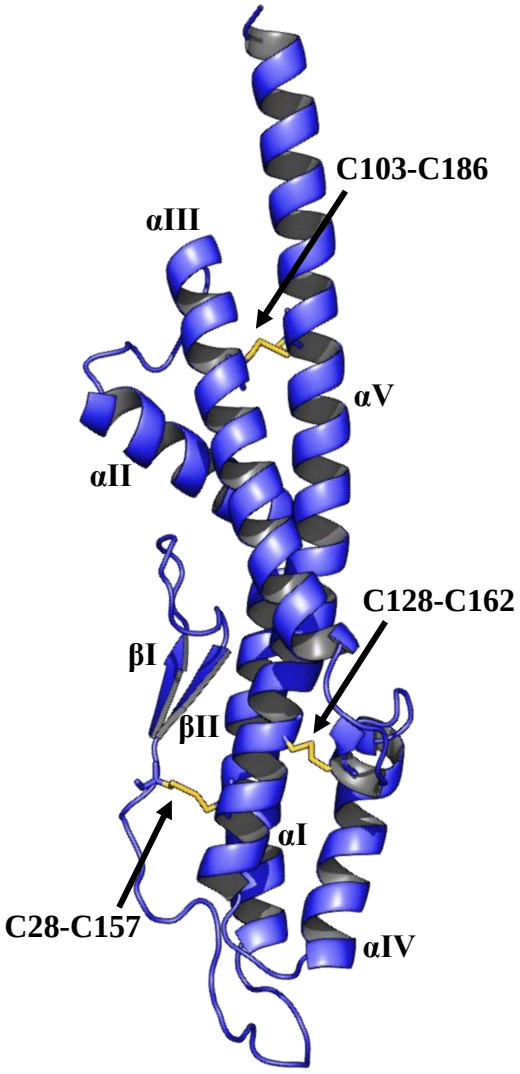

Figure 5-8. Disulphide bond positions within the PyoS2 N-terminal Domain.
Cartoon representation of the PyoS2$_{NTD}$ from the FpvAI:PyoS2$_{NTD}$ structure with disulphide positions predicted by Disulfide By Design (position C11-C26 not shown).

The four PyoS2 disulphide mutants (expressed with their cognate ImS2-His$_6$ immunity protein) were expressed in *E. coli* BL21(DE3) cells, followed by purification using Ni^{2+}-affinity chromatography and SEC. These proteins were found to express well (with the exception of PyoS2(C28-C157)) with minimal homodimeric species present (Figure 5-9).

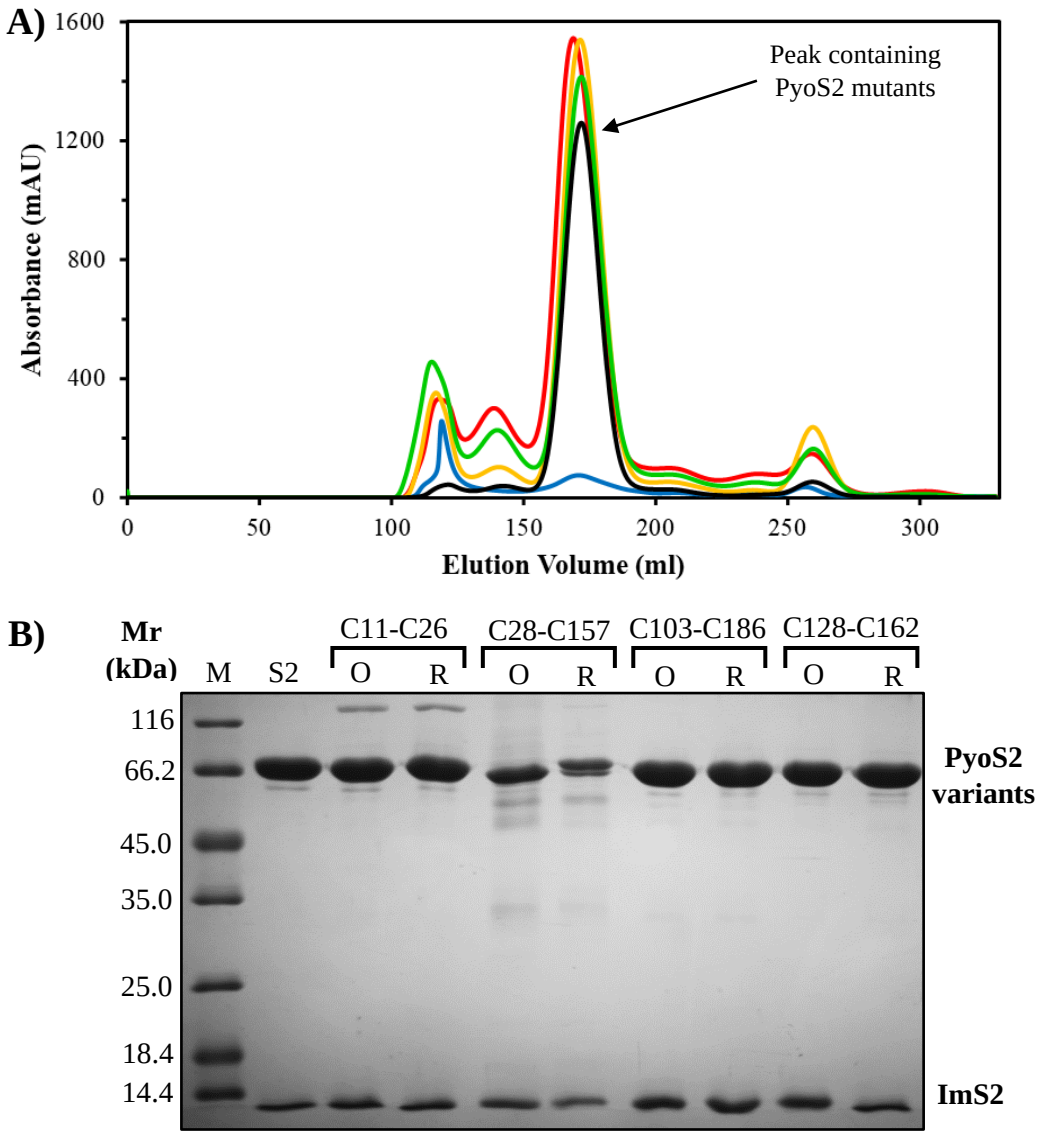

Figure 5-9. Purification of PyoS2-ImS2 disulphide mutants.
A) Elution profile of the measured A_{280nm} for PyoS2 disulphide mutants C11-C26 (*red*), C28-C157 (*blue*), C103-C186 (*yellow*) and C128-C162 (*green*), in addition to PyoS2 (*black*) from a Superdex 200 26/60 column. Proteins eluted in the third peak, highlighted with an arrow, B) 12% polyacrylamide gel of the final SEC purified PyoS2 disulphide proteins (positions denoted above) under different oxidation conditions. M, unstained protein marker (Pierce), S2, PyoS2, O, oxidised with 1 mM diamide, R, reduced with 5 mM DTT.

The formation of disulphide bonds was probed through an *in vitro* fluorescence-based assay in which oxidised and reduced PyoS2 disulphide mutants were labelled with AF488 under denaturing conditions. The presence of disulphide bonds in the oxidised (using diamide) PyoS2 protected them from AF488 labelling (Figure 5-10). The equivalent PyoS2 mutants treated with DTT exhibit significant fluorescence signal.

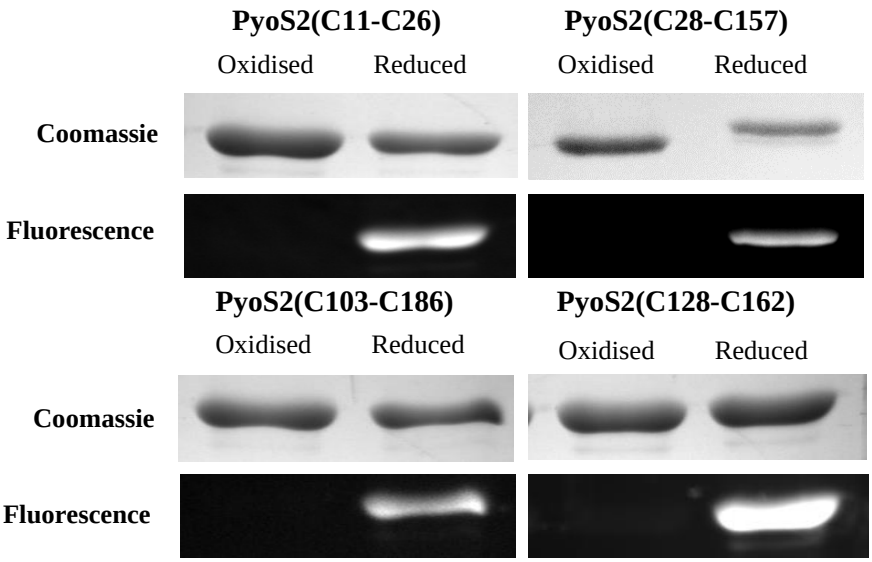

Figure 5-10. Conformation of PyoS2 disulphide bond formation *in vitro* via AF488 labelling. Snapshots from a 12% polyacrylamide gel of PyoS2 disulphide mutants labelled with AF488 after oxidation/reduction treatment. No labelling of free cysteines occurs in the oxidised samples, confirming disulphide bond formation.

Disulphide formation was then further characterized using denaturing ESI-MS (performed by Dr. David Staunton, Molecular Biophysics Suite, Department of Biochemistry, University of Oxford). PyoS2 disulphide species were oxidised or reduced as described previously in section 2.6.1, and their resultant mass spectra were assessed. Reduced PyoS2 disulphide species were additionally denatured and alkylated with iodoacetamide prior to ESI-MS analysis to prevent spontaneous disulphide bond reformation. The oxidised PyoS2 disulphide mutants all exhibited a single peak, from which their molecular weight was calculated. The calculated PyoS2 disulphide mutant molecular weights correspond to that of their predicted masses (Table 5-1). The absence of additional peaks within the ESI-MS spectra suggests no stable reaction intermediate is formed between the diamide and the cysteine residues of the PyoS2 disulphide mutants. The alkylated PyoS2 disulphide mutants all demonstrated a peak shift of ~ 114 Da, corresponding to the presence of two modified carboxyamidomethylcysteine residues. However, this modification was not always the dominant species present in the ESI-MS spectra, with peaks that indicate incorporation of a single alkylated carboxyamidomethylcysteine also present. Taken together, disulphide bond formation can be confirmed for the PyoS2 disulphide mutants *in vitro*, in addition to a mechanism for prevention of disulphide reformation through alkylation of the free cysteines.

Table 5-1. PyoS2 disulphide mutant molecular weights determined by denaturing ESI-MS.

PyoS2 Disulphide Mutant	Predicted Molecular Weight [Da]	Observed Molecular Weight by denaturing ESI-MS [Da]	
PyoS2(C11-C26)‡-ImS2	84739.1	84739.8	84853.4₸
PyoS2(C28-C157)‡-ImS2	84821.1	84820.9	84938.9₸
PyoS2(C103-C186)‡-ImS2	84792.1	84792.7	84906.2₸
PyoS2(C128-C162)‡-ImS2	84741.1	84741.4	84859.4₸

‡Initiator Methionine cleaved.
₸Contains two carboxyamidomethylcysteine residues.

All ESI-MS performed by Dr. David Staunton, Molecular Biophysics Suite, Department of Biochemistry, University of Oxford.

5.2.5. Disulphide formation within the PyoS2$_{NTD}$ does not increase its thermal stability.

N-terminal domains of the PyoS2 disulphide mutants were also expressed in isolation to assess whether disulphide bond formation affected the overall domain structure and stability. PyoS2 N-terminal truncations were generated for three of the disulphide positions (the N-terminal domain of PyoS2(C28-C157) could not be successfully purified) and investigated by far UV-CD spectroscopy. The three disulphide mutant NTDs successfully purified demonstrated near identical secondary structure to native PyoS2$_{NTD}$ indicating correct folding of the domain (Figure 5-11). Thermal melt curves for the oxidised PyoS2 disulphide NTDs indicate that disulphide formation does not affect the thermal stability of the PyoS2$_{NTD}$ domain in PyoS2$_{NTD}$(C103-C186) and PyoS2$_{NTD}$(C128-C162), with these mutants possessing melting temperatures (T_m) of 49 – 50 °C (Figure 5-12A). PyoS2$_{NTD}$(C11-C26) was found to have a reduced T_m of 44 °C, indicating that disulphide bond formation has caused partial destabilisation of the PyoS2$_{NTD}$ domain (Figure 5-12A). This likely results from perturbation of the interaction between the β-hairpin motif (containing the disulphide bond) and α-helical bundle. Reduction and alkylation of the PyoS2 disulphide NTDs (to prevent disulphide reformation) resulted in large shifts in domain melting temperatures, with T_ms of 40 – 44 °C (Figure 5-12B). This is presumably caused by the addition of two carboxyaminomethyl- groups in close proximity to one another; generating steric clashes within the PyoS2$_{NTD}$ domain core. It can therefore be concluded that disulphides formed within the PyoS2$_{NTD}$ do not increase the domain stability.

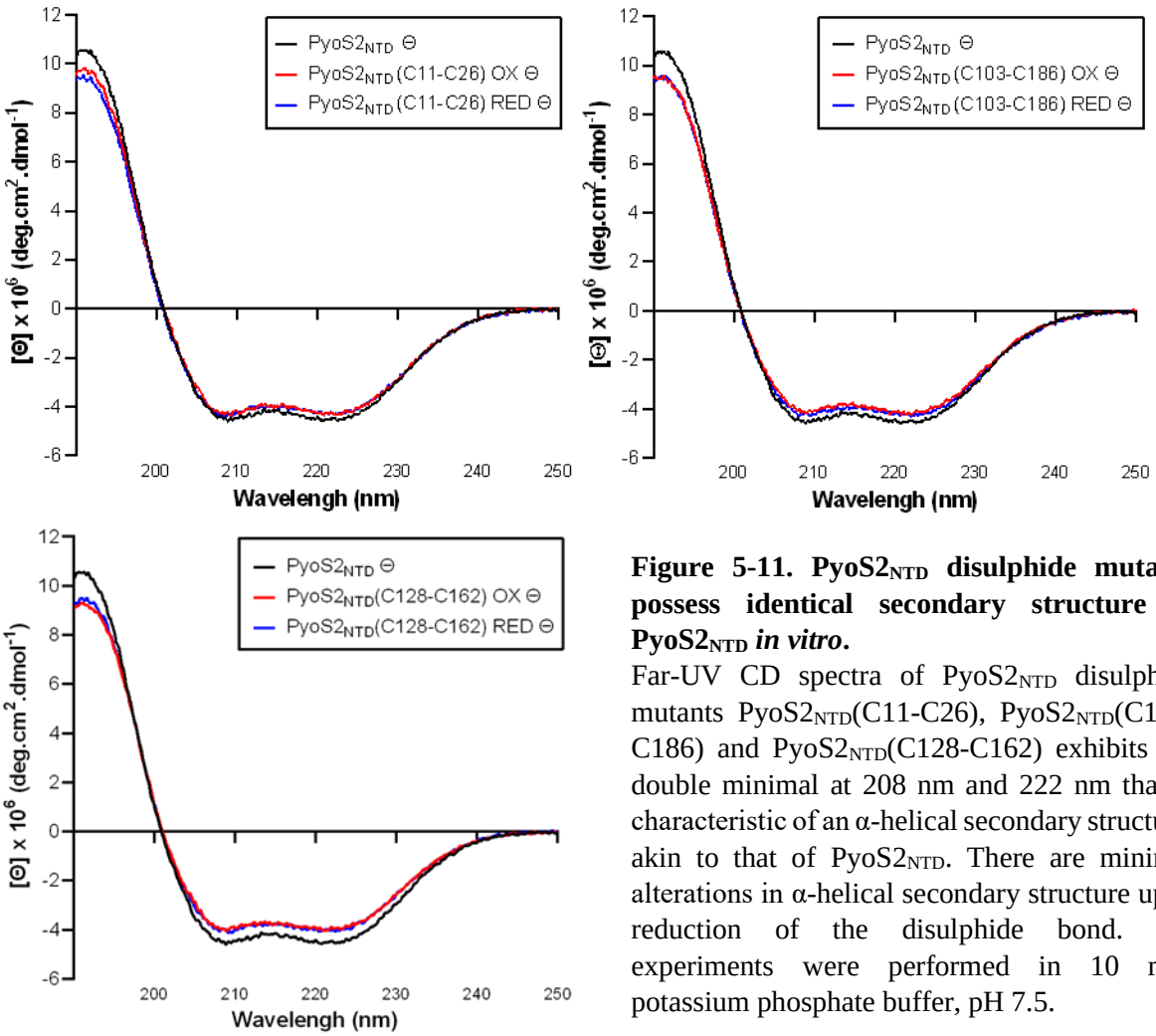

Figure 5-11. PyoS2$_{NTD}$ disulphide mutants possess identical secondary structure to PyoS2$_{NTD}$ *in vitro*.
Far-UV CD spectra of PyoS2$_{NTD}$ disulphide mutants PyoS2$_{NTD}$(C11-C26), PyoS2$_{NTD}$(C103-C186) and PyoS2$_{NTD}$(C128-C162) exhibits the double minimal at 208 nm and 222 nm that is characteristic of an α-helical secondary structure, akin to that of PyoS2$_{NTD}$. There are minimal alterations in α-helical secondary structure upon reduction of the disulphide bond. CD experiments were performed in 10 mM potassium phosphate buffer, pH 7.5.

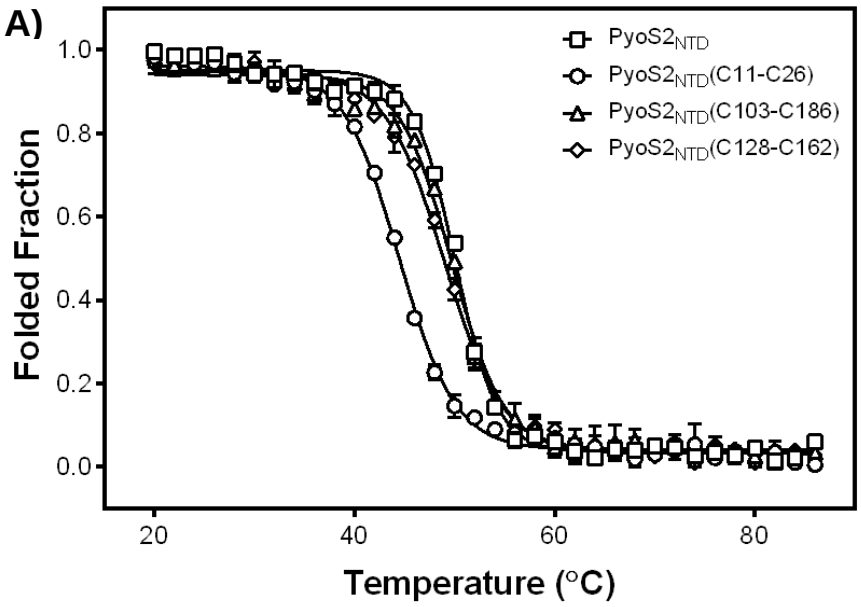

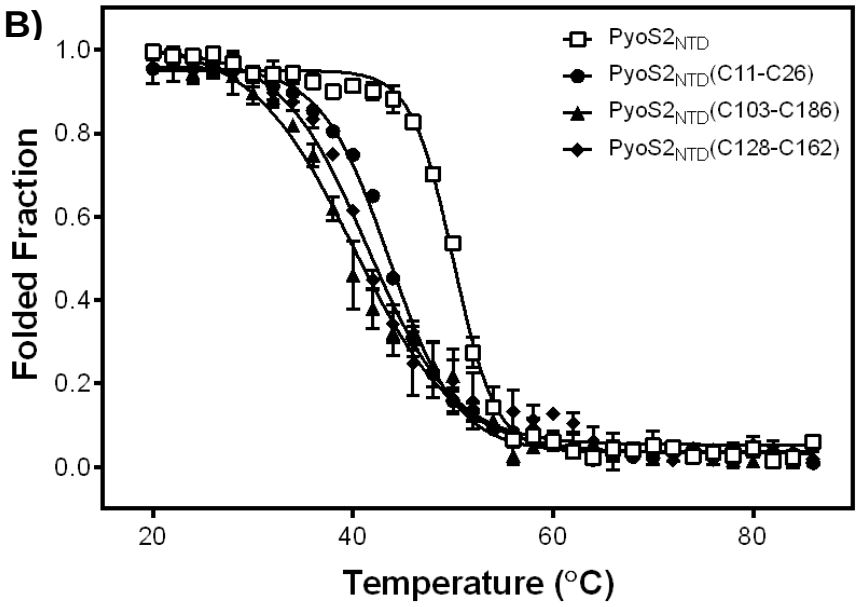

Figure 5-12. Disulphide bond formation within the $PyoS2_{NTD}$ does not increase the thermal stability (T_m) of the domain.
A) Thermal melting curves for isolated N-terminal domains of PyoS2 (□), PyoS2(C11-C26) (○), PyoS2(C103-C186) (Δ) and PyoS2(C128-C162) (◇) after disulphide oxidation obtained by far-UV CD spectroscopy B) Thermal melting curves for isolated N-terminal domains of PyoS2 (□), PyoS2(C11-C26) (●), PyoS2(C103-C186) (▲) and PyoS2(C128-C162) (◆) after disulphide reduction obtained by far-UV CD spectroscopy. All CD experiments were performed in 10 mM potassium phosphate buffer, pH 7.5. Thermal melts were obtained across a temperature gradient of 20 to 86 °C. The normalized average from 3 independent experiments was plotted against temperature with error bars representing the standard deviation.

5.2.6. Unfolding of the PyoS2 β-hairpin motif is required for import.

Utilising the PyoS2 disulphide mutants, delivery of the PyoS2 TonB1-box into the periplasm was investigated. Disulphide bonds were engineered to lock the β-hairpin motif of PyoS2, with PyoS2(C11-C26) preventing β-strand separation, and PyoS2(C28-C157) preventing β-hairpin displacement from the α-helical bundle, respectively. The oxidised PyoS2(C11-C26) and PyoS2(C28-C157) mutants were inactive against *P. aeruginosa* YHP17, as shown by liquid-killing assays and quantified by CFU counts (Figure 5-13 and 5-15). Reduction of the disulphide bonds restored PyoS2 cytotoxic activity for both mutants (Figure 5-13 and 5-15). This confirms that TonB1-box delivery to the periplasm requires flexibility within the β-hairpin; the β-hairpin must displace from the α-helical bundle and furthermore, the β-strands must separate and pass through the FpvAI lumen in an extended conformation.

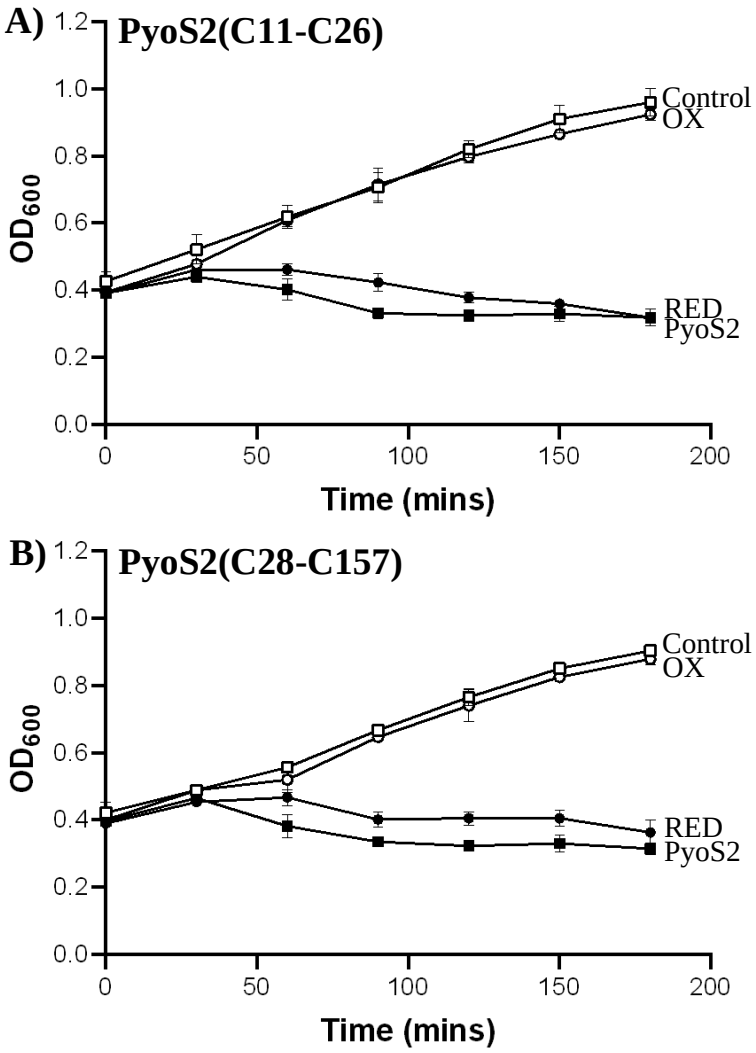

Figure 5-13. Disulphide bond formation within the β-hairpin motif abolishes PyoS2 cytotoxic activity.
P. aeruginosa YHP17 liquid culture killing assays for A) PyoS2(C11-C26) and B) PyoS2(C28-C157) demonstrate that oxidation of the disulphide bond abolishes PyoS2 cytotoxic activity *in vivo*. PyoS2 activity is restored upon reduction of the disulphide bonds. OD_{600nm} measurements averaged from six independent cultures with error bars representing the standard deviation.

5.2.7. Partial unfolding of the PyoS2 α-helical bundle is required for import.

To verify that PyoS2 translocates through FpvAI in an extended conformation, a further pair of disulphide bonds at two different positions within the α-helical bundle of the PyoS2 N-terminal domain (PyoS2(C103-C186) and PyoS2(C128-C162)) were investigated. The oxidised PyoS2(C103-C186) mutant was found to inhibit PyoS2 cytotoxicity against *P. aeruginosa* YPH17 from both liquid-killing assays and quantification by CFU counts (Figure 5-14 and 5-15). Reduction of PyoS2(C103-C186) fully restored cytotoxic activity

(Figure 5-14 and 5-15), suggesting that disulphide formation blocks translocation through prevention of domain unfolding. Interestingly, the oxidised PyoS2(C128-C162) mutant remained active against *P. aeruginosa* YHP17 (Figure 5-14 and 5-15), suggesting this region is imported, regardless of the intramolecular crosslink.

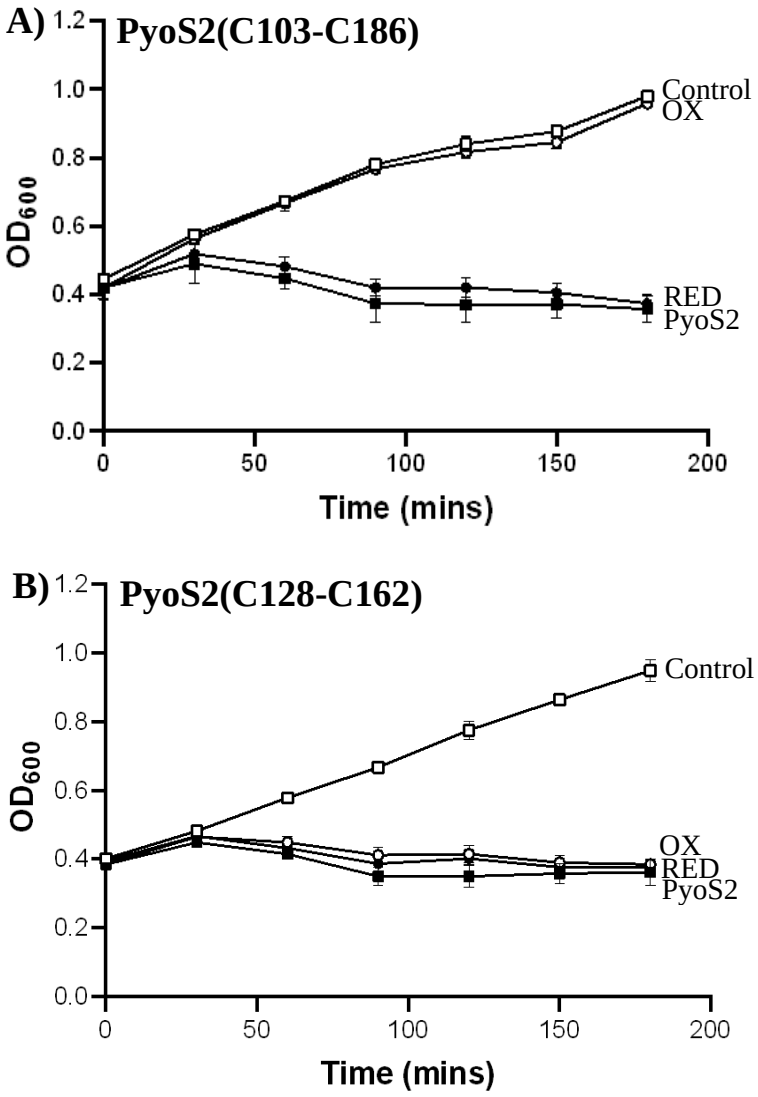

Figure 5-14. Inhibition of PyoS2 cytotoxic activity through disulphide bond formation within the N-terminal domain α-helical bundle is position dependent.
P. aeruginosa YHP17 liquid culture killing assays for A) PyoS2(C103-C186) and B) PyoS2(C128-C162) demonstrate that oxidation of the disulphide bond only abolishes PyoS2 cytotoxic activity for the C103-C186 disulphide mutant. PyoS2(C103-C186) activity is restored upon reduction of the disulphide bond, suggesting unfolding is required for translocation. The PyoS2(C128-C162) mutant remained active after oxidation, suggesting it can translocate in a partially folded state. OD_{600nm} measurements averaged from six independent cultures with error bars representing the standard deviation.

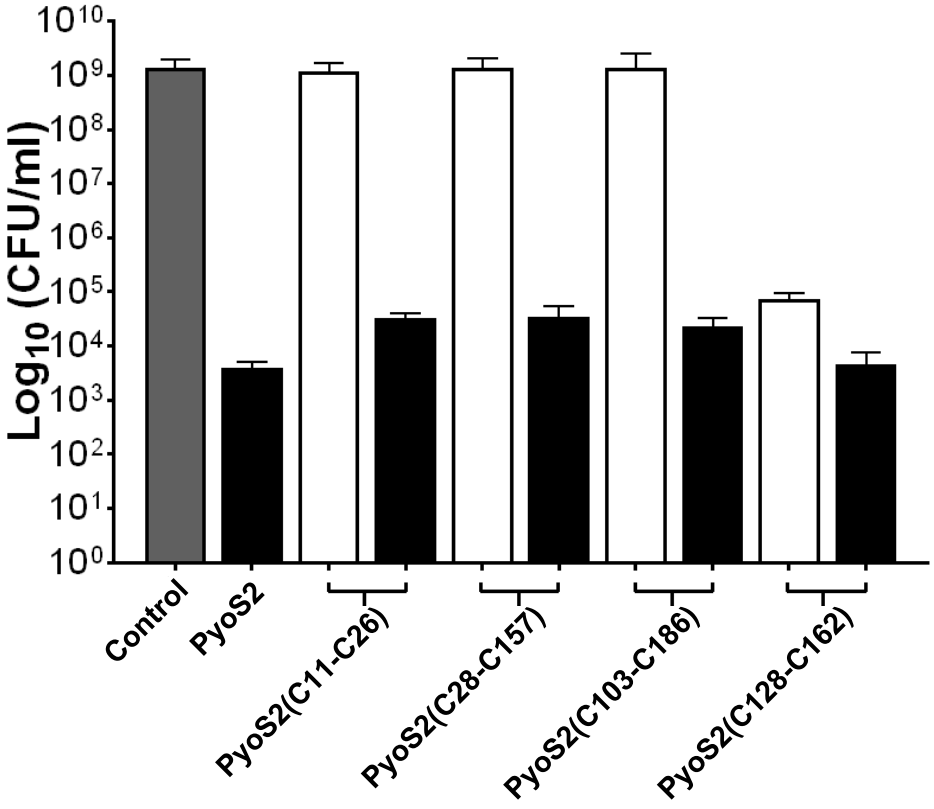

Figure 5-15. Comparison of cytotoxic profiles for the PyoS2 disulphide mutants.
P. aeruginosa YHP17 colony forming units (CFU/ml) from PyoS2 cytotoxicity assay after 3 h incubation shows disulphide positions C11-C26, C28-C157 and C103-C186 inhibit PyoS2 cytotoxicity when oxidised (*white*). This effect is reversed upon disulphide bond reduction (*black*). Disulphide position C128-C162 imparts significantly reduced protection against PyoS2 activity when oxidised. Colony counts from six independent cultures with error bars representing the standard deviation.

Translocation of the PyoS2(C128-C162) disulphide mutant was further investigated utilising kinetic time-course cytotoxicity experiments to identify whether the disulphide bond affects the kinetics of PyoS2 translocation through the FpvAI transporter. The oxidised PyoS2(C128-C162) disulphide mutant displayed an increase in colony forming units (CFU) compared to the reduced mutant (Figure 5-16). Calculation of the half-lives ($t_{1/2}$) of translocation revealed oxidised PyoS2(C128-C162) has a $t_{1/2}$ of 2.5 ± 0.2 minutes, approximately double that of the $t_{1/2}$ of reduced PyoS2(C128-C162) (1.3 ± 0.1 minutes). Thus, whilst the oxidised PyoS2(C128-C162) remains active against *P. aeruginosa*, it pays a kinetic penalty for the presence of the disulphide bond within its N-terminus, slowing translocation through FpvAI.

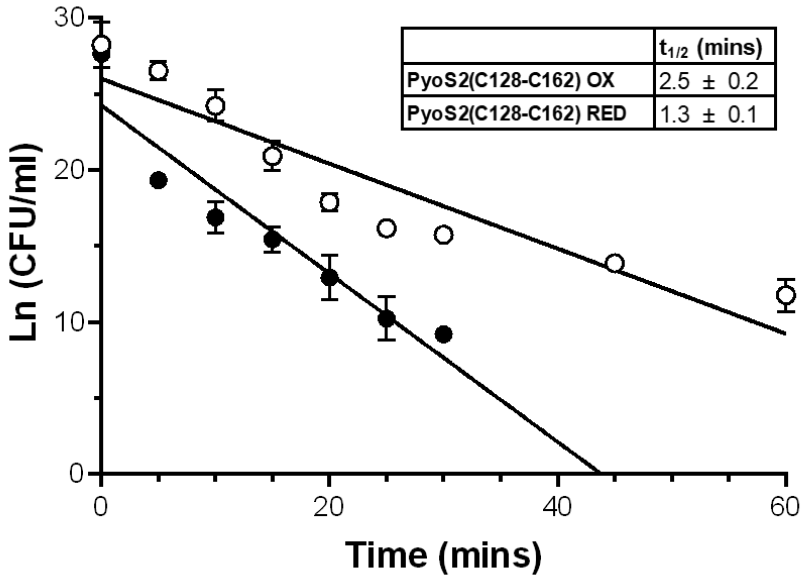

Figure 5-16. Disulphide bond formation within PyoS2(C128-C162) N-terminal domain impedes translocation *in vivo*.

P. aeruginosa YHP17 colony forming units (CFU/ml) from time-course cytotoxicity assays demonstrates that oxidation of the C128-C162 disulphide bond results in a decrease in the PyoS2 translocation rate (○) compared to that of the reduced form (●). Colony counts from four independent cultures (with error bars representing standard deviation) were fitted to a pseudo-first order reaction model and translocation half-lives ($t_{1/2}$) were calculated from the linear plot.

5.3. Discussion.

In this chapter, through a combination of *in vitro* and *in vivo* experiments, I have generated an updated model for the precise mechanism of PyoS2 translocation through its transporter FpvAI, and the structural constraints imposed by the system on this process (Figure 5-17).

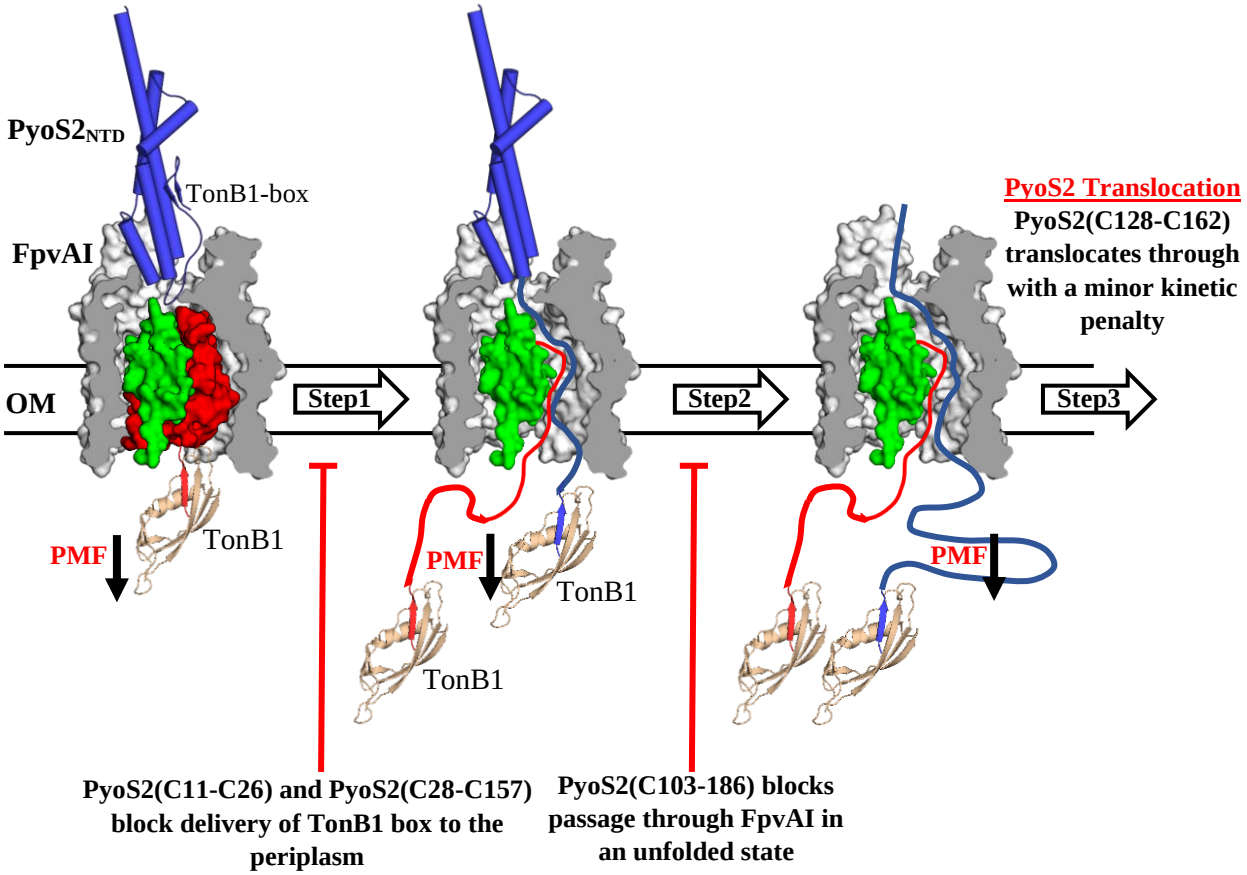

Figure 5-17. Updated model of PyoS2 import through FpvAI and the structural constraints imposed during translocation.
A three-step model for $PyoS2_{NTD}$ import through the FpvAI transporter, supported by *in silico*, *in vitro* and *in vivo* experimental data presented here. Initial binding of $PyoS2_{NTD}$ to FpvAI mimics Fe^{3+}-PVD binding, activating the transporter for uptake and recruiting TonB1 via its TonB1-box. **Step 1.** Force remodelling of the labile portion (*red*) of the FpvAI plug domain occurs in a PMF-dependent manner via contact to the TonB1-ExbB-ExbD complex in the IM (only the C-terminus of TonB1 is shown for clarity). The N-terminus of $PyoS2_{NTD}$ enters the resultant pore formed, facilitating presentation of its own TonB1-box in the periplasm. This process is blocked by disulphides within the β-hairpin motif. **Step 2.** The $PyoS2_{NTD}$ TonB1-box is bound by another copy of TonB1, resulting in the force remodelling of $PyoS2_{NTD}$ itself and driving translocation through the FpvAI lumen. Translocation can be stalled by the presence of intramolecular crosslinks in the form of disulphide bonds (C103-C186). **Step 3.** The entire $PyoS2_{NTD}$ is translocated through the FpvAI lumen, presumably followed by the remainder of the protein for the full-length construct. The PyoS2(C128-C162) mutant can successfully translocate across the OM despite the presence of an intramolecular crosslink, however, import as slowed as a result.

Initiation of PyoS2 import requires the formation of a high-affinity interaction with its translocator FpvAI. PyoS2 has previously been demonstrated to bind FpvAI through its N-terminal domain with a K_d of ~ 240 pM, which outcompetes binding of the native ligand Fe^{3+}-PVD (White *et al.*, 2017). PyoS2 utilises a PRR prior to the first α-helix to bind in the PVD binding cleft, presumably stimulating translocation by molecular mimicry of the native ligand. This PVD binding site constitutes residues from both the β-barrel and globular plug domains (Cobessi *et al.*, 2005; Greenwald *et al.*, 2009), however in order for substrates to translocate, the plug domain must be remodelled, generating a pore through which substrates can diffuse (Braun *et al.*, 2003; Ma *et al.*, 2007). The role of the FpvAI plug in PyoS2 translocation was explored using the *P. aeruginosa* strain PAS033, expressing the FpvAI β-barrel domain alone. This strain has previously been shown to be deficient in PVD uptake *in vivo* (Nader *et al.*, 2011). PyoS2 was found to be unable to parasitize the plugless FpvAI transporter, despite the presence of an unoccluded β-barrel lumen. Abolishment of cytotoxicity resulted from loss of binding between the $PyoS2_{NTD}$ and the transporter, with a fluorescent $PyoS2_{NTD}$ construct unable to label PAS033 cells. The FpvAI plug domain constitutes a sizeable interaction surface for the PyoS2 N-terminus, comprising ~10% of the overall interface surface area between the two proteins in the bound conformation (White *et al.*, 2017). Therefore, it is possible that loss of these interactions, through truncation of the FpvAI plug domain, abolishes this interaction surface between the transporter and the $PyoS2_{NTD}$, and in turn inhibits binding. Alternatively, loss of PyoS2 binding also could indicate increased conformation flexibility within the FpvAI β-barrel without the plug domain present (Nader *et al.*, 2011), compared to that of the full length FpvAI transporter, preventing binding and conferring resistance to PyoS2 activity. The latter appears to be more likely, as intramolecular interactions between FpvAI and $PyoS2_{NTD}$ are primarily mediated by the FpvAI β-barrel domain's extracellular loops, with only a single hydrogen bond formed to the FpvAI plug domain between Tyr200 and the backbone carbonyl of residue Pro41 from $PyoS2_{NTD}$ (White *et al.*, 2017). Indeed, a PyoS2Δ1-45 mutant can still bind to FpvAI *in vitro*, albeit with a 1000-fold reduction in binding affinity, despite abolishment of this hydrogen bond to the FpvAI plug domain.

It had previously been demonstrated that expression of a soluble FpvAI plug domain is able to complement the plugless FpvAI β-barrel in PAS033 and partially restore PVD uptake (Nader *et al.*, 2011). Transformation and expression of the soluble plug domain restored PyoS2 cytotoxic activity against PAS033, in an analogous manner to that demonstrated for

PVD uptake. As such, the soluble plug domain restores both PyoS2 binding and import *in-trans*. However, additional experimentation failed to reconstitute PyoS2 activity through the expression of a fragment of the plug domain comprising the non-labile subdomain only, which is thought to remain associated with the FpvAI β-barrel domain during substrate uptake (discussed in detail in Chapter 6) (Hickman *et al.*, 2017).

During the initial steps of import, PyoS2 must deliver an N-terminal TonB1-box motif into the periplasm to couple to the TonB1 complex, energising uptake (White *et al.*, 2017). The precise mechanism by which this occurs remains unclear, though the unstructured N-terminus of PyoS2 (residues 2 – 10) appears to be involved in its delivery. MD simulations of the PyoS2 unstructured N-terminus, modelled using MODELLER (Webb & Sali, 2016), demonstrate that in a subset of the simulations, the N-terminal residue of PyoS2 spontaneously positions itself above the pore entrance formed by the unplugged FpvAI transporter (Figure 5-18), priming it for import (Dr. Emanuele Paci, University of Leeds, *personal communication*). Indeed, truncation of these residues does not abolish PyoS2 cytotoxicity, but instead decreases the rate of PyoS2 translocation, increasing the $t_{1/2}$ threefold; from 1.2 ± 0.2 minutes to 3.5 ± 0.4 minutes. Unstructured N-terminal regions have previously been shown to be important for presentation of binding motifs in fixed orientations, required for energization of CLB import, as demonstrated previously for ColE9 (Housden *et al.*, 2018). However, no significant binding epitopes are present in the PyoS2 unstructured N-terminus. Instead, the spontaneous positioning of the PyoS2 N-terminus above the open FpvAI pore, and its subsequent delivery into the periplasm, is likely driven by electrostatics. The PyoS2 unstructured N-terminus contains several negatively charged amino acids that impart an overall electronegative charge (pI = 3.67). Localisation of the PyoS2 N-terminal residue above the FpvAI pore likely occurs through electrostatic attraction between this sequence and the positively charged pore entrance (pI = 8.76). Furthermore, a slice through of the FpvAI β-barrel lumen reveals patches of alternating charges (Figure 5-18), which could function to drive directed diffusion of the PyoS2 N-terminus through the pore, prior to contact with the TonB1 complex (Dr. Emanuele Paci, University of Leeds, *personal correspondence*).

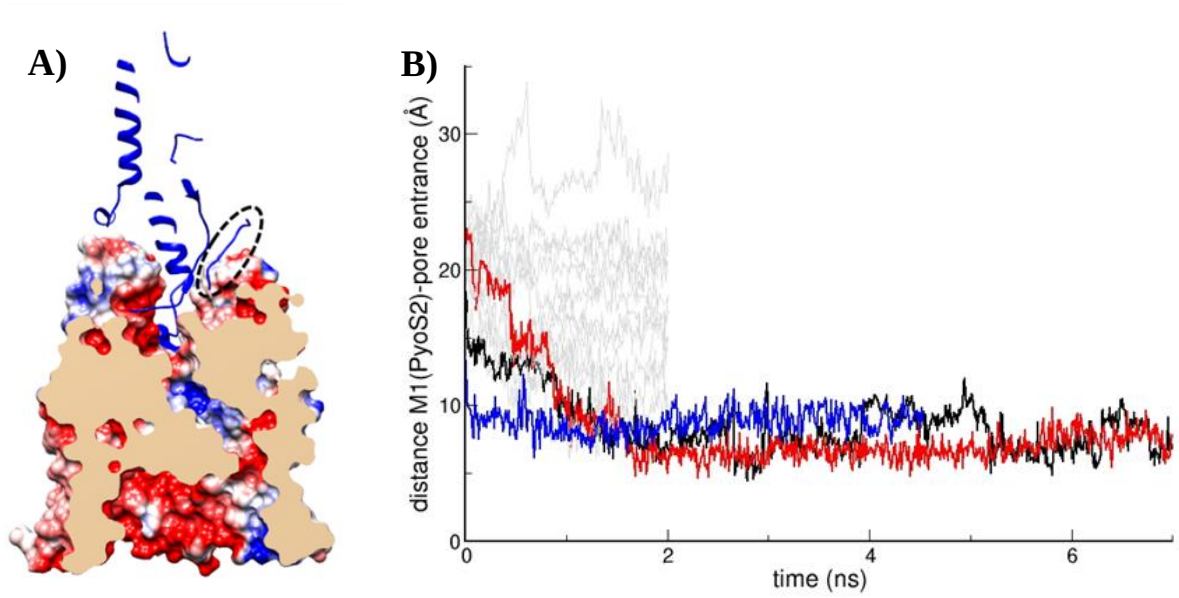

Figure 5-18. MD simulations of PyoS2 unstructured N-terminal residue priming above the FpvAI pore.
A) Transverse of FpvAI receptor (*surface*) with $PyoS2_{NTD}$ bound (*blue*). Removal of the labile plug domain leaves a pore spanning the membrane through the β-barrel. The pore lining is composed of alternating charges and the unstructured PyoS2 N-terminus (*dotted black oval*) is positioned near the pore entrance. B) Distance between the main chain N of Met1 of PyoS2 from the FpvAI pore entrance (identified as the centre of mass of residues Val229, Trp707 and Thr797) demonstrates the unstructured N-terminus of PyoS2 can spontaneously diffuse to the entry of the pore left by the unfolded labile plug. Performing simulations from random conformations of the N-terminal unstructured residues of PyoS2 reveal a small number of cases in which the N-terminus is observed diffusing towards the pore. PyoS2 residues 1 – 10 were modelled prior to simulations using MODELLER (Webb & Sali, 2016). All MD simulations were performed by Daniel Van and Dr. Emanuele Paci, University of Leeds.

Alignment of putative S-type pyocin xNTs with those of PyoS2 and PyoS5 (in which the TonB1-box sequence is characterised) identified an acidic/hydrophobic amino acid pair preceding the putative TonB1-boxes in the majority of pyocin xNT sequences analysed, though its precise distance from the pentapeptide motif varies (Figure 5-19). Conservation of this acid/hydrophobic pair within the xNT motif across the S-type pyocin family could signal its importance for the formation of additional intramolecular interactions with TonB1 outside the TonB1-box, as demonstrated in the FoxA:TonB1 crystal structure (Josts *et al.*, 2019). In addition, the unstructured residues that precede the putative TonB1-boxes are largely electronegative (with the exception of PyoG) and could suggest a conserved mechanism of TonB1-box delivery through TBDTs. This is supported by the substitution of residues 1 – 16 (containing a putative TonB1-box) of the PyoSN xNT onto PyoS2, which

generated an active chimeric pyocin. Thus, the unstructured N-terminus and TonB1-box of S-type pyocins are interchangeable *in vivo*. However, the exact mechanism by which this N-terminal sequence diffuses through the pore, or how diffusion in the direction of the periplasm is favoured, remains unclear.

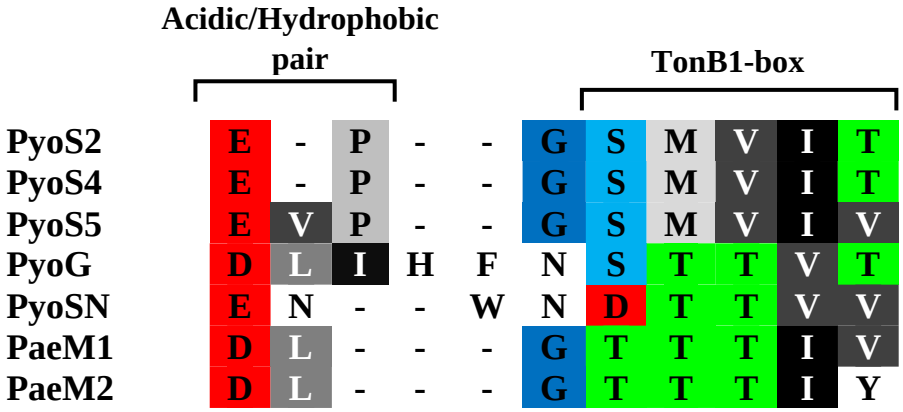

Figure 5-19. An acid/hydrophobic amino acid pair precedes the S-type pyocin TonB1-box. Alignment of xNT sequences of seven S-type pyocins demonstrates the presence of an acid/hydrophobic pair preceding the TonB1-box in most cases. This is closely followed by the TonB1-box, a pentapeptide sequence containing a significant proportion of β-branched amino acids. Amino acids are coloured based on their characteristics: acidic (*red*), hydrophobic (*black and grey*), serine (*cyan*), threonine (*green*) and glycine (*blue*).

It has previously been shown that addition of disulphide bonds into CLBs arrests translocation and inhibits cytotoxicity (Housden *et al.*, 2005; Patzer *et al.*, 2012). The pore through which CLBs translocate is predicted to be too narrow to accommodate an intramolecular crosslink, therefore complete unravelling of the bacteriocin is a prerequisite for translocation. *In vivo* crosslinking data has also demonstrated that PyoS2 crosslinks to residues within the FpvAI β-barrel, suggesting that it must pass through the pore, created by the removal of the labile plug subdomain, to access these positions (White *et al.*, 2017). However, there is no direct evidence to support PyoS2 unfolding during translocation. Attempts to arrest translocation through the introduction of disulphides within the PyoS2 N-terminal domain demonstrated greater tolerance for local structural conservation during import than previously expected. Disulphide formation within the β-hairpin motif (PyoS2(C11-C26) and PyoS2(C28-C157)) inhibited PyoS2 cytotoxicity, which could be reversed upon reduction of the bond. Thus, dissociation of the TonB1-box for delivery into the periplasm is a requisite for PyoS2 import. Interestingly, of the disulphide mutations located within the α-helical bundle, only one (PyoS2(C103-C186)) was able to inhibit PyoS2 cytotoxicity. PyoS2(C128-C162) remained active against *P. aeruginosa*, only suffering a

minor kinetic penalty during import, despite the presence of an intramolecular crosslink. The ability of this partially folded substrate to pass through the FpvAI pore infers a degree of tolerance to the preservation of local structural elements during translocation, which has been shown previously for some CLBs (Duché *et al.*, 1994; Lukacik *et al.*, 2012). These experiments have demonstrated the requirement for partial unfolding of the $PyoS2_{NTD}$ during import, with maintenance of local structural elements tolerated for some regions within PyoS2, whereas others must translocate in a fully extended conformation.

5.4. Conclusions

The work presented in this chapter establishes the structural constrains of PyoS2 import through FpvAI that were not previously clear from *in vitro* crosslinking data, allowing the proposal of an updated model for import (Figure 5-17). The initial formation of a high-affinity interaction between PyoS2 and FpvAI requires the FpvAI plug domain; with an unoccluded FpvAI β-barrel unable to bind the PyoS2 N-terminal domain. Upon TonB1-dependent force remodelling of the FpvAI plug in response to PyoS2 binding, delivery of the PyoS2 TonB1-box into the periplasm occurs, likely guided through the lumen formed by the residues that precede this motif. Formation of an intramolecular crosslink in the β-hairpin abolishes import. Upon contacting TonB1 through its own TonB1-box, PyoS2 is then able to energize uptake through the FpvAI transporter, with a greater degree of tolerance to the presence of local tertiary structural elements than was previously envisaged.

Chapter 6 – General Discussion

6.1. Introduction.

The import of proteins across membrane barriers is a fundamental process in all domains of life. Whereas eukaryotic organisms have developed dedicated import machinery to translocate proteins synthesised in the cytoplasm into organelles such as mitochondria, no analogous mechanisms have been identified in Gram-negative bacteria. Yet proteins are imported by bacteria, which is best exemplified by the multitude of interbacterial competition systems that have evolved to eliminate competing cells (Granato *et al.*, 2019). These systems specifically target vital intracellular components of competing cells and as such, must first navigate the cellular envelope to reach their active site. Some bacterial competition systems rely on dedicated secretion machinery, such as the T3SS, T4SS and T6SS to drive effector protein export from one cell directly into a target cell, utilising energy from ATP hydrolysis or the PMF. This presents a formidable problem for diffusible toxins like CLBs. On the one hand, they must adopt a fold that binds specific structures on the surface of the cell, whilst on the other they must stimulate their own import, without direct access to an intrinsic energy source, that simultaneously disrupts the fold of the toxin. CLBs achieve these objectives by parasitising cell envelope proteins of the target cell, including OM porins, TBDTs, and multidrug efflux pumps, enabling them to contact the energised Tol and Ton systems, which together stimulate import (Papadakos *et al.*, 2012). However, the mechanisms utilised by CLBs during this import process are poorly understood in comparison to the export of protein effectors by dedicated secretion apparatus. The work presented in this study aimed to characterise the molecular mechanisms utilised by TonB-dependent CLBs during import across the cell envelope. Through a multidisciplinary approach, CLB import was addressed from the cellular level down to the atomistic level, revealing new insights into the mechanisms by which TonB-dependent CLBs are imported into bacteria.

6.2.Translocation of PyoSN across the cell envelope.

PyoSN is a recently described non-HNH nuclease-type pyocin that was predicted to exhibit DNase activity through sequence homology to PyoS3. The toxin possesses significant therapeutic potential *in vitro*, exhibiting broad-range activity against *P. aeruginosa* clinical isolates. In Chapter 3, several of the cell envelope components required for PyoSN translocation were identified. As with previously characterised nuclease-type Group B CLBs,

PyoSN utilises a TBDT as its OM receptor/translocator and TonB1 to energise import across the OM (White *et al.*, 2017; Chang *et al.*, 2018). In addition, PyoSN activity was shown to be FtsH-dependent, though the precise mechanism by which this occurs is currently unclear (Figure 6-1).

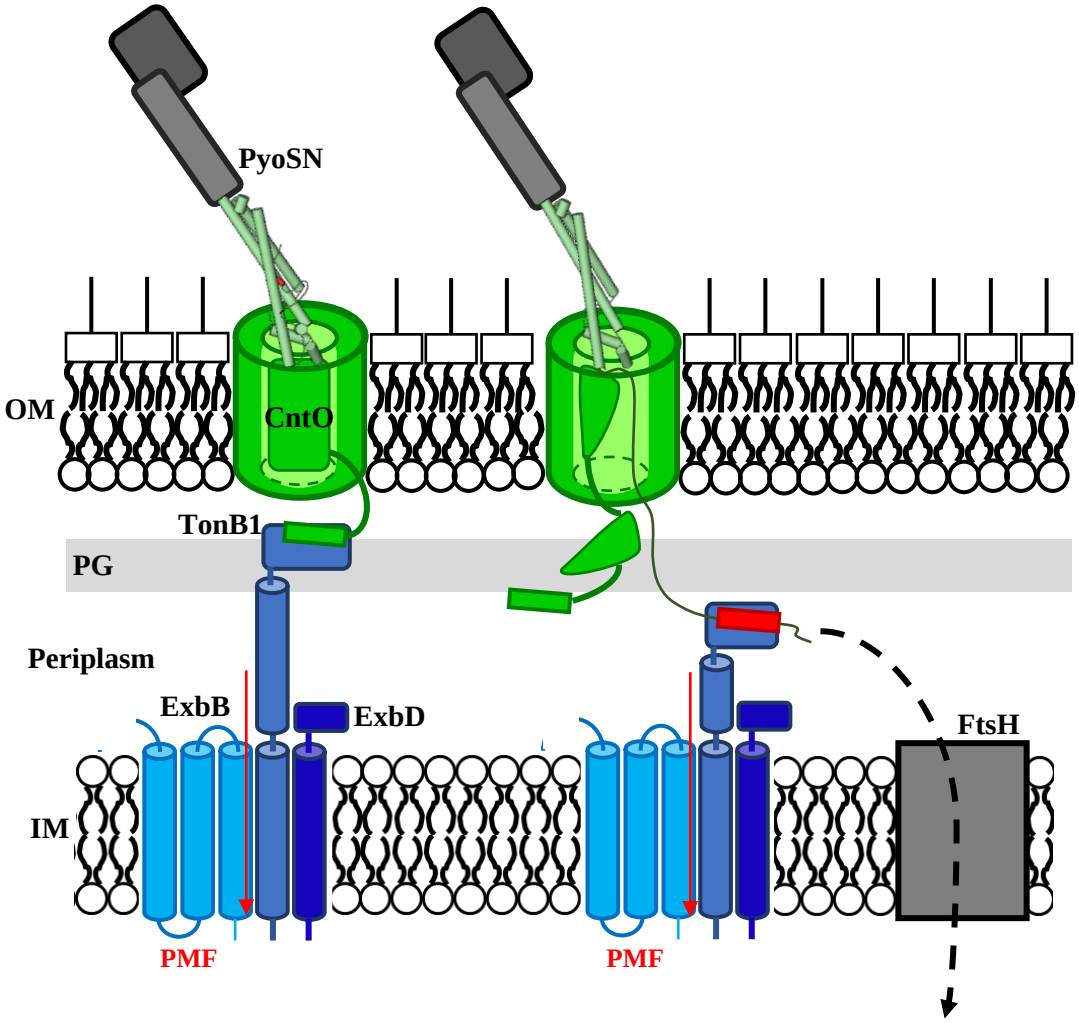

Figure 6-1. Proposed model of PyoSN import across the *P. aeruginosa* cell envelope. A model for PyoSN import across the *P. aeruginosa* cellular envelope based on that described previously for PyoS2 (White *et al.*, 2017). Initial binding of the PyoSN to CntO (*green*) through its N-terminal domain (*pale green*) activates the transporter for uptake, resulting in recruitment of TonB1 via a putative TonB1-box. Force remodelling of the CntO plug domain likely occurs in a PMF-dependent manner via contact to the TonB1-ExbB-ExbD complex (*blue*) in the IM. The xNT of $PyoSN_{NTD}$ enters the resultant pore formed, facilitating presentation of its own TonB1-box (*red*) in the periplasm. The $PyoSN_{NTD}$ TonB1-box is bound by the TonB1 complex, resulting in force remodelling of $PyoSN_{NTD}$ itself and driving translocation of the remainder of the protein through the CntO lumen. Whether PyoSN recruits an additional TonB1 complex, or utilises the one initially recruited by the transporter, is unknown. Once in the periplasm, PyoSN crosses the IM in a process mediated by FtsH (*grey square*).

These components of the cell envelope appear to be well conserved in the import mechanism for S-type pyocins. For example, both PyoS2 and PyoS5 parasitise TBDTs, FpvAI and FptA respectively, as their OM translocator (Denayer *et al.*, 2007; Elfarash *et al.*, 2012, 2014). However, these proteins bind an additional component of the OM in the form of CPA, which likely functions to localise them at the cell surface (McCaughey, Josts, *et al.*, 2016). TonB1 is thought to function in a dual role, binding both the TBDT and the pyocin N-terminus through TonB1 box motifs, energising import into the periplasm (White *et al.*, 2017). PyoSN also uses a TBDT, CntO, in addition to coupling to the TonB1 complex for import. As such, it can be assumed that OM translocation occurs through a similar mechanism to that which has been observed for PyoS2 and PyoS5 import (Figure 6-1). PyoSN is predicted to bind CntO at the extracellular surface, and trigger interactions between the translocator and the TonB1 complex. Force-dependent remodelling of the plug domain would allow PyoSN to commence translocation through the translocator lumen. PyoSN would then couple to TonB1 in the periplasm though an N-terminal TonB box, though whether an additional copy of TonB1 is recruited at this stage remains unclear. PyoSN would then be pulled through the translocator in a PMF-dependent manner by TonB1 in association with its inner membrane stator complex, ExbB-ExbD.

PyoSN is co-synthesised with a cognate immunity protein, ImSN. ImSN is known to bind to PyoSN *in vitro* from comparative studies of PyoS3, inhibiting its DNase activity (Duport *et al.*, 1995). CLB immunity proteins specific for nucleases typically bind to an exosite on the cytotoxic domain, forming a high-affinity interaction and supressing killing activity (Papadakos *et al.*, 2012). PyoSN is predicted to form a high-affinity interaction with ImSN, but the binding interface and thermodynamics of this interaction are presently unknown. Immunity proteins remain associated with nuclease-type CLBs following release into the extracellular medium. At what point ImSN dissociates during PyoSN translocation through CntO remains to be identified. Studies of immunity release during ColE2 import revealed that the process occurs at the cell surface, in addition to requiring the components of the ColE2 translocon, BtuB, OmpF and the Tol complex. Im2 (the cognate immunity protein of ColE2) was not found to cross the cellular envelope during ColE2 translocation, implying dissociation occurs at the cell surface (Duché *et al.*, 2006). Additionally, the dissociation of Im9 from ColE9 during translocation was demonstrated to be PMF-dependent. This suggests that energy transduction from the Tol complex is the driving force for colicin immunity protein release and the

concomitant translocation of the colicin across the OM (Vankemmelbeke *et al.*, 2009). Whether this is also true for S-type pyocins, and more specifically PyoSN, is at present unknown.

From these experiments, CntO appears to be the sole OM component required for import. Several nuclease-type CLBs have been demonstrated to bind two OMPs during translocation. The E-type colicins bind to BtuB as their primary OM receptor, forming a high-affinity complex (Housden *et al.*, 2005). This positions the translocation domain in such a way that it facilitates recruitment of a second OMP, TolC for ColE1 or the porin OmpF for colicins E2 – E9 (Zakharov *et al.*, 2004; Housden *et al.*, 2005). However, this mechanism of cell entry appears to be restricted to Group A bacteriocins, which parasitise the Tol complex (Kleanthous, 2010). The sole member of the Group B bacteriocins that is known to recruit an addition translocator is ColIa, which recruits another copy of its OM receptor Cir (Jakes & Finkelstein, 2010). Whilst it cannot be conclusively ruled out that PyoSN utilises an additional copy of CntO (or another translocator) during import, our understanding of S-type pyocin translocation suggests this is unlikely. In addition to the recruitment of OMPs, some S-type pyocins have been demonstrated to bind CPA, which likely functions to localise the protein at the extracellular surface (McCaughey, Josts, *et al.*, 2016; Behrens *et al.*, 2020). However, no analogous CPA binding domain was identified in PyoSN and its cytotoxic activity against a CPA deficient strain was not impeded. This was surprising due to PyoSN's sequence homology to PyoS3, which is known to bind CPA *in vitro* (McCaughey, Josts, *et al.*, 2016). However, the putative CPA binding motif is found within the PyoS3 N-terminal domain (residues 55 – 150), which shares no homology to that of PyoSN. At present, it appears the PyoSN utilises CntO as the sole OM component for translocation, and as such, functions as the receptor/translocator for OM import.

In the periplasm, the events that culminate in CLB translocation across the IM are poorly characterised. Once in the periplasm, PyoSN might refold prior to transport across the IM, possibly through the actions of a periplasmic chaperone protein, as is demonstrated for ColM. ColM requires the chaperone FkpA in order to refold and elicit its lipid II-hydrolase activity (Hullmann *et al.*, 2008). Whether this refolding process is specific to ColM, CLBs that are active in the periplasm, or all CLBs is unknown; however, there is no evidence that currently supports the requirement of chaperones for nuclease CLBs. As such, the characterisation of additional cofactors required for PyoSN activity is necessary, though identification of periplasmic chaperones appears increasingly unlikely. PyoSN activity was shown to be FtsH dependent, which is thought to be involved in the IM translocation step. Nuclease-type CLBs

have previously been shown to require FtsH for translocation across the IM, with the protease and ATPase activity of FtsH essential for colicin activity (Walker *et al.*, 2007). FtsH is required for the unfolding and degradation of protein substrates from the IM (Langklotz *et al.*, 2012), a process nuclease-type CLBs might mimic during retrograde translocation across the IM. Indeed, the nuclease domain of colicin D and ColE3 undergo proteolytic processing during import across the IM (Chauleau *et al.*, 2011), and as such, PyoSN may be processed in a similar manner during translocation across the IM.

All S-type pyocins for which receptors/translocators are known parasitise TBDTs involved in the uptake of iron, such as FpvAI, FpvAII, FptA and FiuA (Baysse *et al.*, 1999; Elfarash *et al.*, 2012, 2014; Latino *et al.*, 2019). In addition, the recently discovered pyocins PaeM4 and PyoG were found to utilise the HxuC/Hur receptor for import, which is involved in hemin acquisition (Ghequire & Öztürk, 2018; Atanaskovic *et al.*, 2020). The TBDT parasitised by PyoSN is CntO, which is uniquely required for the uptake of pseudopaline; a broad-spectrum metallophore. The *cnt* operon is polycistronic; containing four genes required for the biosynthesis and transporter of pseudopaline. However, only CntO is required for PyoSN activity. The identity of the primary metal ion chelated by pseudopaline is debated, but an intimate association is observed between the *cnt* operon and zinc. *P. aeruginosa* grown in zinc-limited conditions are found to upregulate a host of cell envelope proteins, which are predicted to be involved in zinc uptake, including CntO (Pederick *et al.*, 2015; Mastropasqua *et al.*, 2017). In addition, the *cnt* operon contains a *zur* box in its σ^{70} promotor region, which is negatively regulated by Zur in response to zinc-rich conditions. In zinc-starved conditions, Zur dissociated from the *cnt* operon, facilitating expression (Lhospice *et al.*, 2017). Interestingly, loss of the ZnuABC transporter, the primary zinc uptake pathway in *P. aeruginosa*, results in increased susceptibility to PyoSN in zinc-limited conditions, likely resulting from upregulation of CntO expression to compensate for low intracellular zinc concentrations.

The role of zinc in *P. aeruginosa* pathogenesis is an area of increasing study. Limitation of free zinc appears to be a primary mechanism by which hosts control bacterial infection (Kehl-Fie & Skaar, 2010; Skaar, 2010), and as such, genes involved in zinc uptake are known virulence factors (Mastropasqua *et al.*, 2017). CntO was found to be essential for *P. aeruginosa* growth in airway mucus secretion (AMS) (Gi *et al.*, 2015), in addition to the bacteria's ability to colonise mice (Mastropasqua *et al.*, 2017). Furthermore, the *cnt* operon is found to be upregulated during lung infection (Palmer *et al.*, 2005; Son *et al.*, 2007). As such, further development of PyoSN as a novel therapeutic should be attempted in order to develop new

treatments to combat *P. aeruginosa* lung infection, which disproportionately affects sufferers of the genetic condition CF (Folkesson *et al.*, 2012).

Like other S-type pyocins, PyoSN was predicted to bind to its OM translocator through its N-terminus (Sano *et al.*, 1993). Both PyoS2 and PyoS5 are known to bind to FpvAI and FptA respectively through their N-terminal domains, of which the FpvAI:PyoS2$_{NTD}$ complex has been solved (White *et al.*, 2017; Behrens *et al.*, 2020). In Chapter 4, I attempted to characterise the N-terminal domain of PyoSN and its interactions with several cellular envelope proteins. This culminated in the solution of the PyoSN$_{NTD}$ structure, which further enlightened the structural role of S-type pyocin N-terminal domains in their import across the OM.

PyoSN parasitises the TBDT CntO, and due to the lack of sequence homology with PyoS3, it was reasoned that binding to its specific TBDT involved the N-terminal domain. This was confirmed through Ni^{2+}-affinity pulldown experiments in which PyoSN$_{NTD}$ was found to form a complex with CntO *in vitro*. Attempts to optimise CntO purification in isolation were unsuccessful, therefore an affinity-based purification method was developed, allowing indirect purification of CntO with His-tagged PyoSN$_{NTD}$ as a protein complex. As such, the binding affinity of PyoSN$_{NTD}$ for CntO at present remains uncharacterised. Binding affinities between N-terminal domains of S-type pyocins with their TBDT translocators vary significantly. PyoS2 forms a high-affinity interaction with FpvAI (K_d = ~ 240 pM), allowing it to outcompete the native ligand PVD (White *et al.*, 2017). In contrast, the interactions between PyoS5 and FptA (K_d = 6.5 µM) are substantially weaker (Behrens *et al.*, 2020), and indeed the native ligand pyochelin binds FptA with a K_d ~ three orders of magnitude higher (Hoegy *et al.*, 2009). The binding affinity of PyoSN$_{NTD}$ for CntO is yet to be assessed, however a mechanism for separation of the two proteins after purification must be developed prior to these experiments. It is additionally unknown what affinity CntO binds its native ligand, pseudopaline. Thus, whether the PyoSN$_{NTD}$ is able to outcompete pseudopaline for CntO binding, as demonstrated previously for PyoS2, remains to be seen (White *et al.*, 2017). Attempts were made to crystallise the CntO:PyoSN$_{NTD}$ complex, and whilst crystals formed under a variety of conditions, they failed to diffract to sufficient resolution for high resolution structural studies. As such, these crystallisation conditions require optimisation to ultimately generate a structure of the CntO:PyoSN$_{NTD}$ complex.

However, the structure of the PyoSN$_{NTD}$ in isolation was solved, revealing a kinked three helical bundle fold with an extended N-terminal motif (xNT). The xNT motif contributes

significant buried surface interactions (2960 $Å^2$) within the domain, forming an extensive intramolecular hydrogen bond network to the α-helical bundle. This domain exhibits remarkable structural conservation to the N-terminal domains of PyoS2 and PyoS5 (White *et al.*, 2017; Behrens *et al.*, 2020), despite sharing only 23% and 18% sequence identity, respectively. Alignment of the $PyoSN_{NTD}$ structure with those solved previously for PyoS2 and PyoS5 reveals regions of dissimilarity within their α-helical bundle structures. This is primarily localised within a helical turn motif between αII and αIII, which adopts dissimilar orientation across the three structures. This helix turn is most divergent in the PyoS2 structure, which was solved in complex with its translocator FpvAI. As such, conformation changes within this region could be a direct result of binding to an OM translocator. Previous CLB-receptor complexes have not demonstrated any significant perturbations within the CLB domain upon binding (Kurisu *et al.*, 2003; Buchanan *et al.*, 2007). However, these structures concern CLBs that recruit additional OM translocators, and as such, minimal alterations are observed upon receptor binding (Housden *et al.*, 2005). Whether the variation observed in this helical turn is a requirement of receptor binding, or just a crystallographic artefact, remains to be seen.

Residues 1 – 52 of $PyoSN_{NTD}$ form an xNT that associates laterally with the α-helical bundle, extending up along the face of the domain formed by helices αI and αIII. A similar motif is present in the $PyoS2_{NTD}$ structure (residues 1 – 45), which adopts some secondary structure characteristics, forming a short β-hairpin motif. The xNT present in the $PyoS2_{NTD}$ contains a PRR motif that binds within the PVD binding cleft of FpvAI (White *et al.*, 2017). This is thought to stimulate PyoS2 uptake through molecular mimicry of the target PVD substrate. Whether the $PyoSN_{NTD}$ xNT contains an analogous motif that mimics pseudopaline binding to CntO is currently unknown, and PyoSN residues involved in CntO binding are equally uncharacterised.

However, some functional delineation of the $PyoSN_{NTD}$ xNT has been completed. $PyoSN_{NTD}$ was found to form a high-affinity interaction with TonB1, with a K_d of 61 nM, through a putative TonB1-box. This TonB1-box was mapped to the first 16 residues through a combination of binding and cytotoxicity assays. Sequence alignment of the xNT with other TonB1-dependent S-type pyocins implies that the $PyoSN_{NTD}$ TonB1-box encompasses the pentapeptide sequence DTTVV (residues 10 – 14). These are prototypical amino acids involved in TonB1 binding, which are required for parallel β-strand augmentation of the C-terminal TonB1 β-sheet (Josts *et al.*, 2019). The β-branched amino acids threonine and valine (and isoleucine) exhibit high β-strand propensity, and in addition to methionine, phenylalanine and

tyrosine, are often present in CLB TonB-boxes (Minor & Kim, 1994). The functional importance of these residues can be further inferred from the extensive hydrogen bond network formed between xNT residues 10 – 15, which likely functions to shield both the hydrophobic TonB1 box from the aqueous environment, in addition to locking this sequence in place, protecting it from proteolytic degradation. Truncation of the xNT was found to profoundly affect the $PyoSN_{NTD}$ structure, with a reduction in the domain's thermal stability by 18 °C, resulting in almost complete denaturation of the domain at room temperature. Removal of the $PyoS2_{NTD}$ xNT was also previously shown to result in a reduction in thermal stability (T_m reduction of 6 °C), however this was considerably less significant (White *et al.*, 2017). Removal of the xNT could play a significant role in the import mechanism of PyoSN, whereby xNT dissociation from the α-helical bundle may expediate helical unfolding of the PyoSN N-terminal domain. Indeed, the formation of the high affinity interaction between the $PyoSN_{NTD}$ xNT and TonB1 supports the denaturation of the domain during import in response to TonB1-mediated force. This process of unfolding during import could be further investigated utilising the disulphide lock experiments, as demonstrated for PyoS2 in this study.

Interestingly, despite adoption of near-identical structural topologies, all three S-type pyocin N-terminal domains bind unique TBDTs. From the FpvAI:$PyoS2_{NTD}$ structure, a significant proportion of the interfacial interactions formed by $PyoS2_{NTD}$ (~ 93%) occur with residues from the FpvAI extracellular loops, comprising 13 hydrogen bonds and a salt bridge (White *et al.*, 2017). It is possible that the adoption of this conserved kinked three helical bundle fold is an overarching motif evolved by S-type pyocins to bind the conserved global architecture of TBDTs at a perpendicular angle, as demonstrated by the FpvAI:$PyoS2_{NTD}$ structure. Transporter specificity would be subsequently modulated by distinct intermolecular interactions between the S-type pyocin N-terminus and the TBDT, primarily through the transporter's extracellular loops which possess limited sequence conservation with one another (Noinaj *et al.*, 2010). This is an attractive hypothesis for S-type pyocin N-terminal specificity for disparate TBDTs, supported by their significant deviation in primary sequences, despite adoption of a conserved structural topology. A global conserved three-dimensional structural motif adopted by CLB translocation domains is unlikely to be identified; however, several CLB receptor binding domains are known to assume identical structural topologies. For example, the receptor binding domains of ColM and PaeM are both comprised of a four α-helical bundle, displaying 2.3 Å RMSD between them. These receptor binding domains have significant sequence deviation (25% sequence identity), likely resulting from their specificities for the

specific ferrichrome receptor expressed by their respective target species during import; FhuA for ColM and FiuA for PaeM (Ghequire *et al.*, 2018). In addition, the E-type colicins ColE2 and ColE3 both bind the TBDT BtuB as their primary OM receptor. The ColE2 and ColE3 receptor binding domains adopt identical extended coiled-coil structures, which bind at an oblique angle to BtuB (Kurisu *et al.*, 2003; Sharma *et al.*, 2007). However, these domains share significantly greater sequence identity (91%) than that identified between the S-type pyocin N-terminal domains denoted previously (Sharma *et al.*, 2007).

6.3. Structural constraints of PyoS2 import.

A significant proportion of our understanding of S-type pyocin import across the *P. aeruginosa* OM results from studies concerning PyoS2. An import mechanism for PyoS2 through its OM transporter FpvAI was previously proposed, suggesting that PyoS2 translocates directly through a pore formed by FpvAI upon force-remodelling of the transporter for substrate import, supported by *in vivo* crosslinking data (White *et al.*, 2017). However, the precise mechanism by which this process occurs was poorly understood. In chapter 5, I utilised a combination of *in vitro* and *in vivo* experiments to address the structural constraints of PyoS2 import through FpvAI. These were combined with *in silico* molecular dynamics simulations performed by Daniel Van and Prof. Emanuele Paci (Astbury Centre for Structural Molecular Biology, University of Leeds) to delineate the molecular mechanisms underpinning PyoS2 import.

PyoS2 binds directly to its translocator FpvAI through its N-terminal domain, forming a high-affinity complex (White *et al.*, 2017). PyoS2 is thought to activate FpvAI for translocation through binding to its PVD binding pocket via a PRR motif, which precedes the α-helical bundle. This interaction results in conformational rearrangement in the translocator, akin to Fe^{3+}-PVD binding (Cobessi *et al.*, 2005). The precise mechanism by which TBDTs translocate substrates is disputed, though it is generally accepted that coupling to the TonB1 complex results in structural rearrangement within the globular plug domain that occludes the β-barrel lumen. AFM studies on the TBDT BtuB demonstrate partial removal of the plug domain, termed the labile subdomain, in response to application of force (Hickman *et al.*, 2017). MD simulations of the FpvAI:$PyoS2_{NTD}$ complex support the existence of two mechanically independent subdomains within the FpvAI plug domain: a labile subdomain, which is removed in response to application of force, and a non-labile subdomain, which remains associated with the β-barrel domain (Dr. Emanuele Paci, University of Leeds, *personal communication*). As

such, the precise roles of these subdomains in PyoS2 translocation remain enigmatic. Whilst experiments reported in this study were able to confirm that PyoS2 translocation can be restored *in-trans* through expression of a soluble plug domain, PyoS2 import could not be re-established with the soluble non-labile subdomain alone. As this subdomain is predicted to remain associated with the β-barrel during substrate transport, it was thought that the exogenously expressed non-labile plug subdomain would associate analogously *in-trans*. However, it is possible that the extensive interactions formed with both the labile subdomain and the β-barrel domain imparts stability to the non-labile subdomain *in vivo,* resulting in an unstable construct when the subdomain was expressed exogenously. To further investigate this, FpvAI should be expressed with the non-labile plug subdomain retained (residues 216 – 815), eliminating the possibility of subdomain misfolding, or the requirement for reassociation with the β-barrel domain *in vivo*.

PyoS2 is known to deliver an N-terminal motif containing a TonB1-box into the periplasm to stimulate import. However, the precise mechanism by which this occurs was unknown. It was reasoned that the residues preceding the TonB1-box, which are unstructured in the crystal structure, could play a role in this process, as disordered sequences have previously been demonstrated to be required for CLB translocation (Housden *et al.*, 2018; Jansen *et al.*, 2020). MD simulations suggested (Section 5.3), and experiments confirmed, that the unstructured N-terminus of PyoS2 likely functions to facilitate directed diffusion through the open FpvAI pore. Unlike what has previously been demonstrated for other CLBs like ColE9, the PyoS2 unstructured N-terminus appears to 'prime' the pyocin for import, positioning the N-terminal residue above the entrance to the pore, rather than for presentation of binding epitopes at a defined orientation (Housden *et al.*, 2018). This likely assists in directing diffusion of the N-terminal leader sequence into the pore. The exact mechanism by which the N-terminal leader sequence diffuses through the pore, or how diffusion in the direction of the periplasm is favored, remains unclear. The conservation of an acidic/hydrophobic pair preceding the TonB1-box in all TonB1-dependent S-type pyocin sequences, in addition to the strong preponderance for an overall electronegative charge, implies that electrostatics might be a required for driving diffusion of some, if not all, S-type pyocin N-termini through their transporters, prior to contact with TonB1. The distribution of charged residues lining the FpvAI pore could function to electrostatically 'steer' the PyoS2 leader sequence through the transporter and into the periplasm, whereby contact with the TonB1 complex can subsequently energise import of the rest of the protein.

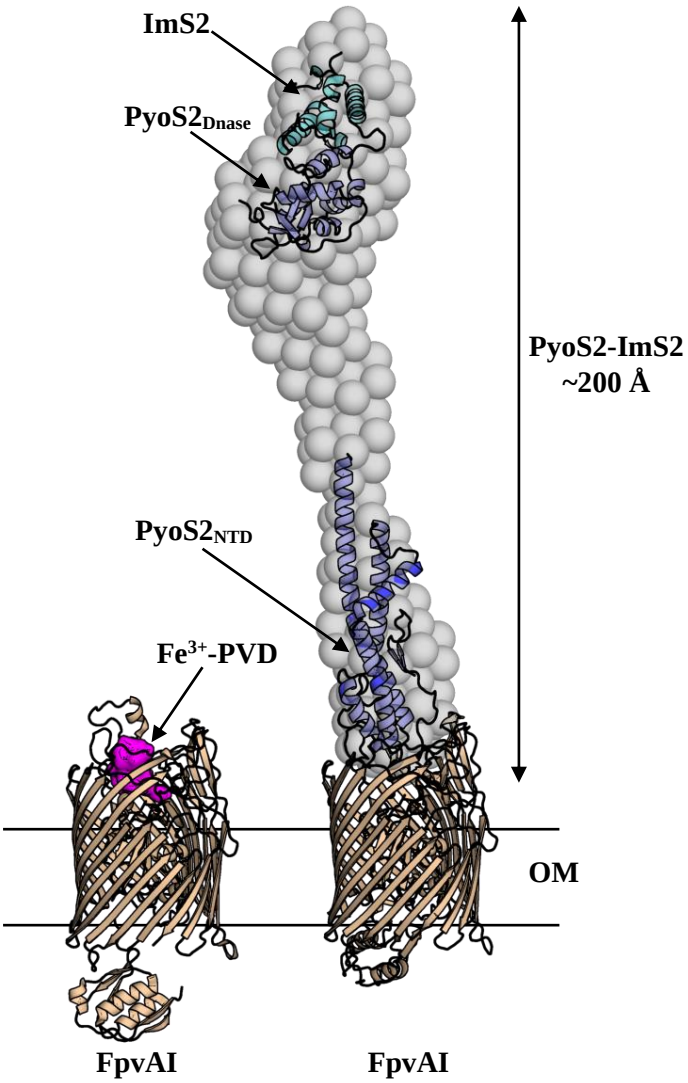

Figure 6-2. Size comparison of substrates translocated by FpvAI – ferripyoverdine and PyoS2. Crystal structures of FpvAI (*peach*) solved in complex with substrates Fe^{3+}-PVD (*magenta*) (PDB ID = 2W16 (Greenwald *et al.*, 2009)) and $PyoS2_{NTD}$ (*blue*) (PDB ID = 5ODW (White *et al.*, 2017)) illustrate the significant size difference between them. PyoS2 possesses additional domains that also presumably translocate through the FpvAI transporter. The crystal structures of both the $PyoS2_{NTD}$, and the $PyoS2_{DNase}$ domain (*blue*) in complex with its immunity protein ImS2 (*cyan*) (PDB ID = 4QKO (Joshi *et al.*, 2015)) were fitted to the SAXS envelope of PyoS2-ImS2, determined previously by Klein *et al* (2016). The remaining SAXS density would be occupied by PyoS2 domains II and III, required for CPA-binding and IM translocation respectively. Taken together, the size of PyoS2-ImS2 (~200 Å in length) greatly exceeds that of Fe^{3+}-PVD.

Whilst the import of target substrates through the lumen of TBDTs can be rationalised, resulting from their small size, the mechanisms by which CLBs pass through the lumen is unclear. For example, both Fe^{3+}-PVD (1.4 kDa) and PyoS2 (74 kDa) utilise the same pore formed by FpvAI during import across the OM, despite the significant disparity in their size.

This is exemplified by the PyoS2 SAXS envelope (Figure 6-2), which extends ~200 Å in length, with a cross section of ~ 35 Å (Klein *et al.*, 2016). Therefore, in order to utilise the ~13 Å pore formed by displacement of the labile plug subdomain of FpvAI, the TonB1-dependent unfolding of PyoS2 during import is the generally accepted mechanism, as demonstrated previously for other CLBs (Penfold *et al.*, 2004; Vankemmelbeke *et al.*, 2013). The structural constraints of this import process were investigated using a combination of MD simulations, coupled with *in vivo* cytotoxicity experiments. MD simulations of $PyoS2_{NTD}$ import (Dr. Emanuele Paci, University of Leeds, *personal communication*) confirmed that the N-terminal domain must unfold during translocation through FpvAI. However, introduction of disulphides within the $PyoS2_{NTD}$ during simulations demonstrated a greater tolerance for local structural conservation during import than previously expected, with two of the disulphide positions tested (C11-C26 and C128-C162) successfully translocating through the FpvAI pore *in silico*. Upon further investigation of these disulphide positions *in vivo*, the formation of an intramolecular disulphide crosslink within the $PyoS2_{NTD}$ was able to arrest translocation in three (PyoS2(C11-C26), PyoS2(C28-C157) and PyoS2(C128-C162)) of the four positions tested. This confirms that complete unfolding of structural elements within the N-terminal domain, particularly the β-hairpin motif, are a prerequisite of PyoS2 import. Yet of the engineered disulphide crosslinks within the $PyoS2_{NTD}$ α-helical bundle, PyoS2(C128-C162) remained active against *P. aeruginosa*, suffering a minor kinetic penalty during import, despite the presence of the intramolecular crosslink. The ability of a partially folded substrate to pass through the FpvAI pore infers a degree of tolerance to the preservation of local structural elements during translocation. However, the import of a partially folded substrate can only occur upon contact with the TonB1 complex, which energises the translocation process. Indeed, oxidised PyoS2(C11-C26) is inactive against *P. aeruginosa in vivo*, despite MD simulations suggesting translocation is viable through the FpvAI pore in a crosslinked state. This is likely due to inability of the disulphide-locked β-hairpin to spontaneously diffuse though FpvAI in the absence of applied 'force', which was utilised during simulations to imitate TonB1-mediated force, or alternatively through disruption of interactions between the TonB1-box with TonB1 in the periplasm. Both the arrest of bacteriocin translocation in response to disulphide formation (Housden *et al.*, 2005; Lukacik *et al.*, 2012), and translocation of bacteriocins containing intramolecular disulphide crosslinks (Duché *et al.*, 1994; Lukacik *et al.*, 2012) have been demonstrated previously, suggesting significant variation in the structural plasticity of CLB import through their requisite transporters. For the mechanism of PyoS2 translocation investigated in this study, it is evident that only partial unfolding of the $PyoS2_{NTD}$ during import

is required, with maintenance of local structural elements tolerated for some regions within PyoS2, whereas others must translocate in a fully extended conformation. How the remaining domains of PyoS2 translocate through FpvAI is not yet clear. Whether the TonB1 complex continues to act upon the TonB1-box, driving translocation of the remaining 480 amino acids, or merely provides the initial mechanical force necessary to overcome an activation barrier, after which translocation proceeds down the energy landscape driven by successive domain refolding, is unknown.

6.4. Analogous protein import systems to CLB translocation.

Examples of protein import across the Gram-negative cell envelope are limited, with no analogous mechanisms to CLB import currently described. However, protein import processes that resemble CLB uptake have been identified in eukaryotes, which can be broadly divided into two distinct categories: protein import into intracellular organelles such as mitochondria, and protein toxin import.

As discussed previously (Section 1.3.4), pre-proteins destined for the mitochondria are synthesised with an N-terminal presequence, which forms an amphipathic α-helix containing both positively charged and hydrophobic faces (Roise *et al.*, 1986). This sequence targets preproteins to the mitochondrial OM surface, whereby it is recognised by the TOM complex. Recognition initially occurs through hydrophobic interactions with Tom20, followed by transfer of the substrate to the central receptor Tom22, which binds the positively charged presequence helix (Abe *et al.*, 2000; Yano *et al.*, 2000). This process is similar to the initial stages of ColE9 translocation, whereby interactions between binding motifs (OBS1 and OBS2) within the unstructured N-terminus and the OmpF lumen primes the colicin for import across the OM (Housden *et al.*, 2018). Like mitochondrial preprotein sequences, the unstructured N-terminus of PyoS2 (residues 2 – 10) is also electrostatically charged; containing several acidic residues that impart a net electronegative charge. This likely functions in the positioning of the PyoS2 N-terminal residue above the electropositive FpvAI pore lumen, in addition to directing diffusion through the transporter to the periplasm. However, it is unlikely that the PyoS2 unstructured N-terminal residues form any significant binding interactions with the FpvAI lumen during uptake, as demonstrated for TOM-mediated protein import and ColE9 import.

The major component of the TOM complex is Tom40, a 19-stranded β-barrel protein that forms the primary protein import channel. The Tom40 pore lumen is ~19 Å in diameter at its widest point (Tucker & Park, 2019), which imparts structural constraints on mitochondrial substrate

import. Mitochondrial proteins are largely translocated in an unfolded conformation, however TOM-mediated translocation of protein-nucleic acid conjugates, in addition to partially folded proteins containing intramolecular disulphide bonds, has been demonstrated previously, albeit at reduced import rates (Vestweber & Schatz, 1989; Schwartz *et al.*, 1999). This suggests some conformational flexibility in mitochondrial protein import, akin to that identified for PyoS2 import through FpvAI in this study. The limit for molecular transport through the Tom40 lumen was found to be ~20 Å, which is close to the diameter of the β-barrel lumen (Schwartz & Matouschek, 1999). This is somewhat larger than that of the pore generated (~13 Å) by FpvAI upon partial unplugging of its labile plug subdomain. At present, the precise conformation that oxidised PyoS2(C128-C162) adopts as it passes through the FpvAI pore lumen is unknown. However, MD simulations suggest that minimal perturbations are incurred within the transporter structure during PyoS2(C128-C162) import. Whether the limits of translocation through FpvAI are similarly increased by further unplugging of the non-labile plug subdomain, allowing larger substrates through the unoccluded β-barrel (~35 – 40 Å) is at present unclear, though this process is highly unlikely to occur *in vivo*.

In addition to secretion of proteins for interbacterial competition, some bacteria secrete additional protein toxins that specifically target eukaryotic cells, resulting in tissue invasion and pathogenicity. For example, anthrax and diphtheria toxins, synthesised by *Bacillus anthracis* and *Corynebacterium diphtheria*, respectively, cause severe pathogeneses during bacterial infection. *P. aeruginosa* also produces protein toxins specific for eukaryotic cells, the most well studied of which is exotoxin A (ETA). Like CLBs, these protein toxins possess modular structure, consisting of domains required for receptor binding, translocation across biological membranes, and cytotoxic activity. In order to reach their cytosolic targets within the eukaryotic cell, some toxins assemble their own translocation machinery, whereas others, like CLBs, hijack host import systems. The anthrax toxin, for example, is comprised of three protein subunits: two enzymatic effectors, oedema factor (OF) and lethal factor (LF), and the protective antigen (PA), which forms the translocation channel (Young & Collier, 2007). Upon binding to cell surface receptors, PA is activated by furin-mediated cleavage to form PA_{63}, which spontaneously self-oligomerises to form a ring shaped heptameric prepore in the cell membrane (Gordon *et al.*, 1995; Jiang *et al.*, 2015). Subsequently, OF and LF bind competitively to high-affinity sites that span the interface of the prepore, forming a series of toxin loaded complexes (Cunningham *et al.*, 2002). Oligomerisation of PA_{63} induces endocytosis of the complex, upon which the acidification of the endosome occurs. This induces

a conformational transition from a prepore to an integral-membrane, ion conductive pore, through which OF and LF can enter the cytosol (Wesche *et al.*, 1998). The structure of the PA_{63} pore revealed a constriction point within the heptameric β-barrel channel, formed by a ring of phenylalanine residues, termed the phi (Φ)-clamp (Krantz *et al.*, 2005). The Φ-clamp is purported to drive the unidirectional import of protein effectors into the cytosol through a charge-state-dependent Brownian ratchet model (Feld *et al.*, 2012; Jiang *et al.*, 2015). A negative electrostatic barrier within the pore hinders the passage of deprotonated acidic residues, which are likely to be protonated in the acidic endosome. As such, residues in the endosome are free to pass through this barrier, whereas deprotonation in the neutral cytosol results in the unidirectional movement of polypeptides through the pore. As demonstrated in this study, loss of the unstructured N-terminal residues of PyoS2 retards translocation across the cell envelope. This region contains several acidic amino acid residues, imparting a net electronegative charge. It is possible that directed diffusion of the unstructured N-terminus through the FpvAI pore also occurs via a Brownian ratchet, with protonation of these residues in the periplasm ensuring unidirectional translocation. Upon contact with the TonB1 complex through the TonB1-box (residues 10 – 14), import is energised, negating the requirement for the ratchet, and facilitating active uptake of PyoS2 across the OM (White *et al.*, 2017).

In addition to promoting unidirectional translocation, the PA_{63} Φ-clamp also functions as a restriction point, forcing the OF and LF effectors to pass through in an unfolded state (Wesche *et al.*, 1998; Jiang *et al.*, 2015). Similarly, the diphtheria toxin (DT) is also known to unfold during translocation into the cytosol. Like CLBs, DT is composed of multiple domains, with an N-terminal enzymatic 'A Domain' and a C-terminal 'B Domain' comprised of translocation and receptor binding domains (Antignani & Youle, 2008). During import, the B domain binds at the target cell surface to the DT receptor, a member of the human heparin-binding epidermal growth factor-like (HB-EGF) growth factor family (Mitamura *et al.*, 1995). This induces endocytosis into clathrin-coated vesicles, which are subsequently delivered to the early endosome (Antignani & Youle, 2008). DT is proteolytically cleaved by furin, generating a disulphide-linked heterodimeric toxin (Gordon *et al.*, 1995). Acidification of the endosome induces partial unfolding in both domains, resulting in exposure of hydrophobic helices within the B Domain, which insert into the endosomal membrane (Antignani & Youle, 2008). The partially folded A Domain translocates through the pore in a pH-dependent manner, and upon reduction of its intramolecular disulphide bond, is released into the cytosol (Papini *et al.*, 1993). The enzymatic A domain elicits cytotoxicity through ADP-ribosylation of elongation factor-2

(EF2), inhibiting proteins synthesis and inducing apoptosis (Collier, 1975). S-type pyocins have also been demonstrated to unfold during import, with the N-terminal translocation domain of PyoSN adopting a force-labile α-helical structure. Dissociation of the xNT from the $PyoSN_{NTD}$ α-helical bundle further destabilises this structure, which likely facilitates translocation through CntO in an unfolded state.

Some bacterial toxins rely on host proteins to facilitate import. ETA, synthesised by *P. aeruginosa*, possesses identical domain architecture to some CLBs, composed of an N-terminal receptor binding domain, a middle domain required for translocation across biological membranes, and a C-terminal cytotoxic domain that exhibits ADP-ribosyltransferase activity (Pastan *et al.*, 1992). The N-terminal domain of ETA binds to target cells via the CD91 receptor (Kounnas *et al.*, 1992). CD91-bound ETA is subsequently endocytosed by the cell and processed through one of two distinct retrograde transport pathways: the KDEL-receptor mediated pathway or the lipid-dependent sorting pathway (Michalska & Wolf, 2015). During KDEL-receptor mediated processing, CD91-bound ETA is internalised into clathrin-coated vesicles, followed by delivery to the early endosome. Within the acidic early endosome, ETA dissociates from the CD91 receptor and undergoes a conformation change, allowing furin-mediated cleavage to generate a disulphide linked heterodimeric toxin (Wedekind *et al.*, 2001). Subsequent unfolding and reduction events involving protein disulphide isomerase result in the dissociation of the cleaved receptor binding domain, and transport of the enzymatic toxin fragment, PE_{37}, to the late endosomes. PE_{37} exploits the Rab9-regulated pathway to reach the trans-Golgi network (TGN), which co-ordinates protein transport within eukaryotic cells (Cancino *et al.*, 2013). Interactions between PE_{37} and the KDEL-receptor within the TGN result in retrograde transport to the endoplasmic reticulum (ER) (Kreitman & Pastan, 1995; Jackson *et al.*, 1999). Alternatively, ETA can reach the ER via the lipid-dependent sorting pathway, in which endocytosis at the extracellular membrane occurs through caveolin-mediated internalisation, and ETA is subsequently trafficked to the ER in a Rab5-dependent manner (Smith *et al.*, 2006). Upon reaching the ER, the translocation domain of PE_{37} hijacks the ER-associated degradation pathway (ERAD) and induces import into the cytosol via Sec61 (Ogata *et al.*, 1990; Theuer *et al.*, 1993). PE_{37} induces apoptosis through the ADP-ribosylation of EF-2, as discussed previously for DT (Iglewski *et al.*, 1977). The ERAD-mediated retrograde translocation of PE exhibits similarities to the mechanism by which nuclease CLBs are postulated to translocate across the IM. FtsH is thought to recognise the IM-associated nuclease

as a misfolded protein, resulting in retrograde translocation into the cytoplasm and, after cleavage by FtsH, release into cytoplasm (Walker *et al.*, 2007; Chauleau *et al.*, 2011).

7. Conclusions.

In summary, this thesis utilised a multidisciplinary approach to uncover the structure and import mechanisms of two TonB1-dependent S-type pyocins, Pyocin SN and Pyocin S2.

7.1. Characterisation of PyoSN Import.

PyoSN is a novel nuclease-type CLB produced by *P. aeruginosa* that exploits several cell envelope proteins during its import into the cytoplasm. PyoSN binds to the OM receptor CntO, a TBDT required for the uptake of the broad-spectrum metallophore pseudopaline. Current understanding of the import process suggests that CntO functions as both the OM receptor and translocator for PyoSN import. This is the first known example of S-type pyocin import through a TBDT receptor that is not implicated in iron uptake. Whilst the identity of the primary metal chelated by pseudopaline for import by CntO remains disputed, there is a clear association between zinc homeostasis and PyoSN activity. The requirement for zinc during *P. aeruginosa* pathogenesis is an area of active research, and PyoSN's potential viability as a novel therapeutic was demonstrated through its successful activity against a majority of strains from a *P. aeruginosa* clinical isolate library.

PyoSN binds CntO through its N-terminal domain, which adopts a kinked three helical bundle fold. Despite sharing no significant sequence identity, this structural topology is conserved with both the N-terminal domains of PyoS2 and PyoS5, which are required for binding to the translocators FpvAI and FptA, respectively. This suggests adoption of a conserved translocator binding motif across the S-type pyocin family, required for binding to TBDTs in the *P. aeruginosa* OM.

PyoSN hijacks the TonB1 complex, composed of TonB1, ExbB and ExbD, during energised import across the OM. PyoSN binds TonB1 through an extended N-terminal motif, which associates laterally with the kinked three helical bundle structure. Removal of the extended N-terminal motif results in significant perturbations in the N-terminal domains, which could function to destabilise the domain during energised import. The TonB1 complex couples the energy dependent steps of PyoSN import to the PMF across the IM. PyoSN binding to CntO likely results in TonB1-dependent force-remodelling of the translocator plug domain, resulting in a pore through which PyoSN can access the periplasm. Exposure of the PyoSN TonB-box, located within the first 16 residues of the extended N-terminal motif, in the periplasm facilitates TonB1 complex binding, and subsequently energises import through CntO. This model of

PyoSN import across the OM is similar to that proposed previously for PyoS2 import through its translocator FpvAI. Once in the periplasm, PyoSN translocates across the IM in an FtsH-dependent manner, eliciting cytotoxicity through its C-terminal non-HNH DNase domain.

7.2.Structural Constraints of PyoS2 Import.

The structure of the N-terminal domain of PyoS2 in complex with its translocator FpvAI has been solved previously. Whilst this structure revolutionised our understanding of S-type pyocin import across the OM, the precise mechanism by which this process occurred remained unclear. The FpvAI plug domain, which occludes the β-barrel lumen in the crystal structure, was found to be essential for PyoS2 cytotoxicity. A *P. aeruginosa* strain expressing a truncated plugless FpvAI receptor was resistant to PyoS2 cytotoxicity. Upon further investigation, resistance to PyoS2 was found to stem from abrogation of PyoS2 binding to the plugless translocator. PyoS2 cytotoxicity could be restored *in-trans*, through expression of a soluble FpvAI plug domain, indicating that an intact plug domain is a requirement for import. To stimulate import, PyoS2 must deliver its TonB1 box into the periplasm in order to engage the TonB1 complex. The PyoS2 unstructured N-terminus (residues 2 – 9) that precede the TonB1 box is required for optimal import across the OM, and likely functions as a leader sequence, positioning the N-terminal residue above the FpvAI pore. Directed diffusion of these residues through the FpvAI pore, likely driven by electrostatics, is thought to facilitate delivery of the TonB1 box to the periplasm prior to energisation of import by the TonB1 complex. Upon contact with TonB1, PyoS2 is able to translocate through the FpvAI pore. The structural constraints of this process suggest that partial unfolding is a requirement of this process; with conservation of some structural elements allowed despite the restrictions imparted by the narrow FpvAI pore (~13 Å).

This study has highlighted the common themes utilised by CLBs during protein import across the Gram-negative cell envelope. Through characterisation of the mechanisms utilised by CLBs, encompassing macromolecular to atomistic detail, I hope that this information will have implications for the development of novel therapeutics to combat the growing threats posed by antibiotic resistant bacteria.

Appendix

Alignments

Alignment I.

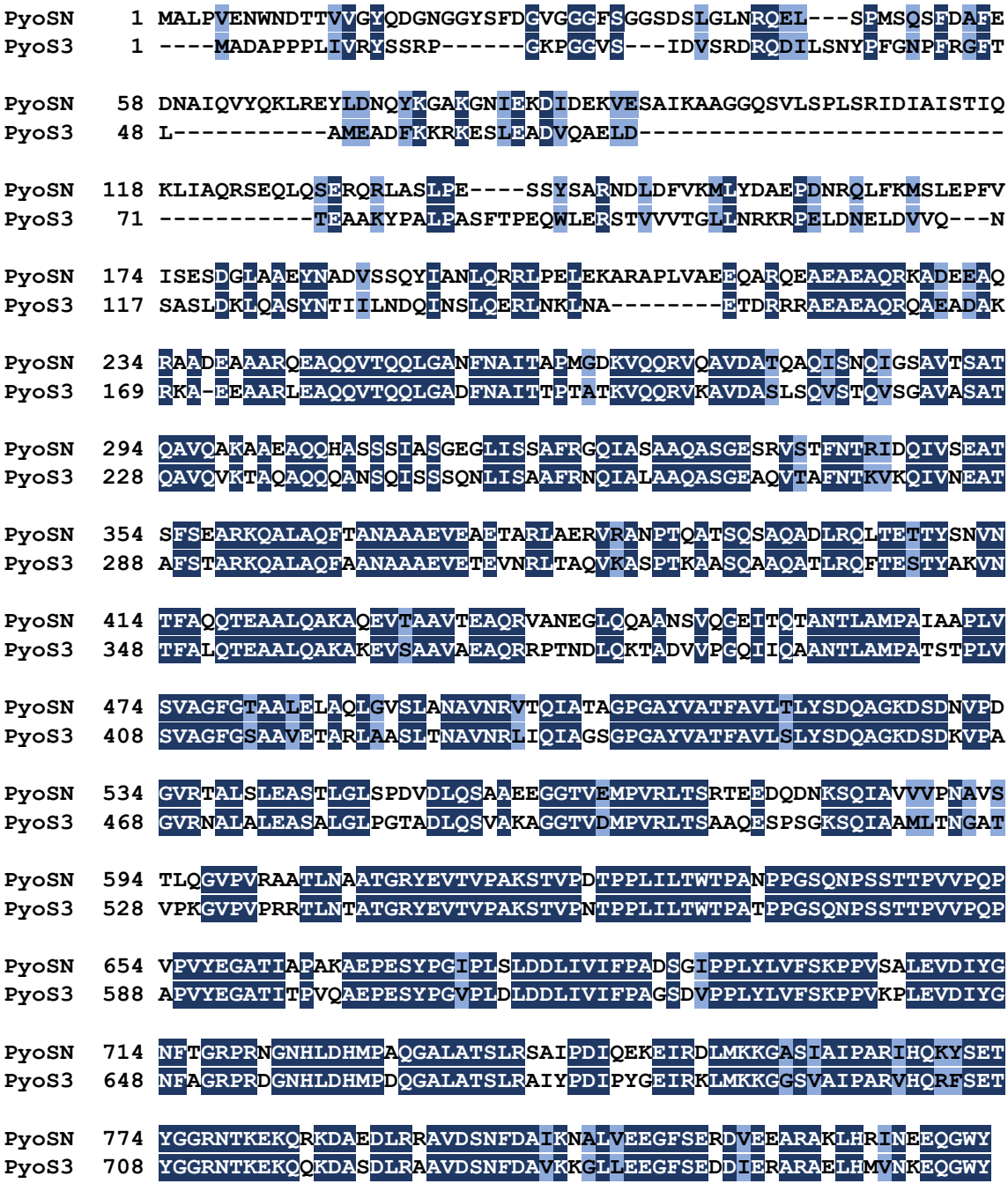

Alignment I. Alignment of Pyocin SN and Pyocin S3
Sequence alignment of Pyocin SN and Pyocin S3 with conserved (*dark blue*) and similar amino acids (*light blue*) are highlighted. Both pyocins share 62.6% sequence identity, primarily in the middle and C-terminal domains (see Figure 3.1.). Alignment was performed with Clustal Omega and annotated using Boxshade.

Alignment II – Sequence alignment of Immunity Proteins ImSN and ImS3.

Alignment II. Alignment of Immunity proteins ImSN and ImS3
Sequence alignment of the cognate immunity proteins of PyoSN and PyoS3, ImSN and ImS3 respectively, with conserved amino acids (*dark blue*) and similar amino acids (*light blue*) highlighted. Both immunity proteins share 45.1% sequence identity. Alignment was performed with Clustal Omega and annotated using Boxshade.

Alignment III – Alignment of CPA-binding domains from PyoS5, PyoS2 and PyoS3.

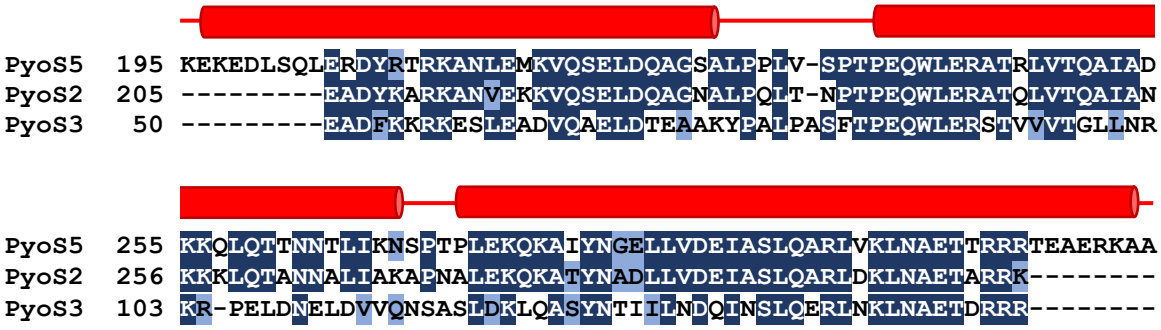

Alignment III. Alignment of S-type pyocin CPA-binding Domains.
Sequence alignment of putative CPA-binding domains from PyoS2 and PyoS3 with the PyoS5 CPA-binding domain (residues 195 – 315) (Behrens *et al.*, 2020). The PyoS5 CPA-binding domain secondary structure is depicted above the alignment (*red*). No analogous sequence within PyoSN aligned with this domain, suggesting PyoSN does not bind to CPA.

Alignment IV – Alignment of unstructured N-terminal regions of TonB1-dependent S-type pyocins

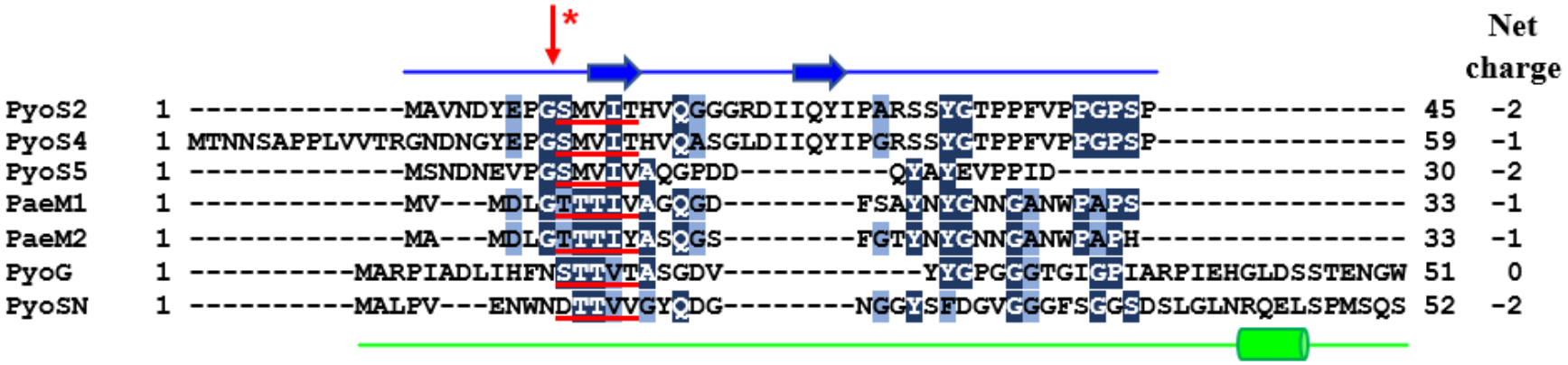

Alignment IV. Conservation of residues and charge across TonB-box sequences in S-Type Pyocin family.
Sequence alignment of unstructured residues of known TonB1-dependent S-type pyocins with the net charge of their predicted unstructured N-termini at pH 7.0. Secondary structural elements adopted within the xNTs of PyoS2 (*blue*) and PyoSN (*green*) are displayed above and below the alignment, respectively. Red arrow denotes the PyoS2Δ1-9 truncation site. Alignment was performed with Clustal Omega and annotated using Boxshade.

Protein Sequences

Pyocin S2

MAVNDYEPGSMVITHVQGGGRDIIQYIPARSSYGTPPFVPPGPSPYVGTGMQEYRKLRSTLDKSHSEL
KKNLKNETLKEVDELKSEAGLPGKAVSANDIRDEKSIVDALMDAKAKSLKAIEDRPANLYTASDFPQK
SESMYQSQLLASRKFYGEFLDRHMSELAKAYSADIYKAQIAILKQTSQELENKARSLEAEAQRAAAEV
EADYKARKANVEKKVQSELDQAGNALPQLTNPTPEQWLERATQLVTQAIANKKKLQTANNALIAKAPN
ALEKQKATYNADLLVDEIASLQARLDKLNAETARRKEIARQAAIRAANTYAMPANGSVVATAAGRGLI
QVAQGAASLAQAISDAIAVLGRVLASAPSVMAVGFASLTYSSRTAEQWQDQTPDSVRYALGMDAAKLG
LPPSVNLNAVAKASGTVDLPMRLTNEARGNTTTLSVVSTDGVSVPKAVPVRMAAYNATTGLYEVTVPS
TTAEAPPLILTWTPASPPGNQNPSSTTPVVPKPVPVYEGATLTPVKATPETYPGVITLPEDLIIGFPA
DSGIKPIYVMFRDPRDVPGAATGKGQPVSGNWLGAASQGEGAPIPSQIADKLRGKTFKNWRDFREQFW
IAVANDPELSKQFNPGSLAVMRDGGAPYVRESEQAGGRIKIEIHHKVRIADGGGVYNMGNLVAVTPKR
HIEIHKGGK

Pyocin S2(C11-C26): Disulphide formed between residues C11 and C26

MAVNDYEPGS**C**VITHVQGGGRDIIQ**C**IPARSSYGTPPFVPPGPSPYVGTGMQEYRKLRSTLDKSHSEL
KKNLKNETLKEVDELKSEAGLPGKAVSANDIRDEKSIVDALMDAKAKSLKAIEDRPANLYTASDFPQK
SESMYQSQLLASRKFYGEFLDRHMSELAKAYSADIYKAQIAILKQTSQELENKARSLEAEAQRAAAEV
EADYKARKANVEKKVQSELDQAGNALPQLTNPTPEQWLERATQLVTQAIANKKKLQTANNALIAKAPN
ALEKQKATYNADLLVDEIASLQARLDKLNAETARRKEIARQAAIRAANTYAMPANGSVVATAAGRGLI
QVAQGAASLAQAISDAIAVLGRVLASAPSVMAVGFASLTYSSRTAEQWQDQTPDSVRYALGMDAAKLG
LPPSVNLNAVAKASGTVDLPMRLTNEARGNTTTLSVVSTDGVSVPKAVPVRMAAYNATTGLYEVTVPS
TTAEAPPLILTWTPASPPGNQNPSSTTPVVPKPVPVYEGATLTPVKATPETYPGVITLPEDLIIGFPA
DSGIKPIYVMFRDPRDVPGAATGKGQPVSGNWLGAASQGEGAPIPSQIADKLRGKTFKNWRDFREQFW
IAVANDPELSKQFNPGSLAVMRDGGAPYVRESEQAGGRIKIEIHHKVRIADGGGVYNMGNLVAVTPKR
HIEIHKGGK

Pyocin S2(C128-C157): Disulphide formed between residues C28 and C157

MAVNDYEPGSMVITHVQGGGRDIIQYI**C**ARSSYGTPPFVPPGPSPYVGTGMQEYRKLRSTLDKSHSEL
KKNLKNETLKEVDELKSEAGLPGKAVSANDIRDEKSIVDALMDAKAKSLKAIEDRPANLYTASDFPQK
SESMYQSQLLASRKFYGEFL**C**RHMSELAKAYSADIYKAQIAILKQTSQELENKARSLEAEAQRAAAEV
EADYKARKANVEKKVQSELDQAGNALPQLTNPTPEQWLERATQLVTQAIANKKKLQTANNALIAKAPN
ALEKQKATYNADLLVDEIASLQARLDKLNAETARRKEIARQAAIRAANTYAMPANGSVVATAAGRGLI
QVAQGAASLAQAISDAIAVLGRVLASAPSVMAVGFASLTYSSRTAEQWQDQTPDSVRYALGMDAAKLG
LPPSVNLNAVAKASGTVDLPMRLTNEARGNTTTLSVVSTDGVSVPKAVPVRMAAYNATTGLYEVTVPS
TTAEAPPLILTWTPASPPGNQNPSSTTPVVPKPVPVYEGATLTPVKATPETYPGVITLPEDLIIGFPA
DSGIKPIYVMFRDPRDVPGAATGKGQPVSGNWLGAASQGEGAPIPSQIADKLRGKTFKNWRDFREQFW
IAVANDPELSKQFNPGSLAVMRDGGAPYVRESEQAGGRIKIEIHHKVRIADGGGVYNMGNLVAVTPKR
HIEIHKGGK

Pyocin S2(C103-C186): Disulphide formed between residues C103 and C186

MAVNDYEPGSMVITHVQGGGRDIIQYIPARSSYGTPPFVPPGPSPYVGTGMQEYRKLRSTLDKSHSEL
KKNLKNETLKEVDELKSEAGLPGKAVSANDIRDE**C**SIVDALMDAKAKSLKAIEDRPANLYTASDFPQK
SESMYQSQLLASRKFYGEFLDRHMSELAKAYSADIYKAQIAILKQTSQE**C**ENKARSLEAEAQRAAAEV
EADYKARKANVEKKVQSELDQAGNALPQLTNPTPEQWLERATQLVTQAIANKKKLQTANNALIAKAPN
ALEKQKATYNADLLVDEIASLQARLDKLNAETARRKEIARQAAIRAANTYAMPANGSVVATAAGRGLI
QVAQGAASLAQAISDAIAVLGRVLASAPSVMAVGFASLTYSSRTAEQWQDQTPDSVRYALGMDAAKLG
LPPSVNLNAVAKASGTVDLPMRLTNEARGNTTTLSVVSTDGVSVPKAVPVRMAAYNATTGLYEVTVPS
TTAEAPPLILTWTPASPPGNQNPSSTTPVVPKPVPVYEGATLTPVKATPETYPGVITLPEDLIIGFPA
DSGIKPIYVMFRDPRDVPGAATGKGQPVSGNWLGAASQGEGAPIPSQIADKLRGKTFKNWRDFREQFW
IAVANDPELSKQFNPGSLAVMRDGGAPYVRESEQAGGRIKIEIHHKVRIADGGGVYNMGNLVAVTPKR
HIEIHKGGK

Pyocin S2(C128-C162): Disulphide formed between residues C128 and C162

MAVNDYEPGSMVITHVQGGGRDIIQYIPARSSYGTPPFVPPGPSPYVGTGMQEYRKLRSTLDKSHSEL
KKNLKNETLKEVDELKSEAGLPGKAVSANDIRDEKSIVDALMDAKAKSLKAIEDRPANL**C**TASDFPQK
SESMYQSQLLASRKFYGEFLDRHMS**C**LAKAYSADIYKAQIAILKQTSQELENKARSLEAEAQRAAAEV
EADYKARKANVEKKVQSELDQAGNALPQLTNPTPEQWLERATQLVTQAIANKKKLQTANNALIAKAPN
ALEKQKATYNADLLVDEIASLQARLDKLNAETARRKEIARQAAIRAANTYAMPANGSVVATAAGRGLI
QVAQGAASLAQAISDAIAVLGRVLASAPSVMAVGFASLTYSSRTAEQWQDQTPDSVRYALGMDAAKLG
LPPSVNLNAVAKASGTVDLPMRLTNEARGNTTTLSVVSTDGVSVPKAVPVRMAAYNATTGLYEVTVPS
TTAEAPPLILTWTPASPPGNQNPSSTTPVVPKPVPVYEGATLTPVKATPETYPGVITLPEDLIIGFPA
DSGIKPIYVMFRDPRDVPGAATGKGQPVSGNWLGAASQGEGAPIPSQIADKLRGKTFKNWRDFREQFW
IAVANDPELSKQFNPGSLAVMRDGGAPYVRESEQAGGRIKIEIHHKVRIADGGGVYNMGNLVAVTPKR
HIEIHKGGK

Pyocin S2Δ1-9: Residues 10 – 689

MSMVITHVQGGGRDIIQYIPARSSYGTPPFVPPGPSPYVGTGMQEYRKLRSTLDKSHSELKKNLKNET
LKEVDELKSEAGLPGKAVSANDIRDEKSIVDALMDAKAKSLKAIEDRPANLYTASDFPQKSESMYQSQ
LLASRKFYGEFLDRHMSELAKAYSADIYKAQIAILKQTSQELENKARSLEAEAQRAAAEVEADYKARK
ANVEKKVQSELDQAGNALPQLTNPTPEQWLERATQLVTQAIANKKKLQTANNALIAKAPNALEKQKAT
YNADLLVDEIASLQARLDKLNAETARRKEIARQAAIRAANTYAMPANGSVVATAAGRGLIQVAQGAAS
LAQAISDAIAVLGRVLASAPSVMAVGFASLTYSSRTAEQWQDQTPDSVRYALGMDAAKLGLPPSVNLN
AVAKASGTVDLPMRLTNEARGNTTTLSVVSTDGVSVPKAVPVRMAAYNATTGLYEVTVPSTTAEAPPL
ILTWTPASPPGNQNPSSTTPVVPKPVPVYEGATLTPVKATPETYPGVITLPEDLIIGFPADSGIKPIY
VMFRDPRDVPGAATGKGQPVSGNWLGAASQGEGAPIPSQIADKLRGKTFKNWRDFREQFWIAVANDPE
LSKQFNPGSLAVMRDGGAPYVRESEQAGGRIKIEIHHKVRIADGGGVYNMGNLVAVTPKRHIEIHKGG
K

Pyocin S2$_{SN1-16}$: PyoSN residues 1 – 16; PyoS2 residues 16 – 689

MALPVENWNDTTVVGYQGGGRDIIQYIPARSSYGTPPFVPPGPSPYVGTGMQEYRKLRSTLDKSHSEL
KKNLKNETLKEVDELKSEAGLPGKAVSANDIRDEKSIVDALMDAKAKSLKAIEDRPANLYTASDFPQK
SESMYQSQLLASRKFYGEFLDRHMSELAKAYSADIYKAQIAILKQTSQELENKARSLEAEAQRAAAEV
EADYKARKANVEKKVQSELDQAGNALPQLTNPTPEQWLERATQLVTQAIANKKKLQTANNALIAKAPN
ALEKQKATYNADLLVDEIASLQARLDKLNAETARRKEIARQAAIRAANTYAMPANGSVVATAAGRGLI
QVAQGAASLAQAISDAIAVLGRVLASAPSVMAVGFASLTYSSRTAEQWQDQTPDSVRYALGMDAAKLG
LPPSVNLNAVAKASGTVDLPMRLTNEARGNTTTLSVVSTDGVSVPKAVPVRMAAYNATTGLYEVTVPS
TTAEAPPLILTWTPASPPGNQNPSSTTPVVPKPVPVYEGATLTPVKATPETYPGVITLPEDLIIGFPA
DSGIKPIYVMFRDPRDVPGAATGKGQPVSGNWLGAASQGEGAPIPSQIADKLRGKTFKNWRDFREQFW
IAVANDPELSKQFNPGSLAVMRDGGAPYVRESEQAGGRIKIEIHHKVRIADGGGVYNMGNLVAVTPKR
HIEIHKGGK

Immunity protein S2

MKSKISEYTEKEFLEFVKDIYTNNKKKFPTEESHIQAVLEFKKLTEHPSGSDLLYYPNENREDSPAGV
VKEVKEWRASKGLPGFKAGLEHHHHHH

Pyocin S2E2: PyoS2 residues 1 – 556; ColE2 residues 449 – 581

MAVNDYEPGSMVITHVQGGGRDIIQYIPARSSYGTPPFVPPGPSPYVGTGMQEYRKLRSTLDKSHSEL
KKNLKNETLKEVDELKSEAGLPGKAVSANDIRDEKSIVDALMDAKAKSLKAIEDRPANLYTASDFPQK
SESMYQSQLLASRKFYGEFLDRHMSELAKAYSADIYKAQIAILKQTSQELENKARSLEAEAQRAAAEV
EADYKARKANVEKKVQSELDQAGNALPQLTNPTPEQWLERATQLVTQAIANKKKLQTANNALIAKAPN
ALEKQKATYNADLLVDEIASLQARLDKLNAETARRKEIARQAAIRAANTYAMPANGSVVATAAGRGLI
QVAQGAASLAQAISDAIAVLGRVLASAPSVMAVGFASLTYSSRTAEQWQDQTPDSVRYALGMDAAKLG
LPPSVNLNAVAKASGTVDLPMRLTNEARGNTTTLSVVSTDGVSVPKAVPVRMAAYNATTGLYEVTVPS
TTAEAPPLILTWTPASPPGNQNPSSTTPVVPKPVPVYEGATLTPVKATPETYPGVITLPEDLIIGFPA
DSGIKPIYVMFRAMESKRNKPGKATGKGKPVGDKWLDDAGKDSGAPIPDRIADKLRDKEFKNFDDFRK
KFWEEVSKDPDLSKQFKGSNKTNIQKGKAPFARKKDQVGGRERFELHHDKPISQDGGVYDMNNIRVTT
PKRHIDIHRGK

Immunity protein 2
MELKHSISDYTEAEFLEFVKKICRAEGATEEDDNKLVREFERLTEHPDGSDLIYYPRDDREDSPEGIV
KEIKEWRAANGKSGFKQGLEHHHHHH

Pyocin S2$_{NTD}$: Residues 1 – 209
MAVNDYEPGSMVITHVQGGGRDIIQYIPARSSYGTPPFVPPGPSPYVGTGMQEYRKLRSTLDKSHSEL
KKNLKNETLKEVDELKSEAGLPGKAVSANDIRDEKSIVDALMDAKAKSLKAIEDRPANLYTASDFPQK
SESMYQSQLLASRKFYGEFLDRHMSELAKAYSADIYKAQIAILKQTSQELENKARSLEAEAQRAAAEV
EADYKLEHHHHHH

FpvAI SD-TB-Plug: Residues 1 – 276: *OM secretion signal underlined*
MPAPHGLSPLSKAFLMRRAFQRRILPHSLAMALSLPLAGYVQAQEVEFDIPPQALGSALQEFGRQADI
QVLYRPEEVRNKRSSAIKGKLEPNQAITELLRGTGASVDFQGNAITISVAEAADSSVDLGATMITSNQ
LGTITEDSGSYTPGTIATATRLVLTPRETPQSITVVTRQNMDDFGLNNIDDVMRHTPGITVSAYDTDR
NNYYARGFSINNFQYDGIPSTARNVGYSAGNTLSDMAIYDRVEVLKGATGLLTGAGSLGATINLIRKK
PTHE

FpvAI Plug$_{NL}$: Residues 215 – 276: *OM secretion signal underlined*
MPAPHGLSPLSKAFLMRRAFQRRILPHSLAMALSLPLAGYVQAQNNFQYDGIPSTARNVGYSAGNTLS
DMAIYDRVEVLKGATGLLTGAGSLGATINLIRKKPTHE

Pyocin SN
MALPVENWNDTTVVGYQDGNGGYSFDGVGGGFSGGSDSLGLNRQELSPMSQSFDAFEDNAIQVYQKLR
EYLDNQYKGAKGNIEKDIDEKVESAIKAAGGQSVLSPLSRIDIAISTIQKLIAQRSEQLQSERQRLAS
LPESSYSARNDLDFVKMLYDAEPDNRQLFKMSLEPFVISESDGLAAEYNADVSSQYIANLQRRLPELE
KARAPLVAEEQARQEAEAEAQRKADEEAQRAADEAAARQEAQQVTQQLGANFNAITAPMGDKVQQRVQ
AVDATQAQISNQIGSAVTSATQAVQAKAAEAQQHASSSIASGEGLISSAFRGQIASAAQASGESRVST
FNTRIDQIVSEATSFSEARKQALAQFTANAAAEVEAETARLAERVRANPTQATSQSAQADLRQLTETT
YSNVNTFAQQTEAALQAKAQEVTAAVTEAQRVANEGLQQAANSVQGEITQTANTLAMPAIAAPLVSVA
GFGTAALELAQLGVSLANAVNRVTQIATAGPGAYVATFAVLTLYSDQAGKDSDNVPDGVRTALSLEAS
TLGLSPDVDLQSAAEEGGTVEMPVRLTSRTEEDQDNKSQIAVVVPNAVSTLQGVPVRAATLNAATGRY
EVTVPAKSTVPDTPPLILTWTPANPPGSQNPSSTTPVVPQPVPVYEGATIAPAKAEPESYPGIPLSLD
DLIVIFPADSGIPPLYLVFSKPPVSALEVDIYGNFTGRPRNGNHLDHMPAQGALATSLRSAIPDIQEK
EIRDLMKKGASIAIPARIHQKYSETYGGRNTKEKQRKDAEDLRRAVDSNFDAIKNALVEEGFSERDVE
EARAKLHRINEEQGWY

Pyocin SNΔ1-52: Residues 53 – 832
MFDAFEDNAIQVYQKLREYLDNQYKGAKGNIEKDIDEKVESAIKAAGGQSVLSPLSRIDIAISTIQKL
IAQRSEQLQSERQRLASLPESSYSARNDLDFVKMLYDAEPDNRQLFKMSLEPFVISESDGLAAEYNAD
VSSQYIANLQRRLPELEKARAPLVAEEQARQEAEAEAQRKADEEAQRAADEAAARQEAQQVTQQLGAN
FNAITAPMGDKVQQRVQAVDATQAQISNQIGSAVTSATQAVQAKAAEAQQHASSSIASGEGLISSAFR
GQIASAAQASGESRVSTFNTRIDQIVSEATSFSEARKQALAQFTANAAAEVEAETARLAERVRANPTQ
ATSQSAQADLRQLTETTYSNVNTFAQQTEAALQAKAQEVTAAVTEAQRVANEGLQQAANSVQGEITQT
ANTLAMPAIAAPLVSVAGFGTAALELAQLGVSLANAVNRVTQIATAGPGAYVATFAVLTLYSDQAGKD
SDNVPDGVRTALSLEASTLGLSPDVDLQSAAEEGGTVEMPVRLTSRTEEDQDNKSQIAVVVPNAVSTL
QGVPVRAATLNAATGRYEVTVPAKSTVPDTPPLILTWTPANPPGSQNPSSTTPVVPQPVPVYEGATIA
PAKAEPESYPGIPLSLDDLIVIFPADSGIPPLYLVFSKPPVSALEVDIYGNFTGRPRNGNHLDHMPAQ
GALATSLRSAIPDIQEKEIRDLMKKGASIAIPARIHQKYSETYGGRNTKEKQRKDAEDLRRAVDSNFD
AIKNALVEEGFSERDVEEARAKLHRINEEQGWY

Immunity protein SN
MNPESIKELVGSLGQSYSELTERKLIPSGSLVKQYEESDWLTLDVDVGIDLEFWAENKISEKLHIVLI
KTMDDIPAYQGELPSPFSRNMEKAMVRSFLGVPDSTKEPFKMPVVGMVGGWDSYTHPERSDVRIFFRY
TPDLKVSTLSFSLKEPGHDLEHHHHHH

Pyocin SN_{TR}: Residues 1 – 699

MALPVENWNDTTVVGYQDGNGGYSFDGVGGGFSGGSDSLGLNRQELSPMSQSFDAFEDNAIQVYQKLR
EYLDNQYKGAKGNIEKDIDEKVESAIKAAGGQSVLSPLSRIDIAISTIQKLIAQRSEQLQSERQRLAS
LPESSYSARNDLDFVKMLYDAEPDNRQLFKMSLEPFVISESDGLAAEYNADVSSQYIANLQRRLPELE
KARAPLVAEEQARQEAEAEAQRKADEEAQRAADEAAARQEAQQVTQQLGANFNAITAPMGDKVQQRVQ
AVDATQAQISNQIGSAVTSATQAVQAKAAEAQQHASSSIASGEGLISSAFRGQIASAAQASGESRVST
FNTRIDQIVSEATSFSEARKQALAQFTANAAAEVEAETARLAERVRANPTQATSQSAQADLRQLTETT
YSNVNTFAQQTEAALQAKAQEVTAAVTEAQRVANEGLQQAANSVQGEITQTANTLAMPAIAAPLVSVA
GFGTAALELAQLGVSLANAVNRVTQIATAGPGAYVATFAVLTLYSDQAGKDSDNVPDGVRTALSLEAS
TLGLSPDVDLQSAAEEGGTVEMPVRLTSRTEEDQDNKSQIAVVVPNAVSTLQGVPVRAATLNAATGRY
EVTVPAKSTVPDTPPLILTWTPANPPGSQNPSSTTPVVPQPVPVYEGATIAPAKAEPESYPGIPLSLD
DLIVIFPADSGIPPLYLVFLEHHHHHH

Pyocin SN_{NTD}: Residues 1 – 205

MALPVENWNDTTVVGYQDGNGGYSFDGVGGGFSGGSDSLGLNRQELSPMSQSFDAFEDNAIQVYQKLR
EYLDNQYKGAKGNIEKDIDEKVESAIKAAGGQSVLSPLSRIDIAISTIQKLIAQRSEQLQSERQRLAS
LPESSYSARNDLDFVKMLYDAEPDNRQLFKMSLEPFVISESDGLAAEYNADVSSQYIANLQRRLPELE
KLEHHHHHH

Pyocin SN_{NTD}Δ1-52: Residues 53 – 205

MFDAFEDNAIQVYQKLREYLDNQYKGAKGNIEKDIDEKVESAIKAAGGQSVLSPLSRIDIAISTIQKL
IAQRSEQLQSERQRLASLPESSYSARNDLDFVKMLYDAEPDNRQLFKMSLEPFVISESDGLAAEYNAD
VSSQYIANLQRRLPELEKLEHHHHHH

$CntO_{PA}$: *OM secretion signal underlined*

MRVSVSLVLGVGLGCSSPALWAETESPAELEVLTVTAEAERAEGPVQGYRANRTASATRTDTRIEDIP
QAISVVPRQVLDDLDSARIERALDFAGGVSRQNNFGGLTMFEYNVRGFTTSEFYRDGFSANRGYMNAP
DSATIERVEILKGPASSLYGRGDPGGTVNLVTKKPQAERFARLHASAGSWDRYRSTLDLNTPLDEEGD
LLYRMNLAVEDSKGFRDYADGQRLLVAPSISWQLDPDTSLLVEAEVVRNRQVFDRGTVAPHNHLGSLP
RSRFFGEPDDGKIDNNNETLQATLRHHFNEQWSLRLASHYKHGHLDGYASENSSLAADGYSLRREYRY
RDFEWHDSITQLDLLGDLHTGSIRHQLLMGLEYERYHNDELILRSIPSRNPYAIDIRRPVYGQPKPPF
GRDDRNHEEVDAMALNLQDQIEFSEKWRGLLGVRFDRYRQDMNATRLNNGRFRETSSQQTQRAATPRI
GVLYQATPEVGLFANASKSFKPNGGTDMAGKAFDPEEGRGYEAGVKLDLLDGRLGMTLAAFHLKKKNV
LTADPSNPGYQQTAGEARSQGFDLQFSGQLTEQLRLIGAYAYIDAEVTKDENIARGSRLLNVPKHSGS
LMGVYEFREGWLHGADAGAAVNYVGERAGDSSDSGFELPAYTTVDLLARYPLASNATLGVNVNNLFDR
RYYERSYNNVWVAPGEPRNLTMSLTLNY

CntO: *E. coli* OmpF signal sequence residues 1 – 23 (*underlined*); CntO residues 23 – 708

MVKRNILAVIVPALLVAGTANAAETESPAELEVLTVTAEAERAEGPVQGYRANRTASATRTDTRIEDI
PQAISVVPRQVLDDLDSARIERALDFAGGVSRQNNFGGLTMFEYNVRGFTTSEFYRDGFSANRGYMNA
PDSATIERVEILKGPASSLYGRGDPGGTVNLVTKKPQAERFARLHASAGSWDRYRSTLDLNTPLDEEG
DLLYRMNLAVEDSKGFRDYADGQRLLVAPSISWQLDPDTSLLVEAEVVRNRQVFDRGTVAPHNHLGSL
PRSRFFGEPDDGKIDNNNETLQATLRHHFNEQWSLRLASHYKHGHLDGYASENSSLAADGYSLRREYR
YRDFEWHDSITQLDLLGDLHTGSIRHQLLMGLEYERYHNDELILRSIPSRNPYAIDIRRPVYGQPKPP
FGRDDRNHEEVDAMALNLQDQIEFSEKWRGLLGVRFDRYRQDMNATRLNNGRFRETSSQQTQRAATPR
IGVLYQATPEVGLFANASKSFKPNGGTDMAGKAFDPEEGRGYEAGVKLDLLDGRLGMTLAAFHLKKKN
VLTADPSNPGYQQTAGEARSQGFDLQFSGQLTEQLRLIGAYAYIDAEVTKDENIARGSRLLNVPKHSG
SLMGVYEFREGWLHGADAGAAVNYVGERAGDSSDSGFELPAYTTVDLLARYPLASNATLGVNVNNLFD
RRYYERSYNNVWVAPGEPRNLTMSLTLNY

TonB1: Residues 109 – 342

GAMATPAELNLGHGELPKTMQVNFVQLEKKAEPTPQPPAAAPEPTPPKIEEPKPEPPKPKPVEKPKPK
PKPKPKPVENAIPKAKPKPEPKPKPEPEPSTEASSQPSPSSAAPPPAPTVGQSTPGAQTAPSGSQGPA
GLPSGSLNDSDIKPLRMDPPVYPRMAQARGIEGRVKVLFTITSDGRIDDIQVLESVPSRMFDREVRQA
MAKWRFEPRVSGGKIVARQATKMFFFKIEKRR

Plasmid Vector Maps

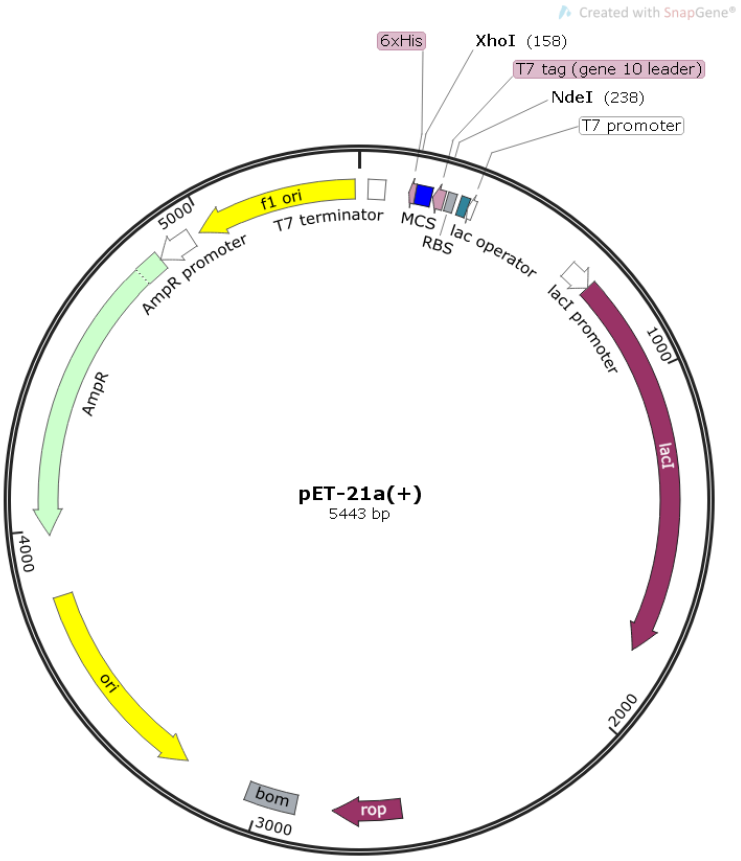

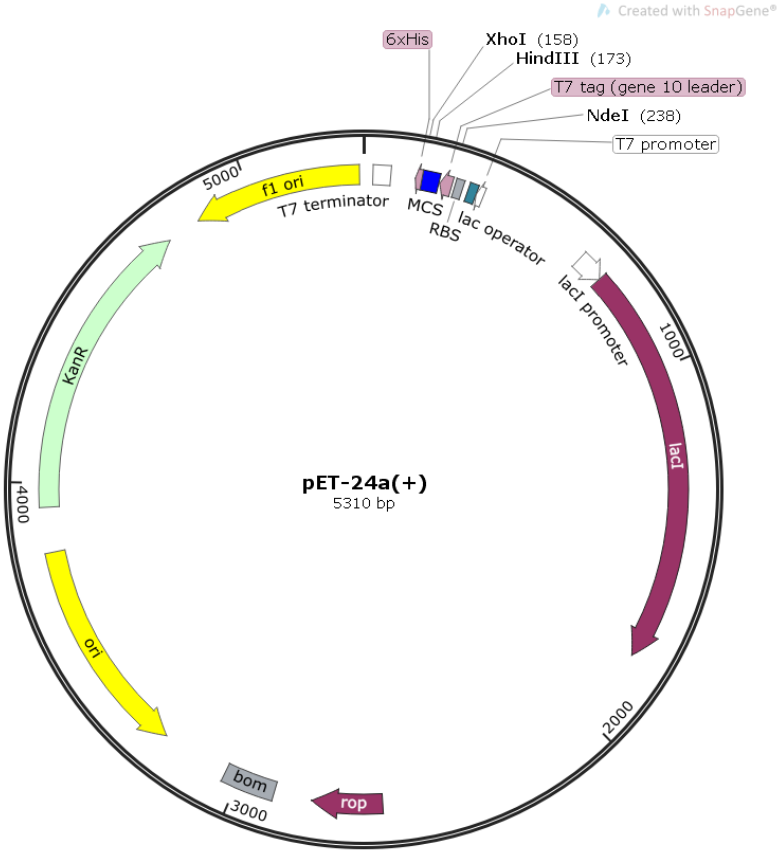

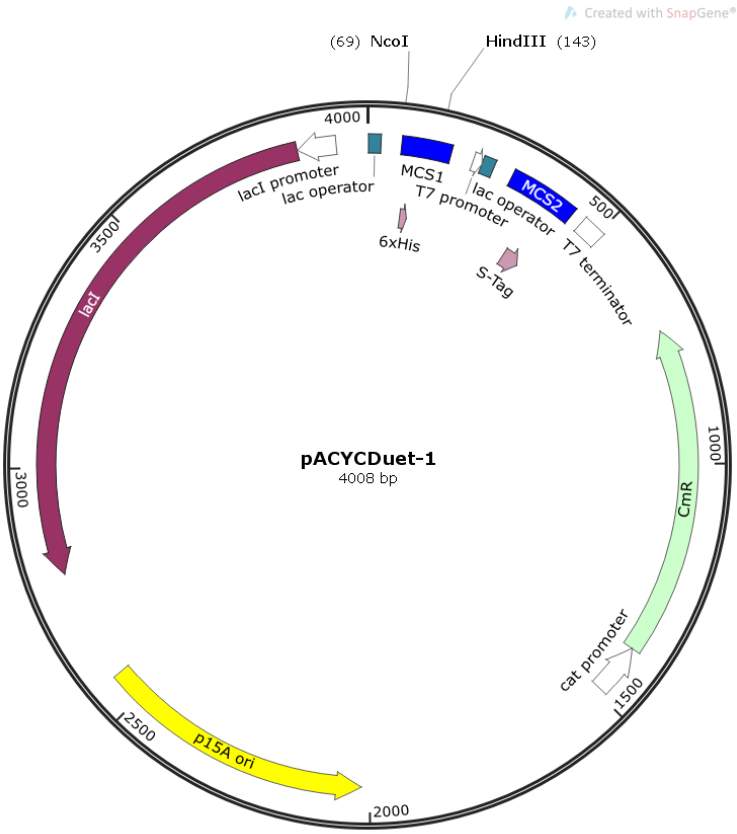
Created with SnapGene®
(69) NcoI
HindIII (143)
4000
lacI promoter
lac operator
MCS1
T7 promoter
lac operator
MCS2
T7 terminator
6xHis
S-Tag
500
3500
lacI
1000
3000
pACYCDuet-1
4008 bp
CmR
cat promoter
1500
2500
p15A ori
2000

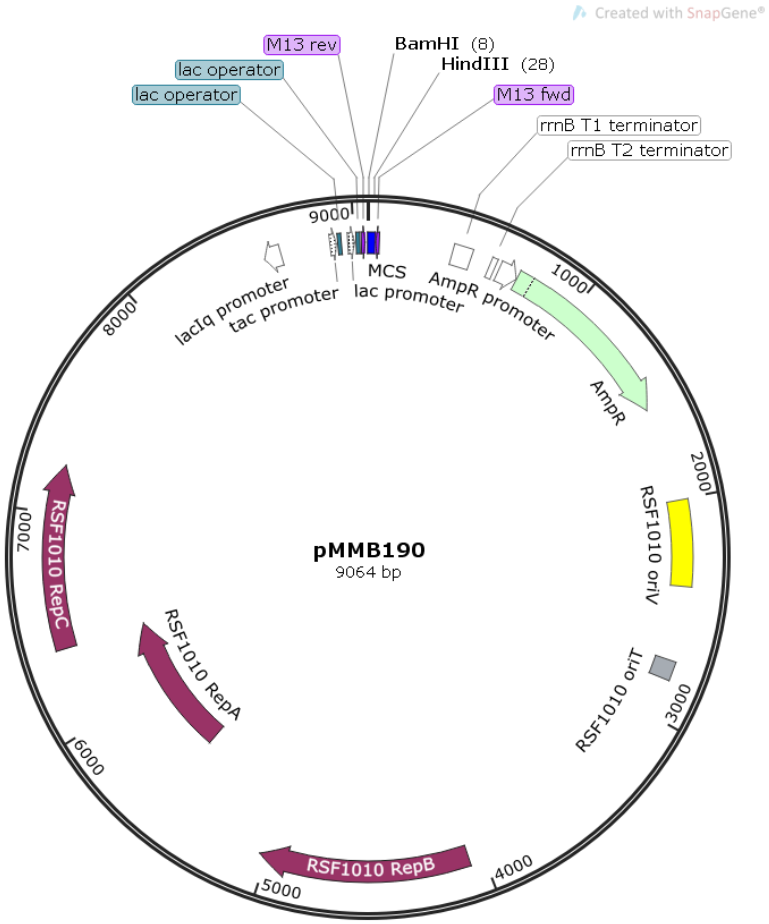
Created with SnapGene®
M13 rev
BamHI (8)
HindIII (28)
lac operator
lac operator
M13 fwd
rrnB T1 terminator
rrnB T2 terminator
9000
lacIq promoter
tac promoter
MCS
lac promoter
AmpR promoter
1000
8000
AmpR
2000
RSF1010 RepC
7000
RSF1010 oriV
RSF1010 RepA
RSF1010 oriT
3000
6000
RSF1010 RepB
4000
5000
pMMB190
9064 bp

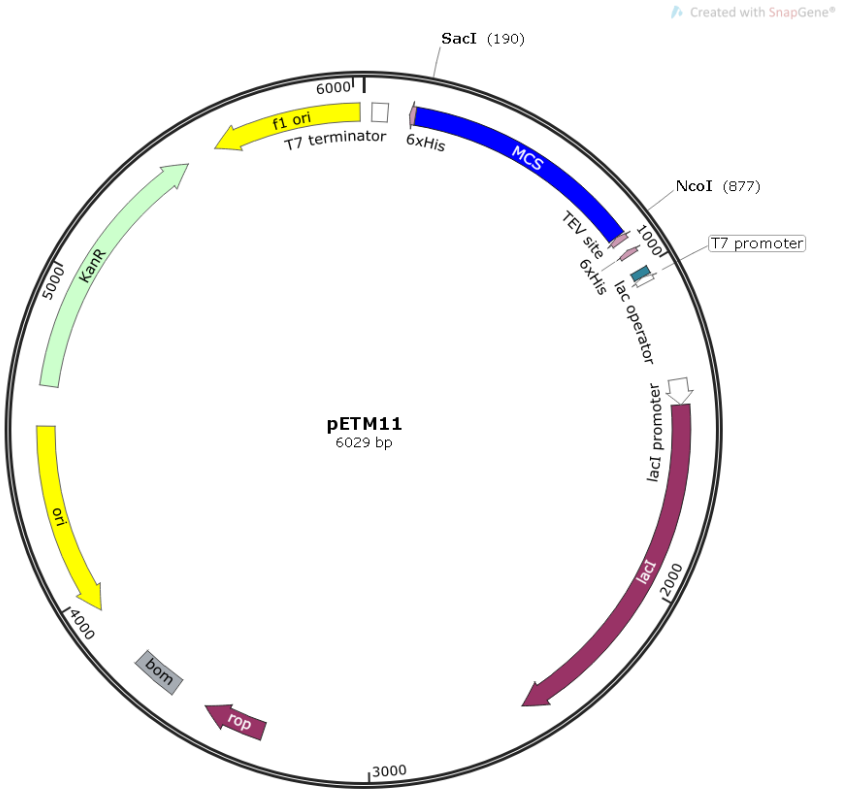
Created with SnapGene®
SacI (190)
6000
f1 ori
T7 terminator
6xHis
MCS
NcoI (877)
TEV site
6xHis
1000
T7 promoter
lac operator
lacI promoter
lacI
2000
3000
rop
bom
4000
ori
5000
KanR
pETM11
6029 bp

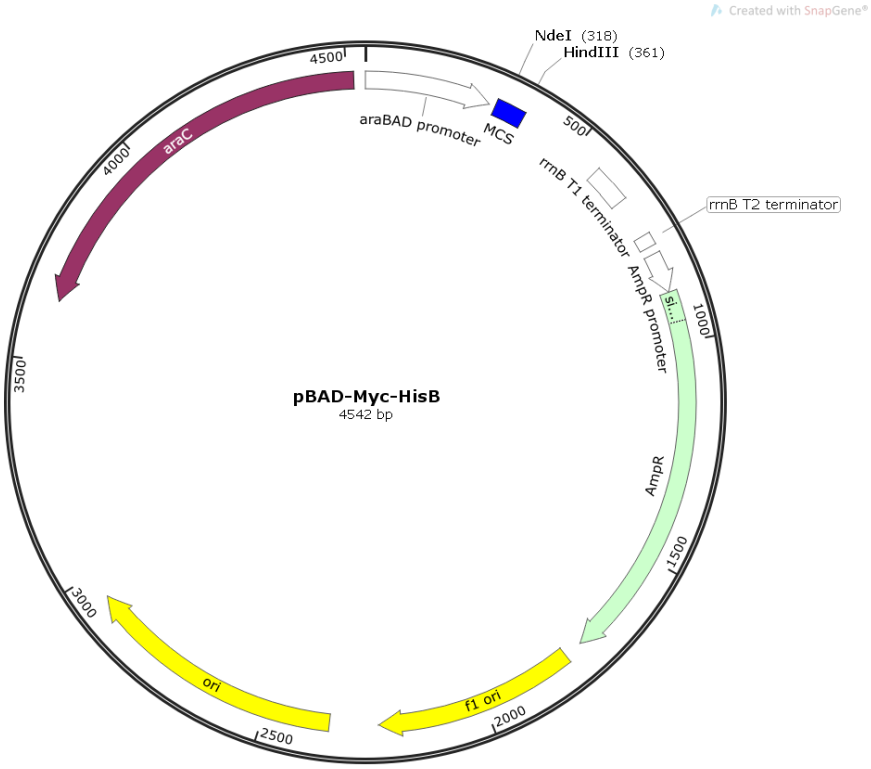
Created with SnapGene®
NdeI (318)
HindIII (361)
4500
araBAD promoter
MCS
500
rrnB T1 terminator
rrnB T2 terminator
AmpR promoter
1000
4000
araC
3500
AmpR
1500
3000
ori
f1 ori
2500
2000
pBAD-Myc-HisB
4542 bp

Table S1. *P. aeruginosa* strains used in this study.

Name	Relevant Characteristics	Source
PA14	Clinical isolate, burn wound	Walker Lab
PA7	Clinical isolate, non-respiratory	
C763	Clinical isolate, CF patient	
J1385	Clinical isolate, CF patient	
J1532	Clinical mucoid isolate, CF patient	
PA62	Environmental isolate, soil	
P1	Clinical mucoid isolate, young CF patient	
P2	Clinical mucoid isolate, young CF patient	
P3	Clinical mucoid isolate, young CF patient	
P4	Clinical mucoid isolate, young CF patient	
P5	Clinical mucoid isolate, young CF patient	
P7	Clinical mucoid isolate, young CF patient	
P8	Clinical mucoid isolate, young CF patient	
P9	Clinical mucoid isolate, young CF patient	
P10	Clinical mucoid isolate, young CF patient	
P11	Clinical mucoid isolate, young CF patient	
P12	Clinical mucoid isolate, young CF patient	
P13	Clinical mucoid isolate, young CF patient	
P14	Clinical mucoid isolate, young CF patient	
P15	Clinical mucoid isolate, young CF patient	
P17	Clinical mucoid isolate, young CF patient	
P18	Clinical mucoid isolate, young CF patient	
P19	Clinical mucoid isolate, young CF patient	
TEP1	Clinical isolate, sepsis	
TEP2	Clinical isolate, sepsis	
TEP3	Clinical isolate, sepsis	
TEP4	Clinical isolate, sepsis	
TEP6	Clinical isolate, sepsis	
TEP7	Clinical isolate, sepsis	
TEP8	Clinical isolate, sepsis	
TEP9	Clinical isolate, sepsis	
TEP10	Clinical isolate, sepsis	
YHP17	Clinical isolate	

Table S2. Plasmid Vector Genotypes used in this study.

Plasmid Vector	Origin	Promotor	Antibiotic Resistance	Reference
pET-21a(+)	pBR322	T7-lac	Ampicillin	Novagen
pET-24a(+)	pBR322	T7-lac	Kanamycin	Novagan
pACYCDuet-1	p15A	T7-lac	Chloramphenicol	Novagen
pMMB190	pMMB66EH	lac-tac	Ampicillin	(Morales *et al.*, 1991)
pETM11	pBR322	T7-lac	Kanamycin	(Dümmler *et al.*, 2005)
pBAD-Myc-HisB	pBR322	araBAD	Ampicillin	Invitrogen

Bibliography

Abe, Y., Shodai, T., Muto, T., Mihara, K., Torii, H., Nishikawa, S. ichi, Endo, T., & Kohda, D. (2000). Structural basis of presequence recognition by the mitochondrial protein import receptor Tom20. *Cell*, **100**(5), 551–560.

Abrusci, P., McDowell, M. A., Lea, S. M., & Johnson, S. (2014). Building a secreting nanomachine: A structural overview of the T3SS. *Current Opinion in Structural Biology*, **25**, 111–117.

Adams, H., Zeder-Lutz, G., Schalk, I., Pattus, F., & Celia, H. (2006). Interaction of TonB with the outer membrane receptor FpvA of *Pseudomonas aeruginosa*. *Journal of Bacteriology*, **188**(16), 5752–5761.

Adams, P. D., Afonine, P. V., Bunkóczi, G., Chen, V. B., Davis, I. W., Echols, N., Headd, J. J., Hung, L. W., Kapral, G. J., Grosse-Kunstleve, R. W., McCoy, A. J., Moriarty, N. W., Oeffner, R., Read, R. J., Richardson, D. C., Richardson, J. S., Terwilliger, T. C., & Zwart, P. H. (2010). PHENIX: A comprehensive Python-based system for macromolecular structure solution. *Acta Crystallographica Section D: Biological Crystallography*, **66**(2), 213–221.

Aeschlimann, J. R. (2003). The role of multidrug efflux pumps in the antibiotic resistance of *Pseudomonas aeruginosa* and other gram-negative bacteria insights from the society of infectious diseases pharmacists. *Pharmacotherapy*, **23**(7), 916–924.

Albrecht-Gary, A.-M., Blanc, S., Rochel, N., Ocaktan, A. Z., & Abdallah, M. A. (1994). Bacterial Iron Transport: Coordination Properties of Pyoverdin PaA, a Peptidic Siderophore of *Pseudomonas aeruginosa*. *Inorganic Chemistry*, **33**(26), 6391–6402.

Alteri, C. J. & Mobley, H. L. T. (2016). The Versatile Type VI Secretion System. *Microbiology Spectrum*, **4**(2). 10.1128/microbiolspec. VMBF-0026-2015.

Andreini, C., Banci, L., Bertini, I., & Rosato, A. (2006). Zinc through the three domains of life. *Journal of Proteome Research*, **5**(11), 3173–3178.

Ankenbauer, R. G., & Quan, H. N. (1994). FptA, the Fe(III)-pyochelin receptor of *Pseudomonas aeruginosa*: A phenolate siderophore receptor homologous to hydroxamate siderophore receptors. *Journal of Bacteriology*, **176**(2), 307–319.

Anraku, Y. (1988). Bacterial Electron Transport Chains. *Annual Review of Biochemistry*, **57**(1), 101–132.

Antignani, A., & Youle, R. J. (2008). Endosome fusion induced by diphtheria toxin translocation domain. *Proceedings of the National Academy of Sciences of the United States of America*, **105**(23), 8020–8025.

Aoki, S. K., Malinverni, J. C., Jacoby, K., Thomas, B., Pamma, R., Trinh, B. N., Remers, S., Webb, J., Braaten, B. A., Silhavy, T. J., & Low, D. A. (2008). Contact-dependent growth inhibition requires the essential outer membrane protein BamA (YaeT) as the receptor and the inner membrane transport protein AcrB. *Molecular Microbiology*, **70**(2), 323–340.

Aoki, S. K., Pamma, R., Hernday, A. D., Bickham, J. E., Braaten, B. A., & Low, D. A. (2005). Microbiology: Contact-dependent inhibition of growth in *Escherichia coli*. *Science*, **309**(5738), 1245–1248.

Araiso, Y., Tsutsumi, A., Qiu, J., Imai, K., Shiota, T., Song, J., Lindau, C., Wenz, L. S., Sakaue, H., Yunoki, K., Kawano, S., Suzuki, J., Wischnewski, M., Schütze, C., Ariyama, H., Ando, T., Becker, T., Lithgow, T., Wiedemann, N., Pfanner, N., Kikkawa, M. & Endo, T. (2019). Structure of the mitochondrial import gate reveals distinct preprotein paths. *Nature*, **575**(7782), 395–401.

Armitage, J. P., & Berry, R. M. (2020). Assembly and Dynamics of the Bacterial Flagellum. *Annual Review of Microbiology*, **74**, 181–200.

Arnold, T., Zeth, K., & Linke, D. (2009). Structure and function of colicin S4, a colicin with a duplicated receptor-binding domain. *Journal of Biological Chemistry*, **284**(10), 6403–6413.

Atanaskovic, I., Mosbahi, K., Sharp, C., Housden, N. G., Kaminska, R., Walker, D., & Kleanthous, C. (2020). Targeted Killing of *Pseudomonas aeruginosa* by Pyocin G Occurs via the Hemin Transporter Hur. *Journal of Molecular Biology*, **432**(13), 3869–3880.

Bakelar, J., Buchanan, S. K., & Noinaj, N. (2016). The structure of the β-barrel assembly machinery complex. *Science*, **351**(6269), 180–186.

Balakrishnan, L., Hughes, C., & Koronakis, V. (2001). Substrate-triggered recruitment of the TolC channel-tunnel during type I export of hemolysin by *Escherichia coli*. *Journal of Molecular Biology*, **313**(3), 501–510.

Barreteau, H., Tiouajni, M., Graille, M., Josseaume, N., Bouhss, A., Patin, D., Blanot, D., Fourgeaud, M., Mainardi, J. L., Arthur, M., Van Tilbeurgh, H., Mengin-Lecreulx, D., & Touzé, T. (2012). Functional and structural characterization of PaeM, a colicin M-like bacteriocin produced by *Pseudomonas aeruginosa*. *Journal of Biological Chemistry*, **287**(44), 37395–37405.

Baysse, C., Meyer, J. M., Plesiat, P., Geoffroy, V., Michel-Briand, Y., & Cornelis, P. (1999). Uptake of pyocin S3 occurs through the outer membrane ferripyoverdine type II receptor of *Pseudomonas aeruginosa*. *Journal of Bacteriology*, **181**(12), 3849–3851.

Bechtluft, P., Nouwen, N., Tans, S. J., & Driessen, A. J. M. (2010). SecB - A chaperone dedicated to protein translocation. *Molecular BioSystems*, **6**(4), 620–627.

Beck, C. M., Diner, E. J., Kim, J. J., Low, D. A., & Hayes, C. S. (2014). The F pilus mediates a novel pathway of CDI toxin import. *Molecular Microbiology*, **93**(2), 276–290.

Behrens, H. M., Lowe, E. D., Gault, J., Housden, N. G., Kaminska, R., Weber, T. M., Thompson, C. M. A., Mislin, G. L. A., Schalk, I. J., Walker, D., Robinson, C. V., & Kleanthous, C. (2020). Pyocin S5 import into *Pseudomonas aeruginosa* reveals a generic mode of bacteriocin transport. *MBio*, **11**(2), 10.1128/mBio. e03230-19.

Behrens, H. M., Six, A., Walker, D., & Kleanthous, C. (2017). The therapeutic potential of bacteriocins as protein antibiotics. *Emerging Topics in Life Sciences*, **1**(1), 65–74.

Berks, B. C. (2015). The Twin-Arginine Protein Translocation Pathway. *Annual Review of Biochemistry*, **84**(1), 843–864.

Berman, H. M., Westbrook, J., Feng, Z., Gilliland, G., Bhat, T. N., Weissig, H., Shindyalov, I. N., & Bourne, P. E. (2000). The Protein Data Bank. *Nucleic Acids Research*, **28**(1), 235–242.

Bingle, L. E., Bailey, C. M., & Pallen, M. J. (2008). Type VI secretion: a beginner's guide. *Current Opinion in Microbiology*, **11**(1), 3–8.

Bonneau, A., Roche, B., & Schalk, I. J. (2020). Iron acquisition in *Pseudomonas aeruginosa* by the siderophore pyoverdine: an intricate interacting network including periplasmic and membrane proteins. *Scientific Reports*, **10**(1), 120.

Bonsor, D. A., Grishkovskaya, I., Dodson, E. J., & Kleanthous, C. (2007). Molecular mimicry enables competitive recruitment by a natively disordered protein. *Journal of the American Chemical Society*, **129**(15), 4800–4807.

Bowman, C. M., Dahlberg, J. E., Ikemura, T., Konisky, J., & Nomura, M. (1971). Specific inactivation of 16S ribosomal RNA induced by colicin E3 *in vivo*. *Proceedings of the National Academy of Sciences of the United States of America*, **68**(5), 964–968.

Braun, M., Endriss, F., Killmann, H., & Braun, V. (2003). In vivo reconstitution of the FhuA transport protein of Escherichia coli K-12. *Journal of Bacteriology*, **185**(18), 5508–5518.

Braun, V. (1975). Covalent lipoprotein from the outer membrane of *Escherichia coli*. *Biochimica et Biophysica Acta (BBA) - Reviews on Biomembranes*, **415**(3), 335–377.

Braun, Volkmar, Patzer, S. I., & Hantke, K. (2002). Ton-dependent colicins and microcins: Modular design and evolution. *Biochimie*, **84**(5–6), 365–380).

Brillet, K., Journet, L., Célia, H., Paulus, L., Stahl, A., Pattus, F., & Cobessi, D. (2007). A β Strand Lock Exchange for Signal Transduction in TonB-Dependent Transducers on the Basis of a Common Structural Motif. *Structure*, **15**(11), 1383–1391.

Brillet, K., Ruffenach, F., Adams, H., Journet, L., Gasser, V., Hoegy, F., Guillon, L., Hannauer, M., Page, A., & Schalk, I. J. (2012). An ABC transporter with two periplasmic binding proteins involved in iron acquisition in *Pseudomonas aeruginosa*. *ACS Chemical Biology*, **7**(12), 2036–2045.

Brockwell, D. J., Paci, E., Zinober, R. C., Beddard, G. S., Olmsted, P. D., Smith, D. A., Perham, R. N., & Radford, S. E. (2003). Pulling geometry defines the mechanical resistance of a β-sheet protein. *Nature Structural Biology*, **10**(9), 731–737.

Brotcke Zumsteg, A., Goosmann, C., Brinkmann, V., Morona, R., & Zychlinsky, A. (2014). IcsA is a *Shigella flexneri* adhesion regulated by the type III secretion system and required for pathogenesis. *Cell Host and Microbe*, **15**(4), 435–445.

Bruce, B. D. (2001). The paradox of plastid transit peptides: Conservation of function despite divergence in primary structure. *Biochimica et Biophysica Acta (BBA) - Molecular Cell Research*, **1541**(1–2), 2–21.

Buchanan, S. K., Lukacik, P., Grizot, S., Ghirlando, R., Ali, M. M. U., Barnard, T. J., Jakes, K. S., Kienker, P. K., & Esser, L. (2007). Structure of colicin I receptor bound to the R-domain of colicin Ia: Implications for protein import. *EMBO Journal*, **26**(10), 2594–2604.

Burger, G., Gray, M. W., Forget, L., & Lang, B. F. (2013). Strikingly bacteria-like and gene-rich mitochondrial genomes throughout jakobid protists. *Genome Biology and Evolution*, **5**(2), 418–438.

Buttner, D. (2012). Protein Export According to Schedule: Architecture, Assembly, and Regulation of Type III Secretion Systems from Plant- and Animal-Pathogenic Bacteria. *Microbiology and Molecular Biology Reviews*, **76**(2), 262–310.

Calmettes, C., Ing, C., Buckwalter, C. M., El Bakkouri, M., Chieh-Lin Lai, C., Pogoutse, A., Gray-Owen, S. D., Pomès, R., & Moraes, T. F. (2015). The molecular mechanism of Zinc acquisition by the neisserial outer-membrane transporter ZnuD. *Nature Communications*, **6**(1), 1–11.

Cancino, J., Jung, J. E., & Luini, A. (2013). Regulation of Golgi signaling and trafficking by the KDEL receptor. *Histochemistry and Cell Biology*, **140**(4), 395–405.

Cascales, E., Bernadac, A., Gavioli, M., Lazzaroni, J. C., & Lloubes, R. (2002). Pal lipoprotein of *Escherichia coli* plays a major role in outer membrane integrity. *Journal of Bacteriology*, **184**(3), 754–759.

Cascales, E., Buchanan, S. K., Duché, D., Kleanthous, C., Lloubès, R., Postle, K., Riley, M., Slatin, S., & Cavard, D. (2007). Colicin Biology. *Microbiology and Molecular Biology Reviews*, **71**(1), 158–229.

Cascales, E., & Christie, P. J. (2003). The versatile bacterial type IV secretion systems. *Nature Reviews Microbiology*, **1**(2), 137–149.

Cascales, E., Lloubès, R., & Sturgis, J. N. (2001). The TolQ-TolR proteins energize TolA and share homologies with the flagellar motor proteins MotA-MotB. *Molecular Microbiology*, **42**(3), 795–807.

Celia, H., Botos, I., Ni, X., Fox, T., De Val, N., Lloubes, R., Jiang, J., & Buchanan, S. K. (2019). Cryo-EM structure of the bacterial Ton motor subcomplex ExbB–ExbD provides information on structure and stoichiometry. *Communications Biology*, **2**, 10.1038/s42003-019-0604-2.

Celia, H., Noinaj, N., Zakharov, S. D., Bordignon, E., Botos, I., Santamaria, M., Barnard, T. J., Cramer, W. A., Lloubes, R., & Buchanan, S. K. (2016). Structural insight into the role of the Ton complex in energy transduction. *Nature*, **538**(7623), 60–65.

Chacinska, A., Koehler, C. M., Milenkovic, D., Lithgow, T., & Pfanner, N. (2009). Importing Mitochondrial Proteins: Machineries and Mechanisms. *Cell*, **138**(4), 628–644).

Chang, C., Mooser, A., Plückthun, A., & Wlodawer, A. (2001). Crystal Structure of the Dimeric C-terminal Domain of TonB Reveals a Novel Fold. *Journal of Biological Chemistry*, **276**(29), 27535–27540.

Chang, J. W., Sato, Y., Ogawa, T., Arakawa, T., Fukai, S., Fushinobu, S., & Masaki, H. (2018). Crystal structure of the central and the C-terminal RNase domains of colicin D implicated its translocation pathway through inner membrane of target cell. *Journal of Biochemistry*, **164**(5), 329–339.

Chauleau, M., Mora, L., Serba, J., & De Zamaroczy, M. (2011). FtsH-dependent processing of RNase colicins D and E3 means that only the cytotoxic domains are imported into the cytoplasm. *Journal of Biological Chemistry*, **286**(33), 29397–29407.

Chevalier, S., Bouffartigues, E., Bodilis, J., Maillot, O., Lesouhaitier, O., Feuilloley, M. G. J., Orange, N., Dufour, A., & Cornelis, P. (2017). Structure, function and regulation of *Pseudomonas aeruginosa* porins. *FEMS Microbiology Reviews*, **41**(5), 698–722). Oxford University Press. https://academic.oup.com/femsre/article/41/5/698/3959603

Chimento, D. P., Mohanty, A. K., Kadner, R. J., & Wiener, M. C. (2003). Substrate-induced transmembrane signaling in the cobalamin transporter BtuB. *Nature Structural Biology*, **10**(5), 394–401.

Clément, E., Mesini, P. J., Pattus, F., & Schalk, I. J. (2004). The Binding Mechanism of Pyoverdin with the Outer Membrane Receptor FpvA in *Pseudomonas aeruginosa* is Dependent on Its Iron-Loaded Status. *Biochemistry*, ***43***(24), 7954–7965.

Cobessi, D., Celia, H., Folschweiller, N., Schalk, I. J., Abdallah, M. A., & Pattus, F. (2005). The crystal structure of the pyoverdine outer membrane receptor FpvA from *Pseudomonas aeruginosa* at 3.6 Å resolution. *Journal of Molecular Biology*, **347**(1), 121–134.

Collier, R. J. (1975). Diphtheria toxin: mode of action and structure. *Bacteriological Reviews*, **39**(1), 54–85.

Corbin, B. D., Seeley, E. H., Raab, A., Feldmann, J., Miller, M. R., Torres, V. J., Anderson, K. L., Dattilo, B. M., Dunman, P. M., Gerads, R., Caprioli, R. M., Nacken, W., Chazin, W. J., & Skaar, E. P. (2008). Metal chelation and inhibition of bacterial growth in tissue abscesses. *Science*, **319**(5865), 962–965.

Cowles, K. N., Moser, T. S., Siryaporn, A., Nyakudarika, N., Dixon, W., Turner, J. J., & Gitai, Z. (2013). The putative Poc complex controls two distinct *Pseudomonas aeruginosa* polar motility mechanisms. *Molecular Microbiology*, **90**(5), 923–938.

Craig, D. B., & Dombkowski, A. A. (2013). Disulfide by Design 2.0: A web-based tool for disulfide engineering in proteins. *BMC Bioinformatics*, **14**(1), 346, 10.1186/1471-2105-14-346

Cuív, P. Ó., Clarke, P., & O'Connell, M. (2006). Identification and characterization of an iron-regulated gene, *chtA*, required for the utilization of the xenosiderophores aerobactin, rhizobactin 1021 and schizokinen by *Pseudomonas aeruginosa*. *Microbiology*, **152**(4), 945–954.

Cunningham, K., Lacy, D. B., Mogridge, J., & Collier, R. J. (2002). Mapping the lethal factor and edema factor binding sites on oligomeric anthrax protective antigen. *Proceedings of the National Academy of Sciences of the United States of America*, **99**(10), 7049–7053.

Cunrath, O., Geoffroy, V. A., & Schalk, I. J. (2016). Metallome of *Pseudomonas aeruginosa*: a role for siderophores. *Environmental Microbiology*, **18**(10), 3258–3267.

Dalbey, R. E., Wang, P., & Kuhn, A. (2011). Assembly of bacterial inner membrane proteins. *Annual Review of Biochemistry*, **80**(1), 161–187.

de Chial, M., Ghysels, B., Beatson, S. A., Geoffroy, V., Meyer, J. M., Pattery, T., Baysse, C., Chablain, P., Parsons, Y. N., Winstanley, C., Cordwell, S. J., & Cornelis, P. (2003). Identification of type II and type III pyoverdine receptors from *Pseudomonas aeruginosa*. *Microbiology*, **149**(4), 821–831.

Dean, C. R., & Poole, K. (1993). Cloning and characterization of the ferric enterobactin receptor gene (*pfeA*) of *Pseudomonas aeruginosa*. *Journal of Bacteriology*, **175**(2), 317–324.

Delano, W. L. (2002). The PyMOL Molecular Graphics System. *DeLano Scientific, Palo Alto, CA, USA*.

Delepelaire, P. (2004). Type I secretion in gram-negative bacteria. *Biochimica et Biophysica Acta (BBA) - Molecular Cell Research*, **1694**(1-3), 149–161.

Delmar, J. A., Su, C. C., & Yu, E. W. (2014). Bacterial multidrug efflux transporters. *Annual Review of Biophysics*, **43**(1), 93–117.

Demchick, P., & Koch, A. L. (1996). The permeability of the wall fabric of *Escherichia coli* and *Bacillus subtilis*. *Journal of Bacteriology*, **178**(3), 768–773.

Deme, J. C., Johnson, S., Vickery, O., Aron, A., Monkhouse, H., Griffiths, T., Hennell James, R., Berks, B. C., Coulton, J. W., Stansfeld, P. J., Lea, S. M. (2020). Structures of the stator complex that drives rotation of the bacterial flagellum. *Nature Microbiology*. **5**, 1553–1564.

Denayer, S., Matthijs, S., & Cornelis, P. (2007). Pyocin S2 (Sa) kills *Pseudomonas aeruginosa* strains via the FpvA type I ferripyoverdine receptor. *Journal of Bacteriology*, **189**(21), 7663–7668.

Devanathan, S., & Postle, K. (2007). Studies on colicin B translocation: FepA is gated by TonB. *Molecular Microbiology*, **65**(2), 441–453.

Doyle, M. T., & Bernstein, H. D. (2019). Bacterial outer membrane proteins assemble via asymmetric interactions with the BamA β-barrel. *Nature Communications*, **10**(1), 1–13.

Driessen, A. J. M., & Nouwen, N. (2008). Protein translocation across the bacterial cytoplasmic membrane. *Annual Review of Biochemistry*, **77**, 643–667).

Duché, D., Baty, D., Chartier, M., & Letellier, L. (1994). Unfolding of colicin A during its translocation through the *Escherichia coli* envelope as demonstrated by disulfide bond engineering. *Journal of Biological Chemistry*, **269**(40), 24820–24825.

Duché, D., Frenkian, A., Prima, V., & Lloubès, R. (2006). Release of immunity protein requires functional endonuclease colicin import machinery. *Journal of Bacteriology*, **188**(24), 8593–8600.

Dudley, M. N. (1990). Overview of gram-negative sepsis. *American Journal of Hospital Pharmacy*, **47**(11 Suppl 3), S3–S6.

Dümmler, A., Lawrence, A., de Marco, A. (2005). Simplified screening for the detection of soluble fusion constructs expressed in *E. coli* using a modular set of vectors. *Microbial Cell Factories*, **4**(1), 1–10

Duport, C., Baysse, C., & Michel-Briand, Y. (1995). Molecular characterization of pyocin S3, a novel S-type pyocin from *Pseudomonas aeruginosa*. *Journal of Biological Chemistry*, **270**(15), 8920–8927.

European Centre for Disease Prevention and Control. (2015). Antimicrobial resistance surveillance in Europe 2015. Annual Report of the European Antimicrobial Resistance Surveillance Network (EARS-Net), 10.2900/6928.

Elfarash, A., Dingemans, J., Ye, L., Hassan, A. A., Craggs, M., Reimmann, C., Thomas, M. S., & Cornelis, P. (2014). Pore-forming pyocin S5 utilizes the FptA ferripyochelin receptor to kill *Pseudomonas aeruginosa*. *Microbiology*, **160**, 261–269.

Elfarash, A., Wei, Q., & Cornelis, P. (2012). The soluble pyocins S2 and S4 from *Pseudomonas aeruginosa* bind to the same FpvAI receptor. *MicrobiologyOpen*, **1**(3), 268–275.

Elias, S., Degtyar, E., & Banin, E. (2011). FvbA is required for vibriobactin utilization in *Pseudomonas aeruginosa*. *Microbiology*, **157**(7), 2172–2180.

Ellison, M. L., Farrow IIII, J. M., Parrish, W., Danell, A. S., & Pesci, E. C. (2013). The Transcriptional Regulator Np20 Is the Zinc Uptake Regulator in *Pseudomonas aeruginosa*. *PLoS ONE*, **8**(9), e75389.

Emsley, P., Lohkamp, B., Scott, W. G., & Cowtan, K. (2010). Features and development of Coot. *Acta Crystallographica Section D: Biological Crystallography*, **66**(4), 486–501.

Farrance, O. E., Hann, E., Kaminska, R., Housden, N. G., Derrington, S. R., Kleanthous, C., Radford, S. E., & Brockwell, D. J. (2013). A Force-Activated Trip Switch Triggers Rapid Dissociation of a Colicin from Its Immunity Protein. *PLoS Biology*, **11**(2), e1001489.

Feld, G. K., Brown, M. J., & Krantz, B. A. (2012). Ratcheting up protein translocation with anthrax toxin. *Protein Science*, **21**(5), 606–624.

Fillat, M. F. (2014). The FUR (ferric uptake regulator) superfamily: Diversity and versatility of key transcriptional regulators. *Archives of Biochemistry and Biophysics*, **546**, 41–52.

Folkesson, A., Jelsbak, L., Yang, L., Johansen, H. K., Ciofu, O., Hoiby, N., & Molin, S. (2012). Adaptation of *Pseudomonas aeruginosa* to the cystic fibrosis airway: An evolutionary perspective. *Nature Reviews Microbiology*, **10**(12), 841–851).

Gasiunas, G., Barrangou, R., Horvath, P., & Siksnys, V. (2012). Cas9-crRNA ribonucleoprotein complex mediates specific DNA cleavage for adaptive immunity in bacteria. *Proceedings of the National Academy of Sciences of the United States of America*, **109**(39), E2579–E2586.

Ghequire, M. G. K., Buchanan, S. K., & de Mot, R. (2018). The ColM family, polymorphic toxins breaching the bacterial cell wall. *MBio*, **9**(1), 10.1128/mBio.02267

Ghequire, M. G. K., & De Mot, R. (2014). Ribosomally encoded antibacterial proteins and peptides from *Pseudomonas*. *FEMS Microbiology Reviews*, **38**(4), 523–568.

Ghequire, M. G. K., Kemland, L., & De Mot, R. (2017). Novel Immunity Proteins Associated with Colicin M-like Bacteriocins Exhibit Promiscuous Protection in *Pseudomonas*. *Frontiers in Microbiology*, **8**, 93.

Ghequire, M. G. K., & Öztürk, B. (2018). A colicin M-type bacteriocin from *Pseudomonas aeruginosa* targeting the HxuC heme receptor requires a novel immunity partner. *Applied and Environmental Microbiology*, **84**(18), 716–734.

Ghequire, M. G. K., Öztürk, B., & De Mot, R. (2018). Lectin-like bacteriocins. *Frontiers in Microbiology*, **9**, 2706.

Ghequire, M. G. K., Swings, T., Michiels, J., Buchanan, S. K., & de Mot, R. (2018). Hitting with a BAM: Selective killing by lectin-like bacteriocins. *MBio*, **9**(2), 10.1128/mBio.02138-17

Ghssein, G., Brutesco, C., Ouerdane, L., Fojcik, C., Izaute, A., Wang, S., Hajjar, C., Lobinski, R., Lemaire, D., Richaud, P., Voulhoux, R., Espaillat, A., Cava, F., Pignol, D., Borezée-Durant, E., & Arnoux, P. (2016). Biosynthesis of a broad-spectrum nicotianamine-like metallophore in *Staphylococcus aureus*. *Science*, **352**(6289), 1105–1109.

Ghysels, B., Dieu, B. T. M., Beatson, S. A., Pirnay, J. P., Ochsner, U. A., Vasil, M. L., & Cornelis, P. (2004). FpvB, an alternative type I ferripyoverdine receptor of *Pseudomonas aeruginosa*. *Microbiology*, **150**(6), 1671–1680.

Ghysels, B., Ochsner, U., Möllman, U., Heinisch, L., Vasil, M., Cornelis, P., & Matthijs, S. (2005). The *Pseudomonas aeruginosa* pir A gene encodes a second receptor for ferrienterobactin and synthetic catecholate analogues. *FEMS Microbiology Letters*, **246**(2), 167–174.

Gi, M., Lee, K. M., Kim, S. C., Yoon, J. H., Yoon, S. S., & Choi, J. Y. (2015). A novel siderophore system is essential for the growth of *Pseudomonas aeruginosa* in airway mucus. *Scientific Reports*, **5**, 14644.

Giovannoni, S. J., Turner, S., Olsen, G. J., Barns, S., Lane, D. J., & Pace, N. R. (1988). Evolutionary relationships among cyanobacteria and green chloroplasts. *Journal of Bacteriology*, **170**(8), 3584–3592.

Gläser, R., Harder, J., Lange, H., Bartels, J., Christophers, E., & Schröder, J. M. (2005). Antimicrobial psoriasin (S100A7) protects human skin from *Escherichia coli* infection. *Nature Immunology*, **6**(1), 57–64.

Glöckner, G., Rosenthal, A., & Valentin, K. (2000). The structure and gene repertoire of an ancient red algal plastid genome. *Journal of Molecular Evolution*, **51**(4), 382–390.

Gomez, N. O., Tetard, A., Ouerdane, L., Laffont, C., Brutesco, C., Ball, G., Lobinski, R., Denis, Y., Plésiat, P., Llanes, C., Arnoux, P., & Voulhoux, R. (2021). Involvement of the *Pseudomonas aeruginosa* MexAB–OprM efflux pump in the secretion of the metallophore pseudopaline. *Molecular Microbiology*, **115**(1), 84–98.

Gorasia, D. G., Veith, P. D., & Reynolds, E. C. (2020). The type IX secretion system: Advances in structure, function and organisation. *Microorganisms*, **8**(8), 1–9.

Gordon, V. M., Klimpel, K. R., Arora, N., Henderson, M. A., & Leppla, S. H. (1995). Proteolytic activation of bacterial toxins by eukaryotic cells is performed by furin and by additional cellular proteases. *Infection and Immunity*, **63**(1), 82–87.

Granato, E. T., Meiller-Legrand, T. A., & Foster, K. R. (2019). The Evolution and Ecology of Bacterial Warfare. *Current Biology*, **29**(11), R521–R537.

Green, E. R., & Mecsas, J. (2016). Bacterial Secretion Systems: An Overview. *Microbiology Spectrum*, **4**(1), 10.1128/microbiolspec.VMBF-0012-2015.

Greenwald, J., Hoegy, F., Nader, M., Journet, L., Mislin, G. L. A., Graumann, P. L., & Schalk, I. J. (2007). Real time fluorescent resonance energy transfer visualization of ferric pyoverdine uptake in *Pseudomonas aeruginosa*: A role for ferrous iron. *Journal of Biological Chemistry*, **282**(5), 2987–2995.

Greenwald, J., Nader, M., Celia, H., Gruffaz, C., Geoffroy, V., Meyer, J.-M., Schalk, I. J., & Pattus, F. (2009). FpvA bound to non-cognate pyoverdines: molecular basis of siderophore recognition by an iron transporter. *Molecular Microbiology*, **72**(5), 1246–1259.

Griko, Y. V., Zakharov, S. D., & Cramer, W. A. (2000). Structural stability and domain organization of colicin E1. *Journal of Molecular Biology*, **302**(4), 941–953.

Gu, Y., Li, H., Dong, H., Zeng, Y., Zhang, Z., Paterson, N. G., Stansfeld, P. J., Wang, Z., Zhang, Y., Wang, W., & Dong, C. (2016). Structural basis of outer membrane protein insertion by the BAM complex. *Nature*, **531**(7592), 64–69.

Hancock, R. E. W., & Brinkman, F. S. L. (2002). Function of *Pseudomonas* porins in uptake and efflux. *Annual Review of Microbiology*, **56**, 17–38.

Hann, E., Kirkpatrick, N., Kleanthous, C., Smith, D. A., Radford, S. E., & Brockwell, D. J. (2007). The effect of protein complexation on the mechanical stability of Im9. *Biophysical Journal*, **92**(9), L79–L81.

Hannauer, M., Barda, Y., Mislin, G. L. A., Shanzer, A., & Schalk, I. J. (2010). The ferrichrome uptake pathway in *Pseudomonas aeruginosa* involves an iron release mechanism with acylation of the siderophore and recycling of the modified desferrichrome. *Journal of Bacteriology*, **192**(5), 1212–1220.

Harmer, C., Alnassafi, K., Hu, H., Elkins, M., Bye, P., Rose, B., Cordwell, S., Triccas, J. A., Harbour, C., & Manos, J. (2013). Modulation of gene expression by *Pseudomonas aeruginosa* during chronic infection in the adult cystic fibrosis lung. *Microbiology*, **159**(11), 2354–2363.

Hawlitschek, G., Schneider, H., Schmidt, B., Tropschug, M., Hartl, F. U., & Neupert, W. (1988). Mitochondrial protein import: Identification of processing peptidase and of PEP, a processing enhancing protein. *Cell*, **53**(5), 795–806.

Hennell James, R., Deme, J. C., Kjær, A., Alcock, F., Silale, A., Lauber, F., Johnson, S., Berks, B. C., & Lea, S. M. (2021). Structure and mechanism of the proton-driven motor that powers type 9 secretion and gliding motility. *Nature Microbiology*, **6**(2), 221–233.

Hermansen, G. M. M., Hansen, M. L., Khademi, S. M. H., & Jelsbak, L. (2018). Intergenic evolution during host adaptation increases expression of the metallophore pseudopaline in *Pseudomonas aeruginosa*. *Microbiology*, **164**(8), 1038–1047.

Hickman, S. J., Cooper, R. E. M., Bellucci, L., Paci, E., & Brockwell, D. J. (2017). Gating of TonB-dependent transporters by substrate-specific forced remodelling. *Nature Communications*, **8**(1), 1–12.

Hill, K., Model, K., Ryan, M. T., Dietmeier, K., Martint, F., Wagner, R., & Pfanner, N. (1998). Tom40 forms the hydrophilic channel of the mitochondrial import pore for preproteins. *Nature*, **395**(6701), 516–521.

Hilsenbeck, J. L., Park, H., Chen, G., Youn, B., Postle, K., & Kang, C. H. (2004). Crystal structure of the cytotoxic bacterial protein colicin B at 2.5 Å resolution. *Molecular Microbiology*, **51**(3), 711–720.

Hoegy, F., Celia, H., Mislin, G. L., Vincent, M., Gallay, J., & Schalk, I. J. (2005). Binding of iron-free siderophore, a common feature of siderophore outer membrane transporters of *Escherichia coli* and *Pseudomonas aeruginosa*. *Journal of Biological Chemistry*, **280**(21), 20222–20230.

Hoegy, F., Lee, X., Noel, S., Rognan, D., Mislin, G. L. A., Reimmann, C., & Schalk, I. J. (2009). Stereospecificity of the siderophore pyochelin outer membrane transporters in fluorescent peudomonads. *Journal of Biological Chemistry*, **284**(22), 14949–14957.

Housden, N. G., Hopper, J. T. S., Lukoyanova, N., Rodriguez-Larrea, D., Wojdyla, J. A., Klein, A., Kaminska, R., Bayley, H., Saibil, H. R., Robinson, C. V., & Kleanthous, C. (2013). Intrinsically disordered protein threads through the bacterial outer-membrane porin OmpF. *Science*, **340**(6140), 1570–1574.

Housden, N. G., Loftus, S. R., Moore, G. R., James, R., & Kleanthous, C. (2005). Cell entry mechanism of enzymatic bacterial colicins: Porin recruitment and the thermodynamics of receptor binding. *Proceedings of the National Academy of Sciences of the United States of America*, **102**(39), 13849–13854.

Housden, N. G., Rassam, P., Lee, S., Samsudin, F., Kaminska, R., Sharp, C., Goult, J. D., Francis, M. L., Khalid, S., Bayley, H., & Kleanthous, C. (2018). Directional Porin Binding of Intrinsically Disordered Protein Sequences Promotes Colicin Epitope Display in the Bacterial Periplasm. *Biochemistry*, **57**(29), 4374–4381.

Housden, N. G., Wojdyla, J. A., Korczynska, J., Grishkovskaya, I., Kirkpatrick, N., Brzozowski, A. M., & Kleanthous, C. (2010). Directed epitope delivery across the *Escherichia coli* outer membrane through the porin OmpF. *Proceedings of the National Academy of Sciences of the United States of America*, **107**(50), 21412–21417.

Hsia, K. C., Chak, K. F., Liang, P. H., Cheng, Y. S., Ku, W. Y., & Yuan, H. S. (2004). DNA Binding and Degradation by the HNH Protein ColE7. *Structure*, **12**(2), 205–214.

Huang, B., Ru, K., Yuan, Z., Whitchurch, C. B., & Mattick, J. S. (2004). tonB3 is required for normal twitching motility and extracellular assembly of type IV pili. *Journal of Bacteriology*, **186**(13), 4387–4389.

Hullmann, J., Patzer, S. I., Römer, C., Hantke, K., & Braun, V. (2008). Periplasmic chaperone FkpA is essential for imported colicin M toxicity. *Molecular Microbiology*, **69**(4), 926–937.

Iadanza, M. G., Higgins, A. J., Schiffrin, B., Calabrese, A. N., Brockwell, D. J., Ashcroft, A. E., Radford, S. E., & Ranson, N. A. (2016). Lateral opening in the intact β-barrel assembly machinery captured by cryo-EM. *Nature Communications*, **7**(1), 1–12.

Iglewski, B. H., Liu, P. V., & Kabat, D. (1977). Mechanism of action of *Pseudomonas aeruginosa* exotoxin A: adenosine diphosphate ribosylation of mammalian elongation factor 2 *in vitro* and *in vivo*. *Infection and Immunity*, **15**(1). 138–144.

Imperi, F., Tiburzi, F., & Visca, P. (2009). Molecular basis of pyoverdine siderophore recycling in *Pseudomonas aeruginosa*. *Proceedings of the National Academy of Sciences of the United States of America*, **106**(48), 20440–20445.

Jackson, M. E., Simpson, J. C., Girod, A., Pepperkok, R., Roberts, L. M., & Lord, J. M. (1999). The KDEL retrieval system is exploited by *Pseudomonas* exotoxin A, but not by *Shiga*-like toxin-1, during retrograde transport from the Golgi complex to the endoplasmic reticulum. *Journal of Cell Science*, **112**(4). 467–475

Jakes, K. S., & Finkelstein, A. (2010). The colicin Ia receptor, Cir, is also the translocator for colicin Ia. *Molecular Microbiology*, **75**(3), 567–578.

Jansen, K. B., Inns, P. G., Housden, N. G., Hopper, J. T. S., Kaminska, R., Lee, S., Robinson, C. V., Bayley, H., & Kleanthous, C. (2020). Bifurcated binding of the OmpF receptor underpins import of the bacteriocin colicin N into *Escherichia coli*. *Journal of Biological Chemistry*, **295**(27), 9147–9156.

Jiang, J., Pentelute, B. L., Collier, R. J., & Hong Zhou, Z. (2015). Atomic structure of anthrax protective antigen pore elucidates toxin translocation. *Nature*, **521**(7553), 545–549.

Jones, D. T. (1999). Protein secondary structure prediction based on position-specific scoring matrices. *Journal of Molecular Biology*, **292**(2), 195–202.

Joshi, A., Grinter, R., Josts, I., Chen, S., Wojdyla, J. A., Lowe, E. D., Kaminska, R., Sharp, C., McCaughey, L., Roszak, A. W., Cogdell, R. J., Byron, O., Walker, D., & Kleanthous, C. (2015). Structures of the Ultra-High-Affinity Protein-Protein Complexes of Pyocins S2 and AP41 and Their Cognate Immunity Proteins from *Pseudomonas aeruginosa*. *Journal of Molecular Biology*, **427**(17), 2852–2866.

Josts, I., Veith, K., & Tidow, H. (2019). Ternary structure of the outer membrane transporter FoxA with resolved signaling domain provides insights into TonB-mediated siderophore uptake. *ELife*, **8**, e48528, 10.7554/eLife.48528

Kehl-Fie, T. E., & Skaar, E. P. (2010). Nutritional immunity beyond iron: a role for manganese and zinc. *Current Opinion in Chemical Biology*, 14(2), 218–224.

Kendrew, J. C., & Parrish, R. G. (1957). The Crystal Structure of Myoglobin. III. Sperm-Whale Myoglobin. *Proceedings of the Royal Society of London. Series A. Mathematical and Physical Sciences*, **238**(1214), 305–324.

Kirkup, B. C., & Riley, M. A. (2004). Antibiotic-mediated antagonism leads to a bacterial game of rock-paper-scissors *in vivo*. *Nature*, **428**(6981), 412–414.

Kleanthous, C. (2010). Swimming against the tide: Progress and challenges in our understanding of colicin translocation. *Nature Reviews Microbiology*, **8**(12), 843–848.

Kleanthous, C., & Walker, D. (2001). Immunity proteins: Enzyme inhibitors that avoid the active site. *Trends in Biochemical Sciences*, **26**(10), 624–631.

Klebba, P. E. (2016). ROSET model of TonB action in Gram-negative bacterial iron acquisition. *Journal of Bacteriology*, **198**(7), 1013–1021.

Klein, Alexander, Wojdyla, J. A., Joshi, A., Josts, I., McCaughey, L. C., Housden, N. G., Kaminska, R., Byron, O., Walker, D., & Kleanthous, C. (2016). Structural and biophysical analysis of nuclease protein antibiotics. *Biochemical Journal*, **473**(18), 2799–2812.

Klein, Astrid, Israel, L., Lackey, S. W. K., Nargang, F. E., Imhof, A., Baumeister, W., Neupert, W., & Thomas, D. R. (2012). Characterization of the insertase for β-barrel proteins of the outer mitochondrial membrane. *Journal of Cell Biology*, **199**(4), 599–611.

Konings, A. F., Martin, L. W., Sharples, K. J., Roddam, L. F., Latham, R., Reid, D. W., & Lamont, I. L. (2013). *Pseudomonas aeruginosa* uses multiple pathways to acquire iron during chronic infection in cystic fibrosis lungs. *Infection and Immunity*, **81**(8), 2697–2704.

Korotkov, K. V., Sandkvist, M., & Hol, W. G. J. (2012). The type II secretion system: Biogenesis, molecular architecture and mechanism. *Nature Reviews Microbiology*, **10**(5), 336–351.

Kounnas, M. Z., Morris, R. E., Thompson, M. R., FitzGerald, D. J., Strickland, D. K., & Saelinger, C. B. (1992). The α2-macroglobulin receptor/low density lipoprotein receptor-related protein binds and internalizes *Pseudomonas* exotoxin A. *Journal of Biological Chemistry*, **267**(18), 12420–12423.

Krantz, B. A., Melnyk, R. A., Zhang, S., Juris, S. J., Lacy, D. B., Wu, Z., Finkelstein, A., & Collier, R. J. (2005). A phenylalanine clamp catalyzes protein translocation through the anthrax toxin pore. *Science*, **309**(5735), 777–781.

Kreitman, R. J., & Pastan, I. (1995). Importance of the glutamate residue of KDEL in increasing the cytotoxicity of *Pseudomonas* exotoxin derivatives and for increased binding to the KDEL receptor. *Biochemical Journal*, **307**(1), 29–37.

Kumazaki, T., & Ishii, S.-I. (1982). Comparative Study on Fibers Isolated from Four R-Type Pyocins, Phage-Tail-Like Bacteriocins of *Pseudomonas aeruginosa*. *Journal of Biochemistry*, 92(5), 1559–1566.

Kurisu, G., Zakharov, S. D., Zhalnina, M. V., Bano, S., Eroukova, V. Y., Rokitskaya, T. I., Antonenko, Y. N., Wiener, M. C., & Cramer, W. A. (2003). The structure of BtuB with bound colicin E3 R-domain implies a translocon. *Nature Structural Biology*, **10**(11), 948–954.

Laffont, C., Brutesco, C., Hajjar, C., Cullia, G., Fanelli, R., Ouerdane, L., Cavelier, F., & Arnoux, P. (2019). Simple rules govern the diversity of bacterial nicotianamine-like metallophores. *Biochemical Journal*, **476**(15), 2221–2233.

Lam, J. S., Taylor, V. L., Islam, S. T., Hao, Y., & Kocíncová, D. (2011). Genetic and functional diversity of *Pseudomonas aeruginosa* lipopolysaccharide. *Frontiers in Microbiology*, ***2***, 118.

Lambert, P. A. (2002). Mechanisms of antibiotic resistance in *Pseudomonas aeruginosa*. *Journal of the Royal Society of Medicine*, **95**(41), 22–26.

Langklotz, S., Baumann, U., & Narberhaus, F. (2012). Structure and function of the bacterial AAA protease FtsH. *Biochimica et Biophysica Acta (BBA) - Molecular Cell Research* **1823**(1), 40–48.

Larsen, R. A., & Postle, K. (2001). Conserved Residues Ser16 and His20 and Their Relative Positioning Are Essential for TonB Activity, Cross-linking of TonB with ExbB, and the Ability of TonB to Respond to Proton Motive Force. *Journal of Biological Chemistry*, **276**(11), 8111–8117.

Larsen, R. A., Thomas, M. G., Wood, G. E., & Postle, K. (1994). Partial suppression of an *Escherichia coli* TonB transmembrane domain mutation (ΔV17) by a missense mutation in ExbB. *Molecular Microbiology*, **13**(4), 627–640.

Latino, L., Patin, D., Chérier, D., Touzé, T., Pourcel, C., Barreteau, H., & Mengin-Lecreulx, D. (2019). Impact of FiuA Outer Membrane Receptor Polymorphism on the Resistance of *Pseudomonas aeruginosa* toward Peptidoglycan Lipid II-Targeting PaeM Pyocins. *Journal of Bacteriology*, ***201***(13), e00164-19, 10.1128/JB.00164-19

Lee, J., Tomasek, D., Santos, T. M., May, M. D., Meuskens, I., & Kahne, D. (2019). Formation of a β-barrel membrane protein is catalyzed by the interior surface of the assembly machine protein BamA. *ELife*, **8**, e49787, 10.7554/eLife.49787

Leiman, P. G., Basler, M., Ramagopal, U. A., Bonanno, J. B., Sauder, J. M., Pukatzki, S., Burley, S. K., Almo, S. C., & Mekalanos, J. J. (2009). Type VI secretion apparatus and phage tail-associated protein complexes share a common evolutionary origin. *Proceedings of the National Academy of Sciences of the United States of America*, **106**(11), 4154–4159.

Levengood, S. K., Beyer, W. F., & Webster, R. E. (1991). TolA: A membrane protein involved in colicin uptake contains an extended helical region. *Proceedings of the National Academy of Sciences of the United States of America*, **88**(14), 5939–5943.

Lewinson, O., Lee, A. T., & Rees, D. C. (2009). A P-type ATPase importer that discriminates between essential and toxic transition metals. *Proceedings of the National Academy of Sciences of the United States of America*, **106**(12), 4677–4682.

Leyton, D. L., Rossiter, A. E., & Henderson, I. R. (2012). From self sufficiency to dependence: Mechanisms and factors important for autotransporter biogenesis. In *Nature Reviews Microbiology*, **10**(3), 213–225).

Lhospice, S., Gomez, N. O., Ouerdane, L., Brutesco, C., Ghssein, G., Hajjar, C., Liratni, A., Wang, S., Richaud, P., Bleves, S., Ball, G., Borezée-Durant, E., Lobinski, R., Pignol, D., Arnoux, P., & Voulhoux, R. (2017). *Pseudomonas aeruginosa* zinc uptake in chelating environment is primarily mediated by the metallophore pseudopaline. *Scientific Reports*, ***7***, 17132.

Llamas, M. A., Mooij, M. J., Sparrius, M., Vandenbroucke-Grauls, C. M. J. E., Ratledge, C., & Bitter, W. (2008). Characterization of five novel *Pseudomonas aeruginosa* cell-surface signalling systems. *Molecular Microbiology*, **67**(2), 458–472.

Llamas, M. A., Sparrius, M., Kloet, R., Jiménez, C. R., Vandenbroucke-Grauls, C., & Bitter, W. (2006). The heterologous siderophores ferrioxamine B and ferrichrome activate signaling pathways in *Pseudomonas aeruginosa*. *Journal of Bacteriology*, **188**(5), 1882–1891.

Lukacik, P., Barnard, T. J., Keller, P. W., Chaturvedi, K. S., Seddiki, N., Fairman, J. W., Noinaj, N., Kirby, T. L., Henderson, J. P., Steven B, A. C., Hinnebusch, J., & Buchanan, S. K. (2012). Structural engineering of a phage lysin that targets Gram-negative pathogens. *Proceedings of the National Academy of Sciences of the United States of America*, **109**(25), 9857–9862.

Lytovchenko, O., Melin, J., Schulz, C., Kilisch, M., Hutu, D. P., & Rehling, P. (2013). Signal recognition initiates reorganization of the presequence translocase during protein import. *EMBO Journal*, **32**(6), 886–898.

Ma, L., Kaserer, W., Annamalai, R., Scott, D. C., Jin, B., Jiang, X., Xiao, Q., Maymani, H., Massis, L. M., Ferreira, L. C. S., Newton, S. M. C., & Klebba, P. E. (2007). Evidence of ball-and-chain transport of ferric enterobactin through FepA. *Journal of Biological Chemistry*, **282**(1), 397–406.

Maki-Yonekura, S., Matsuoka, R., Yamashita, Y., Shimizu, H., Tanaka, M., Iwabuki, F., & Yonekura, K. (2018). Hexameric and pentameric complexes of the ExbBD energizer in the ton system. *ELife*, **7**, e35419, 10.7554/eLife.35419

Malinverni, J. C., Werner, J., Kim, S., Sklar, J. G., Kahne, D., Misra, R., & Silhavy, T. J. (2006). YfiO stabilizes the YaeT complex and is essential for outer membrane protein assembly in *Escherichia coli*. *Molecular Microbiology*, **61**(1), 151–164.

Manson, M. D., Tedesco, P., Berg, H. C., Harold, F. M., & Van der Drift, C. (1977). A protonmotive force drives bacterial flagella. *Proceedings of the National Academy of Sciences of the United States of America*, **74**(7), 3060–3064.

Marshall, B., Stintzi, A., Gilmour, C., Meyer, J. M., & Poole, K. (2009). Citrate-mediated iron uptake in *Pseudomonas aeruginosa*: Involvement of the citrate-inducible FecA receptor and the FeoB ferrous iron transporter. *Microbiology*, **155**(1), 305–315.

Martin, J., Mahlke, K., & Pfanner, N. (1991). Role of an energized inner membrane in mitochondrial protein import: ΔΨ drives the movement of presequences. *Journal of Biological Chemistry*, **266**(27), 18051–18057.

Martin, W. F., Garg, S., & Zimorski, V. (2015). Endosymbiotic theories for eukaryote origin. *Philosophical Transactions of the Royal Society B: Biological Sciences*, **370**(1678), 20140330.

Martin, W. F., & Müller, M. (1998). The hydrogen hypothesis for the first eukaryote. *Nature*, **392**(6671), 37–41.

Mastropasqua, M. C., D'Orazio, M., Cerasi, M., Pacello, F., Gismondi, A., Canini, A., Canuti, L., Consalvo, A., Ciavardelli, D., Chirullo, B., Pasquali, P., & Battistoni, A. (2017). Growth of *Pseudomonas aeruginosa* in zinc poor environments is promoted by a nicotianamine-related metallophore. *Molecular Microbiology*, **106**(4), 543–561.

Mastropasqua, M. C., Lamont, I., Martin, L. W., Reid, D. W., D'Orazio, M., & Battistoni, A. (2018). Efficient zinc uptake is critical for the ability of *Pseudomonas aeruginosa* to express virulence traits and colonize the human lung. *Journal of Trace Elements in Medicine and Biology*, **48**, 74–80.

Maté, M. J., & Kleanthous, C. (2004). Structure-based analysis of the metal-dependent mechanism of H-N-H endonucleases. *Journal of Biological Chemistry*, **279**(33), 34763–34769.

McCaughey, L. C., Grinter, R., Josts, I., Roszak, A. W., Waløen, K. I., Cogdell, R. J., Milner, J., Evans, T., Kelly, S., Tucker, N. P., Byron, O., Smith, B., & Walker, D. (2014). Lectin-Like Bacteriocins from *Pseudomonas* spp. Utilise D-Rhamnose Containing Lipopolysaccharide as a Cellular Receptor. *PLoS Pathogens*, **10**(2), e1003898.

McCaughey, L. C., Josts, I., Grinter, R., White, P., Byron, O., Tucker, N. P., Matthews, J. M., Kleanthous, C., Whitchurch, C. B., & Walker, D. (2016). Discovery, characterization and *in vivo* activity of pyocin SD2, a protein antibiotic from *Pseudomonas aeruginosa*. *Biochemical Journal*, **473**(15), 2345–2358.

McCaughey, L. C., Ritchie, N. D., Douce, G. R., Evans, T. J., & Walker, D. (2016). Efficacy of species-specific protein antibiotics in a murine model of acute *Pseudomonas aeruginosa* lung infection. *Scientific Reports*, **6**, 30201.

McCoy, A. J., Grosse-Kunstleve, R. W., Adams, P. D., Winn, M. D., Storoni, L. C., & Read, R. J. (2007). Phaser crystallographic software. *Journal of Applied Crystallography*, **40**(4), 658–674.

McFarlane, J. S., & Lamb, A. L. (2017). Biosynthesis of an Opine Metallophore by *Pseudomonas aeruginosa*. *Biochemistry*, **56**(45), 5967–5971.

Micenková, L., Bosák, J., Kucera, J., Hrala, M., Dolejšová, T., Šedo, O., Linke, D., Fišer, R., & Šmajs, D. (2019). Colicin Z, a structurally and functionally novel colicin type that selectively kills enteroinvasive *Escherichia coli* and *Shigella* strains. *Scientific Reports*, **9**, 11127.

Michalska, M., & Wolf, P. (2015). *Pseudomonas* Exotoxin A: Optimized by evolution for effective killing. *Frontiers in Microbiology*, **6**, 963.

Michel-Briand, Y., & Baysse, C. (2002). The pyocins of *Pseudomonas aeruginosa*. *Biochimie*, **84**(5–6), 499–510.

Minor, D. L., & Kim, P. S. (1994). Measurement of the β-sheet-forming propensities of amino acids. *Nature*, **367**(6464), 660–663.

Mitamura, T., Higashiyama, S., Taniguchi, N., Klagsbrun, M., & Mekada, E. (1995). Diphtheria toxin binds to the epidermal growth factor (EGF)-like domain of human heparin-binding EGF-like growth factor/diphtheria toxin receptor and inhibits specifically its mitogenic activity. *Journal of Biological Chemistry*, **270**(3), 1015–1019.

Moradali, M. F., Ghods, S., & Rehm, B. H. A. (2017). *Pseudomonas aeruginosa* lifestyle: A paradigm for adaptation, survival, and persistence. *Frontiers in Cellular and Infection Microbiology*, **7**, 39.

Morales, V., Bäckman, M., Bagdasarian, M. (1991). A series of wide-host-range low-copy-number vectors that allow direct screening for recombinants. *Gene*, **97**(1), 39–47.

Mossmann, D., Meisinger, C., & Vögtle, F. N. (2012). Processing of mitochondrial presequences. *Biochimica et Biophysica Acta (BBA) - Gene Regulatory Mechanisms* **1819**(9–10), 1098–1106.

Moynié, L., Milenkovic, S., Mislin, G. L. A., Gasser, V., Malloci, G., Baco, E., McCaughan, R. P., Page, M. G. P., Schalk, I. J., Ceccarelli, M., & Naismith, J. H. (2019). The complex of ferric-enterobactin with its transporter from *Pseudomonas aeruginosa* suggests a two-site model. *Nature Communications*, **10**(1), 1–14.

Murray, T. S., Egan, M., & Kazmierczak, B. I. (2007). *Pseudomonas aeruginosa* chronic colonization in cystic fibrosis patients. *Current Opinion in Pediatrics*, **19**(1), 83–88.

Murshudov, G. N., Skubák, P., Lebedev, A. A., Pannu, N. S., Steiner, R. A., Nicholls, R. A., Winn, M. D., Long, F., & Vagin, A. A. (2011). REFMAC5 for the refinement of macromolecular crystal structures. *Acta Crystallographica Section D: Biological Crystallography*, **67**(4), 355–367.

Nader, M., Journet, L., Meksem, A., Guillon, L., & Schalk, I. J. (2011). Mechanism of ferripyoverdine uptake by *Pseudomonas aeruginosa* outer membrane transporter FpvA: No diffusion channel formed at any time during ferrisiderophore uptake. *Biochemistry*, **50**(13), 2530–2540.

Nakai, M. (2015). The TIC complex uncovered: The alternative view on the molecular mechanism of protein translocation across the inner envelope membrane of chloroplasts. *Biochimica et Biophysica Acta (BBA) - Bioenergetics*, **1847**(9), 957–967.

Nestorovich, E. M., Sugawara, E., Nikaido, H., & Bezrukov, S. M. (2006). *Pseudomonas aeruginosa* porin OprF. Properties of the channel. *Journal of Biological Chemistry*, **281**(24), 16230–16237.

Newstead, S., Ferrandon, S., & Iwata, S. (2008). Rationalizing α-helical membrane protein crystallization. *Protein Science*, **17**(3), 466–472.

Ng, C. L., Lang, K., Meenan, N. A. G., Sharma, A., Kelley, A. C., Kleanthous, C., & Ramakrishnan, V. (2010). Structural basis for 16S ribosomal RNA cleavage by the cytotoxic domain of colicin E3. *Nature Structural and Molecular Biology*, **17**(10), 1241–1246.

Nguyen, V. S., Douzi, B., Durand, E., Roussel, A., Cascales, E., & Cambillau, C. (2018). Towards a complete structural deciphering of Type VI secretion system. *Current Opinion in Structural Biology*, **49**, 77–84.

Nielsen, H., Engelbrecht, J., Brunak, S., & Von Heijne, G. (1997). Identification of prokaryotic and eukaryotic signal peptides and prediction of their cleavage sites. *Protein Engineering*, **10**(1), 1–6.

Nikaido, H. (2003). Molecular Basis of Bacterial Outer Membrane Permeability Revisited. *Microbiology and Molecular Biology Reviews*, **67**(4), 593–656.

Noinaj, N., Guillier, M., Barnard, T. J., & Buchanan, S. K. (2010). TonB-dependent transporters: Regulation, structure, and function. *Annual Review of Microbiology*, **64**, 43–60).

Noinaj, N., Kuszak, A. J., Gumbart, J. C., Lukacik, P., Chang, H., Easley, N. C., Lithgow, T., & Buchanan, S. K. (2013). Structural insight into the biogenesis of β-barrel membrane proteins. *Nature*, **501**(7467), 385–390.

Ochsner, U. A., Johnson, Z., Lamont, I. L., Cunliffe, H. E., & Vasil, M. L. (1996). Exotoxin A production in *Pseudomonas aeruginosa* requires the iron-regulated pvdS gene encoding an alternative sigma factor. *Molecular Microbiology*, **21**(5), 1019–1028.

Oeemig, J. S., Ollila, O. H. S., & Iwaï, H. (2018). NMR structure of the C-terminal domain of TonB protein from *Pseudomonas aeruginosa*. *PeerJ*, **6**, e5412, 10.7717/peerj.5412

Ogata, M., Chaudhary, V. K., Pastan, I., & FitzGerald, D. J. (1990). Processing of *Pseudomonas* exotoxin by a cellular protease results in the generation of a 37,000-Da toxin fragment that is translocated to the cytosol. *Journal of Biological Chemistry*, **265**(33), 20678–20685.

Ogawa, T., Tomita, K., Ueda, T., Watanabe, K., Uozumi, T., & Masaki, H. (1999). A cytotoxic ribonuclease targeting specific transfer RNA anticodons. *Science*, **283**(5410), 2097–2100.

Ohsumi, M., Shinomiya, T., Kageyama, M., & Kasei, M.-. (1980). Comparative Study on R-type Pyocins of *Pseudomonas aeruginosa*. *Journal of Biochemistry*, **87**(4), 1119-1126.

Olejnickova, K., Hola, V., & Ruzicka, F. (2014). Catheter-related infections caused by *Pseudomonas aeruginosa*: Virulence factors involved and their relationships. *Pathogens and Disease*, **72**(2), 87–94.

Otero-Asman, J. R., García-García, A. I., Civantos, C., Quesada, J. M., & Llamas, M. A. (2019). *Pseudomonas aeruginosa* possesses three distinct systems for sensing and using the host molecule haem. *Environmental Microbiology*, **21**(12), 4629–4647.

Palmer, K. L., Mashburn, L. M., Singh, P. K., & Whiteley, M. (2005). Cystic fibrosis sputum supports growth and cues key aspects of *Pseudomonas aeruginosa* physiology. *Journal of Bacteriology*, **187**(15), 5267–5277.

Papadakos, G., Wojdyla, J. A., & Kleanthous, C. (2012). Nuclease colicins and their immunity proteins. *Quarterly Reviews of Biophysics*, **45**(1), 57-103.

Papini, E., Rappuoli, R., Murgia, M., & Montecucco, C. (1993). Cell penetration of diphtheria toxin. Reduction of the interchain disulfide bridge is the rate-limiting step of translocation in the cytosol. *Journal of Biological Chemistry*, **268**(3), 1567–1574.

Park, J. S., Lee, W. C., Yeo, K. J., Ryu, K., Kumarasiri, M., Hesek, D., Lee, M., Mobashery, S., Song, J. H., Kim, S. Il, Lee, J. C., Cheong, C., Jeon, Y. H., & Kim, H. (2012). Mechanism of anchoring of OmpA protein to the cell wall peptidoglycan of the gram-negative bacterial outer membrane. *The FASEB Journal*, **26**(1), 219–228.

Parker, J. L., & Newstead, S. (2012). Current trends in α-helical membrane protein crystallization: An update. *Protein Science*, **21**(9), 1358–1365.

Paschen, S. A., Waizenegger, T., Stan, T., Preuss, M., Cyrklaff, M., Hell, K., Rapaport, D., & Neupert, W. (2003). Evolutionary conservation of biogenesis of β-barrel membrane proteins. *Nature*, **426**(6968), 862–866.

Paškevičius, Š., Starkevič, U., Misiūnas, A., Vitkauskienė, A., Gleba, Y., & Ražanskienė, A. (2017). Plant-expressed pyocins for control of *Pseudomonas aeruginosa*. *PLOS ONE*, **12**(10), e0185782.

Pastan, I., Chaudhary, V., & Fitzgerald, D. J. (1992). Recombinant toxins as novel therapeutic agents. *Annual Review of Biochemistry*, **61**(1), 331–354.

Patzer, S. I., Albrecht, R., Braun, V., & Zeth, K. (2012). Structural and mechanistic studies of pesticin, a bacterial homolog of phage lysozymes. *Journal of Biological Chemistry*, **287**(28), 23381–23396.

Patzer, S. I., & Hantke, K. (1998). The ZnuABC high-affinity zinc uptake system and its regulator Zur in *Escherichia coli*. *Molecular Microbiology*, **28**(6), 1199–1210.

Pawelek, P. D., Croteau, N., Ng-Thow-Hing, C., Khursigara, C. M., Moiseeva, N., Allaire, M., & Coulton, J. W. (2006). Structure of TonB in complex with FhuA, *E. coli* outer membrane receptor. *Science*, **312**(5778), 1399–1402.

Pederick, V. G., Eijkelkamp, B. A., Begg, S. L., Ween, M. P., McAllister, L. J., Paton, J. C., & McDevitt, C. A. (2015). ZnuA and zinc homeostasis in *Pseudomonas aeruginosa*. *Scientific Reports*, **5**, 13139.

Pell, L. G., Kanelis, V., Donaldson, L. W., Howell, P. L., & Davidson, A. R. (2009). The phage λ major tail protein structure reveals a common evolution for long-tailed phages and the type VI bacterial secretion system. *Proceedings of the National Academy of Sciences of the United States of America*, **106**(11), 4160–4165.

Penfold, C. N., Healy, B., Housden, N. G., Boetzel, R., Vankemmelbeke, M., Moore, G. R., Kleanthous, C., & James, R. (2004). Flexibility in the receptor-binding domain of the enzymatic colicin E9 is required for toxicity against *Escherichia coli* cells. *Journal of Bacteriology*, **186**(14), 4520–4527.

Pletzer, D., Braun, Y., & Weingart, H. (2016). Swarming motility is modulated by expression of the putative xenosiderophore transporter SppR-SppABCD in *Pseudomonas aeruginosa* PA14. *Antonie van Leeuwenhoek*, **109**(6), 737–753.

Pohlner, J., Halter, R., & Meyer, T. F. (1987). *Neisseria gonorrhoeae* IgA protease. Secretion and implications for pathogenesis. *Antonie van Leeuwenhoek*, **53**(6), 479–484.

Pommer, A. J., Cal, S., Keeble, A. H., Walker, D., Evans, S. J., Kühlmann, U. C., Cooper, A., Connolly, B. A., Hemmings, A. M., Moore, G. R., James, R., & Kleanthous, C. (2001). Mechanism and cleavage specificity of the H-N-H endonuclease colicin E9. *Journal of Molecular Biology*, **314**(4), 735–749.

Poole, K., & McKay, G. A. (2003). Iron acquisition and its control in *Pseudomonas aeruginosa*: Many roads lead to Rome. *Frontiers in Bioscience*, **8**, d661-d686.

Poole, K., Neshat, S., Krebes, K., & Heinrichs, D. E. (1993). Cloning and Nucleotide Sequence Analysis of the Ferripyoverdine Receptor Gene *fpvA* of *Pseudomonas aeruginosa*. *Journal of Bacteriology*, **175**(15), 4597–4604

Pukatzki, S., Ma, A. T., Revel, A. T., Sturtevant, D., & Mekalanos, J. J. (2007). Type VI secretion system translocates a phage tail spike-like protein into target cells where it cross-links actin. *Proceedings of the National Academy of Sciences of the United States of America*, **104**(39), 15508–15513.

Quintana, J., Novoa-Aponte, L., & Argüello, J. M. (2017). Copper homeostasis networks in the bacterium *Pseudomonas aeruginosa*. *Journal of Biological Chemistry*, **292**(38), 15691–15704.

Radics, J., Königsmaier, L., & Marlovits, T. C. (2014). Structure of a pathogenic type 3 secretion system in action. *Nature Structural and Molecular Biology*, **21**(1), 82–87.

Raetz, C. R. H. (1978). Enzymology, Genetics, and Regulation of Membrane Phospholipid Synthesis in *Escherichia coli*. *Microbiological Reviews*, **42**(3), 614–659.

Raetz, C. R. H., & Dowhan, W. (1990). Biosynthesis and Function of Phospholipids in *Escherichia coli*. *Journal of Biological Chemistry*, **265**(3), 1235–8.

Raetz, C. R. H., & Whitfield, C. (2002). Lipopolysaccharide endotoxins. *Annual Review of Biochemistry*, **71**(1), 635–700).

Ramírez-Estrada, S., Borgatta, B., & Rello, J. (2016). *Pseudomonas aeruginosa* ventilator-associated pneumonia management. *Infection and Drug Resistance*, **9**, 7–18.

Rédly, G. A., & Poole, K. (2005). FpvIR control of *fpvA* ferric pyoverdine receptor gene expression in *Pseudomonas aeruginosa*: Demonstration of an interaction between FpvI and FpvR and identification of mutations in each compromising this interaction. *Journal of Bacteriology*, **187**(16), 5648–5657.

Rendueles, O., Beloin, C., Latour-Lambert, P., & Ghigo, J. M. (2014). A new biofilm-associated colicin with increased efficiency against biofilm bacteria. *ISME Journal*, **8**(6), 1275–1288.

Richardson, L. G. L., Paila, Y. D., Siman, S. R., Chen, Y., Smith, M. D., & Schnell, D. J. (2014). Targeting and assembly of components of the TOC protein import complex at the chloroplast outer envelope membrane. *Frontiers in Plant Science*, **5**, 269.

Roise, D., Horvath, S. J., Tomich, J. M., Richards, J. H., & Schatz, G. (1986). A chemically synthesized pre-sequence of an imported mitochondrial protein can form an amphiphilic helix and perturb natural and artificial phospholipid bilayers. *The EMBO Journal*, **5**(6), 1327–1334.

Roof, S. K., Allard, J. D., Bertrand, K. P., & Postle, K. (1991). Analysis of *Escherichia coli* TonB membrane topology by use of PhoA fusions. *Journal of Bacteriology*, 173(17), 5554–5557.

Ruhe, Z. C., Low, D. A., & Hayes, C. S. (2013). Bacterial contact-dependent growth inhibition. *Trends in Microbiology*, **21**(5), 230–237.

Ruhe, Z. C., Nguyen, J. Y., Xiong, J., Koskiniemi, S., Beck, C. M., Perkins, B. R., Low, D. A., & Hayes, C. S. (2017). CdiA effectors use modular receptor-binding domains to recognize target bacteria. *MBio*, **8**(2), e00290-17, 10.1128/mBio.00290-17.

Ruhe, Z. C., Subramanian, P., Song, K., Nguyen, J. Y., Stevens, T. A., Low, D. A., Jensen, G. J., & Hayes, C. S. (2018). Programmed Secretion Arrest and Receptor-Triggered Toxin Export during Antibacterial Contact-Dependent Growth Inhibition. *Cell*, **175**(4), 921-933.

Sankaran, K., & Wu, H. C. (1994). Lipid modification of bacterial prolipoprotein. Transfer of diacylglyceryl moiety from phosphatidylglycerol. *Journal of Biological Chemistry*, **269**(31), 19701–19706.

Sano, Y., Matsui, H., Kobayashi, M., & Kageyama, M. (1993). Molecular structures and functions of pyocins S1 and S2 in *Pseudomonas aeruginosa*. *Journal of Bacteriology*, **175**(10), 2907–2916.

Saravanan, M., Bujnicki, J. M., Cymerman, I. A., Rao, D. N., & Nagaraja, V. (2004). Type II restriction endonuclease R.KpnI is a member of the HNH nuclease superfamily. *Nucleic Acids Research*, **32**(20), 6129–6135.

Schalk, I. J., & Cunrath, O. (2016). An overview of the biological metal uptake pathways in *Pseudomonas aeruginosa*. *Environmental Microbiology*, **18**(10), 3227–3246.

Schalk, I. J., Hennard, C., Dugave, C., Poole, K., Abdallah, M. A., & Pattus, F. (2001). Iron-free pyoverdin binds to its outer membrane receptor FpvA in *Pseudomonas aeruginosa*: A new mechanism for membrane transport. *Molecular Microbiology*, **39**(2), 351–361.

Schauer, K., Rodionov, D. A., & de Reuse, H. (2008). New substrates for TonB-dependent transport: do we only see the "tip of the iceberg"? *Trends in Biochemical Sciences*, **33**(7), 330–338.

Schindelin, J., Arganda-Carreras, I., Frise, E., Kaynig, V., Longair, M., Pietzsch, T., Preibisch, S., Rueden, C., Saalfeld, S., Schmid, B., Tinevez, J. Y., White, D. J., Hartenstein, V., Eliceiri, K., Tomancak, P., & Cardona, A. (2012). Fiji: An open-source platform for biological-image analysis. *Nature Methods*, **9**(7), 676–682).

Schleiff, E., Jelic, M., & Soll, J. (2003). A GTP-driven motor moves proteins across the outer envelope of chloroplasts. *Proceedings of the National Academy of Sciences of the United States of America*, **100**(8), 4604–4609.

Schramm, E., Mende, J., Braun, V., & Kamp, R. M. (1987). Nucleotide sequence of the colicin B activity gene cba: Consensus pentapeptide among TonB-dependent colicins and receptors. *Journal of Bacteriology*, **169**(7), 3350–3357.

Schwartz, M. P., Huang, S., & Matouschek, A. (1999). The structure of precursor proteins during import into mitochondria. *Journal of Biological Chemistry*, **274**(18), 12759–12764.

Schwartz, M. P., & Matouschek, A. (1999). The dimensions of the protein import channels in the outer and inner mitochondrial membranes. *Proceedings of the National Academy of Sciences of the United States of America*, 96(23), 13086–13090.

Sean Peacock, R., Weljie, A. M., Peter Howard, S., Price, F. D., & Vogel, H. J. (2005). The solution structure of the C-terminal domain of TonB and interaction studies with TonB box peptides. *Journal of Molecular Biology*, **345**(5), 1185–1197.

Shabalin, I. G., Porebski, P. J., & Minor, W. (2018). Refining the macromolecular model–achieving the best agreement with the data from X-ray diffraction experiment. In *Crystallography Reviews*, **24**(4), 236–262.

Sharma, O., Yamashita, E., Zhalnina, M. V., Zakharov, S. D., Datsenko, K. A., Wanner, B. L., & Cramer, W. A. (2007). Structure of the complex of the colicin E2 R-domain and its BtuB receptor: The outer membrane colicin translocon. *Journal of Biological Chemistry*, **282**(32), 23163–23170.

Sharp, C., Bray, J., Housden, N. G., Maiden, M. C. J., & Kleanthous, C. (2017). Diversity and distribution of nuclease bacteriocins in bacterial genomes revealed using Hidden Markov Models. *PLOS Computational Biology*, **13**(7), e1005652.

Shen, B. W., Landthaler, M., Shub, D. A., & Stoddard, B. L. (2004). DNA binding and cleavage by the HNH homing endonuclease I-HmuI. *Journal of Molecular Biology*, **342**(1), 43–56.

Shen, J., Meldrum, A., & Poole, K. (2002). FpvA receptor involvement in pyoverdine biosynthesis in *Pseudomonas aeruginosa*. *Journal of Bacteriology*, **184**(12), 3268–3275.

Shi, L. X., & Theg, S. M. (2013). The chloroplast protein import system: From algae to trees. *Biochimica et Biophysica Acta (BBA) - Molecular Cell Research*, **1833**(2) 314–331.

Shiota, T., Imai, K., Qiu, J., Hewitt, V. L., Tan, K., Shen, H. H., Sakiyama, N., Fukasawa, Y., Hayat, S., Kamiya, M., Elofsson, A., Tomii, K., Horton, P., Wiedemann, N., Pfanner, N., Lithgow, T., & Endo, T. (2015). Molecular architecture of the active mitochondrial protein gate. *Science*, **349**(6255), 1544–1548.

Shrivastava, R., Jiang, X., & Chng, S.-S. (2017). Outer membrane lipid homeostasis via retrograde phospholipid transport in *Escherichia coli*. *Molecular Microbiology*, **106**(3), 395–408.

Shultis, D. D., Purdy, M. D., Banchs, C. N., & Wiener, M. C. (2006). Outer membrane active transport: Structure of the BtuB:TonB complex. *Science*, **312**(5778), 1396–1399.

Silhavy, T. J., Kahne, D., & Walker, S. (2010). The bacterial cell envelope. *Cold Spring Harbor Perspectives in Biology*, 2(5), a000414.

Skaar, E. P. (2010). The battle for iron between bacterial pathogens and their vertebrate hosts. *PLoS Pathogens*, **6**(8), e1000949.

Sklar, J. G., Wu, T., Gronenberg, L. S., Malinverni, J. C., Kahne, D., & Silhavy, T. J. (2007). Lipoprotein SmpA is a component of the YaeT complex that assembles outer membrane proteins in *Escherichia coli*. *Proceedings of the National Academy of Sciences of the United States of America*, **104**(15), 6400–6405.

Sklar, J. G., Wu, T., Kahne, D., & Silhavy, T. J. (2007). Defining the roles of the periplasmic chaperones SurA, Skp, and DegP in *Escherichia coli*. *Genes and Development*, **21**(19), 2473–2484.

Smith, A. D., & Wilks, A. (2015). Differential contributions of the outer membrane receptors PhuR and HasR to heme acquisition in *Pseudomonas aeruginosa*. *Journal of Biological Chemistry*, **290**(12), 7756–7766.

Smith, D. C., Spooner, R. A., Watson, P. D., Murray, J. L., Hodge, T. W., Amessou, M., Johannes, L., Lord, J. M., & Roberts, L. M. (2006). Internalized *Pseudomonas* exotoxin A can exploit multiple pathways to reach the endoplasmic reticulum. *Traffic*, **7**(4), 379–393.

Soelaiman, S., Jakes, K., Wu, N., Li, C., & Shoham, M. (2001). Crystal structure of colicin E3: Implications for cell entry and ribosome inactivation. *Molecular Cell*, **8**(5), 1053–1062.

Son, M. S., Matthews, W. J., Kang, Y., Nguyen, D. T., & Hoang, T. T. (2007). *In vivo* evidence of *Pseudomonas aeruginosa* nutrient acquisition and pathogenesis in the lungs of cystic fibrosis patients. *Infection and Immunity*, **75**(11), 5313–5324.

Szczepaniak, J., Holmes, P., Rajasekar, K., Kaminska, R., Samsudin, F., Inns, P. G., Rassam, P., Khalid, S., Murray, S. M., Redfield, C., & Kleanthous, C. (2020). The lipoprotein Pal stabilises the bacterial outer membrane during constriction by a mobilisation-and-capture mechanism. *Nature Communications*, **11**(1), 1–14.

Takase, H., Nitanai, H., Hoshino, K., & Otani, T. (2000). Requirement of the *Pseudomonas aeruginosa tonB* gene for high-affinity iron acquisition and infection. *Infection and Immunity*, **68**(8), 4498–4504.

Theg, S. M., Bauerle, C., Olsen, L. J., Selman, B. R., & Keegstra, K. (1989). Internal ATP is the only energy requirement for the translocation of precursor proteins across chloroplastic membranes. *Journal of Biological Chemistry*, **264**(12), 6730–6736.

Theuer, C. P., Buchner, J., FitzGerald, D., & Pastan, I. (1993). The N-terminal region of the 37-kDa translocated fragment of *Pseudomonas* exotoxin A aborts translocation by promoting its own export after microsomal membrane insertion. *Proceedings of the National Academy of Sciences of the United States of America*, **90**(16), 7774–7778.

Thomas, S., Holland, I. B., & Schmitt, L. (2014). The Type 1 secretion pathway - The hemolysin system and beyond. *Biochimica et Biophysica Acta (BBA) - Molecular Cell Research*, **1843**(8), 1629–1641.

Tomasek, D., Rawson, S., Lee, J., Wzorek, J. S., Harrison, S. C., Li, Z., & Kahne, D. (2020). Structure of a nascent membrane protein as it folds on the BAM complex. *Nature*, **583**(7816), 473–478.

Tomita, K., Ogawa, T., Uozumi, T., Watanabe, K., & Masaki, H. (2000). A cytotoxic ribonuclease which specifically cleaves four isoaccepting arginine tRNAs at their anticodon loops. *Proceedings of the National Academy of Sciences of the United States of America*, **97**(15), 8278–8283.

Truscott, K. N., Kovermann, P., Geissler, A., Merlin, A., Meijer, M., Driessen, A. J. M., Rassow, J., Pfanner, N., & Wagner, R. (2001). A presequence- and voltage-sensitive channel of the mitochondrial preprotein translocase formed by Tim23. *Nature Structural Biology*, **8**(12), 1074–1082.

Tucker, K., & Park, E. (2019). Cryo-EM structure of the mitochondrial protein-import channel TOM complex at near-atomic resolution. *Nature Structural and Molecular Biology*, **26**(12), 1158–1166.

Turano, H., Gomes, F., Barros-Carvalho, G. A., Lopes, R., Cerdeira, L., Netto, L. E. S., Gales, A. C., & Lincopan, N. (2017). Tn6350, a novel transposon carrying pyocin S8 genes encoding a bacteriocin with activity against carbapenemase-producing *Pseudomonas aeruginosa*. *Antimicrobial Agents and Chemotherapy*, **61**(5), e00100-17.

Turner, R. D., Hurd, A. F., Cadby, A., Hobbs, J. K., Foster, S., J. (2013). Cell wall elongation mode in Gram-negative bacteria is determined by peptidoglycan architecture. *Nature Communications*, **4**, 1496.

Vankemmelbeke, M., Housden, N. G., James, R., Kleanthous, C., & Penfold, C. N. (2013). Immunity protein release from a cell-bound nuclease colicin complex requires global conformational rearrangement. *MicrobiologyOpen*, **2**(5), 853–861.

Vankemmelbeke, M., Zhang, Y., Moore, G. R., Kleanthous, C., Penfold, C. N., & James, R. (2009). Energy-dependent immunity protein release during tol-dependent nuclease colicin translocation. *Journal of Biological Chemistry*, **284**(28), 18932–18941.

Verkhovtseva, Y. V., Filina, Y. Y., & Pukhov, D. E. (2001). Evolutionary role of iron in metabolism of prokaryotes and in biogeochemical processes. *Journal of Evolutionary Biochemistry and Physiology*, **37**, 444–450.

Vestweber, D., & Schatz, G. (1989). DNA-protein conjugates can enter mitochondria via the protein import pathway. *Nature*, **338**(6211), 170–172.

Vetter, I. R., Parker, M. W., Tucker, A. D., Lakey, J. H., Pattus, F., & Tsernoglou, D. (1998). Crystal structure of a colicin N fragment suggests a model for toxicity. *Structure*, **6**(7), 863–874.

Visca, P., Imperi, F., & Lamont, I. L. (2007). Pyoverdine siderophores: from biogenesis to biosignificance. *Trends in Microbiology*, **15**(1), 22–30.

Vollmer, W., Blanot, D., & De Pedro, M. A. (2008). Peptidoglycan structure and architecture. *FEMS Microbiology Reviews*, **32**(2), 149–167.

Voulhoux, R., Filloux, A., & Schalk, I. J. (2006). Pyoverdine-mediated iron uptake in *Pseudomonas aeruginosa*: The Tat system is required for PvdN but not for FpvA transport. *Journal of Bacteriology*, **188**(9), 3317–3323.

Voulhoux, R., & Tommassen, J. (2004). Omp85, an evolutionarily conserved bacterial protein involved in outer-membrane-protein assembly. *Research in Microbiology*, **155**(3), 129–135.

Walburger, A., Lazdunski, C., & Corda, Y. (2002). The Tol/Pal system function requires an interaction between the C-terminal domain of TolA and the N-terminal domain of TolB. *Molecular Microbiology*, **44**(3), 695–708.

Walker, D., Mosbahi, K., Vankemmelbeke, M., James, R., & Kleanthous, C. (2007). The role of electrostatics in colicin nuclease domain translocation into bacterial cells. *Journal of Biological Chemistry*, **282**(43), 31389–31397.

Walker, D., Rolfe, M., Thompson, A., Moore, G. R., James, R., Hinton, J. C. D., & Kleanthous, C. (2004). Transcriptional Profiling of Colicin-Induced Cell Death of *Escherichia coli* MG1655 Identifies Potential Mechanisms by Which Bacteriocins Promote Bacterial Diversity. *Journal of Bacteriology*, **186**(3), 866–869.

Webb, B., & Sali, A. (2016). Comparative protein structure modeling using MODELLER. *Current Protocols in Bioinformatics*, **54**, 5.6.1–5.6.37.

Wedekind, J. E., Trame, C. B., Dorywalska, M., Koehl, P., Raschke, T. M., McKee, M., FitzGerald, D., Collier, R. J., & McKay, D. B. (2001). Refined crystallographic structure of *Pseudomonas aeruginosa* exotoxin A and its implications for the molecular mechanism of toxicity. *Journal of Molecular Biology*, **314**(4), 823–837.

Weinberg, E. D. (2009). Iron availability and infection. *Biochimica et Biophysica Acta (BBA) - General Subjects*, **1790**(7), 600–605).

Wesche, J., Elliott, J. L., Falnes, P., Olsnes, S., & Collier, R. J. (1998). Characterization of membrane translocation by anthrax protective antigen. *Biochemistry*, **37**(45), 15737–15746.

White, P., Joshi, A., Rassam, P., Housden, N. G., Kaminska, R., Goult, J. D., Redfield, C., McCaughey, L. C., Walker, D., Mohammed, S., & Kleanthous, C. (2017). Exploitation of an iron transporter for bacterial protein antibiotic import. *Proceedings of the National Academy of Sciences of the United States of America*, **114**(45), 12051–12056.

Whiteley, M., Bangera, M. G., Bumgarner, R. E., Parsek, M. R., Teitzel, G. M., Lory, S., & Greenberg, E. P. (2001). Gene expression in *Pseudomonas aeruginosa* biofilms. *Nature*, **413**(6858), 860–864.

WHO. (2014). Antimicrobial resistance: Global Report on Surveillance. World Health Organization.

WHO. (2017). Prioritization of pathogens to guide discovery, research and development of new antibiotics for drug resistant bacterial infections, including tuberculosis. *Essential Medicines and Health Products*, **88**, WHO reference number: WHO/EMP/IAU/2017.12.

Wiedemann, N., & Pfanner, N. (2017). Mitochondrial machineries for protein import and assembly. *Annual Review of Biochemistry*, **86**(1), 685–714.

Wiener, M., Freymann, D., Ghosh, P., & Stroud, R. M. (1997). Crystal structure of colicin Ia. *Nature*, **385**(6615), 461–464.

Wilderman, P. J., Vasil, A. I., Johnson, Z., Wilson, M. J., Cunliffe, H. E., Lamont, I. L., & Vasil, M. L. (2001). Characterization of an endoprotease (PrpL) encoded by a PvdS-regulated gene in *Pseudomonas aeruginosa*. *Infection and Immunity*, **69**(9), 5385–5394.

Williams, C. J., Headd, J. J., Moriarty, N. W., Prisant, M. G., Videau, L. L., Deis, L. N., Verma, V., Keedy, D. A., Hintze, B. J., Chen, V. B., Jain, S., Lewis, S. M., Arendall, W. B., Snoeyink, J., Adams, P. D., Lovell, S. C., Richardson, J. S., & Richardson, D. C. (2018). MolProbity: More and better reference data for improved all-atom structure validation. *Protein Science*, **27**(1), 293–315.

Wu, S. L., Li, C. C., Chen, J. C., Chen, Y. J., Lin, C. T., Ho, T. Y., & Hsiang, C. Y. (2009). Mutagenesis identifies the critical amino acid residues of human endonuclease G involved in catalysis, magnesium coordination, and substrate specificity. *Journal of Biomedical Science*, **16**, 6.

Wu, T., Malinverni, J., Ruiz, N., Kim, S., Silhavy, T. J., & Kahne, D. (2005). Identification of a multicomponent complex required for outer membrane biogenesis in *Escherichia coli*. *Cell*, **121**(2), 235–245.

Yang, D., Oyaizu, Y., Oyaizu, H., Olsen, G. J., & Woese, C. R. (1985). Mitochondrial origins. *Proceedings of the National Academy of Sciences of the United States of America*, **82**(13), 4443–4447.

Yano, M., Hoogenraad, N., Terada, K., & Mori, M. (2000). Identification and Functional Analysis of Human Tom22 for Protein Import into Mitochondria. *Molecular and Cellular Biology*, **20**(19), 7205–7213.

Young, J. A. T., & Collier, R. J. (2007). Anthrax toxin: Receptor binding, internalization, pore formation, and translocation. *Annual Review of Biochemistry*, **76**, 243–265.

Zakharov, S. D., Eroukova, V. Y., Rokitskaya, T. I., Zhalnina, M. V., Sharma, O., Loll, P. J., Zgurskaya, H. I., Antonenko, Y. N., & Cramer, W. A. (2004). Colicin occlusion of OmpF and TolC channels: Outer membrane translocons for colicin import. *Biophysical Journal*, **87**(6), 3901–3911.

Zeth, K., Römer, C., Patzer, S. I., & Braun, V. (2008). Crystal structure of colicin M, a novel phosphatase specifically imported by *Escherichia coli*. *Journal of Biological Chemistry*, **283**(37), 25324–25331.

Zhao, Q., & Poole, K. (2000). A second *tonB* gene in *Pseudomonas aeruginosa* is linked to the *exbB* and *exbD* genes. *FEMS Microbiology Letters*, **184**(1), 127–132.

Zhao, T., Zhang, J., Han, X., Yang, J., Wang, X., Vercruysse, M., Hu, H., & Lei, X. (2020). A pseudopaline fluorescent probe for selective detection of *Pseudomonas aeruginosa*. *CCS Chemistry*, **2**, 2405–2417.